ORGANOMETALLIC PI-CONJUGATED MATERIALS: FUNDAMENTAL INVESTIGATIONS AND EXPLORING APPLICATIONS IN OPTOELECTRONICS

By

SUBHADIP GOSWAMI

A DISSERTATION PRESENTED TO THE GRADUATE SCHOOL
OF THE UNIVERSITY OF FLORIDA IN PARTIAL FULFILLMENT
OF THE REQUIREMENTS FOR THE DEGREE OF
DOCTOR OF PHILOSOPHY

UNIVERSITY OF FLORIDA

2015

To my parents, brother and my wife

ACKNOWLEDGMENTS

It has been a fabulous journey over the last five years in UF and I would like to thank almighty for being with me always. Besides, there are many people who contributed to my journey. I certainly know, this little place in the dissertation will not be enough to thank all of them.

First of all, I would like to thank Professor Kirk S Schanze for being such a great adviser and for his help, support and advice throughout my graduate career. His constant encouragement and advice in various aspects of life, both academic and professional helped me to grow as an individual as well as a scientist. I would like to thank him for the kind of freedom he has given me to work and choose my own projects. I immensely enjoyed all the lab responsibilities which helped me to grow my management skills. He always took time to explain critical scientific concepts in a very simple and lucid way to me. I am also grateful to him for giving me the opportunity to present my work in various scientific meetings, especially in KAUST, Saudi Arabia. He is very patient while teaching the efficient way of communicating ideas through emails, manuscripts as well as in power points. I am extremely fortunate to have his believe in every aspect of my work, I hope I did respect them all to the best of my ability.

I am grateful and offer my sincere gratitude to all of my undergraduate chemistry professors in my college as well as IITK in India who fueled the interest of this subject into me. I would like to sincerely thank my all committee members- Prof. Leslie Murray, Prof. Adam Viege, Prof. Daniel Talham, Prof. Franky So, Prof. Ronald Castellano for all the scientific discussion I had with them. My special thanks to Prof. Lisa McElwee-White and Prof. David Richardson for serving in the committee for my oral exam. It is very necessary to have good collaboration in an interdisciplinary research and I am very

fortunate to have such good collaborations. I would like to thank Dr. Aleks Rebane and Geoff wicks from Montana State University for helping me with the two photon absorption; Prof. Omar Abdelsaboor from KAUST for ultrafast transient absorption spectroscopy; Prof. So and Dania from UF materials science department for photovoltaic device fabrication; Prof. John Reynolds and Jeff Hernandez from Georgia Tech for helping me with the photovoltaic device fabrication; Prof John Papanikolas and Melissa Gish from UNC, Chapel Hill for ultrafast transient absorption on isoindigo and DPP compounds.

I am grateful for all the friendship and collaboration inside the Schanze group. Special thanks goes to our former postdoc Dr. Anand Parthasarathy who taught me how to run polymerization reaction, how to measure all the photophysical properties, most importantly he showed me how to take responsibility and perform them with perfection. I would like to thank Russ Winkle for relentlessly running all the DFT calculations for me, Seda Cekli and Dr. Randi Price for a hand in laser instruments or in any other things whenever I needed their help. My “Sisler 420” colleague Dr. Ali Gundogan made my stay enjoyable in the group with many fruitful scientific and fun filled discussions. Our other postdocs Dr. Galyna Dubinina, Dr. Gyu Leem, and Dr. Zhuo Chen were also contributed to my research with their expertise. Julian Wang patiently showed me how to make photovoltaic devices and work with my chromophores for device fabrication. Other than that, I would like to present by sincere gratitude to all present and former member of the group to make my stay memorable in the Schanze group, specially, Junlin Jiang, Yajing Yang, Song Guo, Dave Bullock, Dr. Xuzhi Zhu, Dr. Danlu Wu, Dr. Jie Yang-Cheer, Dr. Dongping Xie, Dr. Hsien-Yi Hsu, Bethy Kim, Ethan Holt, Dr. Jan

Moritz Koenen, Dr. Zhenxing Pan, Dr. Sridhar Rajam, Dr. Rajendra Acharya, Zhiliang Lee and the growing Schanze group family. Raghida Bou Zerdan deserves a special note of thanks for answering my uncountable questions as we were sharing similar chemistry at one point. I would like to thank Dr. Ben Smith, Lori Clark, and Debra Anderson who were always there to help.

I was fortunate to have a nice friend circle outside of my academic environment in Gainesville. I would like to thank Amrita Basu Mullick, Divya Rajan and Akhil Raj Ahir for their friendship and support from the day one in Gainesville, as we came together from India. I must thank all the friends with whom I enjoyed every bit in the cricket field on weekends.

I cannot describe in words my deepest and sincere gratitude to my parents (Mr. Debdas Goswami and Mrs. Tripti Goswami) for their endless unconditional love, support and encouragement. Without them, I would never reached this position. Credit goes to my brother Ranadip Goswami for his love and support.

This dissertation would never be completed without the love and support from my wife Mrs Sucharita Chakraborty. She always asked me a little when I was busy working in the lab or preparing this dissertation. I am and will be always grateful for her persistence and faith in me.

TABLE OF CONTENTS

page

LIST OF TABLES

LIST OF FIGURES

Abstract of Dissertation Presented to the Graduate School
of the University of Florida in Partial Fulfillment of the
Requirements for the Degree of Doctor of Philosophy

ORGANOMETALLIC PI-CONJUGATED MATERIALS: FUNDAMENTAL INVESTIGATIONS AND EXPLORING APPLICATIONS IN OPTOELECTRONICS

By

Subhadip Goswami

August 2015

Chair: Kirk Schanze
Major: Chemistry

This dissertation is focused on synthesis and optoelectronic properties of pi conjugated organometallic polymers and small molecules for non-linear optical property and bulk heterojunction solar cells.

The second and third chapters are focused on the study of gold and platinum containing pi conjugated chromophores to understand the effect of different heavy metals in non-linear absorption as well as photophysical properties. In the second chapter, we have shown, gold is less efficient in populating triplet excited state than platinum because of their weak orbital interaction with the pi conjugated backbone. However, due to low fluorescence quantum yield, the comparative study of these metals on nonlinear absorption was not possible. The third chapter contains the study of these two metals on a charge transfer ligand, where high fluorescence quantum yield was achieved. It was shown that, due to large change in dipole moment for the platinum complexes compare to gold complexes, platinum is much more efficient in showing two photon absorption.

The fourth chapter consists of study with polystyrene containing atactic polymer, where two photon active organometallic chromophores were grafted in varying ratio

along with pure organic chromophores. Efficient singlet to triplet energy transfer was observed in these polymers with increasing platinum concentration and proved by ultrafast transient absorption study. All the polymers were active towards exhibiting upconverted photoluminescence under two photon condition.

Another line of study in this dissertation is synthesizing organometallic materials for photovoltaic application. We have shown that cyclometallated platinum containing donor acceptor chromophores generate triplet excited state efficiently and have suitable HOMO-LUMO energy levels to act as donor materials in photovoltaic devices. Cyclometallated platinum containing diketopyrrolopyrrole polymers are synthesized and shown to have device efficiency of 1.77% with very high fill factor (~65%). The effect of cyclometallated platinum on isoindigo chromophore is also explored and the triplet excited state of isoindigo is detected for the first time. Finally, we have discussed how we can manipulate the morphology of platinum acetylide containing donor-acceptor materials by changing the numbers of terminal long alkyl chains.

CHAPTER 1
INTRODUCTION

Conjugated Polymers

Since the development of polyacetylene by Heeger, MacDiarmid and Shirakawa in 1977, there has been growing interest in the area of conjugated polymers.[1] They showed that polyacetylene (PA) can be doped with halogen vapor to induce conductivity by formation of charge transfer solids between π clouds of polyacetylenes and halogen atoms. In general, the conductive property of the π conjugated polymers can be attributed to the large array of overlapping π orbitals. For example, the ethylene monomer consist of σ bonds formed by three equivalent sp^2 hybrid orbitals and $2p_z$ orbitals are forming weakly overlapping π bonds (Figure 1-1 left). In polyethylene, delocalized π-molecular orbitals (bonding and antibonding) are formed due to the extensive overlap of p_z orbitals with its neighbor p_z orbitals. As the conjugation length of the polymer increases, the increasing orbital overlap of the p_z orbitals lead to lowering of HOMO-LUMO bandgap. Eventually when the bandgap is small enough, the polymer behaves as an organic semiconductor material.

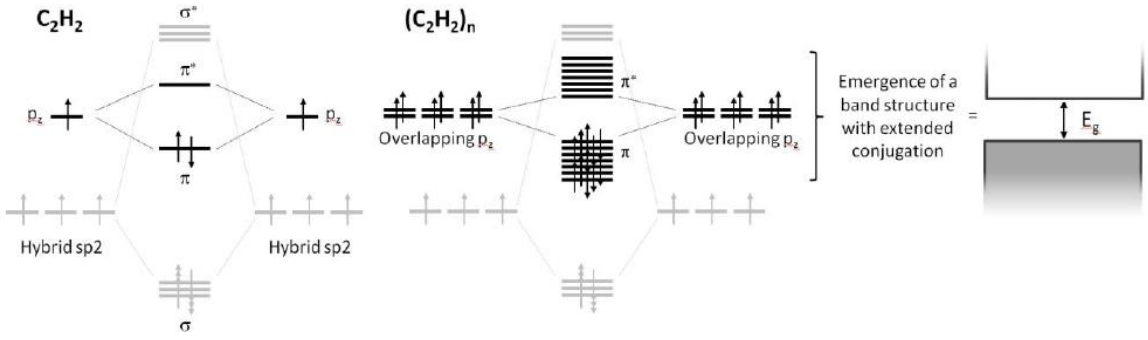

Figure 1-1. Simplified molecular orbital diagram a sp^2 hybridized ethylene-type unit in conjugated system (left); with increased conjugation in polyacetylenes, the π and π* orbitals merged to give rise to HOMO and LUMO molecular orbitals (center); in fully conjugated systems, the band structure is observed with well-defined band gap E_g (right).[2]

Although the band gap in PA is due to Peierls distortion,[3] π-conjugated polymers with aromatic core have intrinsic non-degenerate molecular orbitals arising from their benzenoid and quinoid forms. After these fundamental discoveries of conjugated polymers, chemical modification has allowed the synthesis of conductive polymers for applications in advanced bulk-heterojunction solar cells,[4-7] organic light emitting devices[8,9], and optical sensors[10,11]. Introduction of ionic side chains (cationic and anionic) into the polymer backbone leads to a new family of conjugated materials, called "conjugated poly-electrolytes" or CPEs.[12] Because of their unique photophysical properties, CPEs find application in optoelectronics,[13] biocides,[14] and sensors.[15] The majority of the applications are based on the excited state properties of conjugated organic polymers or oligomers which encourage researchers to study the excited state photophysics of these types of molecules. While singlet excited states have been extensively studied, the triplet excited states are relatively unexplored due to the limited efficiency of singlet to triplet intersystem crossing (ISC) in these compounds. However, organometallic conjugated oligomers and polymers containing heavy metal atoms effectively populate the triplet manifold due to spin-orbit coupling (SOC) and allow the photophysical study of the triplet excited states,[16,17] which have applications in several fields including optical power limiting materials,[18-21] organic light emitting devices,[22-24] photovoltaic devices.[25-27]

Organometallic Materials for Non-linear Absorption

In general, absorption of light by a material corresponds to absorption of a single photon to promote the ground state chromophore to a higher energy state. The energy of the single photon must be equal to the energy difference between the ground state

and excited state for an efficient transition. In 1931, M. Göppert-Mayer first theoretically predicted the possibility of two photon absorption, but lack of a coherent light source precluded validation of the theory.[28] However, very soon after the invention of the laser in 1960, the first experimental evidence for non-linear absorption was observed by using intense coherent radiation from a pulsed ruby-crystal laser.[29] This opened a new field of research called “multiphoton absorption.”

Two photon absorption

Two photon absorption (2PA) is defined by simultaneous absorption of two photons by a ground state chromophore to reach an excited state. The combined energy of the photons is same as the energy difference between ground and excited states, similar to absorption of one photon with twice the energy. However, the selection rule for 2PA is different from that for one photon absorption (1PA).

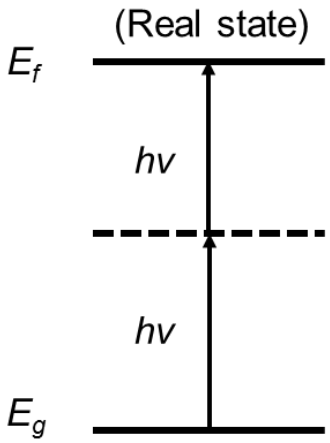

Figure 1-2. Schematic diagram of two photon absorption via an intermediate state.[30]

The short time scale (~ 10 fs) for 2PA can be explained via formation of an intermediate state (Figure 1-2). In the first step, one photon is absorbed by a ground state (E_g) chromophore to reach to the intermediate state and second step consists of absorption of another photon, allowing the molecule to complete its transition to the final

excited state (E_f). The intermediate state is not defined in this process, as it can be between any of an infinite number of eigen states present between E_g and E_f. According to the Heisenberg energy-time uncertainty principle, a large uncertainty in energy leads to very short time scale for 2PA. The instantaneous response time and quadratic dependency on intensity of light make 2PA valuable for photochemical processes to occur in a small focal regions. It is also useful to protect sensitive optical instruments, because two low-energy photons are used instead of one high-energy photon. In live-cell imaging, absorption of two infrared photons can reduce scattering (scattering cross section decreases with increasing wavelength) and decrease background signals to give deep-tissue images. These two properties contribute to the application of 2PA in biological imaging[31-34], photodynamic therapy[35-38], optical power limiting materials[39,40], optical data storage[41,42], photopolymerization[43,44], and lithography[45,46].

Two photon absorption is characterized by a cross section value (σ), which is a molecular property with units of GM (after the name of M. Göppert-Mayer, 1 GM= 10^{-50}cm^4 s photon^{-1}). With advancements in synthetic chemistry and lasers, there has been growing interest in designing new chromophores for 2PA. Key to this is the presence of a ground state dipole moment or the coupling of a transition dipole with the ground state or excited state dipole. In order to have these characteristics, it is necessary but not sufficient to have both electron rich (donor, D) and electron deficient (acceptor, A) chromophores in the same molecule. The other important structural factors for efficient 2PA are coplanarity of the chromophores to increase the charge transfer, symmetry, and conjugation length of the chromophores.

Excited state absorption

Another efficient way to achieve non-linear absorption is by excited state absorption (ESA)[47,48] which occurs when light is absorbed by a chromophore already in an excited state for transition to a higher order excited state. This can take place by either a singlet or triplet excited state and involves slightly longer timescale (ns-μs) compared to 2PA. For organometallic chromophores containing heavy atoms ESA occurs mainly from a triplet excited state T_1 due to strong spin-orbit coupling effect. It has been shown that at high light intensities and for long pulses ESA is the major contributing factor for nonlinear absorption.[47] An effective 2PA cross section β_{eff} is used in the literature to describe two photon absorption when it is difficult to separate the contributions due to ESA and 2PA.

Combination of two Photon absorption and excited state absorption

In heavy atom-containing π-conjugated materials, it is possible to increase the overall nonlinear response by contributions from both 2PA and ESA because of the high absorption coefficient of $T_1 \rightarrow T_n$ transition. On absorption of light, a singlet excited state (S_1) is populated by both one photon absorption (1PA) and two photon absorption (2PA) within ps-fs time scale. The strong spin-orbit coupling effect of the heavy metal induces $S_1 \rightarrow T_1$ intersystem crossing followed by ESA from $T_1 \rightarrow T_n$, which persists within the ns-μs timescale. For platinum acetylide materials ISC takes place with ϕ_{ISC} > 90% in the fs-ns time scale.[49]

The contribution of ESA or 2PA to the overall non-linear process depends on the pulse width of the excitation. In general, non-linear absorption with shorter pulse width excitation (fs-ps) comes from purely 2PA, whereas non-linear behavior under long excitation pulses (ns) is due to the contribution from both 2PA and ESA. Two popular

ways of measuring 2PA cross sections are the non-linear transmission (NLT) and the two photon excited fluorescence or relative fluorescence methods. The NLT method takes into account both 2PA from $S_0 \rightarrow S_1$ and ESA, while the relative fluorescence method pertains to non-linear response from 2PA only due to very short excitation pulse width.

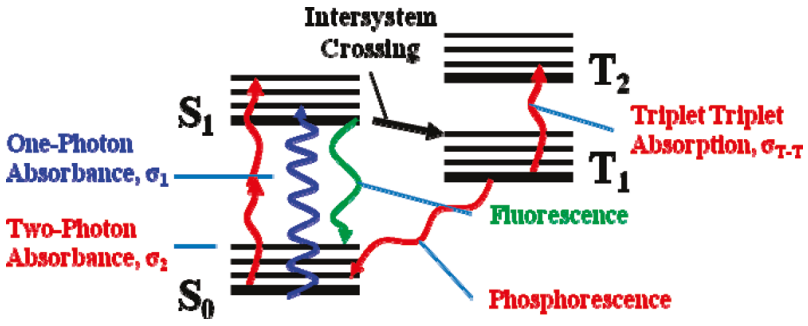

Figure 1-3. Jablonski diagram of a two photon active organometallic chromophore.[49]

Two photon absorption is often observed at double the frequency of the one photon absorption peak. However, it can occur at different energies depending on the symmetry of the chromophore due to difference in selection rules for multiphoton absorption. Efficient spectral overlap of 2PA and ESA from triplet-triplet absorption can result in significant enhancement in overall nonlinear response of the chromophores.

Platinum acetylides: synthesis and photophysics

Since their development in the 1970s,[50] platinum acetylide materials have gained popularity over the years due to their unique photophysical properties and versatile applications. Platinum acetylide was first synthesized by a dehydrohalogenation reaction between the terminally deprotected acetylide hydrogen and *cis*-$Pt(PBu_3)_2Cl_2$. Efficient synthesis of disubstituted platinum acetylide complexes can be accomplished by reacting terminal acetylides with *cis*- $Pt(PBu_3)_2Cl_2$ in the presence of diethylamine and CuI as catalyst at room temperature (Figure 1-4a). Monosubstituted platinum

acetylide complexes can be synthesized by reaction in the presence of refluxing diethylamine.

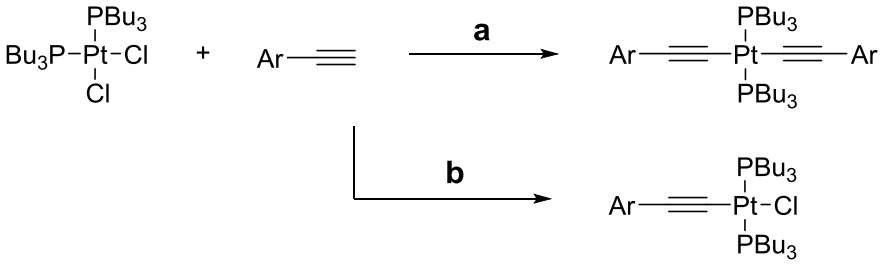

Figure 1-4. Synthesis of platinum acetylide: A) CuI, diethylamine, room temperature, B) diethylamine, reflux.[51,52]

The starting platinum precursor $Pt(PBu_3)_2Cl_2$ can be either the *cis* or *trans* isomer; however, the *cis* isomer converts to *trans* under the basic reaction conditions. It is preferable to start with the *cis* isomer because the "trans effect" of the tributyl phosphine groups labilizes the chloride groups to expedite the reaction. Both isomers can be distinguished by ^{31}P NMR spectroscopy. The phosphorus NMR of platinum acetylide systems are characterized by a strong signal from phosphorus flanked by a couple of platinum satellites due to the interaction of ^{31}P with the NMR-active platinum nucleus ^{195}Pt. The difference in *cis* and *trans* isomers can be determined by the difference in coupling constants $J_{Pt\text{-}P}$.

Photophysics of platinum acetylide

The square planar platinum complex geometry consists of the platinum(II) center and four ligands around the metal center in the same plane with the axial positions vacant. The orbital splitting diagram for a square planar geometry can be explained by removal of axial ligands from octahedral geometry (Figure 1-5), in which, the metal center is surrounded by four ligands in the plane of the metal and two axial ligands in the perpendicular direction. The orbitals $d_{x^2\text{-}y^2}$ and d_{z^2} (e_g set) point directly towards the

ligands, and hence are at higher energy than d_{xy}, d_{xz}, and d_{yz} which are lower in energy, and named as the triply degenerate t_{2g} set of orbitals.

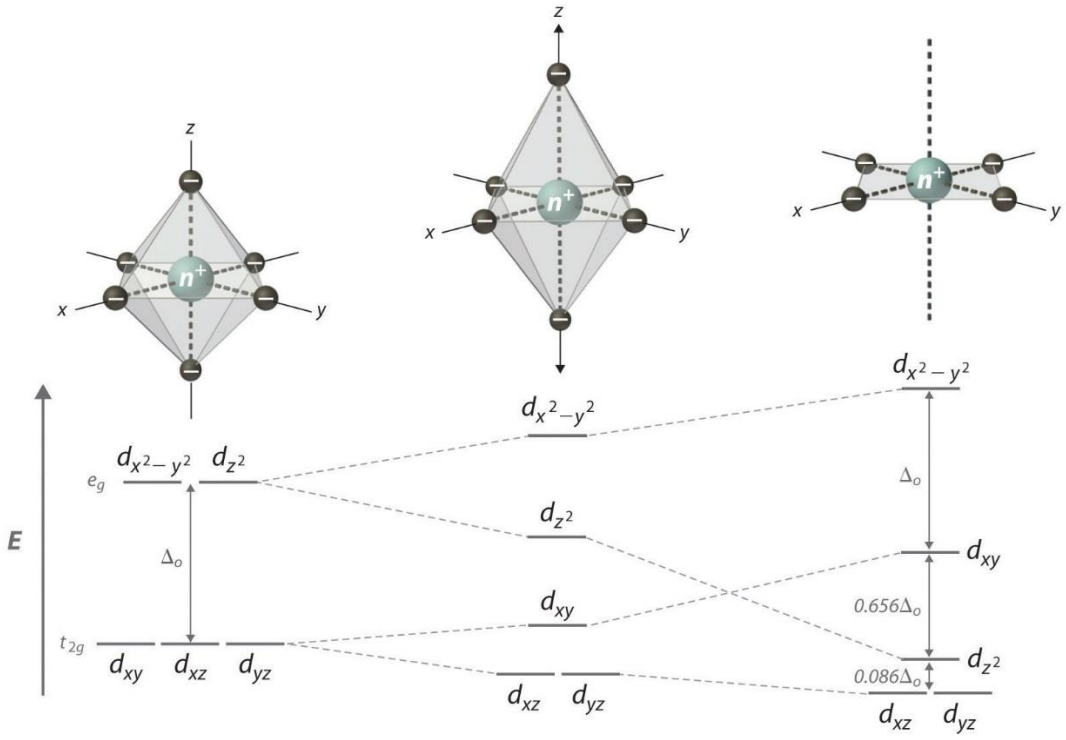

Figure 1-5. Orbital splitting diagram for different metal complex geometry. Adapted from http://chemwiki.ucdavis.edu/Inorganic_Chemistry/Crystal_Field_Theory/Introduction_to_Crystal_Field_Theory/Non-octahedral_Complexes.

In order to derive the d-orbital splitting diagram of the square planar geometry from that of the octahedral geometry, the axial ligands need to be removed. Once the axial ligands start moving away from the metal center (Figure 1-5, middle), the d_{z^2} orbital is stabilized because it points directly towards the axial ligand and $d_{x^2-y^2}$ is destabilized. Upon complete removal of the axial ligands, the z component containing orbitals are all stabilized compared to the x and y component orbitals, as there are no ligands in the z direction (Figure 1-5, right). Although this orbital splitting diagram is typical for square planar geometry, it is subject to change in different ligand geometries.[53] As the Pt(II) ion has a d^8 electronic configuration, the d_{xy} orbital behaves

as the HOMO and $d_{x^2-y^2}$ acts as LUMO. The absorption of light triggers the transition from d_{xy} to $d_{x^2-y^2}$ and, due to the strong antibonding nature of the LUMO, the molecule undergoes significant distortion in the excited state leading to elongation of the square planar Pt-L bonds. This can be envisaged by a simple diagram where d-d excited state potential energy surface is significantly displaced compared to the ground state potential energy surface (Figure 1-6). In this circumstance, the presence of an isoenergetic crossing point between the ground state and excited state leads to a radiationless transition of the excited state via internal conversion (IC) or inter-system crossing (ISC). Other than that, the Laporte-forbidden nature of the d-d transition makes the radiative rate constant (k_r) significantly smaller compared to the non-radiative rate (k_{nr}). This is the reason for the non-emissive nature of platinum complexes with simple inorganic ligands (e.g., $Pt(PBu_3)_2Cl_2$).

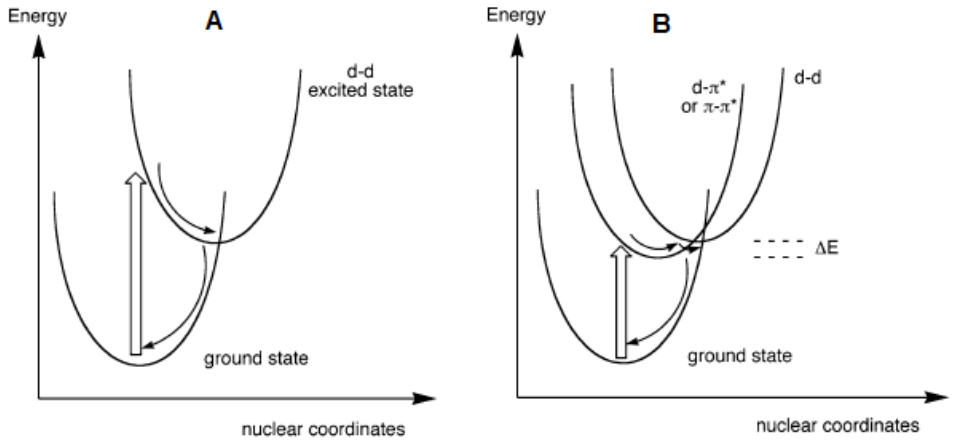

Figure 1-6. Potential energy surface of square planar Pt(II) complexes, (A) when only d-d transition is involved and (B) in presence of other ligands.[53]

However, when π-conjugated ligands are introduced around the Pt(II) ligand environment, the π-π* excited state comes into the play. Although, most of the time π-π* excited states are situated higher in energy compared to the non-emissive d-d

excited states, if the energy gap ΔE is small and thermally accessible, there is probability of a non-radiative transition. A useful strategy to increase ΔE or increase the energy of non-emissive d-d excited state above any emissive excited state is use of a strong ligand field.

Orbital interaction analysis for platinum acetylide

In order to understand the nature of the frontier molecular orbitals involved in π-conjugated organometallic systems, Frapper et al. performed a detailed analysis of the molecular orbitals of the transition metal acetylide polymers.[54] The orbital interaction for the platinum acetylide complex was shown in C_{2v} symmetry by fragmentation analysis for disubstituted metal center. Figure 1-7 depicts the orbital interaction diagram of Pt(II) and two phosphine ligands.

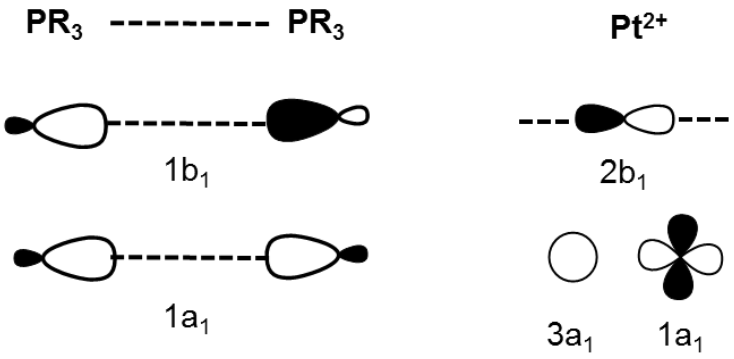

Figure 1-7. Interaction diagram of platinum orbitals with phosphine lone pairs.

Two phosphorus lone pairs can interact with the Pt(II) orbitals (6s + $5d_{x^2-y^2}$, $6p_x$) in a_1 and b_1 symmetry to form σ-interaction. In presence of acetylide ligands, the σ_{M-C} bonding consists of the stabilizing interaction between metal $5d_{z^2}$ and $6p_z$ orbitals with $1a_1$ and $2a_1$ orbitals of acetylide ligands (Figure 1-8).

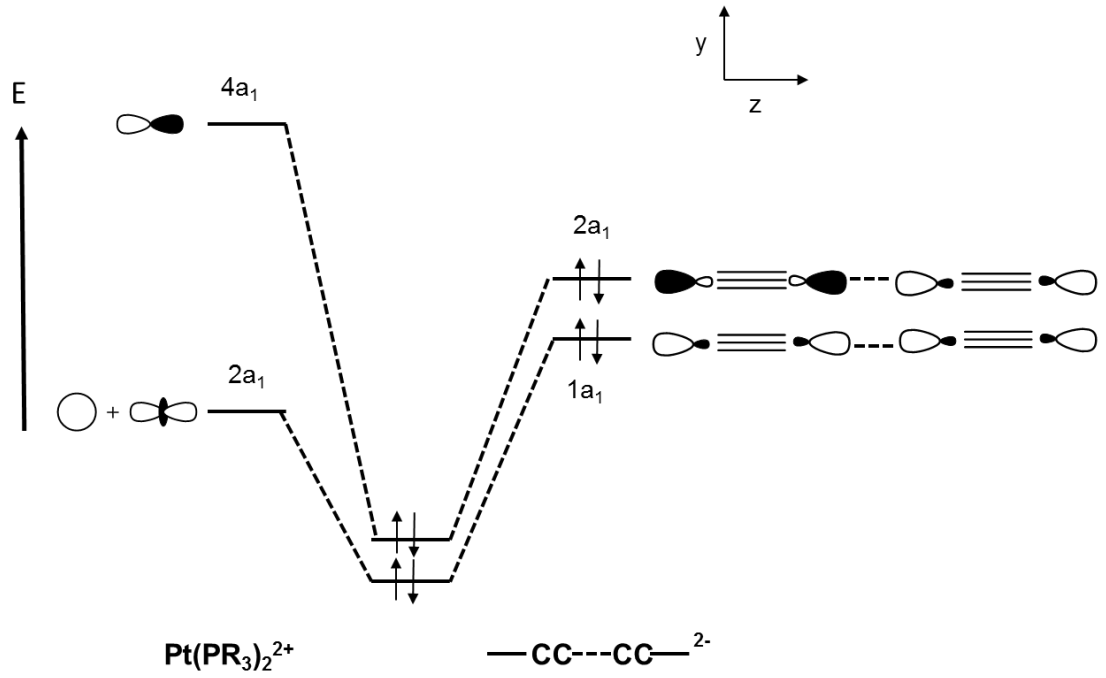

Figure 1-8. Interaction diagram between platinum phosphine fragment and acetylide fragments for σ_{M-C} bonding.

The nature of the highest occupied molecular orbital (HOMO) and lowest occupied molecular orbital (LUMO) is of foremost important for platinum acetylide chromophores and can be estimated by considering the interaction between metal d-orbitals and acetylide orbitals in π-symmetry. Although both the π molecular orbitals from two acetylide ligands are isoenergetic in vacuum, they will split in energy in presence of metal ion to give $1b_1$ and $1b_2$. Among these two, $1b_2$ is higher in energy compared to $1b_1$ because of extensive delocalization for the later. The filled d_{yz} orbital of Pt(II) interacts with $1b_2$ from acetylide resulting a π_{M-C} bonding and an antibonding interaction where the later becomes the HOMO (Figure 1-9A). The main interaction in these orbitals is four electron and destabilizing. It is important to note here, unlike other transition metal complexes, the π* orbitals are higher in energy compared to filled metal orbitals resulting weak back-donation.

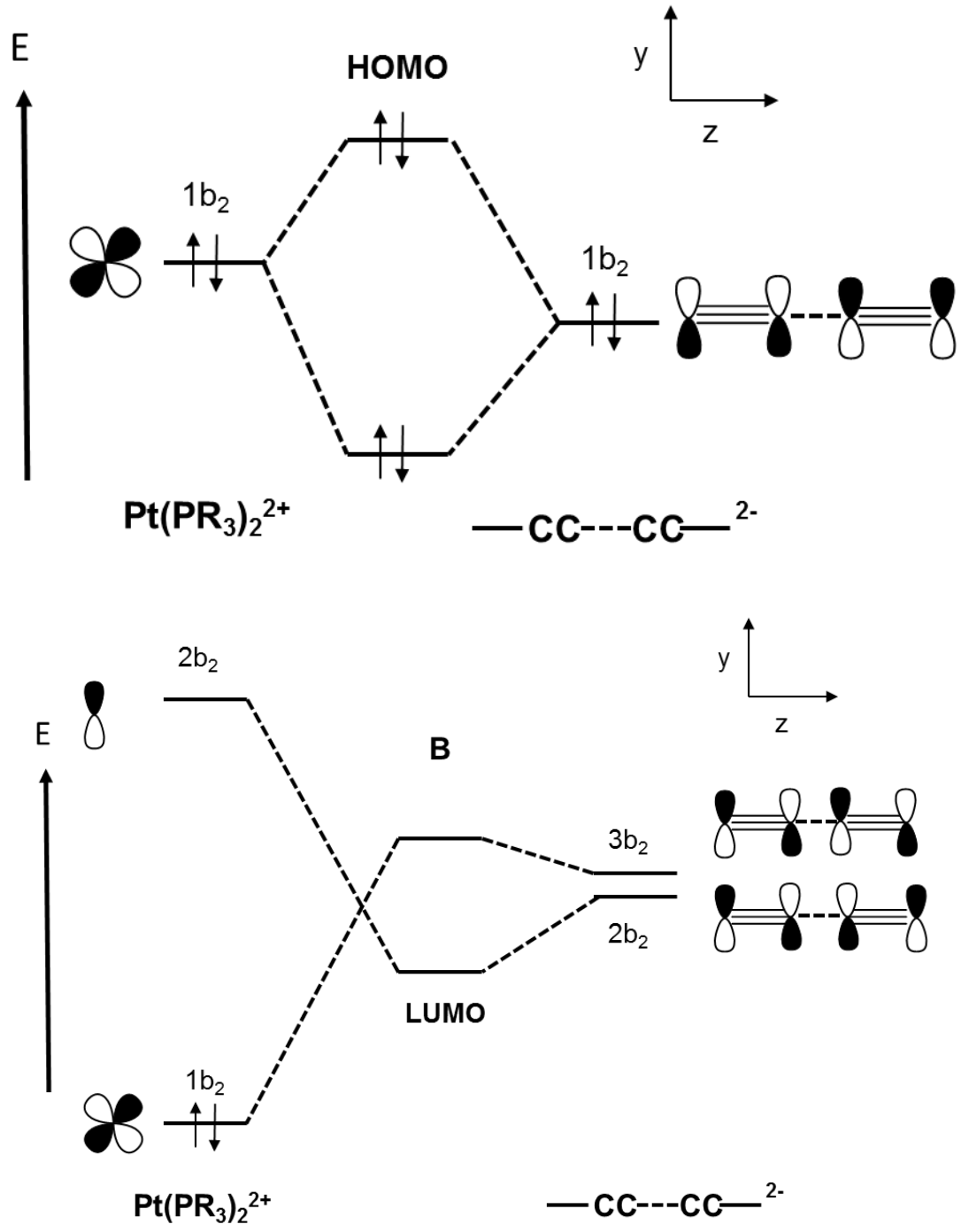

Figure 1-9. Interaction diagram between platinum phosphine and acetylide fragments to form (A) HOMO and (B) LUMO for platinum acetylide system.

Similar to π orbitals of acetylide system, π* orbitals also split in energy ($2b_2$ and $3b_2$), interacting with $6p_y$ through bonding interaction and with $5d_{yz}$ through antibonding interaction. The bonding interaction forms LUMO of the platinum acetylide system (Figure 1-9B).

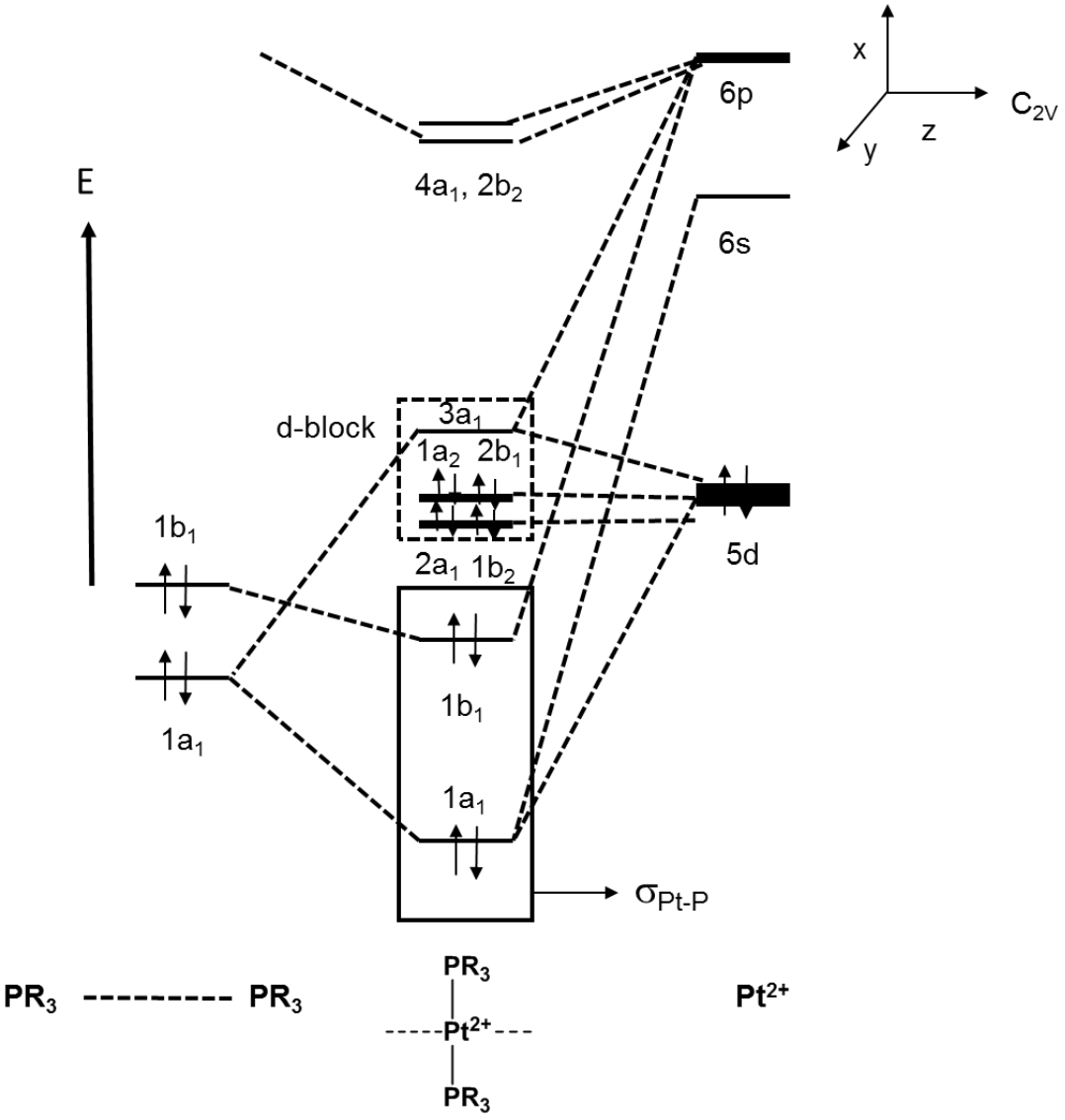

Figure 1-10. Interaction diagram of $Pt(PR_3)^{2+}$. The left hand side shows the lone pairs of phosphine orbitals and the right hand side shows d-orbitals from Pt^{2+}.

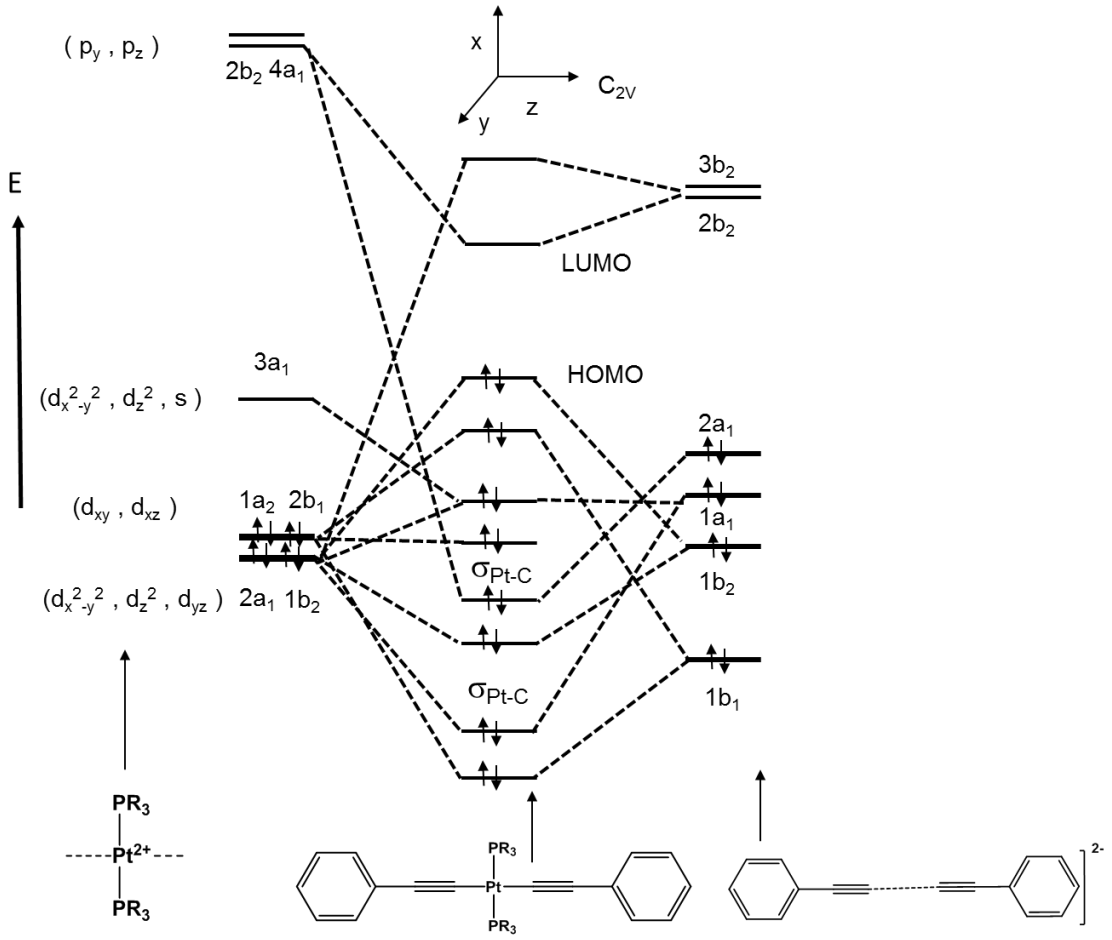

Figure 1-11. The overall interaction diagram for $Pt(Ph{\equiv}C)_2(PR_3)_2$ formed by interaction between $Pt(PR_3)_2$ and acetylide units.

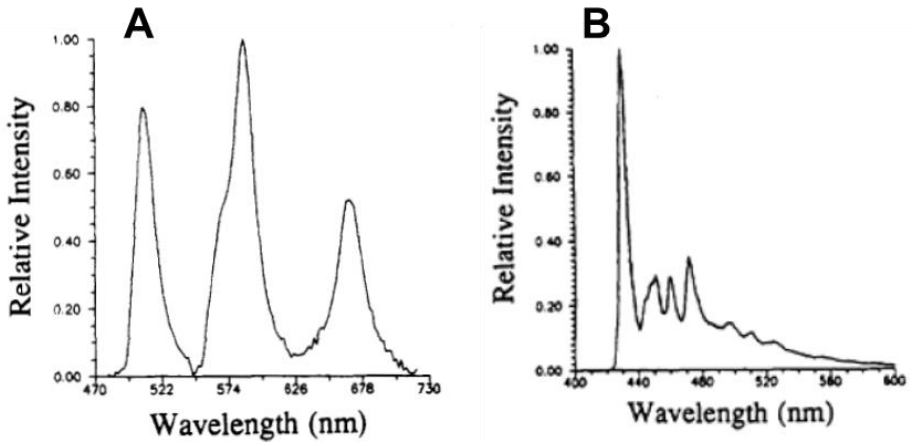

Figure 1-12. The phosphorescence spectra of A) $Pt(C{\equiv}CH)_2(PEt_3)_2$ at room temperature and B)$Pt(C{\equiv}CPh)_2(PEt_3)_2$ at 77K (Figure is adapted with permission from ACS).[55]

Demas et al. first explored the photophysics of platinum acetylide systems with respect to ligand field strength.[55] The platinum complexes *cis*- and *trans*-$Pt(PEt_3)_2Cl_2$ are nonemissive in solution both at room temperature and at 77K, due to the presence of weak-field chloride ligands, which make the d-d excited state the lowest excited state. However, when one of the chloride ligands is substituted by a strong field ligand hydride, the resulting *trans*-$Pt(PEt_3)_2ClH$ shows phosphorescence at 77K. The transition for this emission is attributed to $^3a_{2u}(p_z) \rightarrow {}^1a_{1g}(d_z^2)$, with very little ligand contribution. The replacement of chloride ligands by strong field acetylide ligands leads to $Pt(C{\equiv}CH)_2(PEt_3)_2$ and $Pt(C{\equiv}CPh)_2(PEt_3)_2$, both of which exhibit vibronically structured phosphorescence at low temperature and featureless emission at room temperature. For the acetylide complexes, the transitions are defined as $^1a_{1g}$ $(d_z^2) \rightarrow {}^1a_{2u}$ (π_L).

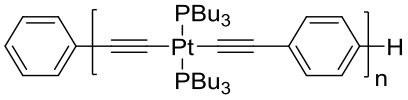

n=1-5, 7

Figure 1-13. The structure of the synthesized platinum acetylide complexes.[52]

However, depending on the conjugation length and structure of the ligand, the metal orbital contribution to the HOMO and LUMO changes. In 2002, Schanze and coworkers reported a series of platinum complexes with increased conjugation length with up to seven Pt centers (Figure 1-13). The absorption spectra dominate the region between 250 nm and 400 nm (Figure 1-14A). With increase in conjugation, the ground state absorption and fluorescence shift to lower energy up to n = 5 due to delocalization of the singlet excited state mediated by the platinum center but levels off between n = 5 and 7. The estimated delocalization length for singlet excited state was n ~6. However,

surprisingly, it was found that the phosphorescence maxima remained almost unchanged with increase in conjugation, and this was attributed to the localization of the triplet excited state with one or two Pt units. The non-radiative rate constant from the triplet excited state was also found to decrease by ~20% with increase in chain length up to n = 7. The S_1-T_1 splitting energy was found in between 0.92 eV and 0.77 eV.

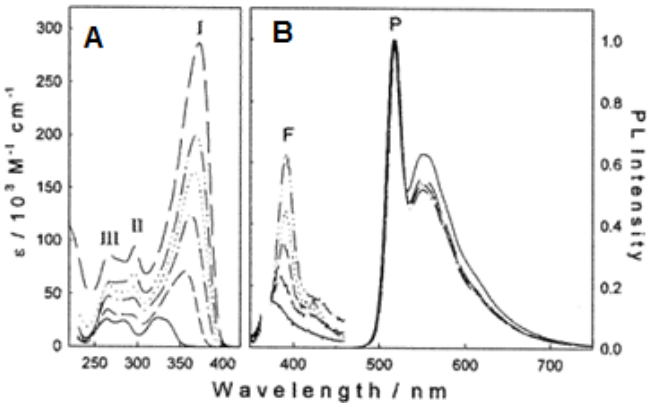

Figure 1-14. The (A) Ground state absorption spectra and (B) emission spectra of the metal complexes (Figure 1-13), F = Fluorescence and P = Phosphorescence.[52]

In another study, Wilson and coworkers synthesized a series of platinum acetylide polymers with varying spacers to investigate the singlet excited state (S_1) and triplet excited (T_1) energy gap (Figure1-15). As expected, with decreasing bandgap in the polymer, the absorption and fluorescence were also shifted towards lower energy. However, with decreasing bandgap, the intensity of phosphorescence was decreased and nonradiative decay was increased, as predicted by the energy gap law. The bandgap of the polymers had no influence on S_1-T_1 energy gap, which remained constant at ~0.7 eV.[56]

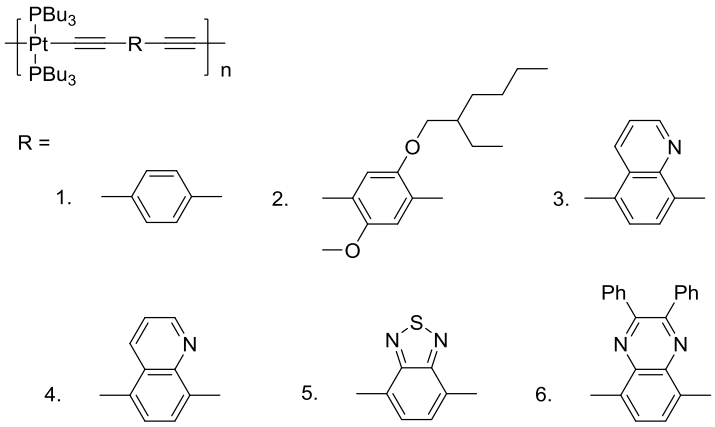

Figure 1-15. Structures of the synthesized platinum acetylide polymers by Wilson et al.[56] (Adapted with permission from AIP).

In order to understand the conductivity in platinum acetylide complexes, Schull and coworkers synthesized a series of complexes with varying phosphine ligands. Although, the conductivity was shown to increase compared to that of the purely organic molecular motif, it remained same for different phosphine ligands in platinum acetylide complexes.[57] Marder and coworkers investigated the electronic coupling through a alkyne-Pt-alkyne bridge in a mixed valence complex. They incorporated two redox active triphenylamine moieties via the platinum center and concluded that the electronic coupling was slightly reduced compared to an all organic alkyne-benzene-alkyne bridge.[58]

Platinum acetylide chromophores for non-linear absorption

Platinum acetylide chromophores are advantageous for nonlinear absorption due to the availability of the large excited state absorption coefficient of $T_1 \rightarrow T_n$, which enhances the overall nonlinear absorption by combination of both 2PA and ESA. One of the first chromophores investigated for nonlinear optical property was bis-((4-(phenylethynyl)phenyl)ethynyl)bis-(tributylphosphine) platinum(II), abbreviated as PE2 (Figure 1-16). It was shown to have nonlinear optical properties via both 2PA and

excited state absorption via $T_1 \rightarrow T_n$. The effective 2PA cross section for this complex was calculated ~235 GM at 595 nm via the nonlinear transmission method. However, the intrinsic 2PA cross section of the platinum PE2 complex was found to be ~ 7GM at 720 nm using femtosecond laser pulses.[59]

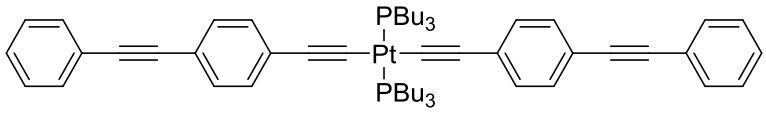

Figure 1-16. Structure of trans-PE2.

In an effort to understand the effect of heterocyclic rings on platinum acetylide chromophores and nonlinear optical properties, the (thienylene phenylene) derivatives (Figure 1-17) were synthesized. The thiophene rings were placed close to the platinum center and also at the terminal positions. The 2PA coefficients were measured with different pulse repetition frequencies. It was observed that with increasing power, 2PA cross sections were increased due to the contribution by excited state absorption from the triplet excited state. The complex with terminal thienyl moieties had lower 2PA cross section value (17GM at 1 MHz) compared to the complex with the thienyl moiety connected to the platinum center.

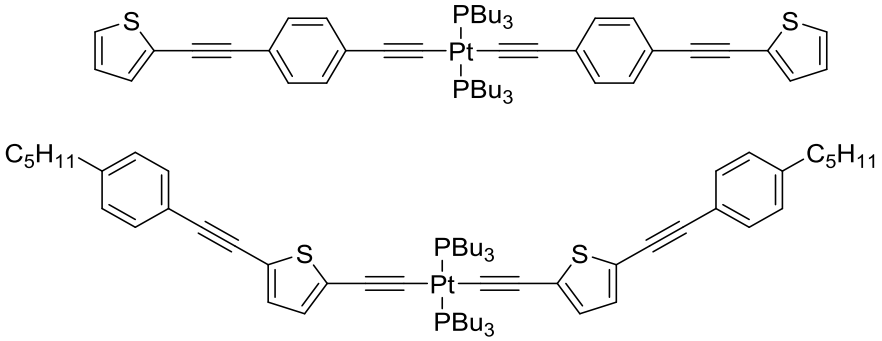

Figure 1-17. Structures of the platinum complexes reported by Glimsdal et al.[59]

In 2007, Rogers and coworkers synthesized a series of platinum acetylide complexes in which the central platinum center was connected to two 2PA chromophores (Figure 1-18). The complexes were synthesized with the general design D-π-D and A-π-A (D= donor and A= Acceptor). In general, all the metal complex exhibit intense ground state absorption from 300 - 400 nm and strong phosphorescence between 500 - 800 nm. The nanosecond transient absorption spectra proved the presence of triplet-triplet absorption from 500 - 950 nm with a λ_{max} of 650 nm. The 2PA cross-section was measured via two photon excited fluorescence method at 720 nm, and the values were found in between 60 -370 GM. The 2PA for these complexes consists of two bands, one of them coincides with $\lambda_{ex} = 2\lambda_{1PA}$ and the other was blue shifted with respect to $\lambda_{ex} = 2\lambda_{1PA}$. It is believed that the coincidence of the band with $2\lambda_{1PA}$ is due to the presence of a non-centrosymmetric conformer in the solution. However, the blue-shifted peak was attributed to the centrosymmetric nature of the platinum acetylide chromophores, which makes the gerade to gerade transition allowed under 2PA conditions.

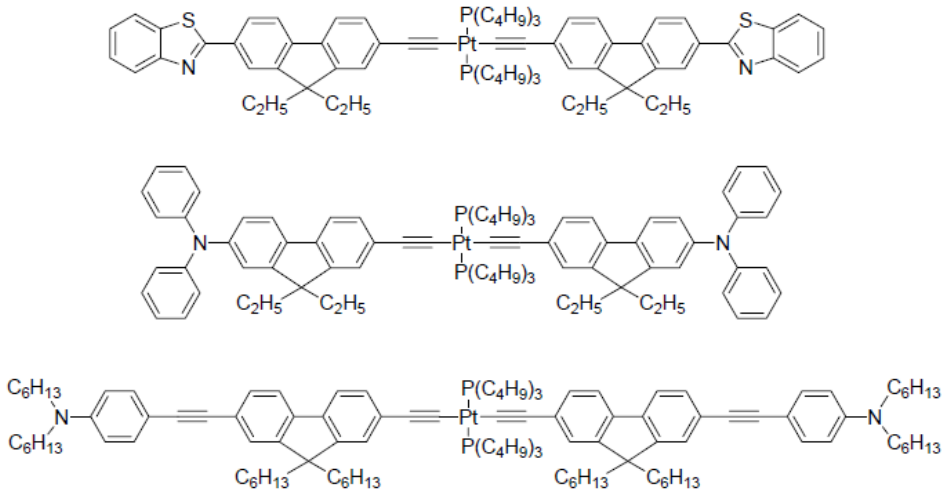

Figure 1-18. Structures of the platinum acetylide complexes reported by Rogers et al.[18]

Kim and coworkers have synthesized a series of platinum acetylide complexes with two photon-active chromophore 4-(diphenylamino)fluorene (DPAF) units and connected with different central aromatic core via platinum center (Figure 1-18). The triplet-triplet absorption spectrum was dependent on the central aromatic core being lower in energy compared to DPAF. The 2PA cross section value for the complexes was found to be 88 - 230 GM with femtosecond pulse. This range is significantly higher compared to the DPAF unit alone (σ_2= 44 GM). The cross sectional value was almost independent of the nature of the central aromatic core, largely due to the "shielding effect" of the platinum center on the dipole moment of DPAF unit towards central aromatic unit.

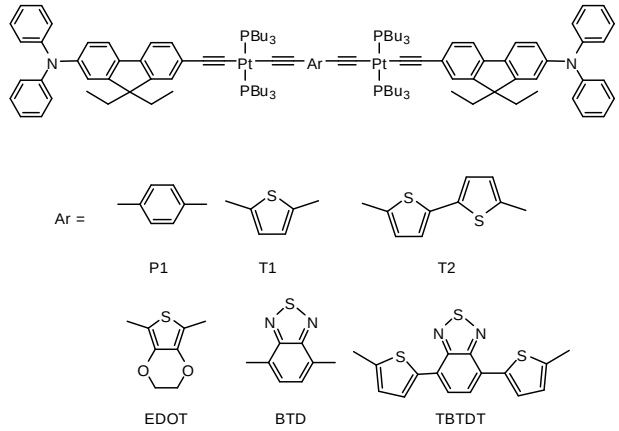

Figure 1-19. Structures of platinum acetylides reported by Kim et al.[60]

Dubinina et al. synthesized a series of cross conjugated *p*-(phenylene vinylene) containing platinum acetylide chromophores. The complexes were found to exhibit a strong 2PA with σ_2 value up to 10000 GM via both NLT and the two photon excited fluorescence method.[19] In order to increase the processibility of these materials, they were incorporated into poly(methyl methacrylate) (PMMA) monoliths and 2 PA cross section value of the monoliths were almost same as those in solution.[61]

Organometallic Polymers for Photovoltaic Devices

With increasing demand for energy and depletion of non-renewable energy resources, it is imperative to investigate alternative renewable energy resources, in particular sunlight. Solar energy is one of the most promising resources because of its abundance and non-polluting nature. One way to convert solar light into electricity is via photovoltaic devices or solar cells which can be categorized as inorganic or silicon (Si) solar cells and organic solar cells. The first practical Si based photovoltaic device was reported by Chapin et al at Bell laboratories in 1954 with power conversion efficiency of 6%. After that, there were several modifications to increase absorptions of the solar spectrum, such as double junction and triple junction solar cells, and hybrid materials were used to increase the solution processibility. However, at this time, a major disadvantage of inorganic solar cells remains their production costs.

Organic semiconducting polymers have gained popularity over the past few years as an alternative renewable energy resources, because of their easy solution processibility, low production cost and inherent ability to fine tune the structural parameters via synthetic chemistry. The first report of an organic solar cell was by Tang at Eastman Kodak research laboratories.[62] In that seminal paper, the effect of using two organic layers instead of one was shown for the first time using copper phthalocyanine as donor and a perylene tetracarboxylic acid derivative as acceptor. The power conversion efficiency achieved using this protocol was ~0.96%. Since then, there have been many advancements in bilayer devices using polymer donor-polymer acceptor,[63] polymer donor-PCBM acceptor[64] and several others. Organic solar cells are also called excitonic solar cells,[4] and the working principle is demonstrated below in Figure 1-20.

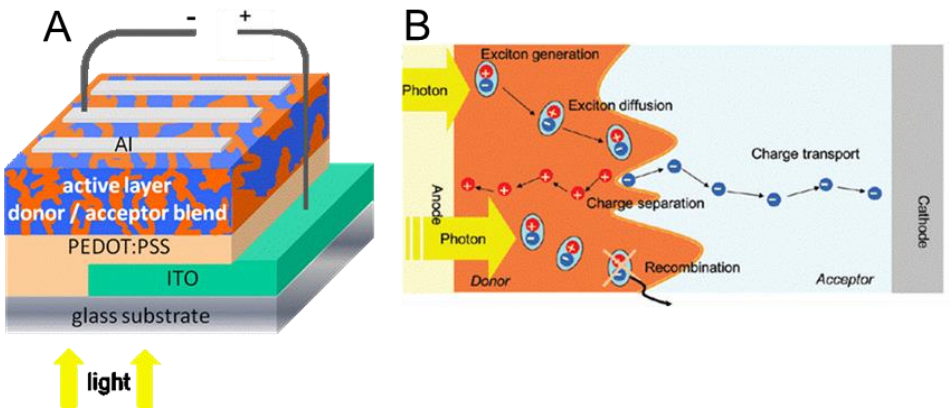

Figure 1-20. (A) The basic architecture of a bulk heterojunction solar cell, (B) the working principle of bulk heterojunction solar cell (right), (adapted with permission from ACS).[65]

Upon irradiation with light, an exciton, a Coloumbically coupled electron and hole pair, is generated in the active layer. Then the exciton diffuses to the donor-acceptor interface. The exciton diffusion length generally depends on the lifetime of the exciton as well as on the diffusivity ($L = (D\tau)^{1/2}$). In a bulk heterojunction device, the typical exciton diffusion length is in the order of 15-20 nm. In order to generate free charge carriers, the excitons need to reach the donor-acceptor interface before they recombine and decay to the ground state. For a bilayer device, it is important to have almost the same phase lengths for the donor or acceptor, preferably equal to the diffusion length of the exciton to prevent charge recombination. The exciton then dissociates into free charge carriers because of the difference in electron affinity between donor and acceptor. The exciton binding energies in organic devices is higher (0.2-0.5 eV) compared to inorganic excitons (<0.03 eV).[66,67] Due to such low binding energy, excitons can be dissociated into free charge carriers at room temperature. The high dielectric constant of the inorganic medium is mainly responsible for the low exciton binding energy in these devices. For organic devices, the low dielectric constant of the

medium makes exciton dissociation unfavorable and this is the reason to incorporate donor-acceptor interface in the device to create additional electric field in the medium. Finally, to generate the photocurrent the free charge carriers travel to their respective electrodes under the driving force generated by the offset of different work function of the electrodes and generate photocurrent.

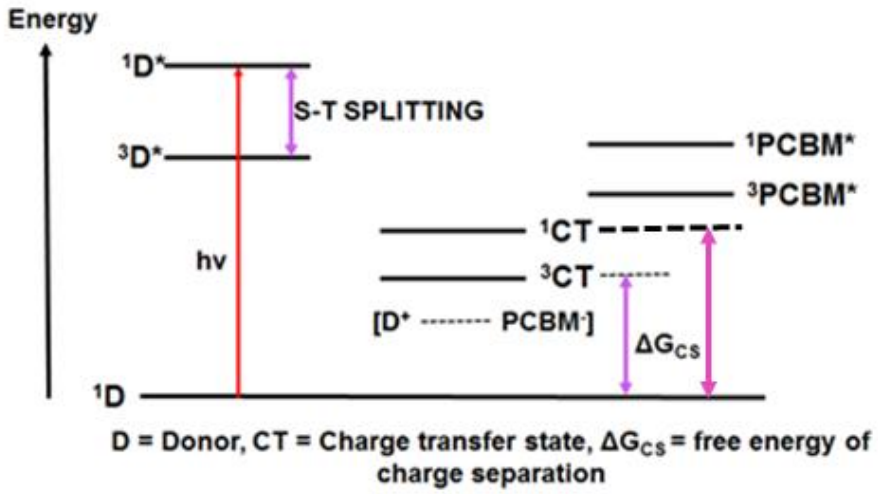

Figure 1-21. Energetics of photoinduced electron transfer (PET).

As the focus of this research is based on organometallic materials, the discussion here is limited to π-conjugated organometallic materials for photovoltaics. Heavy atom containing π-conjugated materials have several advantages compared to inorganic photovoltaics. First, due to the longer lifetime of the triplet excited state, the exciton can diffuse farther to reach the donor-acceptor interface compared a singlet exciton, thus preventing recombination. Second, after charge separation takes place at the donor-acceptor interface, the geminate ion-radical pair still remains spin correlated and if the excitons produced are in triplet excited state, charge recombination can be prohibited due to the electrons spin.[68] Figure 1-21 shows the energetics of photoinduced electron transfer between donor materials and PCBM, which acts as

acceptor in the photovoltaic device. Although, the triplet excitons are preferred for the above mentioned reasons, they have some inherent energetic disadvantages. The driving force for the electron transfer process depends on the difference in energy between the donor and acceptor excited states. Since the triplet exciton is lower in energy compared to singlet exciton (it was shown for most organometallic π-conjugated system, irrespective of the conjugated chromophores ,ΔE_{S-T}~ 0.7 eV [69]), the driving force for electron transfer is higher for singlet excited states, because of their large difference in energy.

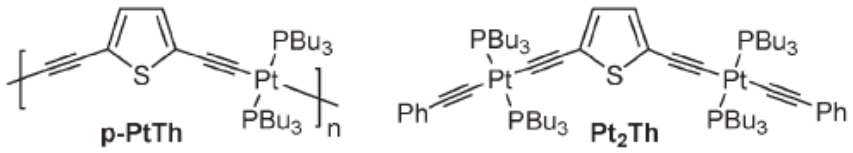

Figure 1-22. The platinum acetylide systems reported by Schanze and coworkers for application in bulk heterojunction solar cells in 2006.

Although the first examples of triplet exciton effects in photovoltaics were reported in bilayer devices using platinum complexes and polymers,[70,71] it was not until 2006 that Schanze and coworkers reported the effect of spin-triplets in bulk-heterojunction solar cells (Figure 1-22). In this work, the active layer was prepared by mixing p-PtTh and PCBM in a 1:4 ratio to obtain a power conversion efficiency of 0.27%. It was shown that the phosphorescence of the polymer at 608 nm was quenched efficiently by PCBM, suggesting facile electron transfer from the triplet excited state of the polymer to PCBM. The anion radical of $PCBM^{-\cdot}$ was also observed by laser flash photolysis at 1050 nm. Yang Yang and coworkers studied the effect of iridium complex doping in a poly(fluorene) - containing organic-inorganic hybrid solar cell with

colloidal CdSe as the acceptor. Efficient triplet exciton generation was observed on the polymer host, followed by an increase in photocurrent.[72]

Holdcroft and his group synthesized an iridium-containing polyfluorene and comparative photophysical and photovoltaic properties to the nonmetallated polymer (Figure 1-23). The phosphorescence of the iridium-containing polymer was efficiently quenched by PCBM, suggesting that electron transfer occurs from the triplet excited state of the polymer to PCBM. However, the frontier orbitals (HOMO and LUMO) remained almost unaffected by metal coordination. The iridium-containing polymer exhibited tenfold increase in photovoltaic efficiency, as well as in external quantum efficiency, compared to the nonmetallated polymer. Although the power conversion efficiency was lower than that of conventional organic solar cells, conceptually this work demonstrated the advantages of triplet exciton compared to singlet excitons.[73]

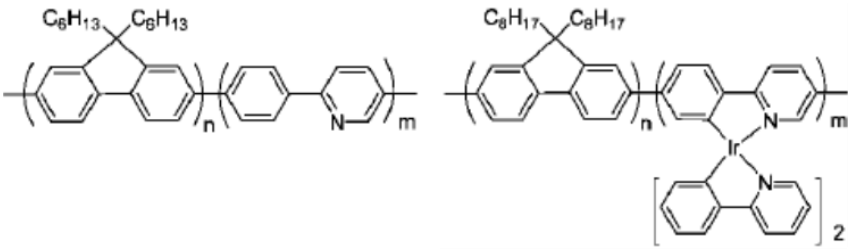

Figure 1-23. Organometallic polymers developed by Holdcroft and his group for bulk heterojunction solar cells (adapted with permission from ACS).[73]

There is a strong relation between the structures of the π-conjugated chromophore and photoinduced electron transfer mechanism. For example, in 2009 Mei et al synthesized a series of platinum acetylide complexes and polymers based on donor-acceptor chromophores to harvest most of the solar spectrum.[25] Nanosecond transient absorption spectroscopy of the polymer:PCBM solution mixture showed no signal from the radical anion of PCBM. However, surprisingly, the fluorescence from the

polymer was quenched significantly with PCBM as a quencher. It was found that the energy of the triplet excited state is lower than the energy of the charge separated state making PET energetically unfavorable from triplet excited state (Figure 1-24).

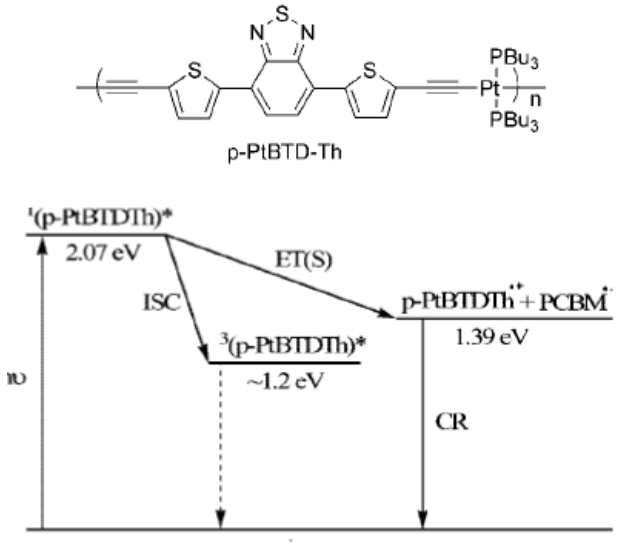

Figure 1-24. Platinum acetylide polymer and energetics reported by Mei et al.in 2010 (adapted with permission from ACS).[25]

Frechet and coworkers synthesized platinum acetylide complexes with varying numbers of terminal thienyl rings based on a similar donor-acceptor chromophore.[74] A strong correlation between the number of terminal thiophene rings and the photocurrent was observed, due to increased light absorption as well as self-assembly of the thiophene rings. A power conversion efficiency of 3% was achieved with these small molecules as donor and $PC_{71}BM$ as acceptor.[74] The platinum 5d orbitals (d_{xy} and d_{xz}) interacted with the alkyne unit of organic π-conjugated system to increase the conjugation.[75] However, due to size and energy mismatch between the 5d and 2p orbitals, the overlap was not strong enough to increase the conjugation length efficiently in a polymer backbone. Clem et al. synthesized a family of π-conjugated polymers with an alternative organometallic architecture, in which a cyclometallated platinum motif

was incorporated in a polymer backbone (Figure 1-25). As the platinum was present at the peripheral position instead of in the main conjugated chain, the conjugation length was significantly increased in this approach. Efficient population of triplet excited state was observed by intersystem crossing mediated by platinum center for both the polymers and verified by singlet oxygen sensitization studies. The thiophene containing polymer Pt-T1 exhibits efficiency up to 1.3% with polymer:PCBM ratio of 1:4.

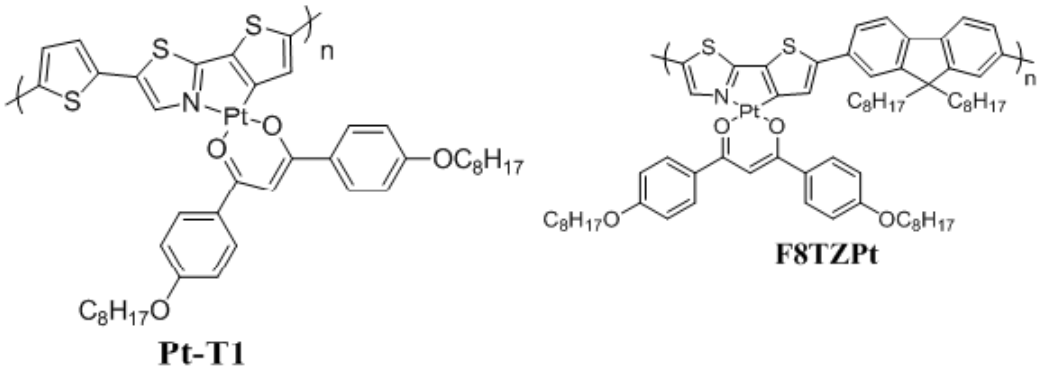

Figure 1-25. Cyclometallated platinum containing polymers reported by Clem et al.

Following a similar line of study, Cheng and coworkers synthesized cyclometallated platinum containing indacenodithiophene polymers for photovoltaic devices.[76] As observed before, electron transfer from the polymer to PCBM took place from a singlet excited state instead of the triplet excited state because of the energetic preference. The highest efficiency observed in this case was 2.9%. Other than platinum, some other metals have been reported recently for application in bulk heterojunction solar cells. Kim and coworkers utilized a multifunctional iridium complex as an energy donor and poly-3-hexylthiophene as energy acceptor (triplet-singlet energy transfer) to improve the photovoltaic device efficiency (Figure 1-26).[77] Polyethylene oxide (PEO) and PCBM were used as an ion channel and electron acceptor. The iridium complex played a multifunctional role here: 1) it acted as an energy donor to the polymer; 2) it

stabilized the exciton; and 3) the sodium ion increases the mobility of free charge carriers to their respective electrodes. Using this approach, the efficiency of the photovoltaic devices increased from 1.6% for P3HT only to 3.4% for 1:3 ratio of pqIrpicNa: PEO.

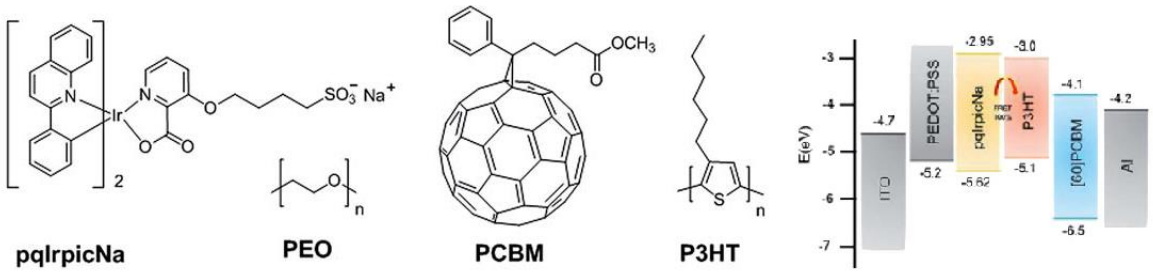

Figure 1-26. Structures of the components used by Kim and coworkers and energy diagram.[77]

Kotowski and coworkers synthesized a ruthenium acetylide complex (1-1) based on a similar TBT (Thienyl-benzothiadiazole-thienyl) chromophore that was reported for platinum acetylide polymer and a small molecule.[78] The cyclic voltammetry study showed that the oxidation potential for the ruthenium acetylide system shifted to 300 mV less positive value compared to the platinum acetylide system due to more electron rich nature of Ru^{II} than Pt^{II}. This fact also produced to more red-shifted absorption in the ruthenium acetylide system. Although, the photovoltaic efficiency observed for this system was quite low, this was the first report that used ruthenium acetylide for bulk heterojunction solar cells. Iridium-containing small molecules have also been used as donor materials for bulk heterjunction solar cells (1-2 in Figure 1-27).[79] Efficient electron transfer from the triplet excited state of the iridium complexes to $PC_{71}BM$ were demonstrated and a power conversion efficiency of 2% was achieved. Cobalt complex 1-3 (Figure 1-27) was synthesized with four arms of terthiophene chains for bulk

heterojunction photovoltaics.[80] It was observed that the ^{3}MLCT state of the complex significantly contributed to the external quantum efficiency of this device and possibly triplet excitons increased the efficiency up to 2.12%.

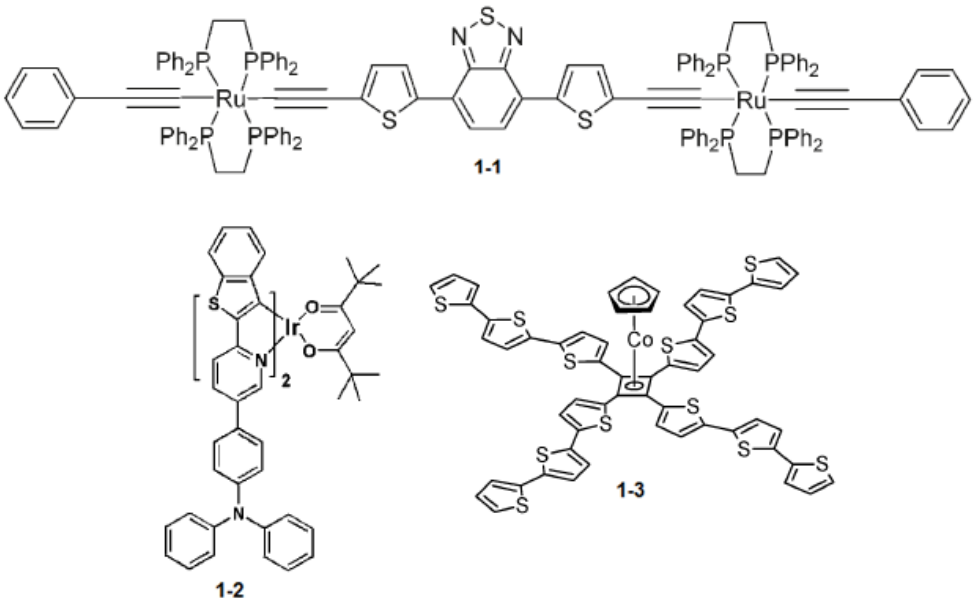

Figure 1-27. Ruthenium-, iridium- and cobalt-containing pi-conjugated small molecules for bulk heterojunction solar cells.[78-80]

Che and coworkers recently reported a series of gold(III) corroles (Figure 1-28) for applications in bulk-heterojunction solar cells by both vacuum deposition and solution processing techniques.[81] All the metal complexes showed the presence of a triplet excited state with an average lifetime of ~25 μs, which was probed by both phosphorescence emission spectroscopy and nanosecond transient absorption spectroscopy. While these materials were used as donor in photovoltaic devices with $PC_{71}BM$ as acceptor, vacuum deposited devices gave efficiency up to 3.0% and solution processed devices showed efficiency of 6%. However, in the solution processed technique, the gold complex was used as a sensitizer to probe the triplet excited state of a donor polymer.

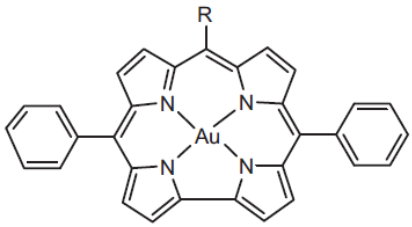

R = C_6H_5; **Au-C1**
R = 4-CF_3-C_6H_4; **Au-C2**
R = C_6F_5; **Au-C3**

Figure 1-28. Structures of the gold complexes reported by Che and coworkers for photovoltaic applications (adapted with permission from John Wiley and Sons).[81]

Recently Huang and coworkers have synthesized a π-conjugated polymer with varying amounts of iridium complex in the main chain (x = 0, 0.01, 0.025, and 0.05%) (Figure 1-29).[82] By increasing the iridium concentration from 0 to 2.5%, the device efficiency increased up to 45%, but with 5% iridium content the efficiency of the device droped. Although a triplet excited state was observed in these polymers, it was believed that the increased efficiency with low iridium content was due to reduction of the back electron transfer process from ^{3}CT to ^{1}T of the polymer. The low PCE with high iridium content was attributed to the low charge carrier mobility of the random iridium complex in the polymer, which decreased the short circuit current.

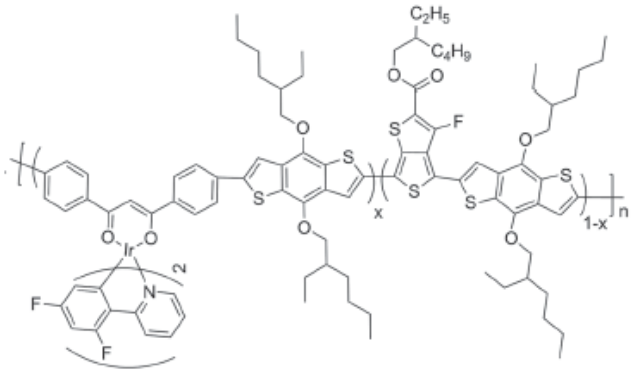

Figure 1-29. Cyclometallated iridium doped conjugated polymer for bulk heterojunction solar cells by Huang and coworkers.[82]

Overview of the Present Study

Heavy atom containing organometallic π-conjugated materials have emerged as important candidates for optoelectronic devices. However, it is obvious that further development of molecular systems in conjunction with increased understainding of their fundamental optical properties is needed for advancement of this field. To help reach this goal, this dissertation is focused on the synthesis and optoelectronic properties of π-conjugated organometallic polymers/small molecules for non-linear optical properties and bulk-heterojunction solar cells.

The second chapter describes research of the photophysics and non-linear optical properties of carbazole-containing π-conjugated oligomers of the type ET-Cbz-TE (E = ethynylene, T = 2,5-thienylene, Cbz = 3,6-carbazole). A detailed investigation is carried out on a series of oligomers that features the Au(I) or Pt(II) acetylide "end groups", as well as a Pt(II)-acetylide linked polymer (CBZ-Au-1 and CBZPt-1, CBZ-Poly-Pt). All of them exhibits weak fluorescence at room temperature. Strong phosphorescence was observed from the platinum complex and polymer compared to the gold complex suggesting efficient spin-orbit coupling for the platinum complex. The triplet excited state was also probed by nanosecond transient absorption spectroscopy. However, no direct evidence of difference in transition metals to 2PA is observed between these two metal chromophores, as both the metal complexes and polymer exhibits 2PA cross section value of 10.- 100 GM.

To better understand the effects of Au(I) and Pt(II) in two photon absorption led to the second project, and discussed in chapter 3. Here, the donor-acceptor ligand (TBT) was end-functionalized with gold(I) phosphine acetylide and platinum(II) phosphine acetylide "auxochromes" (TBT-Au-PMe_3, TBT-Au-PPh_3, TBT-Pt-PMe_3 and

TBT-Pt-PBu_3) to investigate the optoelectronic properties as a function of different heavy metals and phosphine ligands. The gold complexes in general show higher fluorescence quantum yields and longer emission lifetimes compared to the platinum complexes. Pronounced solvatochromism in the fluorescence spectra relative to the ground state absorption spectra suggests an enhanced dipole moment in the excited state of the complexes. The platinum complexes have a larger change in dipole moment for the $S_0 \rightarrow S_1$ transition compared to gold complexes. Stronger intensities of the transient absorption spectra, shorter triplet state lifetimes, and higher singlet oxygen quantum yields suggest more efficient intersystem crossing for the Pt(II) complexes compared to the Au(I) complexes. The 2PA cross section for the Au(I) complexes remain almost the same (~ 100 GM) as the TBT-TMS ligand in the degenerate $S_0 \rightarrow S_1$ transition region but increased slightly to 150 GM towards shorter wavelength. Both Pt(II) complexes exhibit significantly enhanced 2PA compared to the ligand and gold complexes in the S_0-S_1 region, reaching 1000-1200 GM around 750 nm. Overall, the results from this work demonstrates the importance of selection of “heavy transition metals” in achieving high 2PA cross section values.

To investigate singlet energy transfer under both 1-photon and 2-photon excitations, in the fourth chapter, a series of polystyrene based atactic polymers were synthesized with varying ratio of organic to platinum containing organometallic π-conjugated chromophores. As a π-conjugated chromophore 4-(diphenylamino)fluorene (DPAF) was used. The polymers were synthesized by reversible addition−fragmentation transfer (RAFT) polymerization and chromophores were grafted by copper catalyzed “click” reaction onto the polymer. The completion of grafting reaction was monitored by

^{1}H NMR spectroscopy. With increase in platinum content, the photoluminescence quantum yield decreases and fluorescence is replaced by strong phosphorescence at 530 nm. Emission lifetime and ultrafast transient absorption spectroscopy shows singlet energy transfer from DPAF to DPAF-Pt. Excitation of the polymers under 2PA condition exhibits upconverted photoluminescence via the “antenna effect,” with emission spectra similar to those for one photon excitation. Ultrafast transient absorption studies suggest that energy transfer is taking place both by exciton hopping and direct quenching of the excited state. Taken together, these materials are promising candidates for optical power limiting materials.

The fifth chapter describes the effect of different metal complex architectures on photophysical and electrochemical properties on a diketopyrrolopyrrole (DPP) containing donor-acceptor based chromophore. Cyclometallated platinum containing thienyl pyridine auxochrome and platinum acetylide were employed on diketopyrrolopyrrole chromophore to synthesize two metal complexes. It was observed, that fluorescence quantum yield decreased dramatically for cyclometallated complex, suggesting efficient triplet population compared to the platinum acetylide system. Cyclometallated system also has large impact on both the frontier orbitals, whereas platinum acetylide only influence the HOMO energy level of DPP.

The sixth chapter describes the synthesis and photophysical properties of DPP metal complexes and polymers modified with a soluble ancillary ligand for application in bulk heterojunction solar cells. It was observed that the solution state photophysics barely changes with change in ancillary ligand. In the polymeric system, the effect of thiophene vs phenyl substitution in cyclometallated motif was studied for photovoltaic

devices. The thiophene containing polymer was found to exhibit PCE as high as 1.77% with $PC_{71}BM$ as acceptor. The fill factor observed for this polymer is the highest known value to date for an organometallic polymer.

Isoindigo is known as a versatile dye molecule for optoelectronic systems. However, to date the triplet excited state photophysics of this dye have not been studied. As described in the seventh chapter, for the first time we have exposed the triplet excited state of isoindigo by incorporating a cyclometallated platinum motif. The preliminary study on the polymeric system in photovoltaic devices gave PCE of 0.2% and further optimization is in progress.

In the final chapter, we describe the design and synthesis of a series of DPP platinum acetylide complexes with varying numbers of solubilizing alkyl chains at the terminal position. Although the solution state photophysics remain the same for all of the complexes, dramatic differences were observed in thin films. The complex with maximum number of alkyl chains forms *H*-aggregates in contrast to the J-aggregates formed by other complexes. Preliminary photovoltaic studies suggest that the complex without any alkyl chain gives the highest efficiency (0.3%) compared to the other molecules.

CHAPTER 2
PHOTOPHYSICS AND NON-LINEAR ABSORPTION OF GOLD(I) AND PLATINUM(II) ACETYLIDE COMPLEXES OF A THIENYL-CARBAZOLE CHROMOPHORE

Background

Since the discovery of two-photon absorption (2PA) by Göppert-Mayer in the 1930s[28] and the first experimental observation of the effect in 1961,[29] there has been significant research in this field, with investigations seeking to understand the factors that control the 2PA cross-section (σ_2) and to harness the effect in diverse applications. Two-photon absorption has a number of applications ranging from ultrafast optical power limiting via non-linear absorption (NLA),[39,83-85] photodynamic therapy,[86] microscopy,[87] and three-dimensional data storage.[88] Although a variety of organic dyes have proven to be efficient 2PA chromophores, heavy-metal containing organometallic chromophores are especially interesting, in particular with respect to applications in frequency and temporal agile non-linear absorption.[89] Among various organometallic complexes, platinum acetylide containing π-conjugated chromophores are attractive for NLA materials because of their "dual mode" non-linear absorption mechanism.[18,60,90,91] This dual mode comprises of ultrafast 2PA to produce the singlet excited state followed by intersystem crossing (ISC) to a long-lifetime triplet state T1 promoted by the heavy atom effect, which can further absorb photons due to a strongly allowed T_1-T_n absorption.[19,49]

Porphyrin[92-95] and phthalocyanine[96-98] metal complexes have been widely investigated with respect to 2PA and long pulse NLA via the dual mode mechanism;

Goswami, S; Wicks, G; Rebane, A; Schanze, K.S., *Dalton. Trans.* **2014,** 43, 17721- Reproduced by permission of The Royal Society of Chemistry (RSC).

however, metal complexes linked to π-conjugated segments that feature the carbazole moiety have not been well explored.[99] Even though the singlet excited state photophysics for carbazole containing oligomers and polymers are well established, the triplet excited state is relatively unexplored. Introduction of a heavy metal such as platinum or gold into the conjugated backbone of carbazole containing oligomers provides insight into the triplet excited state due to the "heavy atom effect" that is elusive in the strictly organic system.[100,101] Most carbazole derivatives find application in OLEDs or bulk heterojunction solar cells as π electron donor materials; however, there are few reports on organometallic carbazole complexes that exhibit non-linear absorption.[99] Zhou et al reported a carbazole platinum acetylide polymer and a model platinum complex substituting 3,6 position of the aromatic ring, as an efficient optical power limiting material at 532 nm.[102] Tao et al reported a naphthalene platinum acetylide substituted carbazole as a two photon absorbing and two photon induced luminescence molecule with a 2PA cross section (σ_2) of 14 GM (λ_{ex} = 740 nm).[103]

In order to gain fundamental insight into the photophysics and non-linear optical properties of carbazole containing π-conjugated oligomers of the general structure ET-Cbz-TE (T = 2,5-thienylene, Cbz = 3,6-carbazole and E = ethynyl), here we report a detailed investigation of a series of complexes that feature Au(I) or Pt(II) acetylide "end groups", as well as a Pt(II)-acetylide linked polymer (CBZ-Au-1 and CBZ-Pt-1, CBZ-Poly-Pt in Chart 1). We were particularly interested in developing NLA chromophores that have high transparency throughout the visible region, and as such the 3,6-substitution pattern on the Cbz was used which gives rise to a relatively large HOMO-LUMO gap[104] and consequently good optical transparency through most of the visible

region. The photophysical properties of the series of complexes and polymer are fully analyzed, including one and two-photon absorption spectra, photoluminescence spectra, triplet-triplet absorption spectra and singlet oxygen sensitization studies. The results clearly suggest that this set of chromophores has the potential to be used in optical power limiting materials, and the results shed light on how the yield of the triplet state depends on the nature of the heavy metal center. Previous studies have examined in some detail the photophysics of π-conjugated oligomers linked to heavy metals, and this work builds on that base of understanding.[105-107]

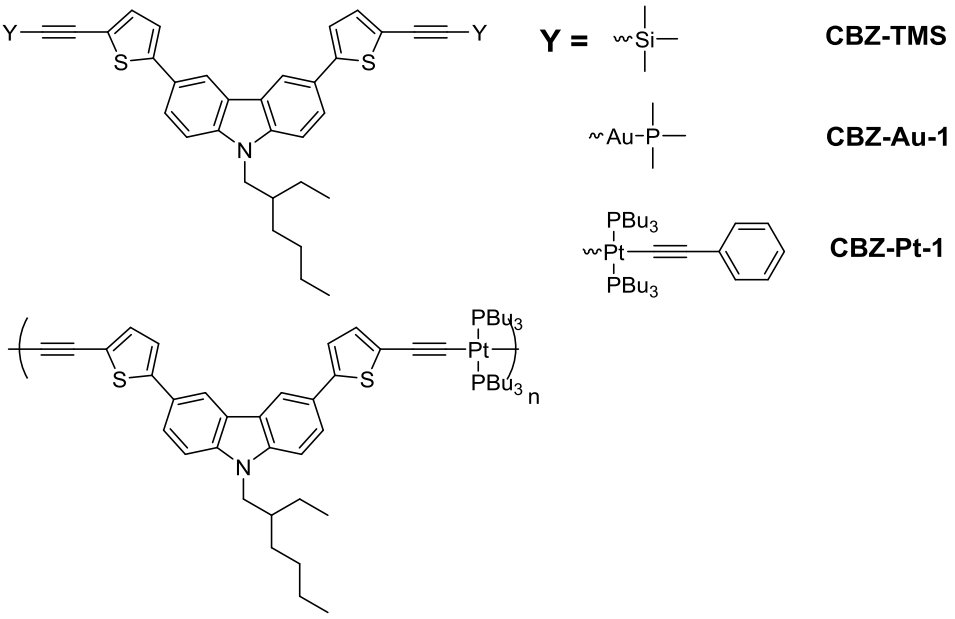

Figure 2-1. Chemical structures of the metal complexes and platinum acetylide polymer.

Results and Discussion

Synthesis

Figure 2-2 describes the synthesis of ET-CBZ-TE ligand. In order to increase the solubility in organic solvents, 2-ethylhexyl alkyl chain was introduced in the first step in

presence of aq. NaOH solution. Bromination of 2-1 was achieved by N-bromosuccinamide (NBS) in THF solution followed by Stille coupling of 2-2 with commercially available 2-(Tributylstannyl) thiophene in presence of $Pd(PPh_3)_4$ catalyst in DMF. The compound 2-3 was reacted with NBS to obtain dibrominated product 2-4 which was further treated with trimethylsilyl acetylene under Sonogashira coupling reaction condition to obtain TMS protected compound CBZ-TMS. Finally, it was treated with potassium carbonate (K_2CO_3) in THF/MeOH solvent mixture at room temperature to obtain ligand L1.

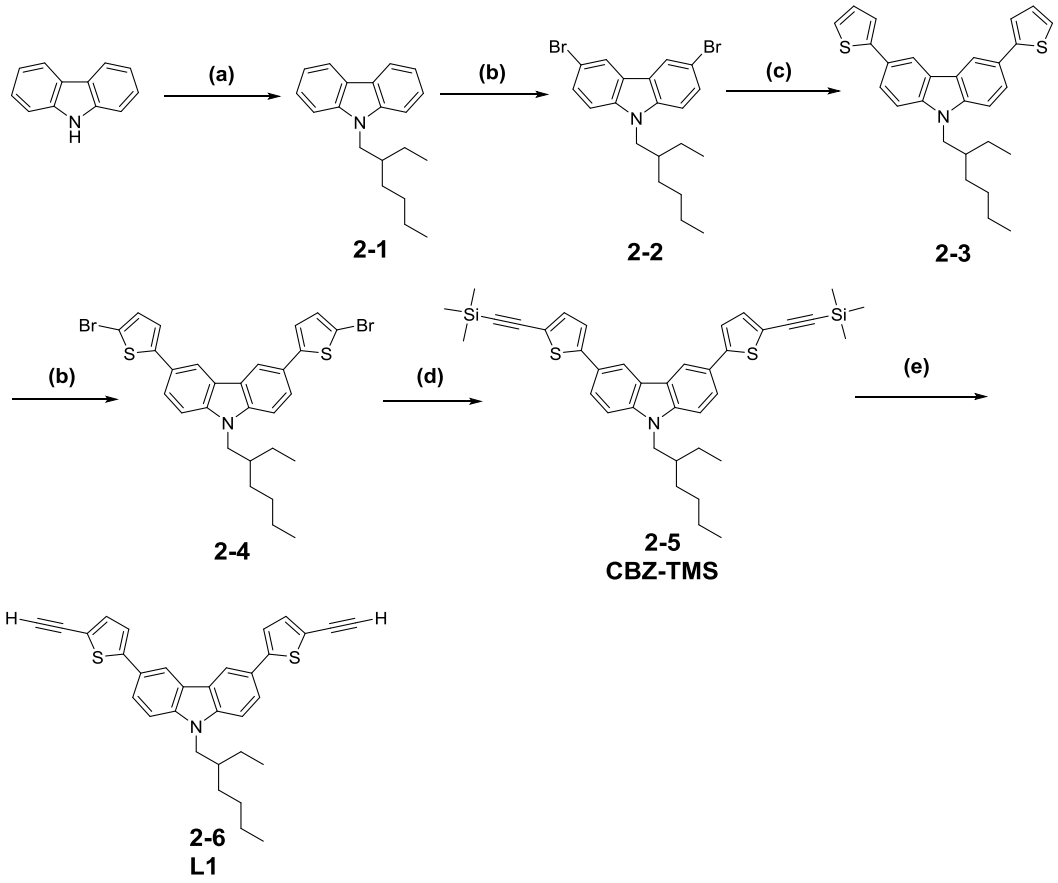

Figure 2-2. The synthetic scheme for the preparation of ligand L1. (a) 2-Ethylhexyl bromide, aq. NaOH, Benzyltriethyl ammonium chloride, toluene, reflux, 15 h; (b) NBS, THF; (c) 2-(Tributylstannyl) thiophene, $Pd(PPh_3)_4$, DMF; (d) Trimethylsilyl acetylene, cis-$Pd(PPh_3)_2Cl_2$, CuI, Diisopropylamine/THF, 70^{o}C ; (e) K_2CO_3, THF/MeOH, rt.

The synthesis of metal complexes and polymer is performed under Hagihara dehydrohalogenation reaction and presented in Figure 2-3. For the synthesis of gold complex CBZ-Au-1, L1 was treated with commercially available PMe_3AuCl in presence of freshly prepared NaOMe in distilled DCM. The complex was obtained as yellow crystalline solid in 84% yield. Terminal hydrogen containing acetylide ligand L1 was treated with 2-7 in DCM/NEt_3 solvent mixture in presence of catalytic amount of CuI to obtain platinum complex CBZ-Pt-1. The platinum acetylide polymer CBZ-Poly-Pt was synthesized by reacting ligand L1 with cis-$Pt(PBu_3)_2Cl_2$ in presence of catalytic amount CuI in toluene/piperidine (1:1) solvent mixture. The crude polymer was purified by precipitation over cold methanol (total 3 times) to obtain bright yellow colored polymer.

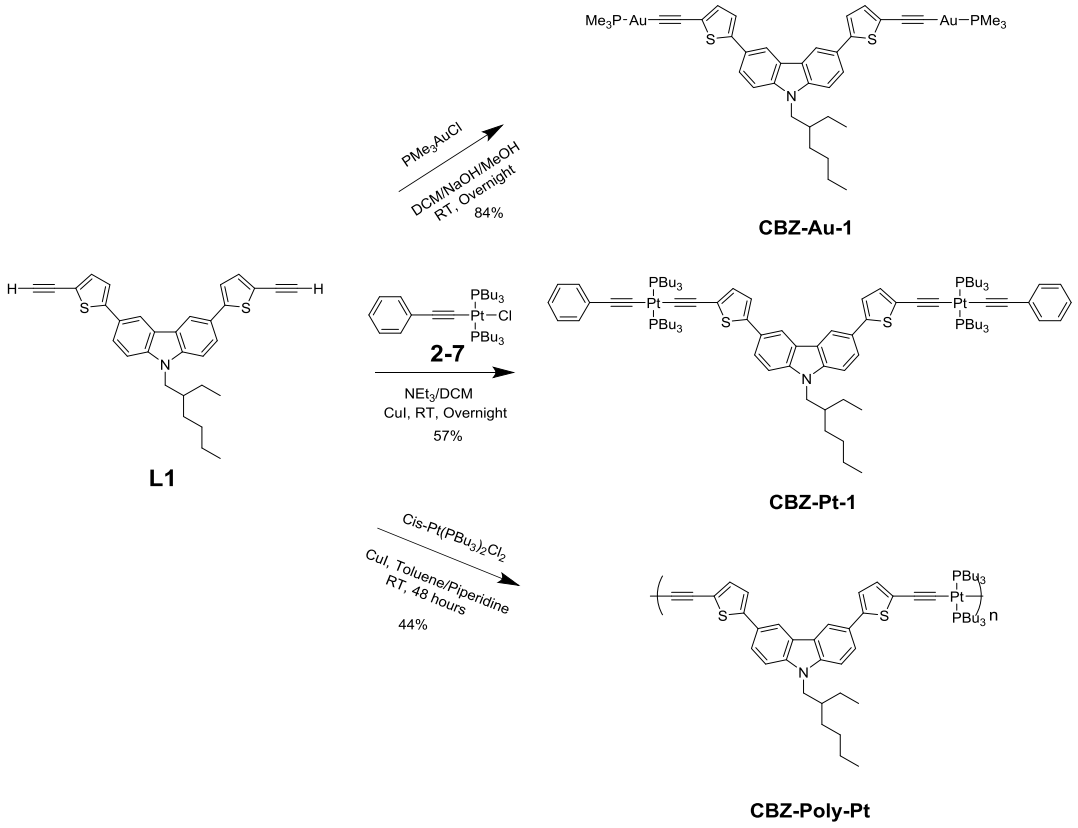

Figure 2-3. Synthetic scheme for the metal complexes and polymer.

Ground State Absorption Spectra

The absorption spectra of the TMS-protected oligomer CBZ-TMS, metal complexes CBZ-Au-1, CBZ-Pt-1 and polymer CBZ-Poly-Pt were measured in THF solution and are shown in Figure 2-4a, and the molar extinction coefficients (ε) and absorption band maxima (λ_{max}) are listed in Table 2-1. In general, the metal complexes, polymer and the free oligomer show strongly allowed absorption in the 300-450 nm region. However, there are interesting and significant differences in the absorption properties across the series. First, the absorption of the free oligomer CBZ-TMS is the most blue shifted of the series, with the principal π,π* transition lying in the near-UV with an onset ~410 nm and λmax = 328 nm. Second, the absorption of the gold(I) congener, CBZ-Au-1, is quite similar to that of CBZ-TMS, but the onset and λ_{max} are slightly red-shifted. This fact can be attributed to the weak interaction between 5d orbitals of the Au(I) centers with the ligand π system.[108] Interestingly, the absorption of the Pt(II) complex and polymer are significantly red-shifted and show enhanced molar absorptivity compared to the free oligomer and Au(I) complex. The absorption onsets are red-shifted by ~25 nm, and the enhanced oscillator strength for the Pt(II) systems is clearly due to enhanced π-conjugation due to mixing of the ligand π-levels with the dπ levels of the Pt(II) centers,[109] (The enhanced molar absorptivity of CBZ-Pt-1 compared to CBZ-Poly-Pt is in part artifact arising because the polymer repeat unit used in the calculation of the absorptivity contains only a single Pt(II) acetylide unit, whereas oligomer CBZ-Pt-1 contains two). Taken together, these results suggest that there is substantial metal-ligand electronic interaction in the Pt(II) systems; however, the interaction is at best weak in the Au(I) complex.

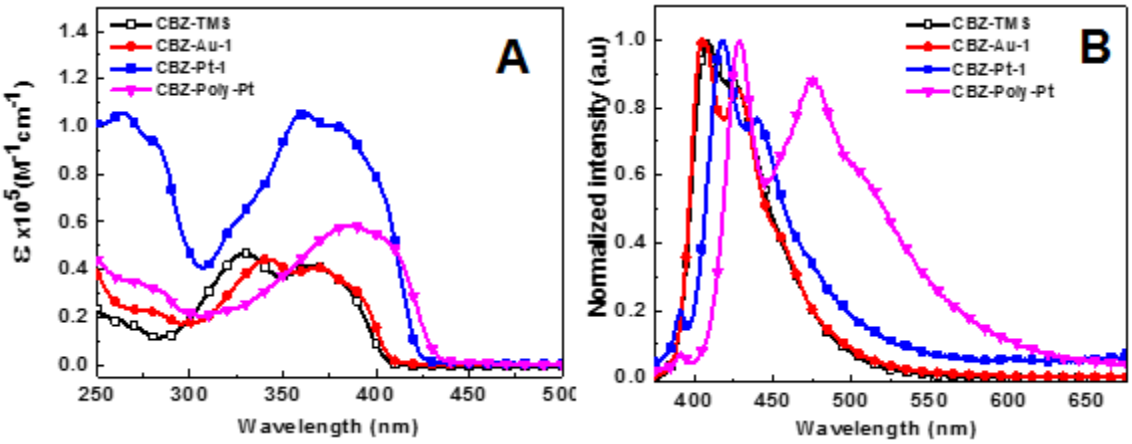

Figure 2-4. (A) Absorption and (B) room temperature emission spectra of CBZ-TMS, CBZ-Au-1, CBZ-Pt-1 and CBZ-Poly-Pt in THF solution. The emission spectra were obtained with excitation wavelength at 350 nm and they are intensity normalized at λ_{max}. Note that the molar absorptivity for CBZ-Poly-Pt is based on the repeat unit concentration, where the repeat unit contains a single Pt(II) center.

Steady-State Photoluminescence Spectroscopy

Room temperature photoluminescence spectra of the oligomer CBZ-TMS, metal complexes CBZ-Au-1, CBZ-Pt-1 and the polymer CBZ-Poly-Pt in deoxygenated THF are shown in Figure 2-4b. At ambient temperature, and with excitation at λ = 350 nm, vibronically structured emission bands were observed that show comparatively low Stokes shift from the absorption. The lifetimes of this emission from the metal complexes (τ_f, Table 2-1) are very short (<200 ps), and on the basis of the small Stokes shift and short lifetimes the emission is attributed to fluorescence from the $^1\pi,\pi^*$ state.[100] The fluorescence spectra show similar trends across the series as noted for the UV-visible absorption spectra. In particular, the emission maxima are red-shifted from free oligomer CBZ-TMS in the sequence CBZ-Au-1 < CBZ-Pt-1 < CBZ-Poly-Pt. Two well defined vibronic peaks were observed in the fluorescence spectrum for all of the systems, which is a signature of 3,6-thienyl substituted carbazole system.[110] The

fluorescence quantum yields (Φ_f, Table 2-1) for the metal complexes and polymer are more than an order of magnitude less than for the free oligomer CBZ-TMS, which can be attributed to efficient $S_1 \rightarrow T_1$ intersystem crossing in the former.

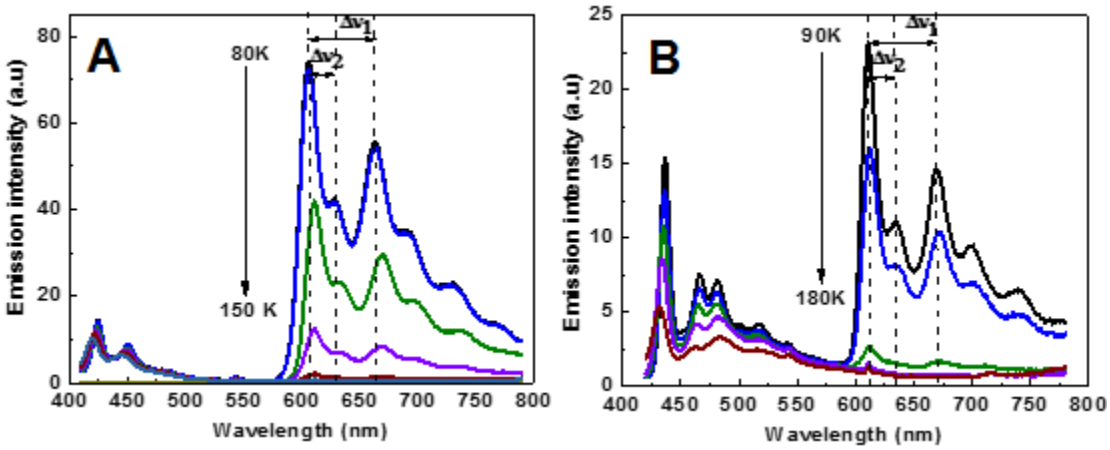

Figure 2-5. Low temperature emission spectra of (A) platinum(II) oligomer CBZ-Pt-1 (temperatures are 80, 90, 100, 120, 135 and 150 K) and (B) platinum(II) polymer CBZ-Poly-Pt in 2-MeTHF (temperatures are 90, 110, 130, 150 and 180 K). The excitation wavelength was 350 nm. The frequencies of the vibronic progressions discussed in the text were determined by the differences shown in the figures.

Close inspection of the fluorescence quantum yield data suggests both the platinum complex CBZ-Pt-1 and the polymer CBZ-Poly-Pt exhibit the most efficient intersystem crossing to the triplet manifold, compared to gold(I) complex CBZ-Au-1, which has a noticeably larger fluorescence yield. This fact can be attributed to stronger spin-orbit coupling effect for platinum(II) than gold(I).[109] Interestingly, gold(I) has a slightly larger spin-orbit coupling constant than platinum(II). We believe that the larger spin-orbit coupling in the platinum(II) systems arises because there is greater dπ-metal/π*-ligand orbital mixing than in the gold(I) system.

In order to understand the effect of the different heavy atoms in promoting phosphorescence in the oligomers, variable temperature photoluminescence

spectroscopy was performed on the series in deoxygenated 2-methyltetrahydrofuran (2-MeTHF) solvent (glass). As shown in Figure 2-5, for the Pt(II) oligomer and polymer, below 130 K a structured emission band is clearly seen in the region from 590-800 nm that is assigned to phosphorescence from the T_1 state. Note that at 80 K, the emission is dominated by the phosphorescence, and given that the room temperature fluorescence yields are ~0.01, we estimate that the 80 K phosphorescence yields for CBZ-Pt-1 and CBZ-Poly-Pt are in the range 0.05 – 0.10.

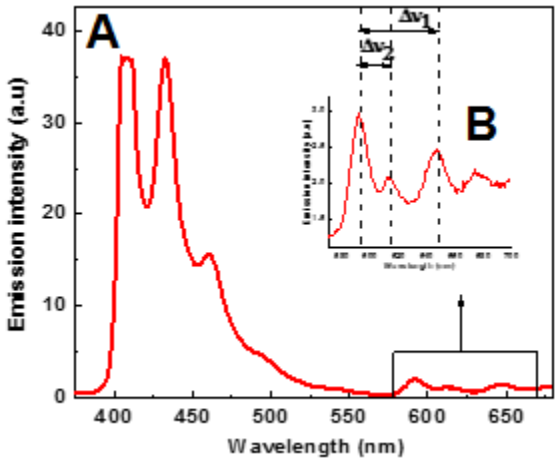

Figure 2-6. Low temperature emission spectrum (77 K) of (A) gold(I) complex CBZ-Au-1 and (B) magnified phosphorescence region. Note that the 0-0 band in the fluorescence is clipped due to the scaling used to show the weak phosphorescence. The frequencies of the vibronic progressions discussed in the text were determined by the differences shown in B.

In contrast to the emission of the Pt(II) systems, even at 80 K the gold(I) complex CBZ-Au-1 exhibits vibronically structured fluorescence and only a weak phosphorescence emission (Figure 2-6). The weak phosphorescence from CBZ-Au-1 can be attributed to less efficient spin-orbit coupling for gold(I) in comparison to platinum(II).[20] In all of the phosphorescence spectra, there are two distinct vibronic progressions observed, assigned as $\Delta\nu_1$ and $\Delta\nu_2$. The coupling frequency differs

Table 2-1. Photophysical properties in THF solution

Compound	λ_{max}/nm	ε/ $M^{-1}cm^{-1}$	λ_{Fl}/nm	ϕ_F [a]	λ_{Phos}/nm[b]	τ_{Fl}/ns[c]	ϕ_Δ [d]	τ_{TA}/μs
CBZ-TMS	328	46,000	407	0.43	-	-	-	0.36
CBZ-Au-1	341	44,000	406	0.04	591	<0.2	0.21± 0.02	0.63
CBZ-Pt-1	362	105,000	418	.003	605	<0.2	0.15± 0.02	0.42
CBZ-Poly-Pt	386	58,000	428	.01	610	<0.2	0.16± 0.02	0.34

Note: [a] Fluorescence quantum yield was measured with respect to quinine sulfate in 0.1 M sulfuric acid (ϕF= 0.54), and the estimated error is ±5 %. [b] Phosphorescence was measured in distilled 2-MeTHF solvent. [c] Lifetime was shorter than lower limit of the picoQuant instrument, 200 ps. All samples are excited at 375 nm. The emission was detected for CBZ-Au-1 at 400 nm and for CBZ-Pt-1 and CBZ-Poly-Pt at 425 nm. [d] Singlet oxygen quantum yield was determined in C6D6 using terthiophene (ϕ^ =0.73) as actinometer

slightly from sample to sample. The $\Delta \nu_1$ is 1430 cm^{-1} for CBZ-Pt-1 and CBZ-Au-1, whereas for CBZ-Poly-Pt $\Delta \nu_1 \approx 1460$ cm^{-1}. For CBZ-Pt-1, CBZ-Au-1 and CBZ-Poly-Pt $\Delta \nu_2 \approx 610$, 575 and 660 cm^{-1}, respectively. The low temperature fluorescence spectra of CBZ-Pt-1 and CBZ-Au-1 exhibit a progression with nearly the same frequency ($\Delta \nu_1 \approx 1430$ cm^{-1}) as the high frequency progression in the phosphorescence. Interestingly, the fluorescence of the polymer exhibits two progressions, one at a similar frequency ($\Delta \nu_1 \approx 1430$ cm^{-1}) and another a higher frequency ($\Delta \nu_1 \approx 2090$ cm^{-1}). The latter may be due to coupling of the singlet state with the C≡C modes

Transient Absorption Spectroscopy

To further explore the properties of the triplet state, ns-μs transient absorption spectroscopy was carried out on deoxygenated THF solutions of the oligomers and polymer. Figure 2-7 compares the transient absorption spectra of oligomer CBZ-TMS with CBZ-Au-1, CBZ-Pt-1 and CBZ-Poly-Pt, immediately following the laser pulse in THF. The transients are quenched by oxygen, and on this basis they are assigned to the absorption of the lowest triplet excited state. The lifetimes of the transient absorption of the triplet state are listed in Table 2-1 (τ_{TA}). The triplet lifetimes for the oligomers are similar, ranging from 0.35 – 0.65 μs, and they vary in the sequence CBZ-Au-1 > CBZ-Pt-1 > CBZ-Poly-Pt. The difference absorption spectra generally consist of ground state bleaching of the S_0-S_1 absorption and broad T_1-T_n absorption in the visible region. Interestingly CBZ-TMS also exhibits triplet absorption, possibly due to the presence of the thiophene units, which are known to enhance ISC in π-conjugated electronic systems.[111]

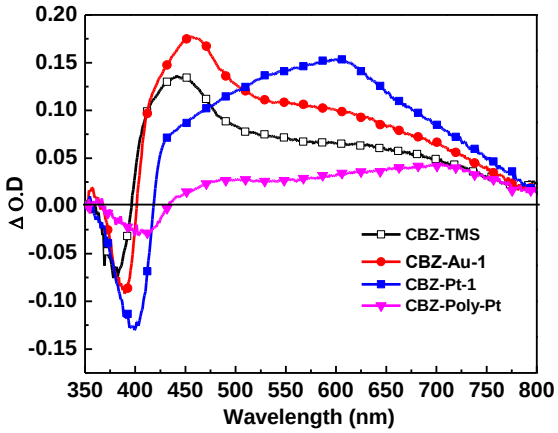

Figure 2-7. Nanosecond transient absorption spectra of the ligand CBZ-TMS, metal complexes CBZ-Au-1, CBZ-Pt-1 and the polymer CBZ-Poly-Pt in deoxygenated THF solution for 45 minutes. All samples were excited at 355 nm with 300 ns of camera delay increment. All the samples have matched absorbance of ~0.7 at the excitation wavelength.

The λ_{max} for T_1-T_n absorption is shifted about 20 nm for the gold complex CBZ-Au-1 and ~164 nm for the platinum complex CBZ-Pt-1 relative to the ligand CBZ-TMS. By comparing the transient absorption signal of the metallated oligomers with the polymer, it is found that the intensity of the signal for the polymer is lower. As the experiment is carried out from samples solutions of matched absorbance, with the same laser power, and the same excitation wavelength, this difference suggests either that the polymer CBZ-Poly-Pt has a lower triplet yield than the metal complexes, or that there is a triplet quenching pathway that operates in the polymer that is not available in the oligomers. One possibility is that triplet-triplet annihilation may take place in the polymer.

As direct excitation of the metal complexes and the polymer produces the triplet state, we examined their ability to sensitize the generation of singlet oxygen ($^1O_2$) in deuterated benzene solution. These experiments were performed by monitoring phosphorescence from $^1O_2$ at 1270 nm. All of the materials sensitize the production of

singlet oxygen, with observed quantum yields ranging from 0.15 – 0.21 (ϕ_Δ ,Table 2-1), consistent with moderately efficient intersystem crossing. However, the singlet oxygen yields are somewhat less than might be expected given that the fluorescence quantum yields of the metallated oligomers are so much less than free oligomer. This may be due to the relatively short triplet lifetimes which result in incomplete triplet energy transfer to oxygen whose concentration is comparatively low in the air saturated solutions.

Two Photon Absorption Spectroscopy

Two photon absorption spectra and cross sections of CBZ-Au-1, CBZ-Pt-1 and CBZ-Poly-Pt were measured in THF by the non-linear transmission (NLT) method and are presented in Fig. 2-8. The comparatively low fluorescence quantum yields for the metal containing oligomers and polymer precluded the use of the two photon excited fluorescence (2PEF) method. The normalized ground state absorption spectra are shown in the plots for comparison. In all three compounds the 2PA cross section values are relatively low in the $S_0 \rightarrow S_1$ transition region, σ_{2PA} ~ 10-100 GM, with only CBZ-Au-1 showing slightly higher values. The cross section intensity increases rapidly toward shorter wavelengths, reaching values of σ_{2PA} ~ 800-1000 GM at 550 nm. Because the maxima of the 2PA spectra are blue-shifted relative to the ground state absorption maxima, we may conclude that these systems display mainly centrosymmetric character.[112] Comparison of the nanosecond transient absorption and 2PA spectra shows that there is a significant overlap between them, especially in the mid-visible region between 500 and 650 nm. This overlap suggests that the complexes will exhibit pronounced long-timescale non-linear absorption via the dual mode mechanism that combines 2PA and excited state absorption by the triplet state.

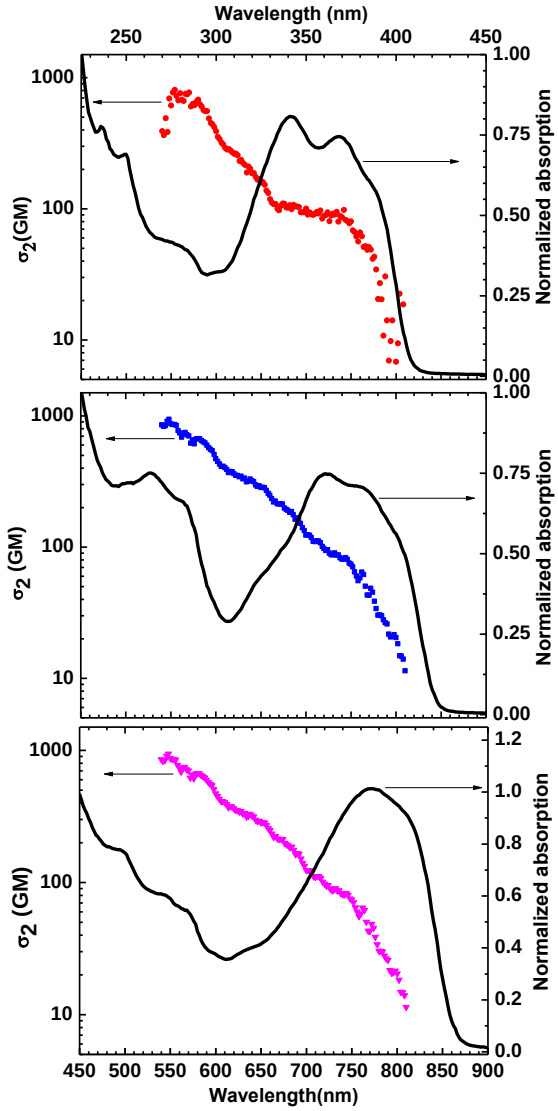

Figure 2-8. 2-Photon absorption spectra of the metal complexes and the polymer are measured with femtosecond pulses via the non-linear transmittance method in THF solution (red filled circles for CBZ-Au-1, blue filled squares for CBZ-Pt-1 and magenta filled diamonds for CBZ-Poly-Pt); corresponding wavelengths are in bottom horizontal scale. One photon absorption spectra (shown by black line) are measured in THF solution and corresponding wavelengths are in upper horizontal scale.

In order to probe the ability of the oligomers and polymers to display non-linear absorption via the dual mode mechanism, open-aperture z-scan experiments were performed by using 1 mM THF sample solutions with 600 nm, 5 ns pulses. Note that 600 nm is more than 100 nm to the red of the onset of the allowed singlet ground state

absorption transition, and consequently excitation at this wavelength is only likely to occur via 2PA. Figure 2-9 compares the representative z-scan results for CBZ-Au-1, CBZ-Pt-1 and CBZ-Poly-Pt. From the z-scan result, it is evident that the non-linear response of these materials varied in the series CBZ-Poly-Pt ~ CBZ-Pt-1 > CBZ-Au-1, with the Pt-oligomer and polymer sample exhibiting approximately 10% reduction in transmittance at the peak of the z-scan.

Recent work from our laboratories has explored the nanosecond z-scan response of a series of Pt-acetylide complexes with high 2PA cross section conjugated ligands.[19] The z-scan response for the present series of carbazole oligomers are somewhat less compared to that of the most active Pt-acetylide oligomers previously investigated. The attenuated response is likely due to the fact that the σ_{2PA} values for the carbazole based oligomers are lower compared to the previously investigated systems. Nonetheless, the response observed in the present series of complexes is respectable and given their relatively good optical transparency, especially for CBZ-Au-1, these chromophores may be useful in non-linear optical applications.

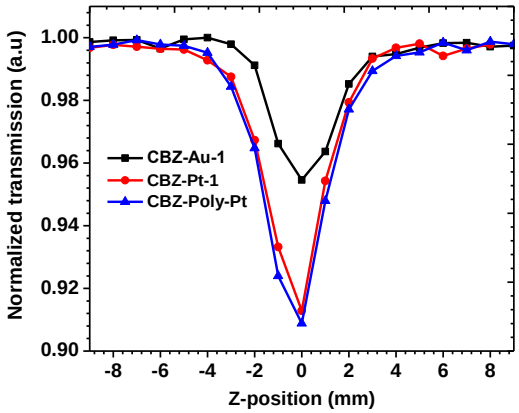

Figure 2-9. Open aperture nanosecond z-scan 1 mM THF solution of CBZ-Au-1, CBZ-Pt-1 and CBZ-Poly-Pt at 600 nm excitation wavelength, 5 ns pulse width.

Summary and Conclusions

This study highlights the photophysical and non-linear absorption properties of a novel series of organometallic chromophores that are based on the carbazole containing ET-Cbz-TE π-conjugated oligomer. The results provide insight regarding the relative effects of the Au(I) and Pt(II) centers on S_1 – T_1 intersystem crossing, radiative decay of T_1 (phosphorescence), and non-linear absorption. Au(I) appears to have relatively little effect on the ground state absorption of the ET-Cbz-TE chromophore, whereas the Pt(II) units induce a significant red-shift. This signals that there is greater mixing of the metal orbitals with the π electron system in the ET-Cbz-TE chromophore for the Pt(II) systems. This results in greater metal induced spin-orbit coupling in the Pt(II) systems, and the effect is manifested in a reduced fluorescence yield and higher phosphorescence yield for CBZ-Poly-Pt ~ CBZ-Pt-1. All of the systems investigated exhibit moderately intense mid-visible transient absorption from a triplet state with a lifetime in the sub-microsecond timescale, consistent with relatively efficient intersystem crossing. Femtosecond non-linear transmittance experiments were utilized to construct the 2-photon absorption spectra of the chromophores. In each case, the 2PA absorption is blue shifted relative to the transition that is degenerate with the primary ground state absorption band. This result is consistent with the centrosymmetric structure of the metallated ET-Cbz-TE chromophore structure. The peak 2PA for this series occurs in the region 550 – 600 nm with σ_{2PA} values > 800 GM.

While the overall non-linear response of this series of organometallic oligomers to nanosecond pulses is lower than that seen in previous studies of Pt-acetylide chromophores, the excellent visible transparency of the ET-Cbz-TE family makes this

system promising for non-linear optical applications where transparency for $\lambda < 500$ nm is a requirement.

Experimental Section

Instrumentation and Methods

All the NMR spectra were recorded using a Varian VXR-300 FT-NMR, operating at 300 MHz for ^{1}H NMR, 121 MHz for ^{31}P NMR and at 75.4 MHz for ^{13}C NMR. Mass spectrometry for the newly synthesized compounds were recorded on a Bruker APEX II 4.7 T Fourier Transform Ion Cyclotron Resonance mass spectrometer (Bruker Daltonics, Billerica, MA). Gel Permeation Chromatography (GPC) analysis of the polymer was performed on a system containing a Shimadzu SPD-20A photodiode array (PDA) detector, using THF as eluent at 1 ml/min flow rate and the system was calibrated with respect to linear polystyrene standards in THF.

Photophysical measurements were conducted with dry HPLC grade THF as solvent in 1 x 1 cm quartz cuvettes unless otherwise noted. UV-visible absorption spectra were obtained on a Varian Cary 100 dual beam spectrophotometer. Room temperature and low temperature emission spectra were recorded on a Photon Technology International (PTI) fluorimeter and collected 90^{o} relative to the excitation beam. The optical density of the sample solutions was kept at ≤0.1 at excitation wavelength. Refractive index corrections were applied for sample and standard solutions for emission quantum yield measurements. Freshly distilled HPLC grade 2-methyl tetrahydrofuran was used for the low temperature experiments. The sample was placed in 1 cm diameter borosilicate glass tube and deoxygenated by 4-5 freeze-pump-thaw cycles under vacuum (10^{-5} Torr) prior to use. Temperatures to 77 K were achieved by using liquid-nitrogen cooled Oxford instrument DN 1704 optical cryostat attached to

an Omega CYC3200 autotuning temperature controller. The reported concentration for polymer refers to the concentration of polymer Repeat Unit (PRU). Solutions for spectroscopic studies were prepared by dilution of stock solutions. Fluorescence lifetimes were collected via a FluoTime 100 Fluorescence Lifetime Spectrometer (PicoQuant, USA).

Nanosecond timescale transient absorption spectroscopy was conducted on a home-built apparatus using third harmonic of a Continuum Surelite series Nd:YAG laser (λ=355 nm, 10 ns FWHM, 7 mJ pulse^{-1}). Probe light was produced by a xenon flash lamp and the transient absorption signal was detected with a gated-intensified CCD mounted on a 0.18 m spectrograph (Princeton PiMax/Acton Pro 180). Samples for transient absorption were contained in a 1 cm path length flow cell with a total volume of 10 ml and continuously circulated at the pump-probe region during the experiment. The optical density of the solutions was kept ≈ 0.7 at 355 nm and samples were degassed with argon for at least 45 minutes before the measurement. Singlet oxygen quantum yields were measured using a Photon Technology International Quantamaster near-IR spectrophotometer containing an InGaAs photodiode detector, an optical chopper and a lock-in amplifier. The optical density was kept below 0.12 for all the samples at excitation wavelength 350 nm.

The open aperture nanosecond time domain Z-scan measurements were performed on a system which employs the third harmonic output of a Continuum Surelite II Nd:YAG laser equipped with a Continuum Surelite OPO PLUS for excitation at 600 and 628 nm. All of the chromophores were excited with a 600 nm laser beam through 50/50 beam splitter. The beam was focused using 50.8 mm focus length, 38.1

mm diameter plano-convex lens. Sample solutions (C= 1.0 mM) were taken in a 1 mm path length cuvette and moved along the focused beam using a manual one-directional translational stage placed exactly behind the focusing lens. The energy of the laser beams were obtained by using Ophir pyroelectric heads and an Ophir Laserstar power/ energy monitor and collected using StarCom32 software.

The laser system for the 2PA measurements comprised a Ti:Sapphire femtosecond oscillator (Lighthouse Inc.), femtosecond regenerative amplifier (Legend F-HE, Coherent Inc.), and an optical parametric amplifier, OPA (TOPAS-C, Light Conversion). The second harmonic of the signal output of the OPA was continuously tunable from 540 to 810 nm with the maximum pulse energy in the range 10 - 30 μJ, and second harmonic of the idler was tunable from 800 to 1070 nm with the maximum pulse energy 10 - 30 μJ. The average pulse duration was 80 - 120 fs (FWHM). A detailed description of the laser system is provided elsewhere.[113] The NLT method has been described previously.[19,114-116] Briefly, the OPA output beam at 100 Hz pulse repetition rate was directed through the sample prepared at concentration, C ~10^{-3} M, in a standard 10 mm spectroscopic cuvette. Two identical 10 mm diameter silicon photodetectors (Thorlabs, DET100A) were used to measure the laser pulse reflected from two glass beam pick-off plates positioned accordingly, before and after the sample. The analog signals from the photodetectors were digitized using a DAQ board (National Instruments, Model PCI-6110). The dependence of the sample transmission (defined as ratio of the signal from the second detector divided by the signal from the first detector) on the incident intensity was evaluated by varying the energy of the incident pulse in the range Pin ≈ 0.3 – 30 μJ using a neutral density filter attenuator wheel (Thorlabs)

mounted on a stepper motor. The estimated accuracy of the measured transmission is about 0.1%. A laser power meter (Nova II, Ophir) was used to measure the average laser power at the input to the sample. The beam diameter at the sample was 0.8 – 1.5 mm and varied depending on the OPA. For calibration of the 2PA cross section a known reference PPV in THF was measured under identical conditions.

General Methods for Synthesis

All reactions were performed under dry and argon atmosphere. THF was dried using solvent purification columns (Glass Contour). All other solvents were used without further purification unless specified. Chloro(trimethylphosphine)gold(I) was purchased from Sigma-Aldrich and used as received. Trimethylsilyl acetylene was purchased from GFS Chemical and was used as received. Potassium tetrachloroplatinate, tetrakis(triphenylphosphine)palladium(0) and bis(triphenylphosphine)palladium(II) dichloride were purchased from Strem Chemicals. Silica gel (230-400 mesh, 60 Å, Silicycle Inc.) was used for column chromatography. Compounds 2-2 and 2-4[117] were synthesized according to the literature procedures. Compounds 2-1 and 2-3 were synthesized by modified literature procedures.[117] Cis-Pt(PBu_3)$_2$$Cl_2$[19] and platinum complex 2-7[118] were synthesized according to the literature procedures.

Synthesis

9-(2-Ethylhexyl)-Carbazole (2-1)

Carbazole (5 g, 30 mmol) and 0.2 gm benzyltriethylammoniumchloride were dissolved in 25 mL of toluene and this light yellow colored suspension was deoxygenated by bubbling with argon for 30 minutes. To this suspension 17.5 gm of 50 w% NaOH (aq) was added at once and it was further deoxygenated for 30 minutes more, in the meanwhile the color of the solution changed to light brown from yellow.

Then 2-ethylhexyl bromide (6.95 g, 36 mmol) was added to the reaction mixture dropwise, and then it was refluxed for 24 hours with vigorous stirring. The organic layer was separated from the aqueous layer and washed with water, brine solution and finally dried over anhydrous Na_2SO_4, filtered and concentrated. The crude yellow liquid was purified by silica gel column chromatography using hexane as eluent to give the titled compound as colorless oil (3 g, 37%). ^{1}H NMR (300 MHz, $CDCl_3$) : δ 8.22 (d, J = 7.7 Hz, 2H), 7.62-7.45 (m, 4H), 7.35 (t, J = 7.4 Hz, 2H), 4.29-4.14 (m, 2H), 2.18 (m, 1H), 1.55-1.33 (m, 8H), 1.06-0.97 (m, 6H).

3, 6-Bis(thiophene-2-yl)-9-(2-ethylhexyl)carbazole (2-3)

Compound 2-2 (3.74 g, 8.55 mmol) and 2-(tributylstannyl) thiophene (7.02 g, 18.81 mmol) were added to 40 mL of dry DMF and purged with argon for 45 minutes. $Pd(PPh_3)_4$ (420 mg, 4 mol %) was added to the reaction mixture under the flow of argon. The orange colored solution was refluxed under argon atmosphere which changed to dark color in an hour. The reflux was continued for 2 more days. The reaction mixture was poured over water and extracted with dichloromethane. The combined organic layer was extracted with brine and finally dried over anhydrous Na_2SO_4. It was filtered and the solvent was evaporated to dryness. The crude product was purified by column chromatography using silica gel as adsorbent and hexane as eluent to obtain 3 as greenish white solid (2 g, 53%). ^{1}H NMR (300 MHz, CDCl3): δ 8.31 (d, J = 1.6 Hz, 2H), 7.70 (dd, J = 8.5, 1.8 Hz, 2H), 7.38-7.30 (m, 4H), 7.24 (d, J = 1.0 Hz, 2H), 7.09 (dd, J = 5.1, 3.6 Hz, 2H), 4.17-4.07 (m, 2H), 2.08-1.99 (m, 1H), 1.42-1.18 (m, 8H) and 0.95-0.80 (m, 6H).

9-(2-Ethylhexyl)-3, 6-bis (5-((trimethylsilyl) ethynyl) thiophen-2-yl)carbazole (2-5)

Compound 2-4 (1.5 g, 2.49 mmol) was dissolved in 30 mL of diisopropylamine and THF (1:4) mixture and deoxygenated by bubbling argon for 45 minutes. Subsequently $Pd(PPh_3)_2Cl_2$ (35 mg, 2 mol %), CuI (20 mg, 4 mol %) were added to the reaction mixture under argon atmosphere and deoxygenated additionally for 30 more minutes. Then trimethylsilylacetylene (0.61 g, 6.23 mmol) was added and reaction mixture was heated at 70^{o}C under inert atmosphere overnight. After confirming the consumption of starting material by TLC, the reaction mixture was evaporated to dryness and the crude product was purified by silica gel chromatography using hexane as eluent to give light yellow colored titled compound (1.43 g, 90.5%). ^{1}H NMR (300 MHz, $CDCl_3$): δ 8.28 (s, 2H), 7.68 (d, J = 8.5 Hz, 2H), 7.37 (d, J = 8.5 Hz, 2H), 7.21 (m, 4H), 4.15 (d, J = 6.9 Hz, 2H), 2.15-1.95 (m, 1H), 1.48-1.17 (m, 8H) , 0.94-0.84 (m, 6H) and 0.27 (s, 18H). ^{13}C NMR (75 MHz, $CDCl_3$): δ 147.41, 141.37, 134.10, 125.52, 124.77, 123.34, 122.01, 121.32, 118.14, 109.88, 99.35, 98.26, 47.89, 39.68, 31.21, 29.03, 24.59, 23.26, 14.26, 11.12 and 0.16 ($SiMe_3$).

Synthesis of L1

TMS protected compound 2-5 (200 mg, 0.314 mmol) was dissolved in 30 mL of MeOH/ THF (1:1) solvent mixture and purged with argon for 30 minutes. K_2CO_3 (216 mg, 1.57 mmol) was added to the reaction mixture and stirred it overnight under argon atmosphere shielded from the light with aluminum foil. The solvents were evaporated to dryness and the residue was dissolved in dichloromethane, washed three times with water and then brine solution. The combined organic layer was dried over anhydrous Na2SO4, filtered and solvent was evaporated under vacuum to give the product as light yellow viscous oil (120 mg, 77%). ^{1}H NMR (300 MHz, $CDCl_3$): δ 8.27 (d, J = 1.6 Hz,

2H), 7.66 (dd, J = 8.5, 1.8 Hz, 2H), 7.35 (d, J = 8.5 Hz, 2H), 7.25 (d, J = 3.8 Hz, 2H), 7.18 (d, J = 3.8 Hz, 2H), 4.14 (m, 2H), 3.38 (s, 2H), 2.07-1.95 (m, 1H), 1.45-1.16 (m, 8H) and 0.91-0.81 (m, 6H). (Due to the instability of the compound 13C NMR was not recorded).

Synthesis of CBZ-Au-1

Compound L1 (40 mg, 0.0813mmol) was dissolved in 5 mL of dichloromethane and purged with argon for 30 minutes. PMe_3AuCl (50 mg, 0.163 mmol) was added to the reaction mixture under argon atmosphere. Then NaOMe (3 ml, 0.813 mmol) (prepared from dissolving 42.7 mg of NaOH in 25 ml of MeOH) was added, which caused formation of a bright yellow precipitate. The reaction mixture was stirred under inert atmosphere overnight. Then the solvent was evaporated to dryness and the yellow residue was dissolved in dichloromethane and passed through a plug of cotton to remove insoluble impurities. The filtrate was evaporated to 5 mL and methanol was added to obtain a yellow precipitate. The precipitate was centrifuged, washed with 20 ml of methanol, hexane and ether respectively and dried under vacuum to obtain 70 mg of complex in 84% yield. ^{1}H NMR (300 MHz, $CDCl_3$): δ 8.27 (s, 2H), 7.66 (d, J = 8.3 Hz, 2H), 7.33 (d, J = 8.4 Hz, 2H), 7.14 (d, J = 3.8 Hz, 4H), 4.14 (d, J = 5.8 Hz, 2H), 2.04 (m, 1H), 1.53 (d, 18H), 1.33 (m, 8H) and 0.88 (m, 6H). ^{13}C NMR (75 MHz, $CDCl_3$): δ 144.94, 141.07, 132.65, 126.05, 124.68, 123.76, 123.36, 121.82, 117.96, 109.62, 47.81, 39.65, 31.21, 29.05, 24.60, 23.25, 16.19, 15.71, 14.26, 11.12. ^{31}P NMR (121 MHz, $CDCl_3$) δ (ppm) 2.06. HRMS (APCI, [M+H]+) m/z calcd for C38H45Au2NP2S2 1036.1873, found 1036.1912.

Synthesis of CBZ-Pt-1

Compound L1 (64 mg, 0.13 mmol) and 2-6 (210 mg, 0.285 mmol) were dissolved in 50 mL of a dichloromethane/triethylamine mixture (1:1 v:v) and deoxygenated for 45 minutes by bubbling argon. After that 5 mg (26 mol %) of CuI was added and the reaction mixture was stirred under inert atmosphere overnight. The solvent was evaporated to dryness under vacuum, and the crude product was purified by silica gel column chromatography using 3:7 DCM/ hexane as an eluent to give the complex as a light yellow solid in 57% yield (140 mg). ^{1}H NMR (300 MHz, CD_2Cl_2): δ 8.29 (s, 2H), 7.70 (d, J = 8.4 Hz, 2H), 7.41 (d, J = 8.5 Hz, 2H), 7.31-7.08 (m, 12H), 6.85 (s, 2H), 4.20 (d, J = 6.5 Hz, 2H), 2.17 (m, 25H), 1.65(m, 24H), 1.53 (m, 24H), 1.44-1.21 (m, 8H), 0.98 (m, 42H). ^{13}C NMR (75 MHz, CD_2Cl_2): δ 142.2, 140.7, 130.9, 129.2, 128.5, 128.0, 126.4, 125.0, 124.3, 123.3, 121.7, 117.5, 115.3 (m), 109.5, 109.2, 107.8 (m), 101.6, 47.8, 39.7, 31.2, 29.1, 26.6, 24.6 (m), 24.2 (m), 23.3, 14.3, 14.1, 11.1 (due to superimposition two carbon is missing). ^{31}P NMR (121 MHz, CD_2Cl_2) δ 4.49 ($J_{Pt\text{-}P}$ = 2340 Hz). HRMS (APCI, [M+H]+) m/z calcd for C96H145NP4Pt2S2 1890.9078, found 1890.9134.

Synthesis of CBZ-Poly-Pt

The ligand L1 (90 mg, 0.183 mmol) and cis-$Pt(PBu_3)_2Cl_2$ (123 mg, 0.183 mmol) was dissolved in 10 mL of piperidine and toluene solvent mixture (1:1) and deoxygenated for 45 minutes by bubbling argon. CuI (5 mg) was added to the reaction mixture and it was stirred at room temperature under argon for 48 hours. The yellow viscous liquid was passed through a short neutral alumina column and filtrate was evaporated to dryness to give a yellow colored film. The residue was dissolved in 5 mL of chloroform and poured it over 200 mL of cold methanol. The obtained yellow

precipitate was centrifuged and the supernatant was removed. The obtained polymer was purified by repeated precipitations (2 times), which resulted in 90 mg of the polymer in 44% yield. ^{1}H NMR (300 MHz, $CDCl_3$): δ 8.25 (bs, 2H), 7.66 (d, 2H), 7.33 (d, 2H), 7.13 (bd, 2H), 6.86 (bd, 2H), 4.15 (d, 2H), 2.32-1.94 (m, 13H), 1.78-1.4 (m, 24H), 1.36 (m, 8H) and 1.1-0.81 (m, 24H). ^{31}P NMR (121 MHz, $CDCl_3$): δ 4.41 ($J_{Pt\text{-}P}$ = 2335.3 Hz). GPC: Mw = 24800, Mn = 9400 g/mol, PDI = 2.6.

CHAPTER 3
PHOTOPHYSICS AND NON-LINEAR ABSORPTION OF GOLD(I) AND PLATINUM(II) DONOR-ACCEPTOR-DONOR CHROMOPHORES

Background

Organometallic π-conjugated materials have emerged as one of the frontier research fields over the past few decades, owing to their application in organic light emitting diodes (OLEDs),[119-121] organic photovoltaic devices (OPVs),[25,75,79,80] and materials for non-linear absorption.[18,19,122] Two photon absorption (2PA) can be considered as one of the efficient ways of achieving non-linear absorption. After 2PA was first theoretically predicted in the 1930s,[28] and its first experimental observation in 1961,[29] there has been growing interest to develop new materials based on their non-linear optical characteristics. Two photon absorption has applications ranging from optical power limiting material via non-linear absorption,[83,123,124] imaging to data storage,[125] and photodynamic therapy.[37] Among various organometallic chromophores, heavy atom containing chromophores are unique in achieving efficient non-linear absorption by a "dual mode" pathway because of the facility of harvesting the triplet excited states via the spin-orbit coupling (SOC) effect.[18,49] The "dual mode" pathway is a combination of $S_0 \rightarrow S_1$ transition via absorption of 2PA or 1PA followed by intersystem crossing to the triplet excited state and excited state absorption from $T_1 \rightarrow T_n$.[49]

The general design strategy for efficient two photon absorption involves, synthesizing chromophores with a large transition dipole moment as well as permanent dipole moment between ground state (g) and excited state (e).[30] This is achieved by using donor (D) and acceptor (A) chromophores with a π-conjugated spacer in several fashions that includes D-π-A, D-π-D, A-π-A and several others.[30] Apart from that, D-A-D structural motif is popular for generating quadrupolar chromophores for applications not

only in non-linear absorption but also in optoelectronic devices.[25,126] Among different organometallic architectures, metal acetylide containing small molecules and polymers are of interest due to strong interactions between the metal d-orbitals and the π-system of the ligand.[127] In this work, we have studied TE-BTD-ET (E = ethynylene, T = 3-hexyl-2,5-thienylene, BTD = 2,1,3-benzothiadiazole) containing organometallic complexes for optoelectronic properties as well as 2 PA, where BTD acts as acceptor and T acts as a donor. While this paper was under preparation Angelis and co-workers reported platinum acetylide and a ruthenium acetylide of the same ligand studied here, as an efficient second-order nonlinear optical materials.[21]

A comparative study of gold(I) and platinum(II) acetylide systems with a thienyl carbazole chromophore was shown before by Schanze and coworkers .[128] It was observed from the low-temperature photoluminescence study that gold(I) is less efficient in populating the triplet excited state compared to platinum(II). Due to low fluorescence quantum yield of those metal complexes and polymer, nonlinear transmission (NLT) method was employed to estimate the 2PA behavior. However, no direct evidence was observed for the inherent effect of different heavy metals from the 2PA spectra. To address this issue, the current work involves the synthesis of four different gold(I) and platinum(II) complexes of the TE-BTD-ET ligand and complete photophysical characterization including ground state absorption, emission, nanosecond transient absorption, singlet oxygen sensitization. The high fluorescence quantum yield of the metal complexes and the ligand allow 2PA measurement via two photon excited fluorescence method. In order to understand the effect of the phosphine ancillary ligands on the photophysical properties, two gold(I) complexes were synthesized with

trimethyl phosphine and triphenyl phosphine ligands (TBT-Au-PMe_3 and TBT-Au-PPh_3, respectively) and two platinum(II) complexes were synthesized with trimethyl phosphine and tributyl phosphine ligands (TBT-Pt-PMe_3 and TBT-Pt-PBu_3, respectively). Analytical purity of the metal complexes were confirmed from ^{1}H NMR, ^{13}C NMR, ^{31}P NMR, and mass spectral studies. The results clearly suggest that the platinum complexes have significantly higher triplet yields, polarity as well as 2PA cross sections than the gold complexes, and they have potential to be used as efficient optical power limiting materials.

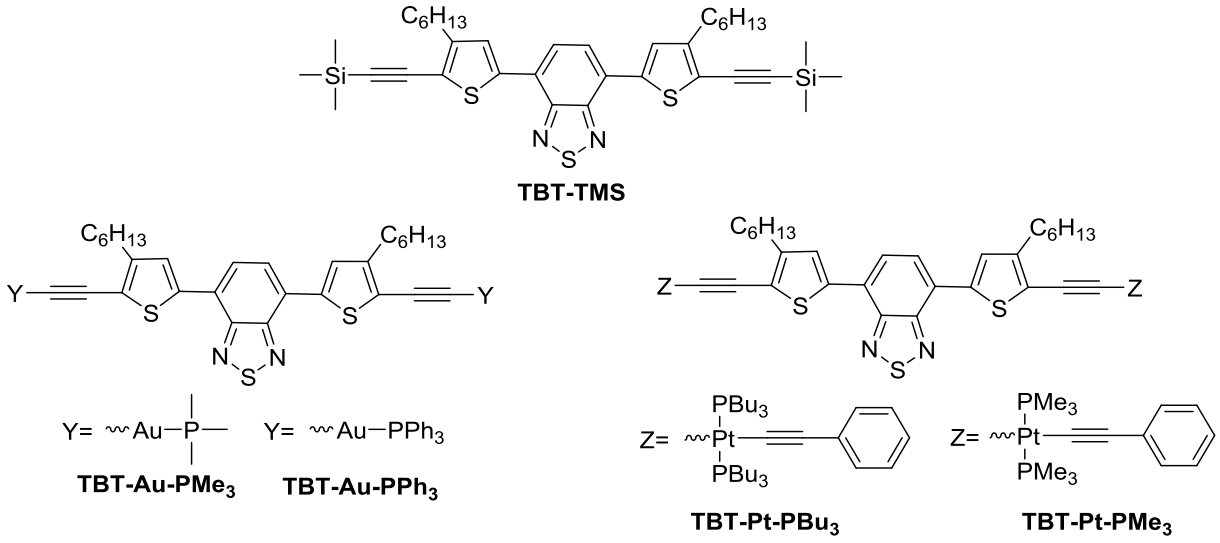

Figure 3-1. Chemical structures of the metal complexes and ligand.

Results and Discussion

Synthesis

Figure 3-2 illustrates the synthesis of donor-acceptor ligand TBT-H, containing 3-hexylthiophene as donor and .2,1,3-benzothiadiazole as an acceptor unit. In the first step, commercially available 3-hexylthiophene was treated with n-BuLi at -78˚C in anhydrous THF and the lithiated compound was quenched with 2-isopropoxy-4,4,5,5-tetramethyl-1,3,2-dioxaborolane to obtain the intermediate 3-1. The compound 3-1 was

treated with 4,7-dibromo derivative of 2,1,3-benzothiadiazole under Suzuki cross coupling condition to obtain 3-2 as a bright orange compound. In the next step, 3-2 was brominated with NBS in $CHCl_3$/ AcOH solvent mixture to obtain bright red colored dibrominated compound 3-3. Sonogashira reaction between 3-3 and trimethylsilylacetylene afforded TMS protected compound TBT-TMS. It was finally deprotected under basic condition to obtain TBT-H in 95% yield.

The synthesis of the metal complexes were performed via Hagihara dehydrohalogenation reaction. The terminally deprotected ligand TBT-H was reacted with commercially available PMe_3AuCl under basic condition to obtain the gold complex TBT-Au-PMe_3. All the other metal complexes of the series were synthesized via in-situ deprotection followed my dehydrohalogenation in the same reaction vessel. The TMS protected compound TBT-TMS was reacted with tetra-n-butylammonium fluoride (TBAF) and PPh_3AuCl in piperidine/THF solvent mixture to obtain red colored gold complex TBT-Au-PPh_3. For the synthesis of platinum acetylide complexes, the intermediates 3-4 and 3-5 were synthesized by following literature procedures. The TMS protected ligand was insitu deprotected and reacted with 3-4 and 3-5 to isolate the platinum acetylide complexes TBT-Pt-PBu_3 and TBT-Pt-PMe_3 respectively. The gold(I) complexes were found unstable towards silica gel column chromatography and purified via recrystallization. Both the platinum(II) complexes were purified by silica gel column chromatography and recrystallization from methanol. Apart from TBT-Pt-PBu_3, all the metal complexes were isolated as crystalline solid.

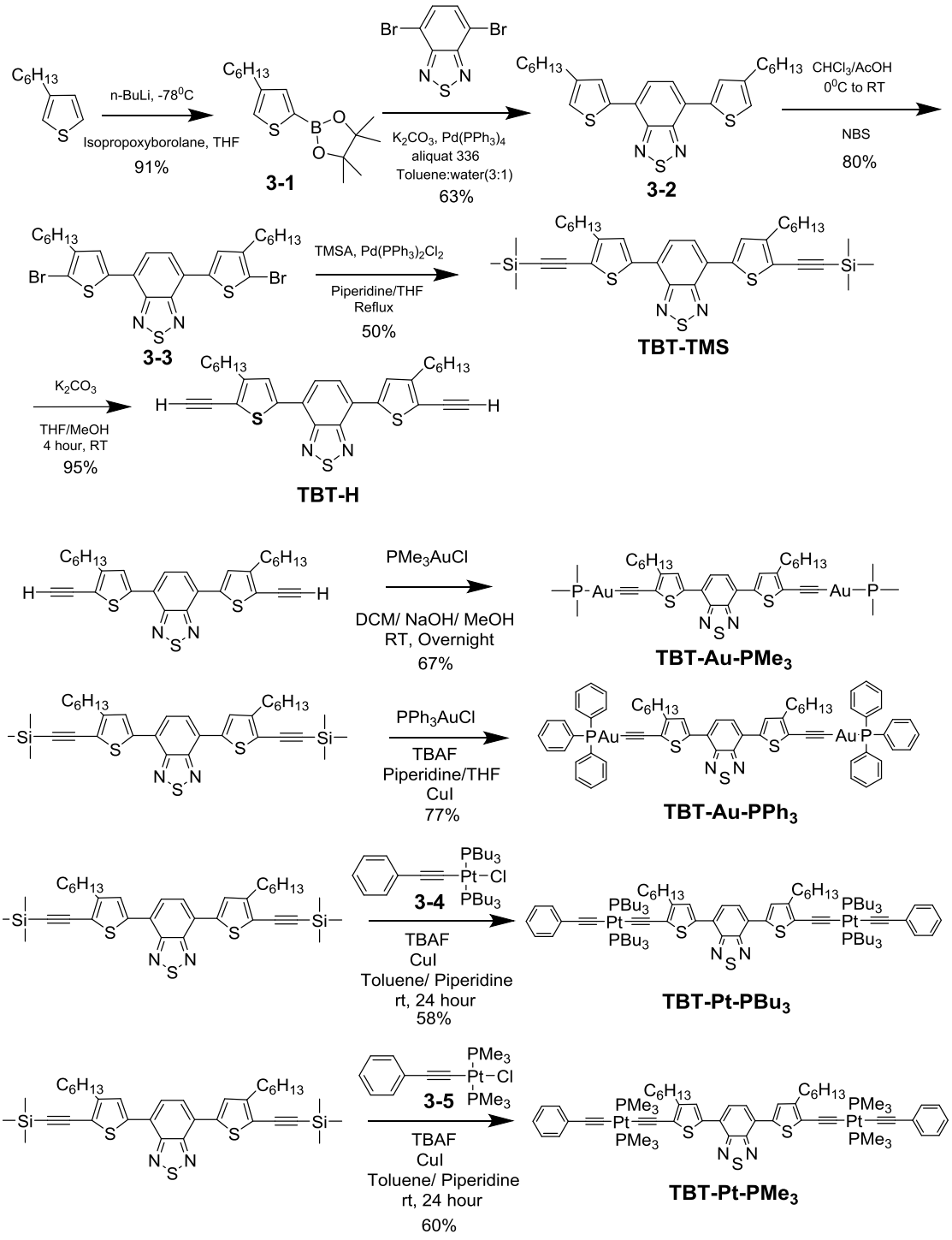

Figure 3-2. The synthetic scheme for acetylide containing TBT chromophores and metal complexes.

Electrochemistry.

In an attempt to identify the effect of heavy metals on the redox properties of TBT, electrochemical studies were performed in dry dichloromethane solvent. In this experiment platinum was used as working and counter electrodes and Ag/Ag^+ as quasi-reference electrode in 0.1 M NBu_4PF_6 electrolyte solution. All potentials were reported with respect to Fc/Fc^+ redox couple and the potential values are listed in Table 3-2. Cyclic voltammograms are presented in Figure 3-3

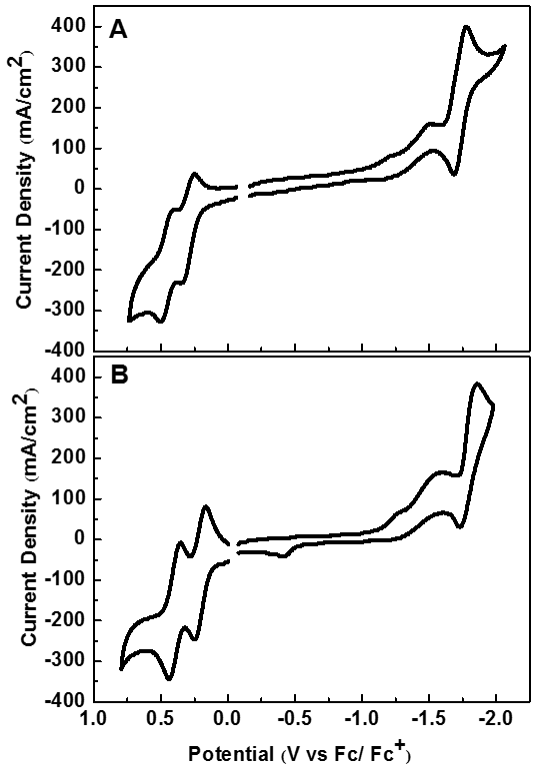

Figure 3-3. Cyclic Voltammograms of the metal complex (A) TBT-Pt-PMe_3 and (B) TBT-Pt-PBu_3 in dichloromethane with 0.1 M TBAPF6 as the supporting electrolyte. It was scanned at 100 mV s^{-1}. All the potentials are referenced to Fc/Fc^+ couple as an internal standard.

In general for the platinum(II) complexes, the CVs exhibit a single reversible reduction wave and two reversible oxidation waves. This feature is similar to the cyclic voltammogram of the TBT unit only, which suggests that all the redox behavior is

centered on the chromophore and the metals have little influence.[25] The oxidation and reduction potential values changed slightly from the previously reported platinum acetylide complexes with similar TBT π-conjugated chromophore but without the hexyl chain substitution at 3-position of thiophene.[25] Small difference in redox potential values is observed between TBT-Pt-PMe_3 and TBT-Pt-PBu_3. Increase in oxidation potential and lower reduction potential for TBT-Pt-PBu_3 compared to TBT-Pt-PMe_3 is probably due to increased electron density in the former by tributylphosphine group. However, the gold(I) complexes gave irreversible behavior in electrochemical measurement which is in accordance with the literature report from Castellano and coworkers on gold(I) containing phenanthroline complexes.[129] The electrochemical band gap was calculated by taking the difference between first oxidation and reduction potential values. Tributylphosphine substituted TBT-Pt-PBu_3 has slightly smaller bandgap compared to TBT-Pt-PMe_3, which is in agreement with the optical absorption studies.

Table 3-1. Electrochemical properties of the platinum complexes.[a]

Compound	$E_{1/2}$/V		$E_{1/2}$/V		ΔE_g ^{Echem}/ eV[b]	ΔE_g ^{opt}/ eV[c]
	Red_1	Red_2	Ox_1	Ox_2		
TBT-Pt-PMe_3	-1.73	-	0.29	0.46	2.02	1.91
TBT-Pt-PBu_3	-1.79	-	0.21	0.40	2.00	1.89

Note: [a] Measured in CH_2Cl_2 using 0.1 M NBu_4PF_6 as supporting electrolyte. It was scanned at 100 mV s^{-1}. All the potentials are referenced to Fc/Fc^+ couple as an internal standard. [b] Electrochemical band gap was calculated by taking the difference between first oxidation potential and reduction potential. [c] Optical band gap was calculated by measuring onset of uv-absorption spectra.

UV-Visible Absorption Spectroscopy.

Ground state absorption spectra of the metal complexes and the ligand TBT-TMS in THF solution are presented in Figure 3-4A. In general the absorption spectra

exhibit two bands which is typical for BTD containing donor-acceptor chromophores.[25,130] The high energy band is due to the π-π* transition of the conjugated backbone and the low energy transition is assigned to the charge transfer transition.[25] It is important to note that, density functional theory (DFT) calculation on these metal complexes predicts the longer wavelength transition is completely due to HOMO→LUMO transition. The molar extinction coefficients (ε) and absorption band maxima (λ_{max}) are provided in Table 3-2.

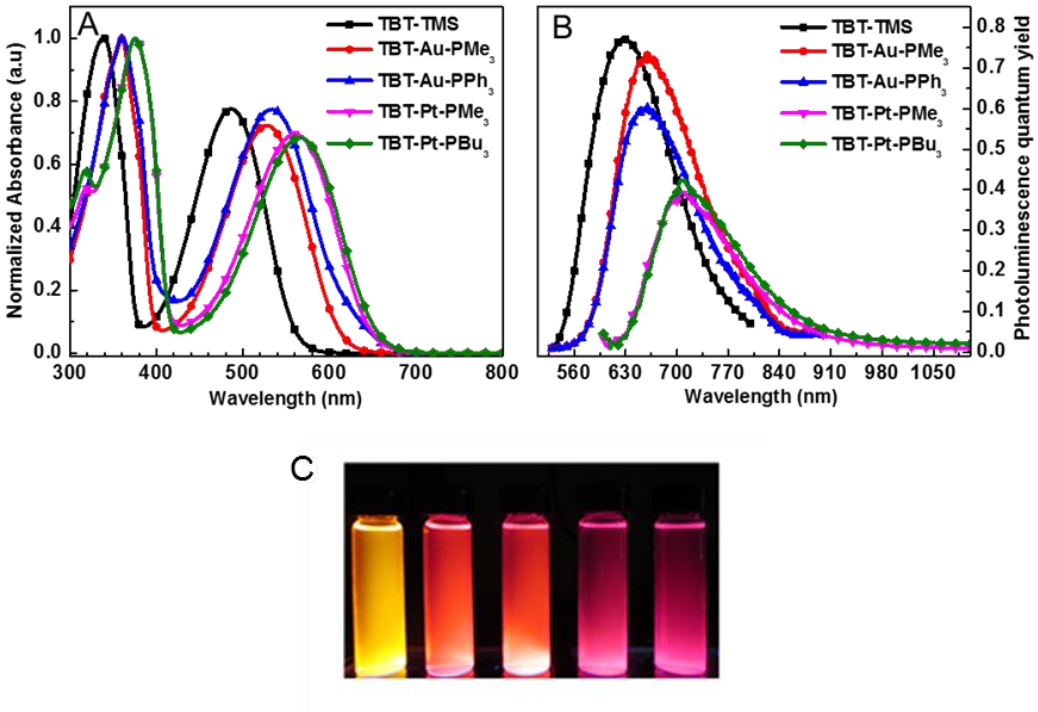

Figure 3-4. The (A) ground state absorption spectra of the metal complexes and ligand in THF solution, (B) photoluminescence spectra of the metal complexes and ligand in THF solution, (C) solution of the metal complexes under uv light, from left to right- TBT-TMS, TBT-Au-PMe_3, TBT-Au-PPh_3, TBT-Pt-PMe_3 and TBT-Pt-PBu_3.

Inspection of the absorption spectra shows that the absorption of the metal complexes is significantly red shifted from the ligand TBT-TMS, suggesting increase in conjugation through mixing of the metal d-orbitals with the π-system of the ligand.[54] This

fact is also supported from the DFT calculations (APPENDIX B). However, there are significant differences across the series. The onset of absorption for the gold complexes TBT-Au-PMe_3 and TBT-Au-PPh_3 is blue shifted compared to the platinum congeners of the series TBT-Pt-PMe_3 and TBT-Pt-PBu_3. This enhanced conjugation for platinum acetylides can be attributed to better orbital overlap of Pt-5d orbitals with conjugated π-orbitals of the ligand[131] and also the DFT calculation provides evidence for contribution of additional terminal acetylide group of the platinum acetylides to the HOMO. For both gold(I) and platinum(II) complexes there are differences observed in absorption spectra at longer wavelength with change in ancillary phosphine ligand. There is 30 nm of red shift in onset of absorption for TBT-Au-PPh_3 in comparison to TBT-Au-PMe_3. On the other hand, the onset of absorption for TBT-Pt-PBu_3 is ~5 nm red shifted compared to TBT-Pt-PMe_3 The difference in electron donating ability of the phosphine ligands alter the charge density in metal-dπ orbitals and hence the extent of pπ-dπ interaction also changes. This fact is an indirect evidence of the contribution of metal to ligand charge transfer (MLCT) character to Th→BTD charge transfer transition of the ligand.

In order to understand the polarity of the ground state, solvent dependent absorption spectra were measured for ligand TBT-TMS and metal complexes TBT-Au-PMe_3, TBT-Pt-PMe_3. The absorption spectra blue shifted with increased polarity of the solvents (Figure 3-5 A, C, E). In general low energy absorption band was more affected by the change in solvent polarity compared to the high energy absorption band, likely due to its charge transfer character. The shift in absorption spectra for the metal complexes are larger compared to the ligand, possibly due to enhanced polarity of the metal complexes in ground state. The gold(I) and platinum(II) metal complexes have

almost the same changes in absorption spectra with change in solvent polarity, suggesting similar change in dipole moment on excitation.

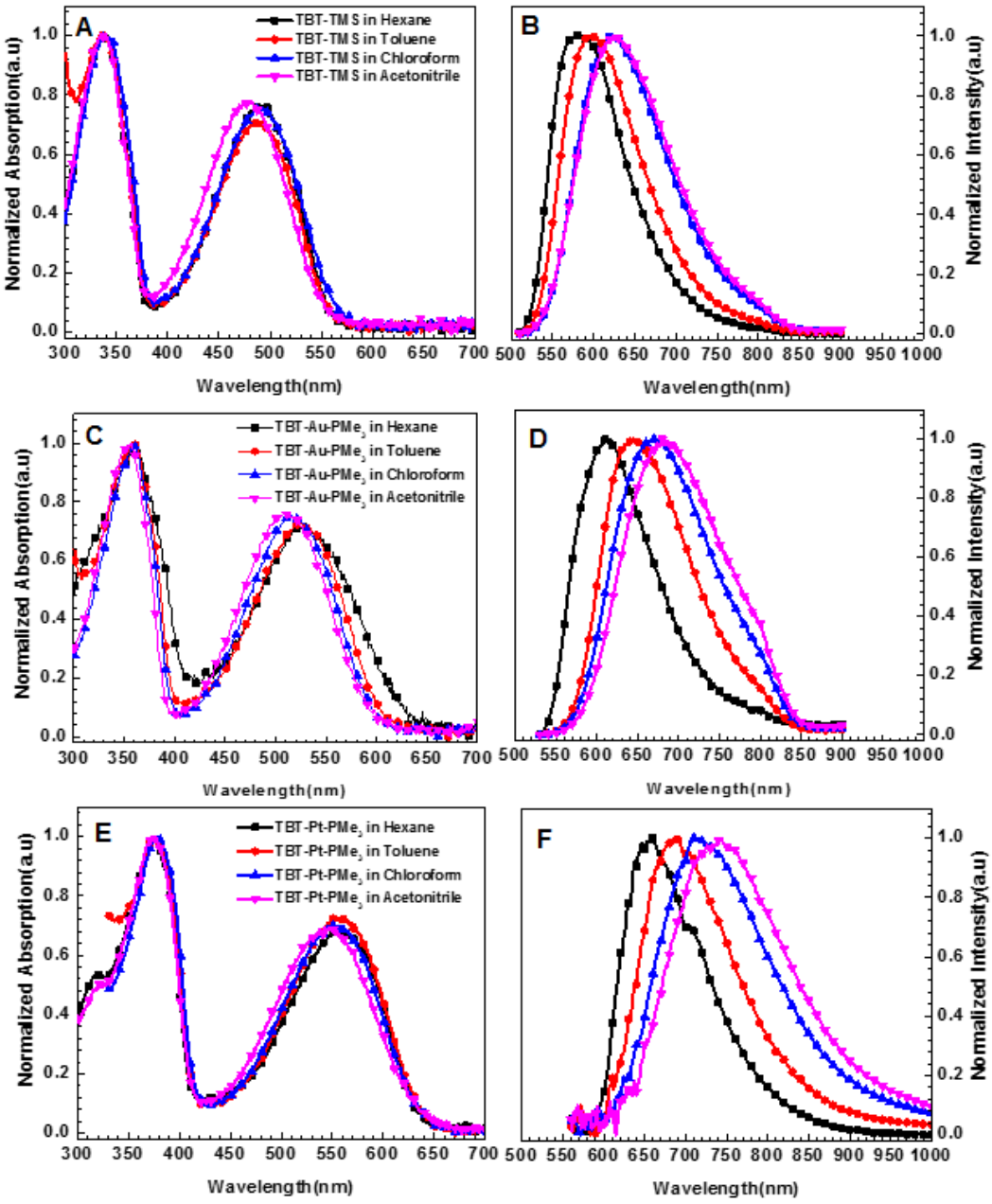

Figure 3-5. Solvent dependent study of ground state absorption (left panel) and emission (right panel) of TBT-TMS (A and B), TBT-Au-PMe_3 (C and D) and TBT-Pt-PMe_3 (E and F).

Steady State Photoluminescence Spectroscopy

The photoluminescence spectra of the ligand and metal complexes were recorded in THF and shown in Figure 3-4B. They all exhibits featureless broad emission band and very small Stokes shift relative to the lowest energy band. This fact along with the emission lifetimes in the order of nanoseconds suggests that emission can be assigned to the fluorescence from lowest singlet excited state. The trend in the emission spectra observed is same as in absorption spectra. Bathochromic shift was observed upon metallation of the ligand TBT-TMS, suggesting enhanced π-conjugation. As expected, the onset of emission is further red shifted for platinum acetylide complexes compared to gold acetylide complexes due to the contribution of both from Pt-5d orbitals and terminal acetylide moiety.

The fluorescence band maxima (λ_{em}), fluorescence quantum yields (ϕ_{fl}) and lifetimes (τ_{fl}) are listed in Table 3-2. All the metal complexes exhibit lower ϕ_{fl} and shorter τ_{fl} compared to the ligand TBT-TMS. In general ϕ_{fl} and τ_{fl} values are higher for gold complexes than the platinum complexes. The radiative rate of decay (k_r) for the metal complexes and ligand are calculated from fluorescence quantum yield and singlet excited state lifetime. In general k_r remains almost the same across the series (~ 10^8 s^{-1}). However the difference in fluorescence quantum yield of the metal complexes with the ligand suggests an alternative non-radiative pathway is in effect. We suggest, this is due to intersystem crossing from $S_1 \rightarrow T_1$ excited state. If we assume the non-radiative decay from $S_1 \rightarrow S_0$ remains same for the metal complexes and ligand, then it is possible to estimate the rate of intersystem crossing (k_{isc}) and quantum yield of intersystem crossing efficiency (ϕ_{isc}). The gold complexes have k_{isc} values in the order of ~10^6 s^{-1}

whereas the platinum complexes populate the triplet excited state 3-4 times faster with a rate in the order of (~10^7). Overall platinum complexes have significantly higher ϕ_{isc} values compared to the gold complexes indicating intersystem crossing is less efficient in gold(I) congeners compared to platinum(II) congeners which is in accordance with the previous literature reports.[20,128]

The emission maxima exhibit a bathochromic shift as the solvent polarity increases. Compared to the ground state absorption spectra, a greater change is observed in the emission profile for the metal complexes and ligands in response to the change in solvent polarity which is in accordance with the literature about BTD containing donor-acceptor chromophores.[132] This is possibly due to direct excitation of the ground state chromophores to less polar Frank-Condon excited state and then non-radiative decay to the more polar charge transfer excited state from where the emission occurs.[133] Excited state dipole moments (μ_e) of these set of chromophores were estimated by using Lippart-Mataga equation,

$$v_a - v_f = \left[2\left(\mu_e - \mu_g\right)^2 \Delta f\right](hca^3) + Constant \qquad (3\text{-}1)$$

Where,

$$\Delta f \cong \left[\frac{\varepsilon - 1}{2\epsilon + 1} + \frac{n^2 - 1}{2n^2 + 1}\right] \qquad (3\text{-}2)$$

The Stokes shift ($v_a - v_f = \bar{\nu}$) is plotted with solvent orientation polarizability (Δf) of different solvents. The ground state dipole moments (μ_g) of the ligand and the metal complexes were estimated from DFT calculations performed in gas phase (0.18 D for TBT-TMS, 9.62 D for TBT-Au-PMe_3 and 18.6 D for TBT-Pt-PMe_3). The effective radii of Onsager cavity (a) for the metal complexes were estimated by calculating molecular dimensions from DFT (6.2 Å for TBT-TMS, 6.6 Å for TBT-Au-PMe_3 and 7.4 Å for TBT-

Pt-PMe_3). From the slope of the linear plot along with the estimated value of Onsager cavity (a), the difference in dipole moment between ground and excited state is estimated. In general the positive values of $\mu_e - \mu_g$ suggests the increased dipole moments in excited state which made them more responsive towards the change in solvent polarity. Compared to the ground state both the metal complexes and ligand have higher dipole moment values in excited state (11.2 D for TBT-TMS, 23.6 D for TBT-Au-PMe_3 and 34.6 D for TBT-Pt-PMe_3). The trend in polarity of the molecules (TBT-TMS < TBT-Au-PMe_3 < TBT-Pt-PMe_3) remains same both in ground and excited states.

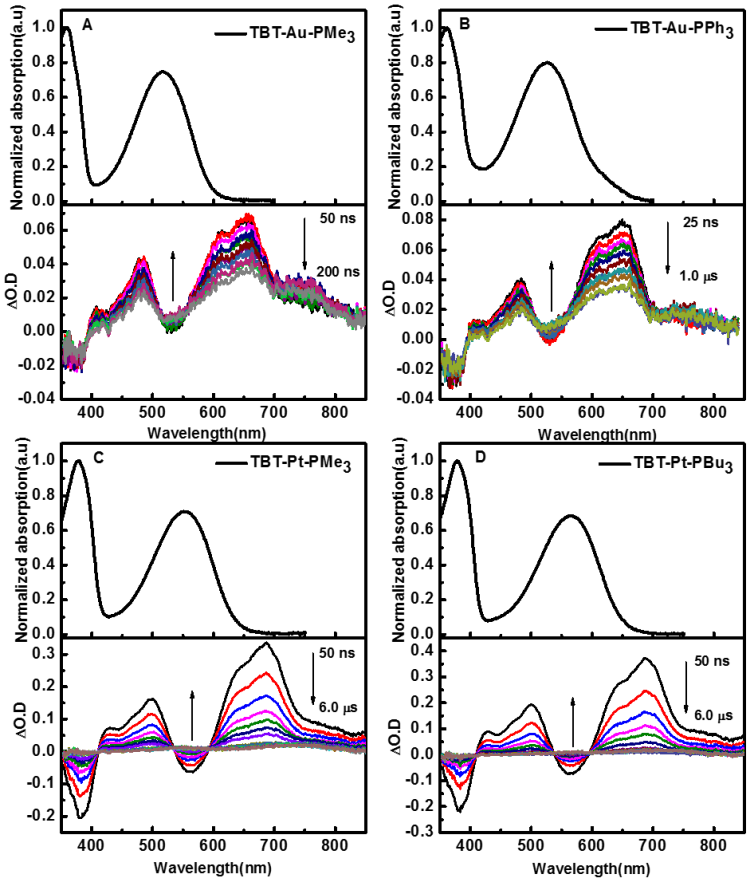

Figure 3-6. Ground state absorption (top panels) and transient absorption spectra (bottom panels) of the metal complexes. Transient absorption spectra obtained in deoxygenated THF solution with λ_{exc} of 355 nm.

Nanosecond Transient Absorption Spectroscopy

As phosphorescence was not observed from the metal complexes and thus nanosecond transient absorption spectroscopy was performed in THF, seeking evidence of triplet excited state population. Figure 3-6 shows the transient absorption of the metal complexes (bottom panel) along with their ground state absorption spectra (top panel). In general all of the transient absorption spectra consist of a broad absorption band at 600 - 800 nm region with strong bleaching at the ground state absorption band. All of the transients are quenched by molecular oxygen, suggesting their assignment to long-lived triplet excited state. There was no evidence of triplet – triplet absorption observed for the ligand TBT-TMS. Several important points emerge on careful inspection of the spectra.

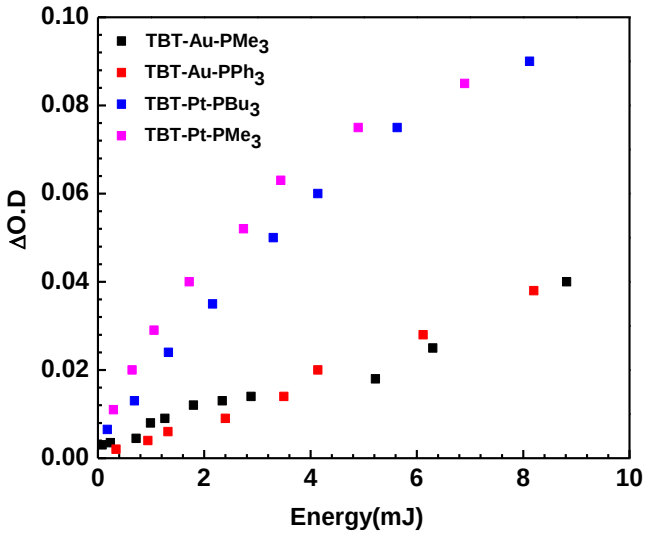

Figure 3-7. Energy dependent transient absorption study of the metal complexes at 480 nm.

The intensity of the signal for gold(I) congeners are in general 4~5 times lower compared to platinum(II) congener. As the experiment is performed with sample

solutions of matched absorbance and with the same laser power, this result clearly suggests gold(I) complexes have significantly lower triplet yield compared to the platinum(II) complexes.

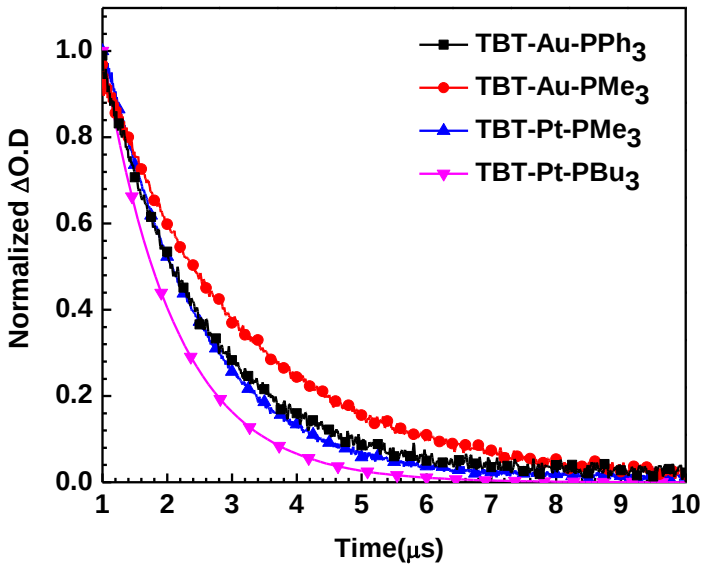

Figure 3-8. Lifetime of the triplet excited state of the metal complexes at 480 nm after excitation at 355 nm in deoxygenated THF solution.

Energy dependent transient absorption study of the metal complexes is performed at 480 nm (Figure 3-7). It is evident from the slope of the ΔO.D vs energy (mJ) plot that the intersystem crossing efficiencies for the platinum complexes is ≈ 3-4 times higher compared to the gold complexes, and this fact is in accordance with the estimated values of k_{isc} and ϕ_{ISC}. In order to measure the triplet excited lifetime of the metal complexes single wavelength transient absorption spectra are measured at 480 nm (Figure 3-8). Gold(I) complexes have slightly longer triplet state lifetime compared to the platinum(II) complexes, possibly due to slow $T_1 \rightarrow S_0$ intersystem crossing process.

Singlet oxygen sensitization experiment is an indirect evidence of triplet excited state population by monitoring the phosphorescence from singlet oxygen at 1270 nm. All of the materials sensitized the formation of singlet oxygen in deuterated benzene

solutions and the quantum yield (ϕ_Δ) varies in the series TBT-Pt-PMe_3> TBT-Pt-PBu_3> TBT-Au-PPh_3> TBT-Au-PMe_3 (Table 3-2). The singlet oxygen quantum yields are consistent with triplet excited state population, as platinum(II) congeners being more efficient in intersystem crossing, are in general shows higher quantum yields compared to gold(I) congeners. Although, the triplet excited state lifetime of TBT-Au-PPh_3 is longer compared to TBT-Au-PMe_3, due to efficient intersystem crossing yield in the former, the singlet oxygen quantum yield is higher for TBT-Au-PPh_3 in comparison with TBT-Au-PMe_3.

Two Photon Absorption Spectroscopy

In order to assess two photon cross sections, the THF solutions of these metal complexes and ligand were excited by Ti-Sapphire pumped oscillator system (pulse duration <100 fs) and presented in Figure 3-9. Relatively high fluorescence quantum yields of these complexes allow to measure two photon absorption by two photon excited fluorescence method (2PEF).[134] All the measurements were performed with air saturated solutions. Normalized one photon absorption spectra are shown in the same plot for comparison. In general there is a significant blue shift of two photon absorption spectra compared to the ground state absorption consistent with the centrosymmetric nature of the molecules.[112,135]

Ligand TBT-TMS has two photon absorption cross section $\sigma_{2PA} \approx 120$ GM in the region close to $S_0 \rightarrow S_1$ one photon transition. The 2PA spectra of the gold(I) metal complexes show a well-defined peak at 780 -800 nm and another broad absorption band at < 775 nm. In general, the 2PA spectra for the gold complexes are slightly red shifted compared to the 2PA spectra of TBT-TMS. This fact can be attributed to the

slight increase in conjugation length mediated by the gold dπ orbitals and this trend is in accordance with the ground state absorption spectra.

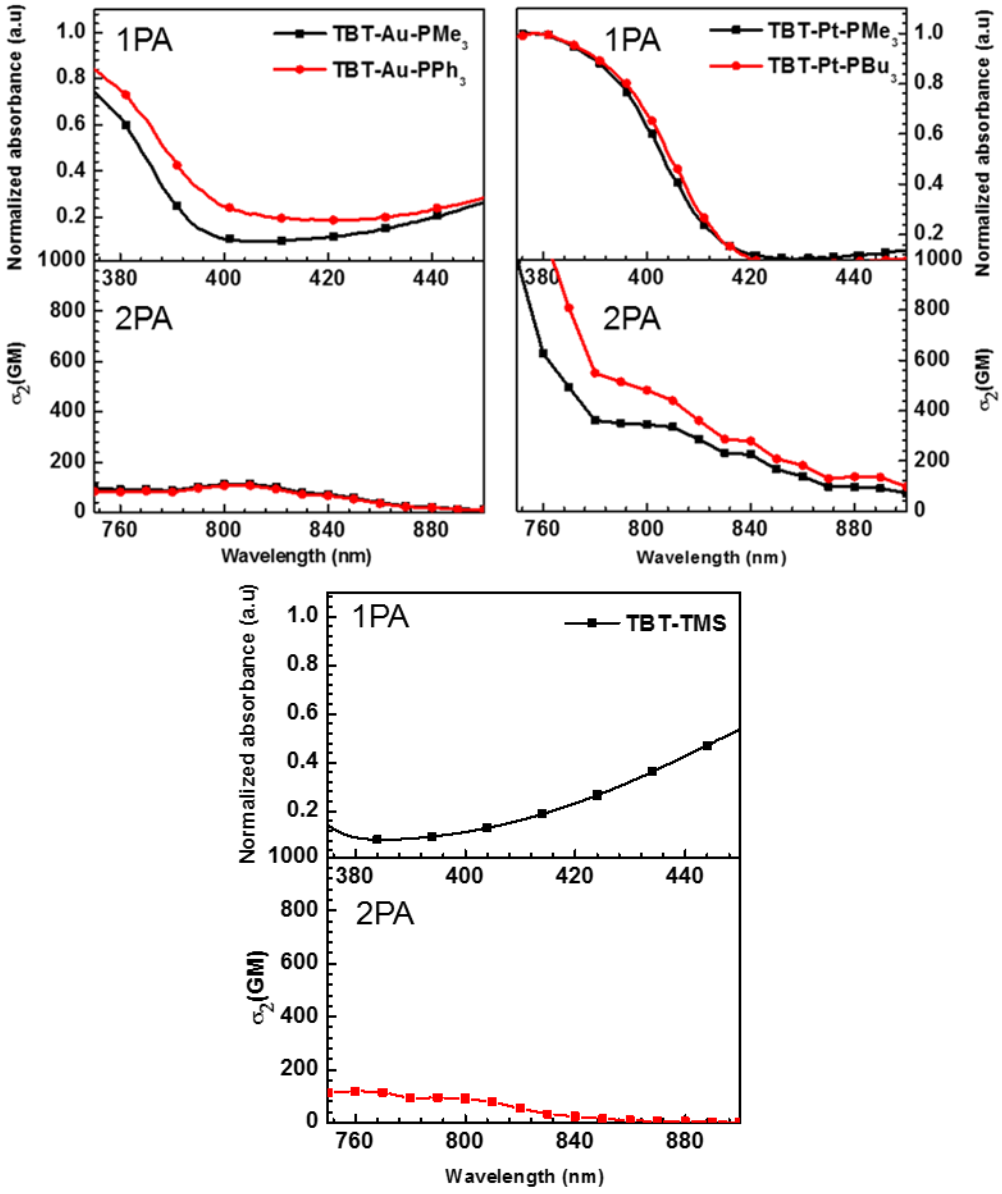

Figure 3-9. Two photon absorption spectra (bottom panel) and one photon absorption spectra (top panel) of the metal complexes and ligand in THF solution. Corresponding wavelengths are in x-axis. Two photon absorption cross section and normalized absorption are shown in the corresponding y-axis.

Table 3-2. Summary of photophysical properties.[a]

Compound	λ_{max} (nm)	ε ($x10^3$) ($M^{-1}cm^{-1}$)	λ_{em} (nm)	ϕ_{fl}[b] (%)	k_r ($x10^8$) (s^{-1})	k_{isc} ($x10^7$) (s^{-1})	ϕ_{isc}	τ_{fl} (ns)	τ_{TA}/ µs	ϕ_{Δ}[c] (%)
TBT-TMS	487	133	628	77	1.0	-	-	7.5	-	-
TBT-Au-PMe_3	519	27	659	73	1.1	1.1	0.10	6.5	2.14	9
TBT-Au-PPh_3	527	30	654	60	1.0	3.3	0.20	6.3	1.54	17
TBT-Pt-PMe_3	555	35	696	39	1.0	11	0.46	4.4	1.43	31
TBT-Pt-PBu_3	566	32,	704	42	1.0	11	0.45	4.3	1.10	26

Note: [a] All the photophysical properties were recorded in tetrahydrofuran; λ_{max} is the absorption maxima, ε is the molar extinction coefficient, λ_{em} is the emission band maxima, ϕ_{fl} is the fluorescence quantum yield, k_r, k_{isc}, and ϕ_{isc} are the rate constant for radiative decay, rate constant for non-radiative decay and the intersystem crossing quantum yield respectively, τ_{fl} and τ_{TA} are the lifetime of fluorescence and triplet excited state respectively, $\phi\Delta$ is the singlet oxygen quantum yield. [b] Fluorescence quantum yield was measured with respect to Rhodamine B as actinometer in absolute ethanol (ϕ_{fl} = 0.49). [c] Singlet oxygen quantum yield was measured in C_6D_6 using terthiophene (Φ_{Δ} = 0.73) as actinometer.

Although, two photon cross section value for gold(I) complexes remain almost the same as ligand TBT-TMS at 780 - 800 nm, they have slightly higher values reaching ≈ 150 GM at shorter wavelength region. Surprisingly, for platinum(II) complexes the 2PA cross section values are 200 - 600 GM at 800 - 900 nm region reaching 1000 GM at < 800 nm. One of the main factors that influence 2PA is transition dipole moment going from the ground state to first excited state (μ_{ge}). The dipole moment for the metal complexes in singlet excited state is calculated from solvent dependent emission spectra by utilizing Lippart-Mataga equation. Enhanced two photon absorption for platinum(II) complexes can be assigned to their larger change in dipole moment upon excitation compared to gold(I) complexes. However very slight differences were observed in 2PA with change in ancillary phosphine ligands..

Discussion

In general heavy atom containing π-conjugated chromophore enhances nonlinear absorption from contribution of both $S_0 \rightarrow S_1$ transition via 2PA and ESA from $T_1 \rightarrow T_n$. However, if the non-linear absorption is measured by using two photon excited fluorescence method, it is possible to isolate the contribution of $S_0 \rightarrow S_1$ 2PA from ESA by using short pulse width lasers. Although Pt(II) is ~4 times efficient in populating triplet excited state in comparison to Au(I), as the 2 PA measurements were performed by 2 PEF method, we believe platinum is inherently able to induce higher 2PA irrespective of the triplet excited state contribution. One of the important factor that contributes to the 2PA in a two level model is change in dipole moment between ground and excited state and it can be expressed by the following equation-

$$\sigma_2 = \frac{2(2\pi)^4 {f_{\text{opt}}}^4}{15(nch)^2}|\mu|^2|\Delta\mu|^2(2\cos^2\theta + 1)g(2\nu_{\text{L}})$$

Where μ and $\Delta\mu$ are transition dipole moment and the difference in permanent dipole moments between ground and excited state respectively.[136] It can be clearly understood from this equation the greater the $\Delta\mu$, the higher the σ_2 value can be achieved. From solvatochromic behavior of gold and platinum acetylide complexes, it was shown that platinum complexes have larger change in dipole moment in excited state than gold complexes and hence higher 2PA cross section values.

Davies and coworkers showed that between gold(I) and ruthenium(II) acetylide complexes, the later shows 3-5 times higher quadratic nonlinearity and this was attributed to the electron rich nature of ruthenium.[137] In similar line, one possible reason for higher change in dipole moment for platinum complexes is its electron rich nature (16 electron) compared to gold (14 electron) center. Jia and coworkers reported a family of trimetallic acetylide complexes based on triazine core with gold(I) and ruthenium(II).[138] The ruthenium complexes were found to have red shifted absorption compared to gold complexes. They have shown the HOMO was less influenced by gold nonbonding d-orbitals because of their low energy, however, ruthenium d-orbitals are situated above the HOMO energy level and significant orbital mixing provides extensive conjugation. From the DFT calculations on TBT-Pt-PMe_3 and gold(I) complexes, it was observed that gold d orbitals have less contribution in HOMO in comparison to platinum d-orbitals (APPENDIX B).

Unlike other transition metals gold(I) undergoes further stabilization of filled $5d_z^2$ orbital when it mixes with 6s orbital due to their low energy gap and produce two hybrid

orbitals (see below). This high s orbital content of the frontier orbital makes it isolobal with proton.[139] We anticipate, this could be another reason of less conjugation in gold(I) complexes in comparison to platinum complexes as Au(I) behaves like a H^+ only.

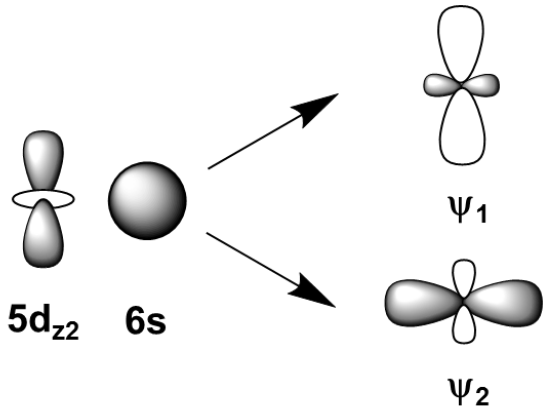

Figure 3-10. Hybridization of $5d_z^2$ and 6s orbital of gold (I).

Another striking difference observed between gold(I) and platinum(II) complexes is in their quantum yield of intersystem crossing (ϕ_{ISC}). The enhanced triplet-triplet absorption for platinum complexes is also supported by TD-DFT calculations. The major transition involved in transient absorption is from singly occupied HSOMO→LUMO+1 and to higher energy LUMOs. HSOMO has more metal orbital contribution for platinum complexes compared to gold complexes. In order to show the charge distribution in the triplet excited state, charge difference density (CDD) diagrams were constructed for these metal complexes (APPENDIX B). Compared to gold(I), platinum(II) donates significant amount of electron density to the electron deficient part of the molecule. However, there is no significant difference observed for different phosphine ancillary ligands for both gold(I) and platinum(II) complexes.

Summary and Conclusions

In this work, the synthesis of a series of four donor-acceptor organometallic complexes was carried out. In an attempt to study the impact on triplet excited properties and 2PA influenced by different heavy metals, Au(I) and Pt(II) “auxochromes” were appended at the terminal position of ligand TBT-TMS. The photophysical results clearly demonstrates the effect of platinum in populating the triplet excited state more efficiently. The ground state absorption spectra exhibits a very slight bathochromic shift for gold(I) complexes compared to platinum(II) complexes, supporting the concept of isolobal relation of $Au(I)^+$ with H^+.[139] We have also demonstrated the effect of ancillary phosphine ligands on photophysical properties and proved their contribution to the overall charge transfer character of these complexes. Enhanced solvatochromic response of the metal complexes in emission spectra suggests their increased polar character in excited state compared to ground state. Strong nanosecond transient absorption signal of the platinum complexes validates efficient mixing of platinum dπ orbitals with pπ orbitals of the ligand and hence strong spin-orbit coupling. In an effect to estimate the comparative rate of ISC of these metal complexes, nanosecond transient absorption spectroscopy was performed with varying the laser power. The slope of the change in optical density vs laser power suggests, platinum complexes populating the triplet excited states at 4 times faster rate than the gold complexes.

While the gold complexes have almost similar two photon absorption cross sectional values as TBT-TMS, significantly higher cross sectional values for platinum complexes proved the importance transition metals in nonlinear absorption. This study will help in understanding the importance of selection of heavy metals in manipulating the triplet excited states as well as two photon absorption behavior.

Experimental Section

Instrumentation and Methods

All the NMR spectra were recorded by using an INOVA 500 FT-NMR operating at 500 MHz for ^{1}H NMR, operating at 125 MHz for ^{13}C NMR and Mercury-300 FT-NMR operating at 75.4 MHz for ^{13}C NMR. The mass spectral analysis for the newly synthesized complexes were recorded in Mass Spectrometry services at University of Florida.

Photophysical Measurements were performed with dry and HPLC grade tetrahydrofuran (THF) in a 1 X 1 cm^2 quartz cuvettes unless otherwise noted. All the solutions for photophysical characterizations were prepared by diluting a stock solution unless otherwise mentioned. Ground state UV-Visible absorption spectra were obtained by a Shimadzu UV-1800 dual beam spectrophotometer. Corrected room temperature emission spectra were obtained in a Photon Technology International (PTI) spectrophotometer and collected at 90° relative to the excitation beam. The absorptivity of the solutions for fluorescence quantum yield and molar extinction coefficient were kept within $\leq$0.1. Refractive index corrections for solvents were employed for fluorescence quantum yield calculations for both sample and standard solutions. Fluorescence lifetimes were recorded with a PicoQuant FluoTime 100 Compact Fluorescence Lifetime Spectrophotometer using time-correlated single photon counting (TCSPC) instrument. The sample solutions were excited with a PDL-800B Picosecond Pulsed Laser (375 nm) and the concentration was kept at ~ 0.1.

Nanosecond transient absorption spectroscopy was performed on a home-built instrument using the third harmonic of a Continuum Surelite series Nd:YAG laser (λ_{exc}=

355 nm, 10 ns FWHM, 7 mJ per pulse). Probe light for this pump-probe spectroscopy was produced by a xenon flash lamp, and the signal was detected with a gated-intensified CCD mounted on a 0.18 M spectrograph (Princeton PiMax/Acton Pro 180). The concentration of the sample solutions were adjusted to O.D. ≈ 0.7 at 355 nm wavelength and deoxygenated with argon for 45 minutes to 1 hour before the measurement. The solutions were taken in 1 cm path length flow cell (10 mL) and continuously circulated at the pump-probe region during the experiment.

The cyclic voltammetry (CV) study of the samples were obtained from a BAS CV-50W voltammetric analyzer (Bioanalytical Systems, Inc., www.bioanalytical.com) in dry and freshly distilled dichloromethane (CH_2Cl_2) solution in the presence of 0.1 M tetra-n-butylammonium hexafluorophosphate ($TBAPF_6$) as electrolyte. Three electrodes were used during the measurement, a platinum microdisk (2 mm^2) as the working electrode, a platinum wire as the auxiliary electrode and a silver wire as the reference electrode. The sample concentration was adjusted 1 mM and the sweep rate was maintained at 100 mV/s. A positive pressure of argon was maintained during the measurement. All the electrochemical potential obtained are calibrated with respect to a ferrocene internal standard (E(Fc/Fc+) = 0.43 V vs SCE in CH_2Cl_2).

For two photon absorption, a Millenia eV laser (2nd harmonic of Nd:YAG, 532 nm) was used to pump a Spectra-Physics Tsunami femtosecond Ti:Sapphire laser with a repetition rate of 80 MHz. The output of the Ti:Sapphire laser was tuned to 980 nm, had pulse widths of < 100 fs,and had a power of 375 mW. Steady-state emission spectra were collected on a Fluoromax-3 spectrophotometer.

All calculations were carried out using DFT as implemented in Gaussian 09[1] Rev. C.01. Geometries were optimized using the B3LYP functional along with the 6-31G(d) basis set for C, H, N, the 6-31+G(d) basis set for P, S, and the SDD basis set for Au, Pt. To minimize computational cost, solubilizing butyl moieties were replaced with methyl groups, and thiophene hexyl groups were replaced by hydrogen. Thus only one Pt complex was computed, as they only differed in length of the solubilizing alkyl chains. These models are designated by the addition of a prime (') to their name, thus the model for PtMe is termed as PtMe'. All singlet optimizations were started from idealized geometries without symmetry constraints. Triplet optimizations were started from the optimized singlet geometry and used the unrestricted B3LYP functional. All optimized structures were characterized by vibrational frequency calculations and were shown to be minima by the absence of imaginary frequencies. Time-dependent DFT calculations were performed for all optimized structures at the same level of theory with the same basis sets. Structures and orbitals were visualized using Chemcraft Version 1.7,[2] which was also used to generate charge difference density plots

General Methods for Synthesis

All the reactions were performed under an argon atmosphere unless mentioned. THF and toluene were dried using solvent purification columns (Glass contour) under argon atmosphere. The starting material 3-Hexylthiophene was purchased from Sigma Aldrich. Bis(triphenylphosphine)palladium(II)dichloride, Tetrakis(triphenylphosphine)palladium(0), Chloro(trimethylphosphine)gold(I) were purchased from Strem Chemicals. Trimethylsilyl acetylene was obtained from GFS chemical and used as received. The intermediate for the reactions, 3-1, 3-2, 3-3, 4,7-

Dibromobenzo[c]-1,2,5-thiadiazole,[140] 3-4 [118]and 3-5[141] were synthesized by following literature procedure.

Synthesis

Synthesis of TBT-TMS

In a 50 mL Schlenk flask, a mixture of 3-3 (605 mg, 0.965 mmol), $Pd(PPh_3)_2Cl_2$ (13.5 mg, 0.019 mmol) and CuI (7.4 mg, 0.04 mmol) were combined and vacuum-argon cycled for three times. A deoxygenated mixture of THF/piperidine (15 mL, 4:1) was added to the reaction mixture under argon atmosphere. Trimethylsilyl acetylene (TMSA) (470 mg, 4.78 mmol) was added promptly to the reaction mixture via syringe and heated to 60˚C overnight under an argon atmosphere. The solvents were removed under vacuum and the crude product was purified by column chromatography on silica with hexane/ dichloromethane (9:1) as eluent. The product was isolated as dark red solid in 50% yield. ^{1}H NMR (500 MHz, $CDCl_3$): δ 7.88 (s, 1H), δ 7.77 (s, 1H), δ 2.78 (t, 2H, J= 7.6 Hz), δ 1.82-1.68 (m, 2H), δ 1.48-1.32 (m, 6H), δ 0.94 (t, 3H, J= 6.6 Hz), δ 0.31 (s, 9H). ^{13}C NMR (125 MHz, $CDCl_3$, δ): 152.40, 149.66, 138.78, 128.46, 125.54, 125.42, 119.91, 103.04, 97.60, 31.61, 30.10, 29.73, 28.98, 22.63, 14.12.

Synthesis of TBT-H

In a 100 mL round bottom flask TBT-TMS (125 mg, 0.19 mmol) was dissolved in 20 mL of THF/MeOH (1:1) solvent mixture and deoxygenated by bubbling with argon for 30 minutes. Finely grounded K_2CO_3 (105 mg, 0.76 mmol) was added to the reaction mixture under argon atmosphere and stirred for 4 hours at room temperature shielded from light with aluminum foil. After TBT-TMS was consumed, the solvents were evaporated under vacuum. The crude product was dissolved in dichloromethane and washed with water three times and brine one time. The combined organic phase was

dried over anhydrous Na_2SO_4, filtered and evaporated under vacuum to obtain the product as red solid in 95 % yield. ^{1}H NMR (500 MHz, $CDCl_3$): δ 7.86 (s, 1H), δ 7.79 (s, 1H), δ 3.55 (s, 1H), δ 2.74 (m, 2H), δ 1.67 (m, 2H), δ 1.32 (m, 6H), δ 0.86 (t, J= 7.0 Hz, 3H).

Synthesis of TBT-Au-PMe_3

In a 100 mL round bottom flask TBT-H (80 mg, 0.15 mmol) was dissolved in 15 mL of distilled dichloromethane and 7.26 mL of NaOMe (Prepared from dissolving 42.7 mg of NaOH in 25 mL of MeOH) was added to the reaction mixture. The dark orange solution was deoxygenated with argon for 30 minutes. In a mixture of 20 mL dichloromethane/methanol (1:3), PMe_3AuCl (0.31 mmol) was dissolved and added to the reaction mixture promptly under argon atmosphere. The reaction mixture changed color from dark orange to wine red. It was stirred overnight under an argon atmosphere at room temperature, protecting from light with aluminum foil. The solvents were evaporated under vacuum. The crude product was dissolved in DCM and passed through a cotton plug to remove any insoluble impurities. The solvents were evaporated and the crude product was recrystallized from DCM/ diethyl ether solvent mixture to obtain the product as purple shiny solid in 67% yield. ^{1}H NMR (500 MHz, $CDCl_3$): δ 7.93 (s, 1H), δ 7.72 (s, 1H), δ 2.80 (m, 2H), δ 1.72 (m, 2H), δ 1.54 (d, J= 10 Hz, 9H), δ 1.34 (m, 6H), δ 0.89 (t, J= 6.7 Hz, 3H). ^{13}C NMR (125 MHz, $CDCl_3$, δ): 152.62, 147.34, 136.79, 128.68, 125.52, 125.32, 125.01, 96.42, 31.80, 30.24, 29.79, 29.18, 22.70, 15.91, 15.62, 14.22. ^{31}P NMR (121 MHz, CDCl3) δ (ppm): 0.80. HRMS (APCI, [M+H] +) m/z calcd for C36H48Au2N2P2S3 1061.85, found 1061.19.

Synthesis of TBT-Au-PPh_3

In a 100 mL round bottom flask TBT-TMS (27 mg, 0.041 mmol) was taken and dissolved in 10 mL of previously deoxygenated THF/piperidine (1:1) solvent mixture. After that PPh_3AuCl (40.6 mg, 0.082 mmol) and CuI (1.44 mg, 0.0076 mmol) were added to the reaction mixture under argon atmosphere subsequently. After that TBAF (1M in THF, 0.15 mL, and 0.15 mmol) was added to the reaction mixture and immediately the color changed from orange to dark red. The residue was washed with deionized water several times. The crude product was dissolved in minimal amount of DCM and excess amount of methanol was added to it. The dark red precipitate formed was isolated by vacuum filtration and washed with copious amount of methanol to obtain the product in 77% yield. ^{1}H NMR (500 MHz, $CDCl_3$): δ 7.93 (s, 1H), δ 7.70 (s, 1H), δ 7.45 (m, 15 H), δ 2.80 (t, J= 7.7 Hz, 2H), δ 1.60 (m, 2H), δ 1.31 (m, 6H), δ 0.85 (t, J=6.7 Hz, 3H). ^{13}C NMR (125 MHz, $CDCl_3$, δ): 152.58, 147.55, 136.97, 134.27, 134.22, 131.58, 128.70, 31.79, 30.25, 29.81, 29.17, 22.69, 14.21 (the acetylene carbons were not seen here). ^{31}P NMR (121 MHz, $CDCl_3$) δ (ppm): 42.13. HRMS (APCI, [M+H]+) m/z calcd for C66H60Au2N2P2S3 1433.2798, found 1433.2785.

Synthesis of TBT-Pt-PBu_3

In a round bottom flask, TBT-TMS (53 mg, 0.080 mmol) and 3-4 (130 mg, 0.18 mmol) were taken and dissolved in previously deoxygenated 10 mL piperidine/ toluene (1:1) solvent mixture. After that CuI (4 mg, 0.021 mmol) and TBAF (1M in THF, 0.32 mL, 0.32 mmol) were added to the reaction mixture subsequently under argon atmosphere. The color of the reaction mixture immediately changed from orange to dark purple. It was left stirring overnight under argon atmosphere. Silica gel was added to the reaction mixture and solvents were evaporated under vacuum. The crude product was purified

by column chromatography on silica with dichloromethane/ hexane as eluent. The product was isolated as dark purple viscous oil in 58% yield. Subsequent recrystallization with methanol failed to give solid product. ^{1}H NMR (500 MHz, $CDCl_3$): δ 7.92 (s, 1H), δ 7.67 (s, 1H), δ 7.29-7.08 (m, 5H), δ 2.72 (t, J= 7.6 Hz, 2H), δ 2.15 (m, 12H), δ 1.61 (m, 14 H), δ 1.51-1.41 (m, 12 H), δ 1.34 (m, 6H), δ 0.96-0.88 (m, 21 H). ^{13}C NMR (125 MHz, $CDCl_3$, δ): 152.78, 143.33, 134.47, 130.80, 129.01, 128.74, 127.86, 126.53, 125.30, 124.87, 124.72, 120.23, 109.32, 107.66, 101.06, 31.98, 30.62, 29.92, 29.47, 26.43, 24.41, 23.88, 22.77, 14.18, 13.91. ^{31}P NMR (121 MHz, $CDCl_3$) δ (ppm): 3.25 (J_{Pt-P} = 2349.8 Hz). HRMS (MALDI, M+) m/z calcd for C94H148N2P4Pt2S3 1915.9025, found 1915. 9061.

Synthesis of TBT-Pt-PMe$_3$

Compound TBT-TMS (31 mg, 0.046 mmol) and 3-5 were dissolved in deoxygenated piperidine/toluene (10 mL, 1:1) solvent mixture. After that CuI (3 mg, 0.012 mmol) and TBAF (1M in THF, 0.2 mL, 0.2 mmol) were added to the reaction mixture. The purple colored solution was left stirring over night at room temperature under argon atmosphere. Silica gel was added to the reaction mixture and the solvents were evaporated under vacuum. The crude product was purified by column chromatography on silica gel with hexane/ethyl acetate eluent and then recrystallized with methanol to obtain the product as purple crystalline solid in 60% yield. ^{1}H NMR (500 MHz, $CDCl_3$): δ 7.93 (s, 1H), δ 7.71 (s, 1H), δ 7.36 (m, 2H), δ 7.25 (t, J= 7.5 Hz, 2H), δ 7.17 (m, 1H), δ 2.75 (m, 2H), δ 1.83-1.71 (m, 20H), δ 1.35 (m, 6H), δ 0.92 (t, J= 6.8 Hz, 3H). ^{13}C NMR (125 MHz, $CDCl_3$, δ): 152.69, 144.40, 135.10, 131.06, 128.85, 127.97, 125.59, 125.34, 124.89, 109.25, 100.47, 31.87, 30.62, 29.99, 29.43, 22.70,

15.57, 14.17. ^{31}P NMR (121 MHz, $CDCl_3$) δ (ppm): -20.52 (J_{Pt-P} = 2289.32 Hz). HRMS (MALDI, M+) m/z calcd for C58H76N2P4Pt2S3 1411.3429, found 1411.3420.

CHAPTER 4
POLYSTYRENE BASED ARRAYS OF PI-CONJUGATED ORGANOMETALLIC CHROMOPHORES: TWO PHOTON LIGHT HARVESTING ASSEMBLIES

Background

Two photon absorption (2PA) has been the forefront of research for decades since its invention in 1930s[28] due to its application in several fields, including optical power limiting material,[39,83,85,142] three dimensional data storage,[143-145] biological imaging,[31,146] and photodynamic therapy.[86] Platinum(II) containing organometallic π-conjugated chromophores are an important class of materials because of the accessibility of "dual mode" nonlinear pathway and high 2PA cross section in these materials.[18] The "dual mode" pathway comprises excitation of chromophores from ground state to singlet excited state by two photon absorption, followed by intersystem crossing (ISC) to triplet excited state (T_1) facilitated by heavy atom platinum, which then undergoes $T_1 \rightarrow T_n$ absorption. In order to increase the processibility of platinum acetylide containing materials, polymers are advantageous over small molecules because of their inherent ability to cast films. However, compared to small molecules there have been limited number of studies on platinum acetylide polymers or incorporation of platinum acetylide monomers in polymer matrix, for 2PA.[147,148] Wong and coworkers have examined a series of platinum acetylide polymers based in fluorene, carbazole, thiazole and compared their optical power limiting property with their non-metallated version.[102] To compare the triplet excited state property of different heavy metals, our group reported a platinum acetylide polymer based on π-conjugated thienyl carbazole system.[128] Attempt has been made to incorporate the small molecules into poly(methyl methacrylate) (PMMA) matrix to process them into films for optical power limiting property by Malmström and co-workers.[83]

While π-conjugated polymers impart several advantages, conformational disorders create traps in the polymer chains which can significantly reduce the exciton delocalization. Our group reported a series of PMMA non-conjugated copolymers grafted with platinum acetylide containing two photon absorbing chromophores via free radical polymerization.[149] However, the maximum loading of chromophores achieved in that process was 12%. “Energy transfer” have been one of the most efficient way of harvesting the light energy since its inception in 1969.[150] The ability to graft multiple chromophores (donor = D, acceptor = A) in varying ratio to the non-conjugated polymer backbone allows to unravel energy transfer mechanism in more detail. Recently Schubert and co-workers reported a series of polymers featuring PMMA based backbone and oligo(phenylene ethynylene) (OPE) as pendant chromophores.[151] Singlet-singlet and triplet-triplet energy transfer has been reported recently from our group based on non-conjugated polystyrene backbone.[152,153]

The objective of the present study is to investigate the energy transfer from singlet to triplet excited state in a non-conjugated polymer backbone and utilize this phenomenon for two photon absorption. Previous studies have shown that 4-(diphenylamino)fluorene (DPAF) is an effective chromophore for non-linear absorption phenomena.[18,60] In presence of platinum, it can exhibit 2PA in 600 - 800 nm region with cross section values 100 - 200 GM via “dual mode” pathway. Thus, we have selected this chromophore unit to attach to the non-conjugated polystyrene backbone via “click chemistry” to generate a series of polymers and the model complex is synthesized for comparative study with polymers. The analytical purity of the polymers is characterized by ^{1}H NMR, IR and gel-permeation chromatography (GPC). The photophysical property

of these polymers as well as the model complex are studied by steady state absorption, emission, nanosecond and femtosecond transient absorption spectroscopy, two photon excited photoluminescence spectroscopy. The results presented here clearly demonstrate the polymers with platinum show efficient energy transfer from singlet to triplet excited state and their utility as efficient two photon absorbing material.

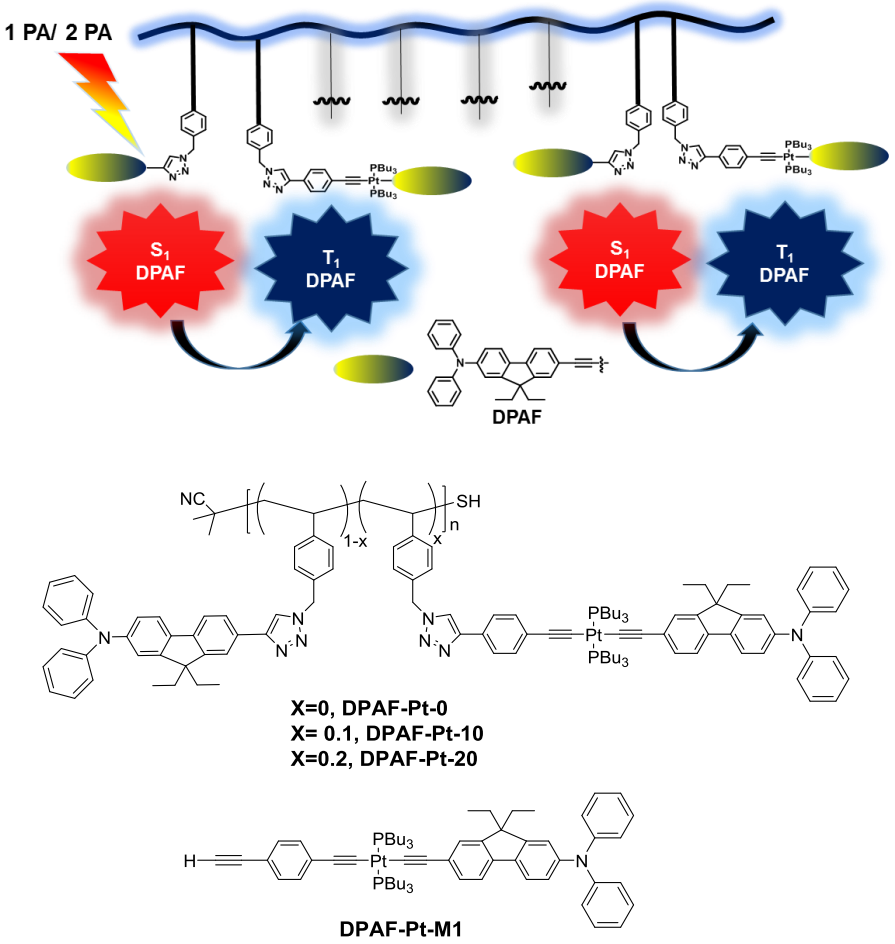

Figure 4-1. The cartoon showing energy transfer in the polymer and chemical structures of the polymers and the model complex discussed herein.

Results and Discussion

Design Strategy and Synthesis of Polymers

The structure of the polymers and the model platinum complex are shown in Figure 4-1. These polymers feature an atactic polystyrene backbone, grafted with two

pendant π-conjugated chromophores where non-metallated DPAF acts as energy donor and metallated DPAF acts as acceptor. As mentioned before, DPAF chromophore is selected because of its efficient 2PA properties. The design strategy for these polymers was to dilute the number of platinum centers in the polymer backbone and harvest the light energy from non-metallated DPAF to populate the triplet excited state for efficient 2PA properties. The polymers are designated as DPAF-Pt-*x*, where *x* represents the percentage of platinum chromophore.

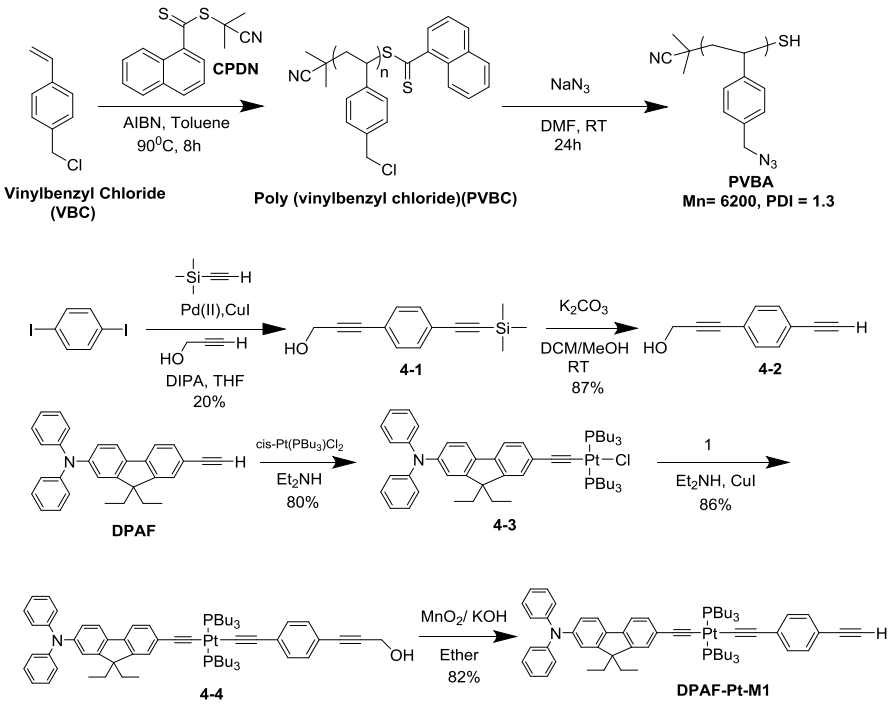

Figure 4-2. Synthesis of polymer and the monomers with terminal alkyne group.

The precursor azide substituted polymer PVBA was synthesized via reversible addition-fragmentation transfer polymerization (RAFT) according to literature procedures with molecular weight of 6200 and PDI of 1.30.[154] Metallated DPAF-Pt-M1 and non-metallated DPAF were synthesized according to literature procedures.[155] Finally, the DPAF-Pt-*x* polymers were prepared by grafting DPAF-Pt-M1 and DPAF onto

the polystyrene backbone in varying ratios utilizing Cu(I) catalyzed azide-alkyne cycloaddition reaction (CuAAC "click") between the azide group and terminal alkyne of the monomers.

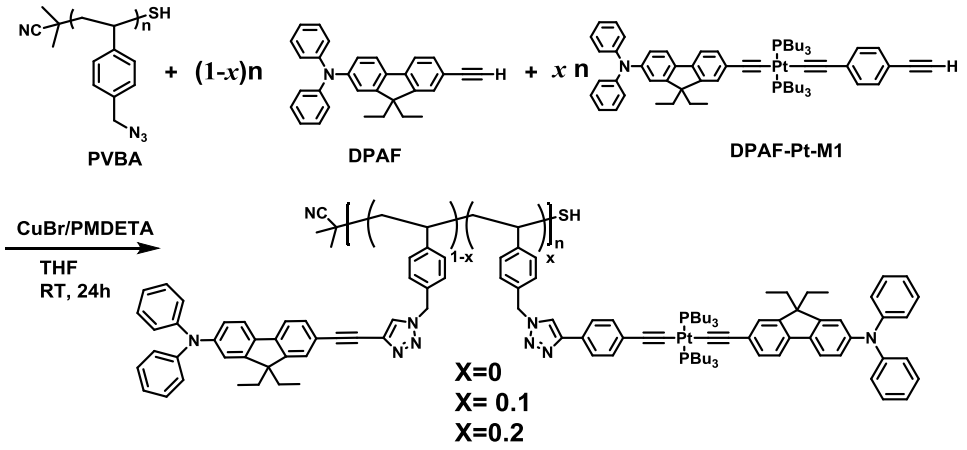

Figure 4-3. Synthesis of platinum containing polymers by click reaction.

Structural Characterization

The polymerization reaction and grafting of the π-conjugated chromophores via "click reaction" were confirmed from GPC traces as well as NMR spectroscopy. The unimodal distribution of GPC traces after the polymerization reaction and the "click" reaction suggests absence of any crosslinking or branching in the polymer chain. Significant shift is observed in the GPC traces after the "click" reaction towards lower retention time, suggesting an increase in the molecular weight (Figure 4-5).

The azide polymer PVBA is characterized by two sets of protons in ^{1}H NMR; peaks at 6.93 and 6.43 ppm are coming from a and b respectively (Figure 4-4). The other signature peak for this polymer is at 4.19 ppm (c) which is due to benzylic protons. The complete disappearence of this signal upon "click" reaction and appearance of signal at 5.38 ppm due to the protons next to triazole rings, confirms the quantitative grafting of the chromophores to the polymer backbone. The downfield shift of the

protons next to the triazole ring is due to more electron withdrawing nature of triazole ring compared to azide functionality. The additional shoulder at 0.36 ppm for DPAF-Pt-10 and 0.34 ppm for DPAF-Pt-20 confirms the presence of two terminal $–CH_3$ of fluorene from two different chromophores (organic DPAF and organometallic DPAF-Pt). From the integration values of terminal $–CH_3$ of PBu_3 at 0.87 ppm, it is possible to calculate the loading ratio of platinum chromophore. The calculated values are in close proximity of loading ratio (9.2% for DPAF-Pt-10 and 19% for DPAF-Pt-20). As an alternative, chromophore ratios can also be estimated from optical absorption spectra of the polymers.

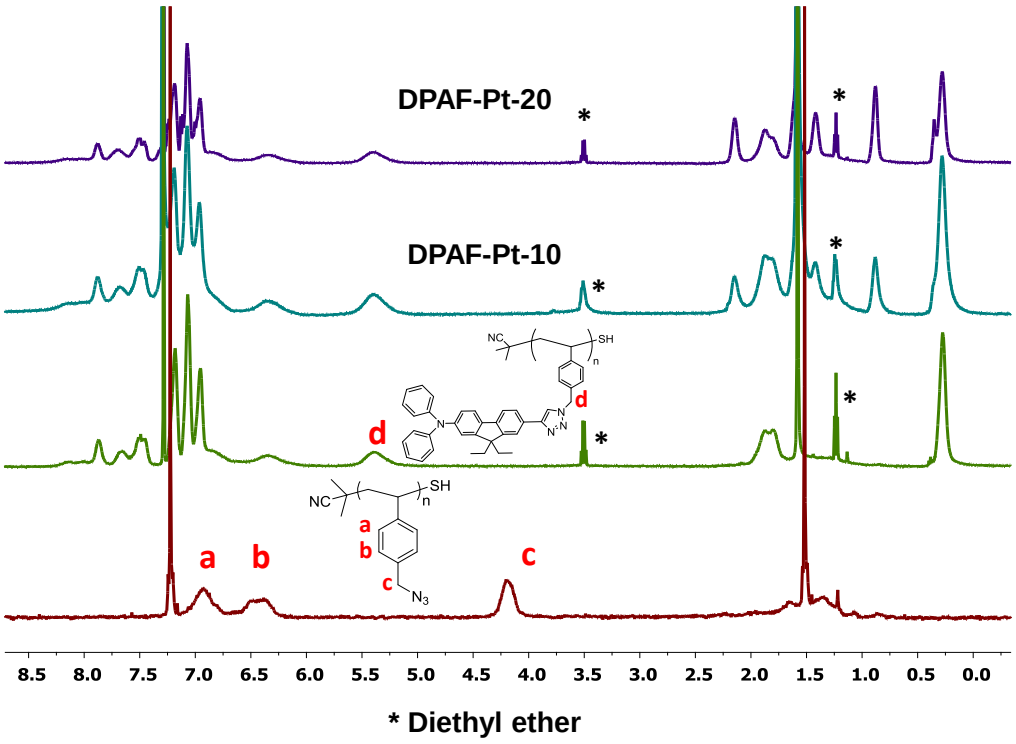

Figure 4-4. ^{1}H NMR spectra of PVBA, DPAF-Pt-0, DPAF-Pt-10 and DPAF-Pt-20. The detailed NMR spectra with integration values are shown in the supporting information.

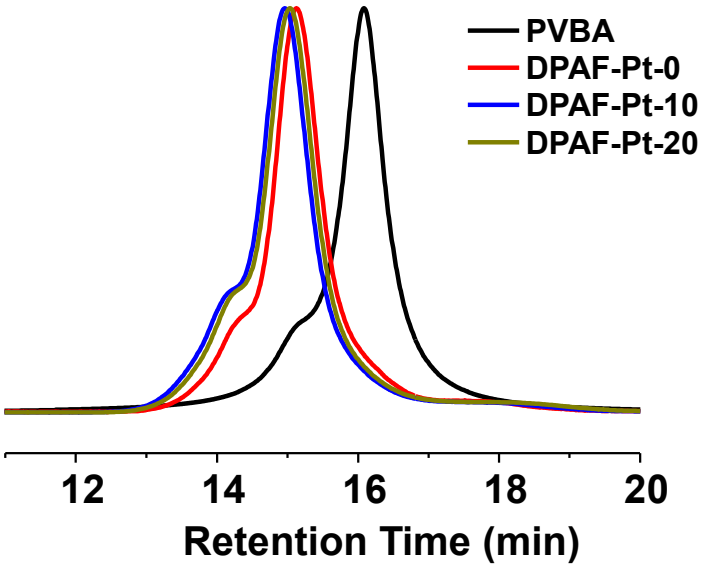

Figure 4-5. GPC traces of polymers. The black line shows the GPC trace for precursor polymer PVBA (Mn= 6200 kg/ mol, PDI= 1.3), red line shows the GPC trace for DPAF-Pt-0 (Mn= 15100 kg/ mol, PDI= 1.28), blue line shows the GPC trace for DPAF-Pt-10 (Mn= 17500 kg/ mol, PDI= 1.33) and the greenish-yellow line shows the GPC trace for DPAF-Pt-20 (Mn= 16500 kg/ mol, PDI= 1.33).

Ground State Absorption and Emission Spectroscopy

The ground state absorption spectra of all the chromophores were recorded in THF solution and presented in Figure 4-6 (A). The spectral shape for all the polymers remain almost the same as model complex DPAF-Pt-M1 and dominated by strong absorption in near UV region. The absorption is mainly due to π-π*transition. However, blue shift in absorption maxima is observed for the polymers compared to the model complex which is in accordance with the literature report for non-conjugated polymers.[149] Insignificant amount of red shift is observed in increasing the platinum loading ratio due to inherent red shifted absorption of DPAF-Pt-M1. The molar extinction coefficients (ε) and absorption maxima (λ_{max}) for the polymers and model complex are

provided in Table 4-1. The molar extinction coefficient of the polymers is increased with increasing amount of DPAF-Pt chromophore.

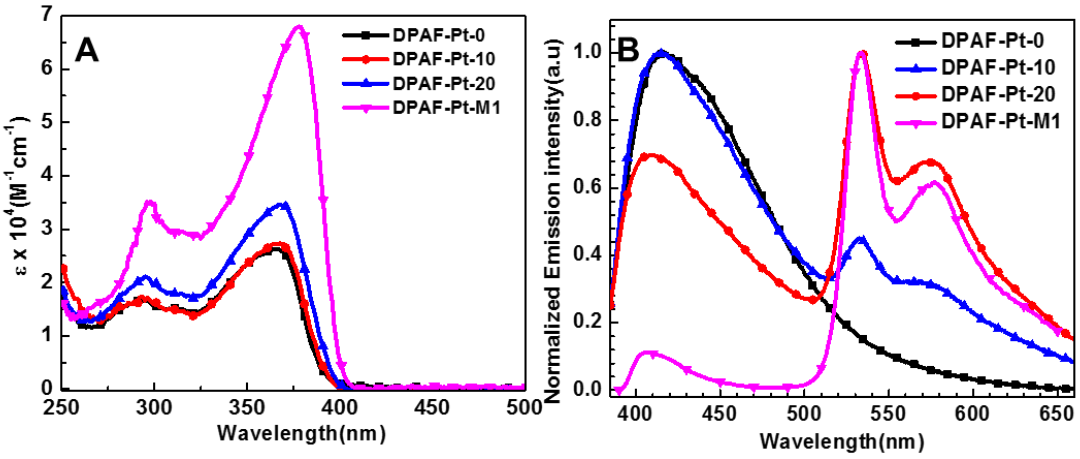

Figure 4-6. (A) Ground state absorption spectra and (B) photoluminescence spectra of the polymers and model complex in deoxygenated THF solution.

Figure 4-6 (B) shows the emission spectra of the polymers and model complex, recorded in deoxygenated THF solution by exciting them at maximum absorption wavelength. The spectra of the model complex DPAF-Pt-M1 features an intense vibronically structured phosphorescence band at 534 nm and less intense fluorescence at 405 nm. This phosphorescence emission is typical for platinum substituted DPAF chromophores.[18,149] No phosphorescence is observed for DPAF only polymer DPAF-Pt-0, which is dominated by a strong broad fluorescence peak at 417 nm. With increasing platinum concentration in the polymer backbone, intensity of phosphorescence increases at 534 nm. The fluorescence quantum yield decreases significantly from DPAF-Pt-0 to DPAF-Pt-20 in the order DPAF-Pt-0 > DPAF-Pt-10 > DPAF-Pt-20, suggesting efficient energy transfer from singlet excited state of DPAF to triplet excited state of DPAF-Pt. Singlet excited state lifetime of the polymers were monitored at 450 nm in THF solution by exciting at 375 nm. In general, all show bi-exponential decay with

a major component and a minor component. The major component for DPAF-Pt-0 has a lifetime of 1.72 ns and can be attributed to the singlet excited state lifetime. The minor component has a lifetime of 0.52 ns, and we suggest this may be due to reorganization of the polymer backbone in the excited state. With increasing platinum content, the lifetime of the major component decreased dramatically due to increasing rate of energy transfer from singlet excited state to the triplet excited state of DPAF-Pt. However, for DPAF-Pt-10 and DPAF-Pt-20, the minor component has longer lifetime compared to DPAF-Pt-0.

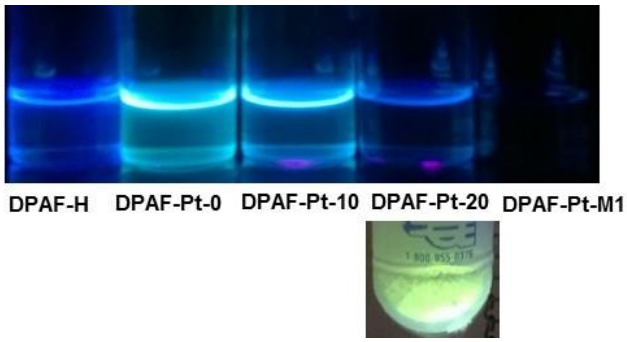

Figure 4-7. The emission color of the polymers and model complexes under UV excitation. DPAF-Pt-20 shows intense green phosphorescence upon five freeze-pump-thaw cycles.

Table 4-1. Summary of Photophysical properties.[a]

Compound	λ_{max} (nm)	$\lambda_{max\ (Fl)}$ (nm)	$\lambda_{max\ (Ph)}$ (nm)	ε [b] ($M^{-1}cm^{-1}$) x10^4	Φ_{fl}[c]	Φ_{Ph} [d]	τ_{Fl} (ns)
DPAF-Pt-0	365	415	-	2.5	63%	-	1.72 (72.6%) 0.52 (27.4%)
DPAF-Pt-10	366	417	532	2.8	15%	2%	0.23 (63.4%) 1.35 (36.4%)
DPAF-Pt-20	368	409	533	3.4	6%	10%	0.14 (80.0%) 1.30 (20.0%)
DPAF-Pt-M1	378	407	533	7.0	-	27%	<0.2

Note: [a] All the photophysical properties were recorded in THF, [b] Molar extinction coefficient and the molecular weight of the polymer repeat unit (PRU) is used for calculation, [c] Fluorescence quantum yield was recorded with respect to quinine sulfate as actinometer (ϕ_{Fl} = 0.54), [d] Phosphorescence quantum yield was recorded with respect to $Ru(Bpy)_3^{2+}.3\ H_2O$ (ϕ_{Ph} = 0.038).

Transient Absorption Spectroscopy

In an effort to detect the triplet excited state and provide further insight into the energy transfer process, nanosecond-microsecond (ns-μs) transient absorption (TA) spectroscopy was performed in deoxygenated THF solution and presented in Figure 4-8. All the samples were excited by the third harmonic of a Nd-YAG laser at 355 nm with 5 ns pulse width.

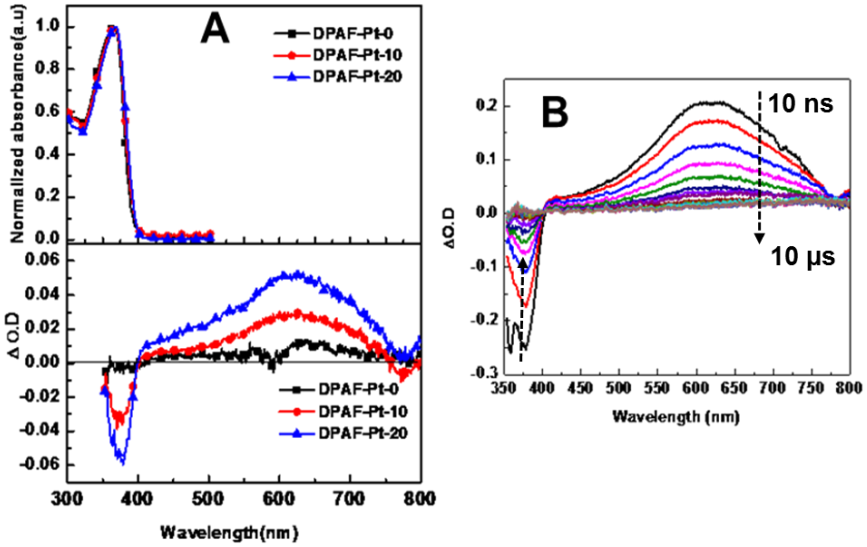

Figure 4-8. The (A) ground state absorption spectra of the polymers are shown in the top panel and nanosecond transient absorption spectra in the bottom panel. Initial delay 10 ns following a 15 ns laser excitation pulse with 50 ns camera delay increment were used, (B) the nanosecond transient absorption spectra of the model complex DPAF-Pt-M1. Initial delay 50 ns following a 15 ns laser excitation pulse with 500 ns camera delay increment were used. All the spectra were recorded in deoxygenated THF with λ_{exc} = 355 nm.

In general, the transient absorption spectra consist of a ground state bleach at 300 - 400 nm and broad transient absorption signal at 400 - 800 nm. The polymer without platinum, DPAF-Pt-0 has almost no signal in transient absorption spectroscopy. However, with increasing platinum concentration, due to transfer of energy from singlet excited state (S_1) to triplet excited state (T_1) and subsequent absorption from $T_1 \rightarrow T_n$,

transient signal rises at 600 nm. In comparison to the model complex DPAF-Pt-M1 (Figure 4-8 B), the transient absorption signals are weak for polymers. As all the measurements were performed with the same laser power and same solution concentration (Absorption ≈ 0.7 at 355 nm), it can be concluded that the model complex has higher triplet yield compared to the polymer.

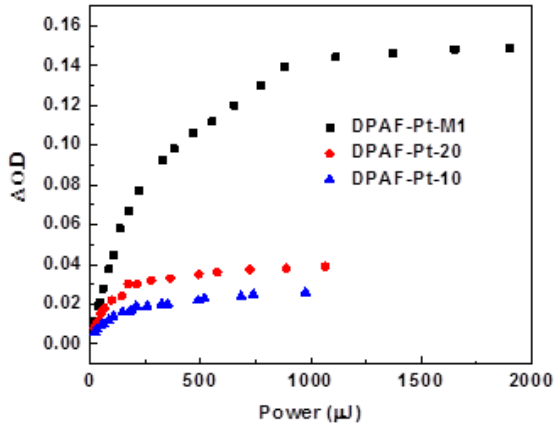

Figure 4-9. Laser power dependent comparative transient absorption spectroscopy of the model complex and the polymers DPAF-Pt-10 and DPAF-Pt-20. The absorption of all of them was kept ~ 0.7 at 355 nm.

To further compare the triplet yield of the polymers and the model complex, laser power dependent transient absorption study was performed at 600 nm (Figure 4-9). The model complex DPAF-Pt-M1 has higher triplet state absorption compared to the polymers DPAF-Pt-10 and DPAF-Pt-20, which is in agreement with the previous measurement of transient absorption across the visible wavelength region. The slope of difference in absorbance (ΔO.D) vs power (μJ) is calculated for all the chromophores and the range is kept under 250 μJ to avoid saturation of the metal center. Compared to the slope of DPAF-Pt-M1 (0.0004), the slope for DPAF-Pt-20 and DPAF-Pt-10 are 0.0002 and 0.0001, respectively. However, the amount of platinum centers (10% and 20%) are 1/5th and 1/10th of the amount present on the model complex (100%). Taking

that into account, calculated slopes are 2.5 times higher compared to the theoretical values. We believe this enhancement in triplet yield in DPAF-Pt-20 and DPAF-Pt-10 is due to energy transfer from the non-metallated DPAF centers in the polymer to the metallated center.

Femtosecond/picosecond (fs/ps) spectroscopy was carried out with three polymers to understand the dynamics of energy transfer and shown in Figure 4-10. A ground state bleach was observed for all the polymers at < 460 nm and singlet excited state absorption was observed above 460 nm with a maximum at 525 nm. However, significant differences were observed for the singlet excited state dynamics.

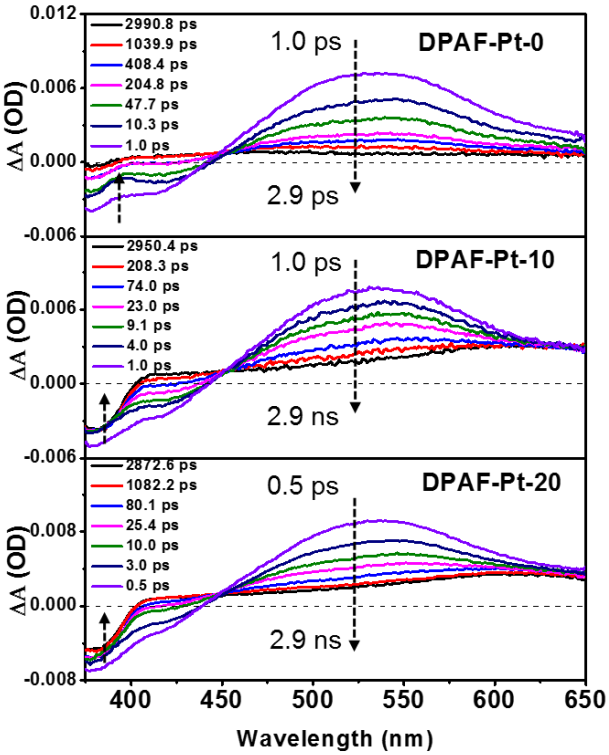

Figure 4-10. Ultrafast transient absorption spectra of the polymers DPAF-Pt-0 (top panel), DPAF-Pt-10 (middle panel), DPAF-Pt-20 (bottom panel) at λ_{exc}= 355 nm with laser power of 0.5 mW.

The homopolymer DPAF-Pt-0 spectra are observed within 1 ps following excitation pulse and only dominated by decay of the singlet excited state to ground state with no other spectral evolution. For DPAF-Pt-10, immediately after excitation at 1 ps, there is another feature rising after 600 nm and according to ns-μs transient absorption spectroscopy, this state can be unambiguously assigned to triplet excited state. In comparison to DPAF-Pt-10, DPAF-Pt-20 is populating the triplet excited state faster (within 0.5 ps), which is expected due to higher platinum chromophore concentration in this polymer. The kinetics of singlet excited state decay is presented in Figure 4-11 and lifetime data are shown in Table 4-2. All the polymers exhibit three components in decay processes. The major component of the decay gets faster with increasing amount of platinum, i.e., it increases in the series DPAF-Pt-0 > DPAF-Pt-10 > DPAF-Pt-20.

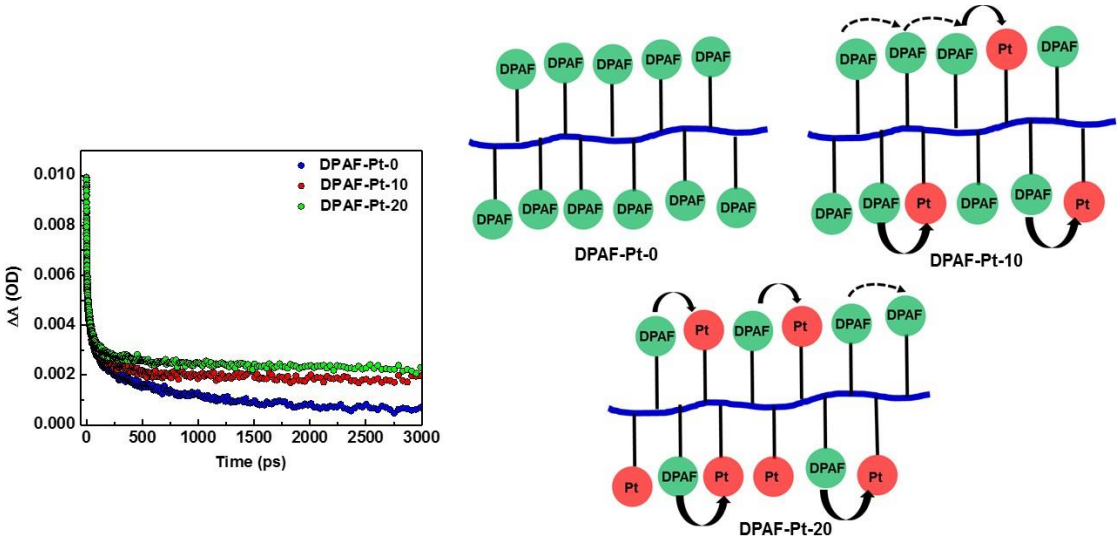

Figure 4-11. Ultrafast transient kinetics of the polymers DPAF-Pt-0, DPAF-Pt-10 and DPAF-Pt-20, monitored at 530 nm and the cartoons explaining the lifetime data of the singlet excited state of the polymers.

We believe, the fast component is due to direct energy transfer from singlet excited state of DPAF to triplet excited state of DPAF-Pt chromophore, when they are in close proximity. Another way of singlet energy transfer is by “exciton hopping” when the

acceptor is away from donor part. With increasing platinum concentration in the chromophore, the number of steps needed for hopping to acceptor decreases as well as there are more chromophores for direct quenching to occur. We attribute the intermediate component to the “exciton hopping” process, which increases in the order of DPAF-Pt-0 > DPAF-Pt-10 > DPAF-Pt-20. The minor component we attribute to the excited state decay, which is singlet excited state for DPAF-Pt-0 and triplet excited state for the platinum containing polymers.

Table 4-2. Kinetic data from ultrafast transient absorption spectroscopy.[a]

Compound	τ1 (ps)	τ2 (ps)	τ3 (ps)
DPAF-Pt-0	628 (11%)	42.5 (16%)	3.71 (73%)
DPAF-Pt-10	280 (10%)	38.1 (20%)	3.46 (70%)
DPAF-Pt-20	409 (2%)	29.1 (8%)	2.67 (90%)

Note: [a] The singlet excited state decay was monitored at 530 nm.

Two Photon Excited Photoluminescence Spectroscopy

To understand whether the energy transfer is equally efficient under two photon excitation, deoxygenated polymer solutions were excited by femtosecond laser pulse at 750 nm and the emission was monitored over a wide range of wavelength (Figure 4-12). All the polymers and platinum model complex DPAF-Pt-M1 shows upconverted photoluminescence spectra. As expected, DPAF-Pt-0 exhibits intense fluorescence only under two photon condition. Strong phosphorescence was observed for both DPAF-Pt-10 and DPAF-Pt-20. Interestingly, the comparative fluorescence and phosphorescence intensity were similar to that observed under one photon excitation. Due to higher platinum chromophore concentration, model complex DPAF-Pt-M1 exhibits intense phosphorescence with minimal fluorescence, which is in agreement with the one photon

emission spectra. This experiment, along with the visible transparency of these polymers, clearly proves all the polymers have potential to be used as optical power limiting material.

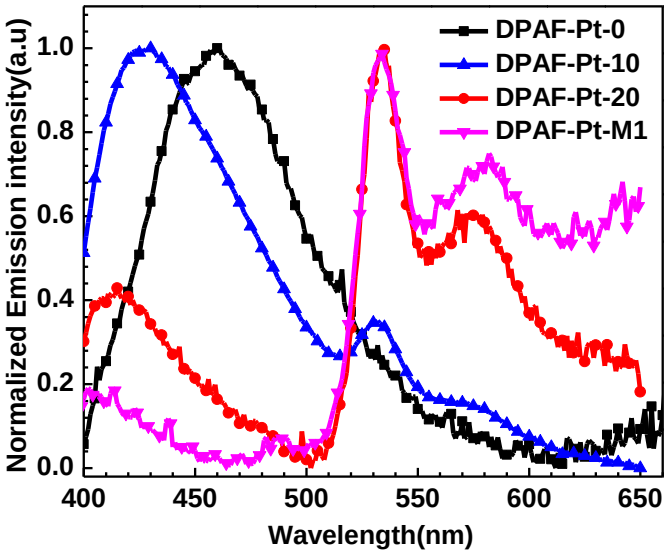

Figure 4-12. Two photon induced luminescence spectra of deoxygenated THF solution of polymers and the model complex.

Summary and Conclusions

We have carried out the synthesis of a series of atactic polystyrene polymer grafted with varying ratio of two photon active metallated and non-metallated DPAF chromophore. The results clearly demonstrate the impact of increasing amount of DPAF-Pt chromophore on photophysical properties specifically on triplet excited state properties. Increasing amount of platinum in the polymer backbone exhibits increase in phosphorescence intensity and lowers the fluorescence quantum yield. Decrease in singlet excited state lifetime in the series DPAF-Pt-0 > DPAF-Pt-10 > DPAF-Pt-20 suggests energy transfer from nonmetallated DPAF part to metallated DPAF part of the polymer backbone. We suggest the energy transfer is taking place from S_1 state of

DPAF to S_1 state of DPAF-Pt, followed by energy transfer to T_1 state of DPAF-Pt. Laser power dependent nanosecond-microsecond transient absorption study shows higher triplet excited state production for DPAF-Pt-M1 compared to the platinum containing polymers. However, comparison of slopes at lower power suggests DPAF-Pt-10 and DPAF-Pt-20 has higher rate of intersystem crossing than what is expected for such a low platinum containing polymers and this is due to energy transfer from singlet excited state of DPAF. A detailed kinetic study of this process by ultrafast transient absorption spectroscopy is also performed. The energy transfer takes place via DPAF to DPAF-Pt within 2-3 ps and via DPAF to DPAF hopping within 30-40 ps. The polymers as well as the platinum model complex exhibits excellent upconverted photoluminescence under 2 PA condition.

Overall the excellent visible transparency of these polymers, diluted platinum centers in the polymer chain, two photon induced upconverted emission makes this system excellent candidate for optical power limiting property.

Experimental

Instrumentation and Methods

NMR spectra were recorded by using an INOVA 500 FT-NMR at 500 MHz for ^{1}H NMR, and at 125 MHz for ^{13}C NMR. Phosphorus NMR were recorded in Mercury-300 FT-NMR operating at 75.4 MHz. Gel permeation chromatography for the polymers was performed by using a system consisting of a Shimadzu LC-6D pump, Agilent mixed-D column and a Shimadzu SPD-20A photodiode array detector. THF was used as an eluent with a flow rate of 1 ml/ min. The system was calibrated using linear polystyrene standards in THF.

The photophysical measurements were carried out in deoxygenated, HPLC grade tetrahydrofuran (THF) solvent in 1x1 cm quartz cuvettes unless otherwise mentioned. UV-visible absorption spectra were obtained by a Shimadzu UV-1800 dual beam spectrophotometer. Steady state emission spectra were recorded by using Photon Technology International (PTI) spectrophotometer and collected at 90˚, relative to the excitation beam. The optical density for all samples was kept ≤0.1 at excitation wavelength, unless otherwise mentioned. Emission quantum yield measurements were performed by taking into account corrections for refractive index of the solvents used. Singlet excited state lifetime was measured by using PicoQuant FluoTime 100 Compact Fluorescence Lifetime Spectrophotometer by time-correlated single photon counting (TCSPC) and the solutions were excited by a PDL-800B Picosecond Pulsed Diode Laser at 375nm.

Nanosecond transient absorption spectra were performed with a THF solution of the sample and the optical density was maintained at ≈0.7 at 355 nm. The samples were taken in a 1cm path length flow cell and deoxygenated by bubbling argon for at least 45 minutes prior to measurement. The spectra were measured in a home-built apparatus with the third harmonic of a Continuum Surelite series Nd:YAG laser (λ = 355 nm, 10 ns FWHM, 7 mJ per pulse). White probe light was produced by xenon flash lamp, and the transient absorption signal was detected with a gated-intensified CCD mounted on a 0.18 m spectrograph (Princeton PiMax/Acton Pro 180).

The femtosecond transient absorption spectra for the polymers were measured at KAUST using Ti:Sapphire femtosecond regenerative amplifier (Spectra-Physics)

operating at 800 nm with 35 fs pulses and a repetition rate of 1 kHz. The samples were excited at 355 nm. The details of the instrumentation are reported elsewhere.[156]

General Methods for Synthesis

All the reactions were performed under dry argon atmosphere. THF and toluene were used directly from dry solvent purification columns (Glass contour). All the other solvents for reaction were used directly from commercial resources and without any further purification unless specified. The synthetic scheme for the polymer and monomers are provided above in Figure 4-2 and Figure 4-3. Both the model complex, DPAF and DPAF-Pt-M1 were synthesized by following literature procedures.[155] The synthesis of cis-$Pt(PBu_3)_2Cl_2$ was performed according to the literature procedure.[19] The synthetic description of precursor polymer PVBA is described elsewhere.[154] Copper (I) iodide (CuI), Copper (I) bromide (CuBr), Phenyl acetylene, *N,N,N′,N″,N″*-pentamethyldiethylenetriamine (PMDETA) were purchased from Sigma-Aldrich. Palladium catalyst Bis(triphenylphosphine)palladium(II) dichloride $[Pd(PPh_3)_2Cl_2]$ was purchased from Strem Chemicals and Trimethylsilyl acetylene (TMSA) was purchased from GFS chemical. CuBr was stirred overnight in acetic acid, washed with acetone and vacuum dried to purify before use in the click reaction.

General Protocol for Synthesis of DPAF-Pt-0 to DPAF-Pt-20: Example of DPAF-Pt-20

A solution of PVBA (20 mg, 0.13 mmol), DPAF (45.5 mg, 0.11 mmol), DPAF-Pt-M1 (32 mg, 0.03 mmol), PMDETA (24 mg, 0.14 mmol) were dissolved in 10 mL of dry THF and the light yellow colored solution was deoxygenated by purging with argon for 45 minutes. After that CuBr (20 mg, 0.14 mmol) was added to the reaction mixture under an argon atmosphere and the color was changed from light yellow to green over

the course of 30 minutes. The reaction mixture was left stirring overnight under argon atmosphere for 24 hours at room temperature. After the reaction, the mixture was passed through a short neutral alumina column to remove the residual copper catalyst. The solvent was evaporated under vacuum and precipitated over diethyl ether. The precipitate was collected by centrifugation and dissolved in minimal amount of THF, and re-precipitate in diethyl ether again. This process was repeated three times and then the precipitate was dried under vacuum for 24 hours to isolate the polymer as light greenish yellow solid (83 mg, 88% yield).

CHAPTER 5
PHOTOPHYSICS OF ORGANOMETALLIC PLATINUM(II) DERIVATIVES OF THE DIKETOPYRROLOPYRROLE CHROMOPHORE

Background

Diketopyrrolopyrrole (DPP) dyes can be easily considered as one of the most versatile building block studied in recent years due to its potential application in optoelectronic devices especially in bulk heterojunction solar cells (BHJs),[157,158] dye sensitized solar cells (DSCs)[159] and organic field effect transistors (OFETs).[160,161] It was first introduced by Farnum *et al.*[162] in 1974 and soon became popular because of its excellent properties such as bright red color, high thermal stability, high melting point and interesting photophysical aspects.[163,164] DPP dyes containing unsubstituted amide-nitrogen remain insoluble in almost all organic solvents due to the presence of strong intermolecular H-bonding between the lactam rings.[163,164] The central amide-nitrogen atom can be easily functionalized with aliphatic side chains to improve its solubility in organic solvents, as well as to improve the processibility of DPP containing materials.[163,164] Apart from its amide-nitrogen atom, the DPP core can also be substituted in the 3 and 6 positions by thiophene,[165] phenyl,[166] selenophene,[166] furan[167] etc to fine tune its optoelectronic properties. Thiophene is favored over phenyl as a donor because of its smaller dihedral angle with the DPP core which leads to enhanced planarity of the system and stronger donor-acceptor charge transfer.[168]

While the singlet excited state photophysics of DPP containing molecules are well studied,[166] the triplet excited states are relatively less explored, due to the low

efficiency of $S_1 – T_1$ intersystem crossing (ISC).[169] Considering the importance of triplet excited states in optoelectronic systems it is important to understand the properties of the triplet states in DPP chromophores. In this regard, it is well-known that heavy metal atom substitution of π-conjugated organic chromophores is an effective means to induce efficient ISC, due to the effects of spin-orbit coupling induced by the mixing of the metal centered dπ orbitals with the π-electron system.[170-173] This method has been widely used, both to afford fundamental insight into triplet chromophore properties, but also as a means to significantly enhance the efficiency of emission in phosphorescent light emitting diodes that feature heavy metal inorganic and organometallic phosphors.[119,174,175] To date there are very few reports on heavy-metal substituted DPP complexes. In 2000 Langhals *et al.* reported various transition metal complexes utilizing DPP dianions with the goal to improve the fluorescence quantum yield of DPP chromophores.[176] In this study metals such as Au(I) and Pt(II) were coordinated to the DPP amide-nitrogens; however, the photophysics of the complexes was dominated by the singlet excited state of the ligand reflecting the relatively poor interaction between the DPP π-electron system and the metal centers. In 2012 McCusker *et al.* reported iridium containing DPP complexes which displayed efficient $S_1 – T_1$ ISC and a long-lived triplet excited state.[169]

Platinum acetylide π-conjugated oligomers and polymers have been widely investigated due to the ability of the heavy-metal center to induce strong-spin orbit coupling which enhances the triplet yield and often induces efficient phosphorescence at ambient temperature.[171,177-186] Since the triplet exciton has a longer lifetime compared to the singlet exciton, platinum acetylide containing polymers have been explored as the

active materials in photovoltaic devices to improve the exciton diffusion.[25,65,68,187] Due to inefficient orbital overlap between Pt 5d and C 2p orbitals in the acetylide linkage, the effective conjugation length is limited, which could be detrimental for photovoltaic response.[188] In an effort to overcome this issue, a cyclometallated platinum motif has been incorporated in the conjugated polymer backbone. In this design, not only is the effective conjugation length increased, but additional planarity is provided to the π-electron system.[188,189]

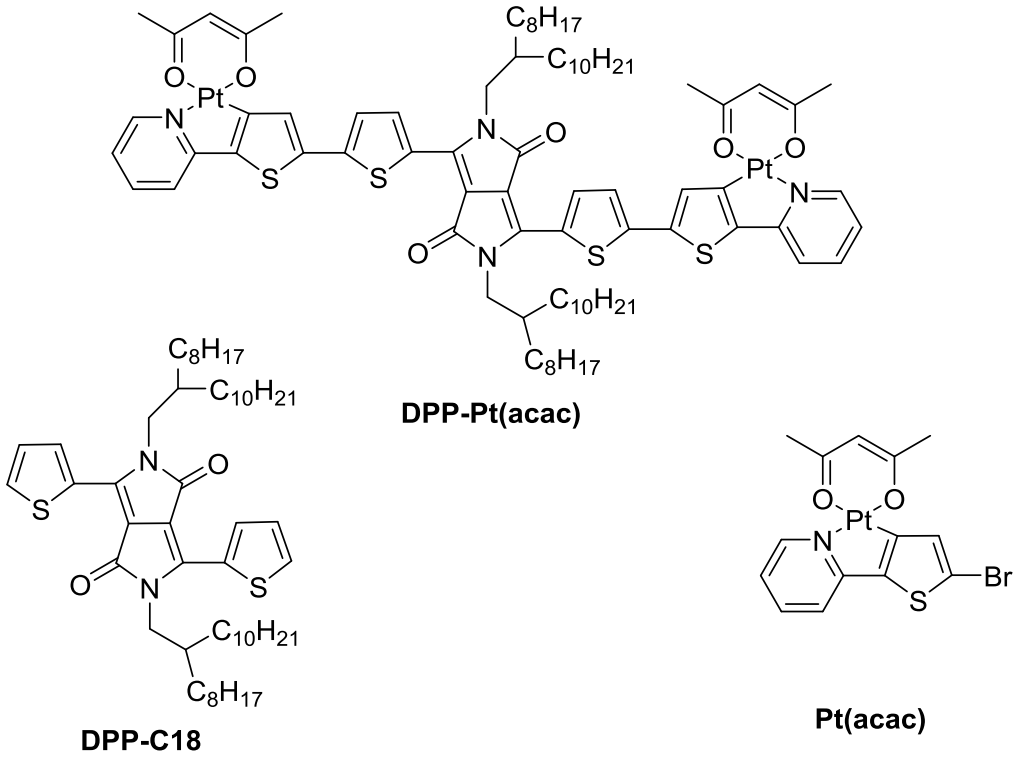

Figure 5-1. Structure of the metal complex and the precursors.

In the present section, we present the results of a detailed investigation of the optoelectronic properties of the two platinum-substituted DPP π-conjugated chromophores DPP-Pt(acac) and DPP-Pt(CC) (Figure 5- 1 and Figure 5-2). This study provides insight into the effects of these two different heavy metal architectures on the photophysical properties of the DPP chromophore. The ground state redox potentials of

the chromophores were determined by solution electrochemistry, and the results were used to estimate the HOMO and LUMO energy levels. The photophysical properties of the chromophores were characterized using absorption, photoluminescence and time-resolved absorption spectroscopy on timescales from sub-picoseconds to microseconds. Density functional theory (DFT) computations were performed to understand the molecular orbitals involved in both the singlet and triplet excited state photophysics and support the experimental data. The results reveal that in both platinum DPP derivatives the metal auxochromes have a significant effect on the chromophores' photophysics. The most profound effect is a reduction in the fluorescence yields accompanied by enhanced triplet yield due to the spin-orbit coupling induced by the metal auxochromes. The effects are most pronounced in DPP-Pt(acac) indicating that the orthometallated platinum auxochrome is able to induce spin-orbital coupling to a greater extent compared to the platinum acetylide substituents. To the best of our knowledge this is the first detailed report of triplet excited state photophysics of DPP containing metal-organic chromophore influenced by different platinum complex architectures. We note that a LETTER has recently been published concerning CT complex formation between DPP-Pt(acac) and a tetra-cationic porphyrin acceptor.[190] It was shown there, DPP-Pt(acac) can perform electron transfer in ultrafast time scale (1-2 ps) to tetra-cationic porphyrin, PCBM and TCNE. However, the charge recombination is slow and persists into ns scale. It is important to note here, fast electron transfer and slow charge recombination is one of the essential criteria for photovoltaic device operation.

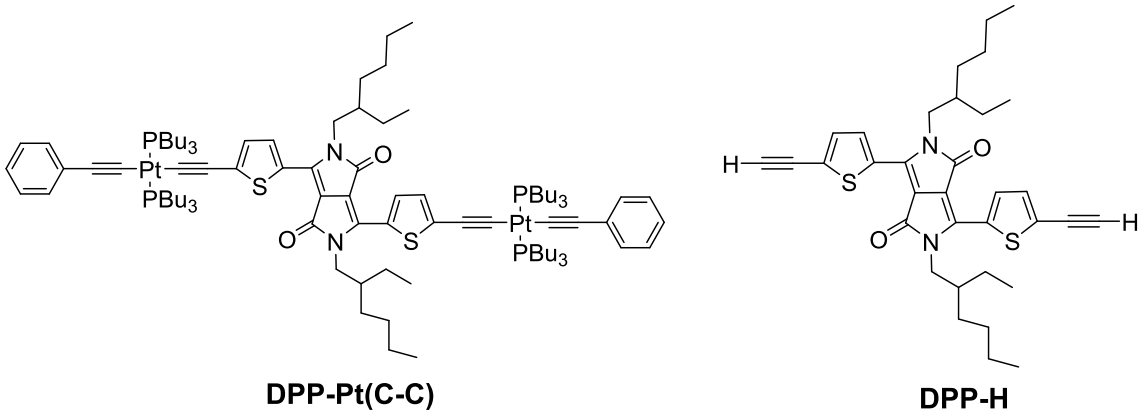

Figure 5-2. Structure of the ligand and platinum acetylide containing DPP complex.

Results and Discussion

Structures and Synthesis

The compounds that are the focus of the study described herein are shown in Figure 5-1 and 5-2. Each compound features a diketopyrrolopyrrole (DPP) core chromophore flanked on both ends by organometallic auxochromes linked via 2,5-thienylene (Th) units. The Th-DPP-Th unit is a donor-acceptor-donor (DAD) π-conjugated system that has been studied extensively for application in organic solar cells and organic transistor applications.[160,191,192] As outlined below, the platinum(II) auxochromes extend the π-conjugation and introduce spin-orbit coupling into the excited state wave functions**.**

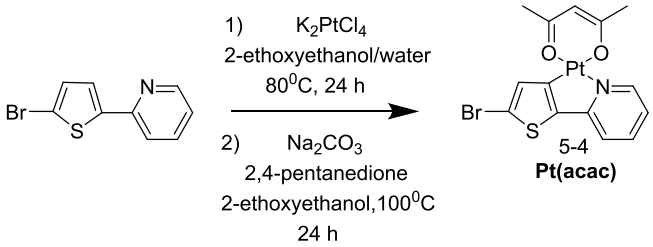

Figure 5-3. Synthetic scheme of DPP-Pt(acac) complex.

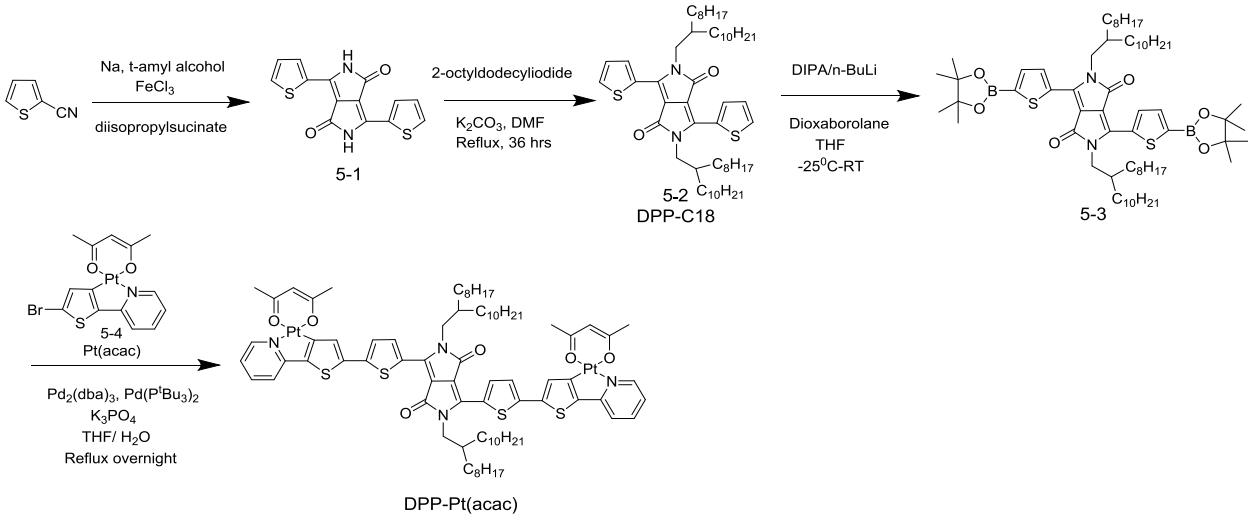

Figure 5-3. Continued.

The DPP-Pt(CC) system was the first target to be synthesized, and it was prepared by reaction of DPP-H with *trans*-Ph-CC-Pt(PBu_3)$_2$Cl under Hagihara conditions (Figure 5-4). Note that DPP-Pt(CC) is N,N'-substituted with 2-ethylhexyl (2-EH) groups and these combined with the PBu_3 groups at the Pt-acetylide centers are sufficient to impart the material with good solubility properties in solvents such as THF and $CHCl_3$. In subsequent work, we developed a method to cross couple the previously reported[193] bis-boronic ester derivative of DPP with Pt(acac) under Suzuki conditions. Initial attempts at this reaction utilized a 2-EH substituted version of the DPP chromophore, and unfortunately it was found that the product was nearly insoluble. Mass spectral analysis of the insoluble material revealed that it had the correct molecular mass. Therefore, based on this insight we were motivated to prepare the DPP chromophore with 2-(octyl)dodecyl substituents to improve solubility (DPP-C18). Subsequent reaction of the bisboronate ester (5-3 in Figure 5-3) with Pt(acac) afforded DPP-Pt(acac) which has good solubility in THF and $CHCl_3$.

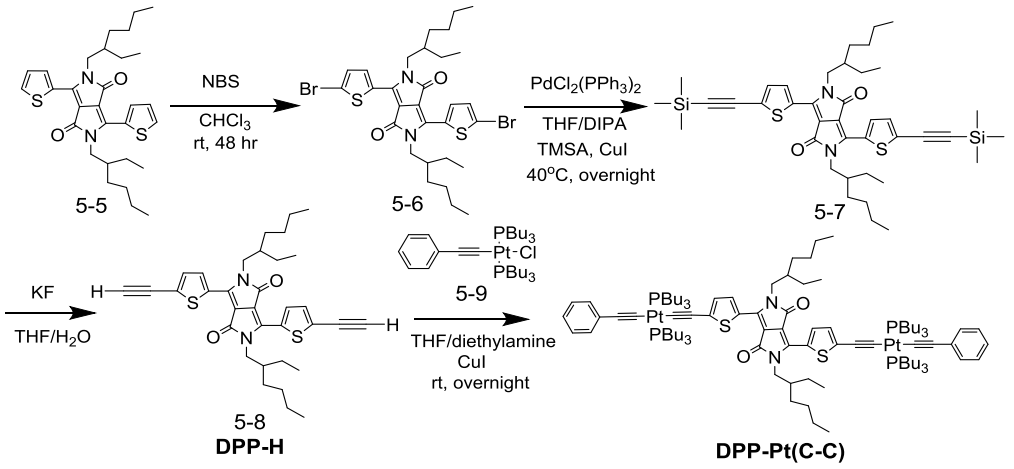

Figure 5-4. The synthetic scheme of platinum acetylide complex DPP-Pt(C-C).

Electrochemistry

In order to identify the redox levels for the various DPP compounds and understand how the platinum units modify the frontier orbital energy levels, electrochemical studies were carried out using cyclic and differential pulse voltammetry (CV and DPP, respectively). These studies were conducted using platinum working and counter electrodes and a Ag/Ag^+ quasi-reference electrode in CH_2Cl_2/0.1 M NBu_4PF_6 electrolyte. All potentials are reported relative to a Fc/Fc^+ internal standard. Cyclic voltammograms of these two complexes are shown in Figure 5-5 and the electrochemical data is summarized in Table 5-1. All the plots are scaled to the same X-axis, in order to make the comparison among their redox behavior.

First, the electrochemistry of the core DPP unit is modeled by DPP-C18. This compound exhibits a single reversible reduction at -1.68 V along with two reversible oxidations at +0.53 and 1.04 V. The cyclic voltammogram of DPP-Pt(CC) is qualitatively similar to that of DPP-C18, in that a single reversible reduction is observed along with two reversible oxidations. The reduction of the DPP-Pt(CC) occurs at the same potential as for the DPP model, whereas the oxidation waves are shifted to less positive

potentials (0.16 and 0.45 V). These differences indicate that the platinum acetylide auxochrome has little effect on the energy of the LUMO, whereas the HOMO is raised by approximately 0.35 eV (see below).

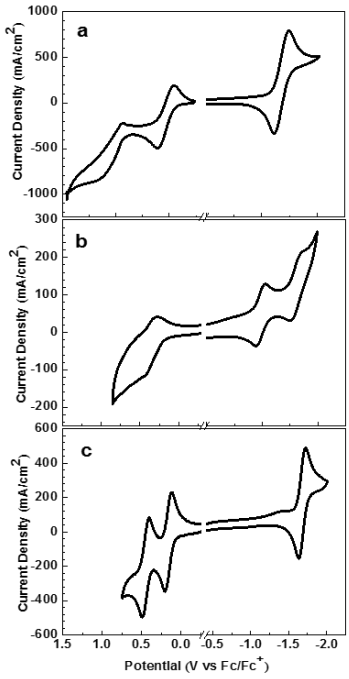

Figure 5-5. Cyclic voltammograms of a) DPP-C18, b) DPP-Pt(acac) and c) DPP-Pt(CC) in dichloromethane solvent with 0.1 M $TBAPF_6$ as the supporting electrolyte. It was scanned at 100 mV s^{-1}. All the potentials are referenced to Fc/Fc^+ couple as an internal standard.

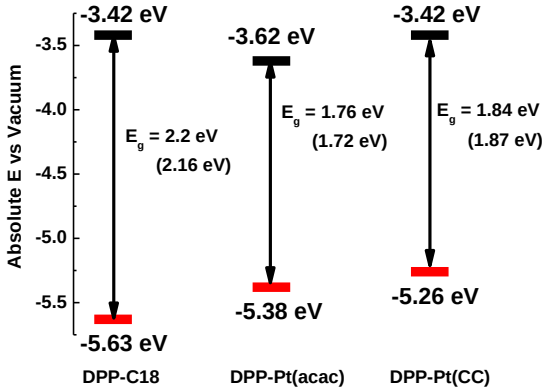

Figure 5-6. Frontier orbital energy levels of DPP chromophores. E_g is the calculated electrochemical bandgap, and the values in parenthesis calculated from the onset of the long wavelength absorption band (optical bandgap).

The electrochemistry of DPP-Pt(acac) is more complex compared to the other two compounds. First, this oligomer exhibits two nicely reversible reductions at -1.48 and -1.8 V. The first reduction is shifted to a less cathodic potential compared the other DPP chromophores. In addition, DPP-Pt(acac) exhibits two oxidation waves, the first of which appears to be reversible whereas the second is at best quasi-reversible. By using differential pulse voltammetry, the peak potentials are estimated as 0.28 and 0.43 V. Here again, the first oxidation is shifted to a less positive potential compared to that of DPP-C18.

By using electrochemical data, it is possible to calculate the energies of the HOMO and LUMO levels for the three DPP oligomers; the values are listed in Table 5-1, and Figure 5-6 illustrates the trends for the three compounds, along with the computed electrochemical bandgaps. This presentation clearly illustrates the effects that the two different platinum auxochromes have on the frontier energy levels. Specifically, it can be seen that in DPP-Pt(CC) the Pt-acetylide units increase the HOMO energy level relative to that of DPP-C18, but have little effect on the LUMO. Nevertheless, the electrochemical bandgap is reduced by ~0.35 eV due to the effect of the Pt-acetylide units on the HOMO level. By contrast, it is evident that in DPP-Pt(acac) the orthometallated Pt units lower the LUMO and increase the HOMO level, and as a consequence, these “substituents” have a significant effect on the bandgap. The larger effect of the Pt(acac**)** units may not be surprising, given that it is likely that the 2 additional thienyl-pyridine units (a total of four additional arylene rings compared to DPP-C18) have the effect of substantially increasing the overall π-conjugation in the oligomers.

Density functional theory (DFT) calculations were carried out on the oligomers, and in Table 5-1 compares the experimental HOMO and LUMO energies (electrochemistry) with the DFT computed levels. In each case, DFT overestimates the absolute orbital energies by ~1 eV; however, in general the trends in the computed orbital energies agree with the experimental values. Thus, as can be seen, the DFT computed HOMO energies increase in the order DPP-C18 **<** DPP-Pt(acac) < DPP-Pt(CC). The calculations correctly simulate the relative LUMO energies of DPP-C18 and DPP-Pt(acac); however, the HOMO for DPP-Pt(CC) is predicted to be 0.3 eV higher relative to that of DPP-C18, which is not in agreement with the electrochemistry.

Table 5-1. Electrochemical properties of DPP-Pt(acac) and DPP-Pt(CC).[a]

Compound	$E_{1/2}$/V		$E_{1/2}$/V		HOMO / eV	LUMO/ eV
	Red_1	Red_2	Ox_1	Ox_2		
DPP-C18	-1.68	-	0.53	1.04[b]	-5.63 (-4.97)	-3.42 (-2.51)
DPP-Pt(acac)	-1.48	-1.8	0.28[b]	0.43[b]	-5.38 (-4.59)	-3.62 (-2.70)
DPP-Pt(CC)	-1.68	-	0.16	0.45	-5.26 (-4.37)	-3.42 (-2.21)

Note: [a] Measured in CH_2Cl_2 using 0.1 M NBu_4PF_6 as supporting electrolyte. It was scanned at 100 mV s^{-1}. All the potentials are referenced to Fc/Fc^+ couple as an internal standard. [b] Determined from DPV. The computed HOMO and LUMO energy levels are shown in parenthesis.

UV-Visible Absorption Spectroscopy

Ground state absorption spectra of the metal complexes DPP-Pt(acac), DPP-Pt(CC) and the related precursors are examined in THF and are shown in Figure 5-7 (panels a and c). The metal complexes DPP-Pt(acac) and DPP-Pt(CC) feature absorption throughout the near-UV and visible regions.

The spectra are dominated by an intense absorption band in the mid-visible (500 - 750 nm), and weaker absorption in the 300-450 nm region. The low energy transition

is due to a donor-acceptor charge transfer transition, while higher energy features arise from π,π* transitions.[166] The molar absorptivity (ε) and absorption band maxima (λ_{max}) are provided in Table 5-2.

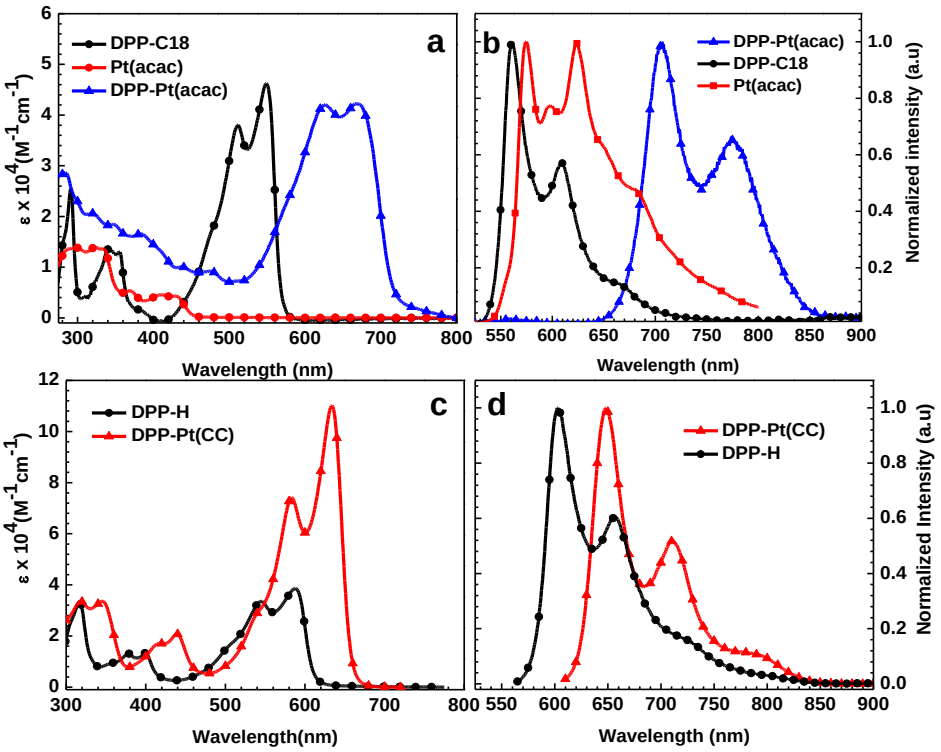

Figure 5-7. Absorption and fluorescence spectra in THF solution. a) and b) DPP-Pt(acac) and related precursors; c) and d) DPP-Pt(CC) and DPP-H. The emission spectra were obtained by exciting the sample solutions at 590 nm.

Significant differences in spectral shape and the large bathochromic shift (117 nm) of DPP-Pt(acac) from the precursor molecule DPP-C18 reveal that considerable additional π-conjugation is imparted by the cyclometallated platinum auxochromes that are appended at the ends of the conjugated electronic system. This notion is supported from the DFT and TD-DFT calculations, which show that the long-wavelength electronic transition is purely of HOMO → LUMO character, and that the HOMO and LUMO have significant contributions from the terminal cyclometallated thienyl-pyridine moieties

(APPENDIX C). It is important that the HOMO and LUMO contain only small contributions from Pt-based orbitals, suggesting that the long wavelength HOMO-LUMO transition is dominated by the carbon and heteroatom π-electron system. It is believed that metal-to-ligand charge transfer does not contribute much, if any, to the oscillator strength in the long wavelength band. In addition, note that the spectrum of DPP-Pt(acac) exhibits additional absorptivity in the 300 - 500 nm region, corresponding to the region where the localized Pt(acac) metal-to-ligand charge transfer transitions occur (compare in Figure 5-7a). Note that the significant bathochromic shift of the long wavelength absorption is consistent with the prediction based on the electrochemical bandgap (Table 5-1)-

Table 5-2. Summary of photophysical properties.[a]

Compound	λ_{max} (nm)	ε x 10^5 ($M^{-1}cm^{-1}$)	λ_{em} (nm)	ϕ_{fl} [b]	$k_r/10^8$ (s^{-1})	$k_{isc}/10^8$ (s^{-1})	ϕ_{isc}	τ_{fl}/ns	τ_{TA}/μs
DPP-C18	549	4.6	560.9	0.86	1.5	-	-	5.8	-
Pt(acac)	297, 322, 406	1.32	574.8, 623.4	-	-	-		-	-
DPP-Pt(acac)	667	4.2	706.2	0.022	1.2	53	0.97	0.18	0.16
DPP-H	588	3.9	603.1	0.66	1.5	-	-	4.34	-
DPP-Pt(CC)	633	11	648.6	0.53	1.7	1.3	0.40	3.2	1.1

Note: [a] In THF solution. λ_{max} is the absorption band maximum; ε is the molar extinction coefficient; λ_{em} is the emission band maximum; ϕ_{fl} is the fluorescence quantum yield; k_r, k_{nr} and k_{isc} are the radiative decay, non-radiative decay and intersystem crossing rate constants, respectively; ϕ_{isc} is the intersystem crossing quantum yield; τ_{fl} is the fluorescence lifetime; τ_{TA} is the triplet excited state lifetime from TA decay. Estimated error in the data is ± 5% of the reported values. [b] Quantum yield measured using tetraphenylporphyrin in toluene (ϕ_F=0.09) as actinometer.

The Pt-acetylide capped complex DPP-Pt(CC) also exhibits a significant red shift (46 nm) and increased oscillator strength compared to the free acetylene chromophore, DPP-H. These features indicate that there is a significant interaction between Pt-based dπ orbitals and the π-system of the DPP chromophore. Indeed, this interaction is reflected in the molecular orbital plots which are derived from the DFT calculations (APPENDIX C). By analogy to DPP-Pt(acac), the long wavelength band is essentially purely of HOMO → LUMO character; the MO plots reveal that Pt dπ orbitals contribute to the HOMO and to a lesser extent to the LUMO of the DPP chromophore. This observation is consistent with previous work on Pt-acetylide complexes featuring π-conjugated acetylide ligands, where it has been suggested that the long wavelength absorption may even have a small degree of Pt-to-ligand metal-to-ligand charge transfer (MLCT).[194-196]

Referring back to Figure 5-6, which compares the electrochemical and optical bandgaps (the latter are values in parenthesis), it can be seen that there is excellent agreement in the values. This is consistent with the notion that the lowest energy transitions are primarily HOMO – LUMO in character. Moreover there is a degree of charge transfer (quadrupolar chromophores) in the optical transitions, as the LUMO orbitals are concentrated more in the DPP core. The charge transfer can be visualized by the charge difference density (CDD) plots obtained from the time-dependent (TD)-DFT calculations (APPENDIX D).

Photoluminescence Spectroscopy

Photoluminescence spectra of DPP-Pt(acac), DPP-Pt(CC) and their precursors were recorded in deoxygenated THF solution and they are also presented in Figure 5-7

(panels b and d). In general both of the metal complexes exhibit a vibronically structured emission that has a relatively small Stokes shift relative to the lowest absorption band. This fact, coupled with the lifetimes indicate that the emission can be assigned as fluorescence from the lowest singlet state. Note that the fluorescence for DPP-Pt(acac) and DPP-Pt(CC) are significantly red-shifted from their respective precursor chromophores. The emission spectrum of the Pt(acac) model complex was also obtained, and it is also shown in Figure 5-7b; this complex exhibits phosphorescence which is blue-shifted substantially from the fluorescence of DPP-Pt(acac). In a previous related study, Castellano, Ziessel and co-workers reported weak phosphorescence emission at 77 K from a DPP chromophore that contained conjugated Ir(III) units in the wavelength region between 950 and 1100 nm (1.1 - 1.3 eV).[169] In the present study, we carried out careful near-infrared emission spectroscopy experiments (ambient temperature, vacuum degassed samples) seeking evidence for phosphorescence from both DPP-Pt(acac) and DPP-Pt(CC). Unfortunately no definitive evidence for phosphorescence emission in the 900 - 1400 nm range for the DPP metal complexes was obtained in these experiments.

Fluorescence quantum yields (ϕ_{fl}) and lifetimes (τ_{fl}) for the various DPP chromophores are listed in the Table 5-2, along with other photophysical parameters. The fluorescence quantum yields for the unmetallated chromophores DPP-C18 and DPP-H are relatively high (0.86 and 0.66, respectively) and the fluorescence lifetimes are on the order of 5 ns. Interestingly, the radiative decay rates for the set of DPP chromophores are relatively constant at 1.5×10^8 s^{-1}. Each of the metal complexes displays a reduced quantum yield and lifetime compared to the non-metallated DPP

units. First, for the orthometallated system DPP-Pt(acac), the emission parameters are dramatically reduced relative to DPP-C18. On the other hand, for the acetylide linked DPP-Pt(C-C) complex the reduction in ϕ_{fl} and τ_{fl} is modest compared to DPP-H. Interestingly, the radiative decay rates for the metallated chromophores are very similar to those of the non-metallated systems (1.2 - 1.6 x 10^8 s^{-1}). This correspondence in radiative rates across the series indicates that the reduced fluorescence yields and lifetimes for the metallated chromophores is due to an increase in a non-radiative decay channel. We suggest that this channel is $S_1 \rightarrow T_1$ intersystem crossing. If we assume that the rate of internal conversion from $S_1 \rightarrow S_o$ is constant across the series (and it accounts for the balance of the singlet decay for DPP-C18), it is possible to estimate the intersystem crossing yield and rate constant, ϕ_{isc} and k_{isc}, respectively. These parameters are listed in Table 5-2 for the metallated chromophores. Here it can be seen that intersystem crossing in DPP-Pt(acac) is highly efficient, with ϕ_{isc} ~ 0.97. The triplet yield in the acetylene linked DPP-Pt(CC) chromophore is still respectable at ϕ_{isc} ~ 0.40; however, it is clearly considerably less than in the orthometallated complex. Importantly, the difference in triplet yields arises because intersystem crossing is nearly 50-fold faster in DPP-Pt(acac), reflecting a significant effect of the orthometallated auxochromes on the rate of intersystem crossing.

Transient Absorption Spectroscopy

A key objective of this work is to understand how the triplet state yield is affected by incorporation of two different platinum auxochromes into the DPP chromophore. The low to moderate quantum yields of emission and fluorescence lifetimes suggest that intersystem crossing is efficient in both of the metal complexes. However, since

phosphorescence was not detected from the metal complexes, ns/μs transient absorption (TA) spectroscopy was performed to probe the triplet state. Figure 5-8 shows the TA difference spectra along with corresponding ground state absorption spectra. Several correlations emerge on careful inspection of the spectra.

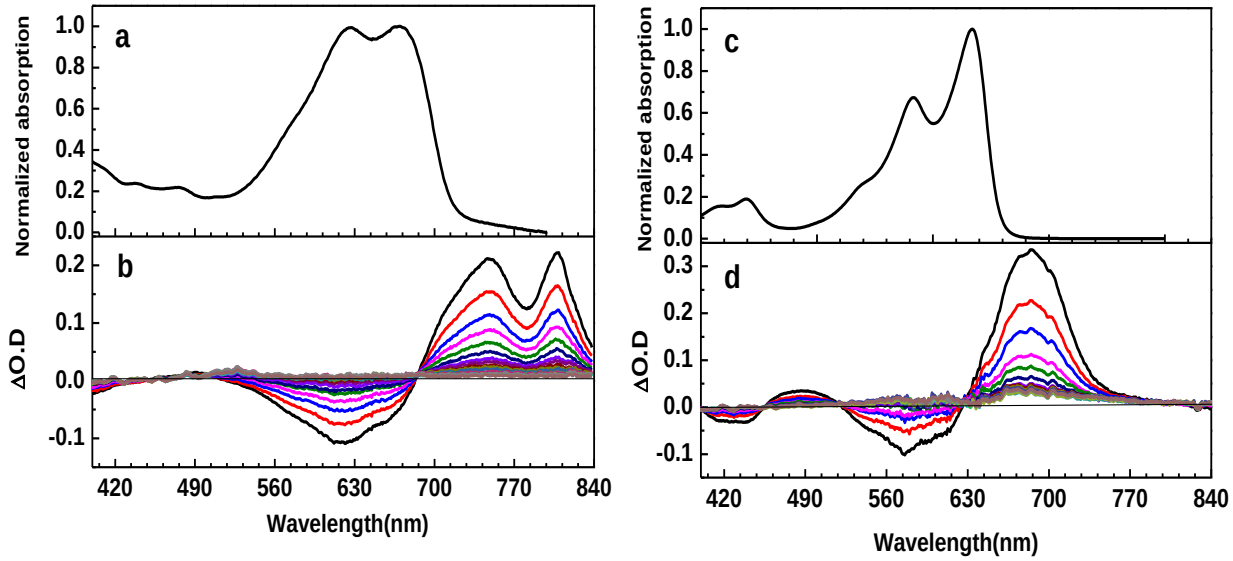

Figure 5-8. Ground state absorption (top panels) and transient absorption spectra (bottom panels). Transient spectra obtained in degassed THF solution. Initial delay 50 ns following 10 ns laser excitation pulse. a) and b) DPP-Pt(acac) transient absorption obtained with excitation at 625 nm and delay increments of 50 ns. c) and d) DPP-Pt(CC**)** transient absorption obtained with excitation at 532 nm and delay increment of 500 ns.

In general, both of the complexes gave a strong TA difference signal in the range from 500 - 800 nm. In each case, the primary TA presents as a derivative-shaped feature, with strong bleaching in the ground state absorption band with the appearance of a strong excited state absorption band to the red of the ground state band. The transients decay with lifetimes of 0.16 μs and 1.1 μs for DPP-Pt(acac) and DPP-Pt(CC), respectively, and they are quenched by oxygen, consistent with assignment to the triplet state. This assignment is further supported by the fact that similar TA difference absorption spectra were observed for Ir-substituted DPP complexes reported by

Castellano and Ziessel and assigned to the triplet-triplet absorption.[169] Importantly, excitation of the unmetallated chromophore DPP-C18 under the same conditions gave rise to no observable transient absorption due to a triplet state, consistent with the notion that intersystem crossing is promoted by the Pt auxochromes in the metal complexes. We note that the considerably shorter triplet lifetime for DPP-Pt(acac) compared to DPP-Pt(CC) is consistent with the other photophysical data by indicating that spin-orbit coupling is stronger in the former complex. The enhanced spin-orbit coupling not only increases the rate of $S_1 – T_1$ ISC, but also the rate of non-radiative decay, $T_1 – S_0$.[141]

In order to gain additional insight into the nature of the triplet-triplet absorption, TD-DFT calculations were carried out on the lowest triplet state of DPP-Pt(CC)' and DPP-Pt(acac)' (here the ' indicates the alkyl groups were truncated to $–CH_3$). These calculations show that the triplet-triplet absorption is dominated by strongly allowed one-electron transitions involving the excited electron and hole to/from the adjacent filled/occupied levels (e.g., HSOMO $\rightarrow$ LUMO + 1 and HOMO – 1 $\rightarrow$ LSUMO). This is by analogy to the "mid-gap" transitions observed in doped conjugated polymer systems, and explains the red-shift of the oscillator strength of the primary transition in the triplet state.[197] The TD-DFT calculations are able to closely predict the experimentally observed triplet-triplet absorptions (677 and 804 nm, respectively for DPP-Pt(CC)' and DPP-Pt(acac)'). Finally, the charge difference density plots for the triplet-triplet absorption suggest that there is an even greater degree of charge-transfer in this transition compared to the absorption of the ground state (APPENDIX C). This is likely due to the strong contribution of the higher unfilled levels (LUMO + 1) in the triplet-triplet

absorption, where LUMO +1 is more strongly localized on the DPP core of the chromophore.

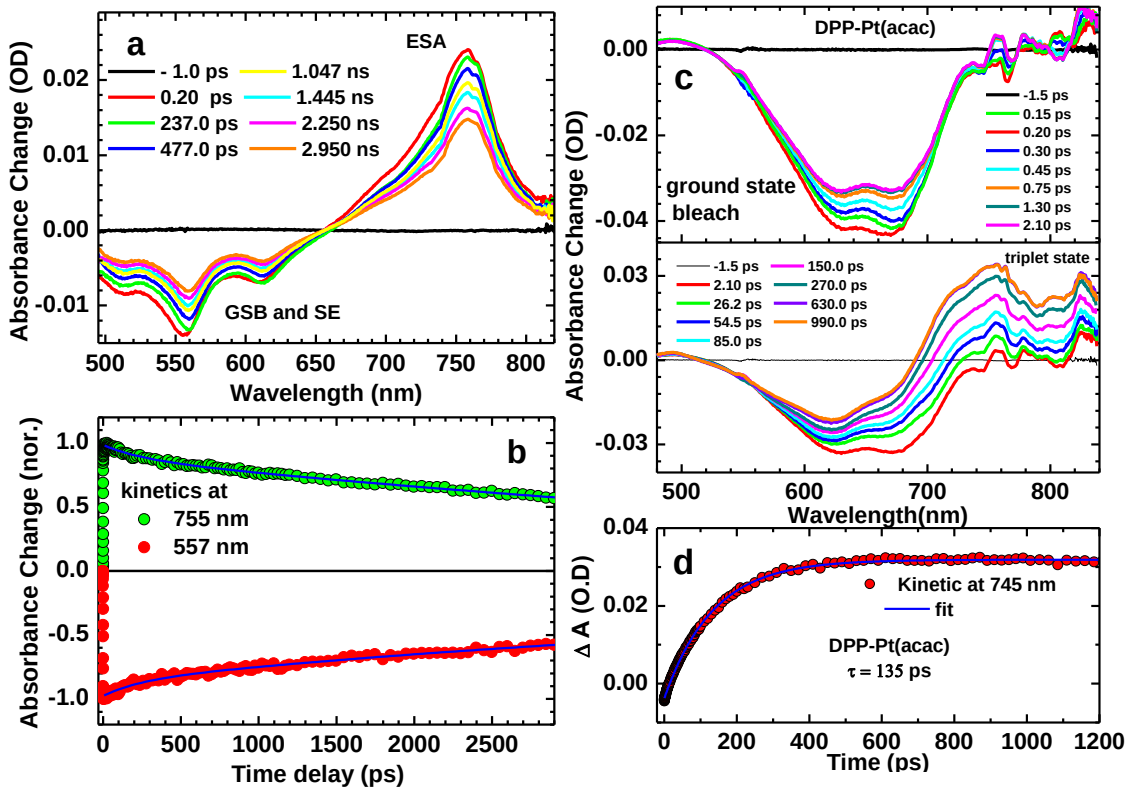

Figure 5-9. Femtosecond transient absorption spectra of DPP-C18**,** a) at different time delay increments after 475 nm excitation and b) the kinetics at 557 nm and 755 nm. Femtosecond transient absorption spectra of DPP-Pt(acac), c) at different time intervals after 550 nm excitation and d) the kinetics at 745 nm. All experiments were conducted in with samples dissolved in dichloromethane. Some data in this figure reproduced with modification from ref. [190], copyright American Chemical Society Publications 2014.

Finally, in order to gain further insight into the fast intersystem crossing in DPP-Pt(acac), femtosecond/picosecond TA spectroscopy was carried out. For comparison, the TA spectrum of DPP-C18, which does not undergo intersystem crossing, was also obtained. First, as shown in Figure 5-9a, in addition to the ground state bleach and stimulated emission in the spectral range of 490-650 nm, a positive absorption band appears at 760 nm. The spectrum is present within 200 fs following excitation, and the

only spectral evolution observed is slow decay. This spectrum is due to the absorption of the S_1 state of the DPP chromophore. It is worth noting that the lifetime of DPP is much longer than the maximum time window of the ps TA system (3 ns), and therefore an accurate decay lifetime cannot be extracted from fitting the data on this timescale. However, it is obvious that the excited state decay is fast. In addition, there no spectroscopic signature for the intersystem crossing within our time window of 3 ns, by contrast to what is observed for DPP-Pt(acac**)**.

The fs/ps TA time resolved difference spectrum for DPP-Pt(acac) is shown in Figure 5-9c. Immediately following 100 fs excitation pulse the difference spectrum is dominated by bleaching in the ground state absorption. Over a timescale of a 500 ps a broad absorption band that peaks at ~750 nm grows-in, concomitant with a blue shift in the zero-crossing point in the difference spectrum. The absorption feature that grows corresponds well with the long-lived transient absorption observed by ns-μs TA and is assigned to the triplet state. A kinetic plot obtained at 745 nm (Figure 5-9d) exhibits an exponential rise with τ = 135 ps, giving an intersystem crossing rate of $k_{isc} \sim 7.4 \times 10^9\ s^{-1}$. Note that this is excellent agreement with the rate estimated from the fluorescence parameters (Table 5-2).

Summary and Conclusions

We have carried out a detailed study of the electrochemical and photophysical properties of two novel diketopyrrolopyrrole containing metal complexes DPP-Pt(acac) and DPP-Pt(CC) featuring cyclometallated platinum and platinum acetylide auxochromes. The results clearly illustrate the effects of the different platinum auxochromes on the optical properties, and most importantly, on the spin-orbit coupling induced S-T transitions. The electrochemical data reveal that the platinum units have a

significant effect on the frontier orbital energy levels of the chromophore, and these effects are manifested by red-shifts of the long-wavelength absorption band relative to the unmetallated DPP chromophore. The effect is larger for DPP-Pt(acac), possibly in part due to the increased overall length and planarization of the π-electron system. Fluorescence and transient absorption spectroscopy show that both platinum auxochromes increase the rate of intersystem crossing, giving rise to substantial triplet yields in both DPP-Pt(acac) and DPP-Pt(CC**)**. The effect is substantially larger for the former system, revealing that the Pt(acac) auxochrome is able to more effectively induce spin-orbital coupling in the π-electron system. The enhanced spin-orbit coupling is also manifest in a substantially larger triplet decay rate in DPP-Pt(acac) compared to DPP-Pt(CC**)**.

This work shows that the addition of platinum centers onto the DPP chromophore gives rise to interesting modifications in the excited state properties of the chromophore, especially with respect to the introduction of enhanced spin-orbit coupling induced intersystem crossing, combined with substantial red-shifting in the long wavelength transition. The Pt(acac) complex exhibits substantial visible and near-infrared light absorption. Taken together, the properties of these chromophores could be useful in energy conversion applications, and future studies from our labs will explore the application of these oligomers and related polymers in organic solar cells.

Experimental

Instrumentation and Methods.

NMR spectra were recorded by using a Mercury-300 FT-NMR, operating at 300 MHz for ^{1}H NMR, 121 MHz for ^{31}P NMR and at 75.4 MHz for ^{13}C NMR. ^{1}H (500 MHz) was recorded on a Varian Inova-500 FT-NMR. Mass spectrometry for the newly

synthesized compounds was recorded in Mass Spectrometry Services, which is located in house at the University of Florida.

All photophysical measurements were performed with dry, HPLC grade tetrahydrofuran (THF) in 1 x 1 cm quartz cuvettes. Solutions for photophysical measurements were prepared by dilution of the stock solution unless otherwise mentioned. Steady state absorption spectra were obtained by a Shimadzu UV-1800 dual beam spectrophotometer. Corrected room temperature emission spectra were recorded on a Photon Technology International (PTI) spectrophotometer and collected at 90^0, relative to the excitation beam. The optical density for all samples during emission measurements was kept $\leq$0.1 at the excitation wavelength. Corrections for refractive index of the solvents were employed for both the sample and standard solutions for emission quantum yield measurements. Fluorescence lifetime data were recorded with a PicoQuant FluoTime 100 Compact Fluorescence Lifetime Spectrophotometer by time-correlated single photon counting (TCSPC) and the sample solutions were excited by a PDL-800B Picosecond Pulsed Diode Laser (375nm).

Nanosecond transient absorption spectroscopy was measured on an in-house apparatus using third harmonic of a continuum Surelite series Nd:YAG laser (λ=532 nm for DPP-Pt(CC) and 625 nm for DPP-Pt(acac) by using an OPO Plus parametric oscillator, 10 ns fwhm, 180 $\mu J\text{-pulse}^{-1}$). Probe light was produced by a xenon flash lamp and the transient absorption signal was detected by using a gated intensified CCD mounted on a 0.18M spectrograph (Princeton PiMax/Acton Pro 180). The sample solution concentrations were adjusted to O.D $\approx$ 0.7 at excitation wavelength and were deoxygenated with argon for at least 45 minutes before the measurement. Samples for

transient absorption were taken in a 1 cm pathlength flow cell (10 mL) and continuously circulated at the pump-probe region during the experiment.

In the femtosecond pump–probe transient absorption experiments, white light probe pulses were generated in a 2 mm-thick sapphire plate by a few μJ pulse energy of the fundamental output of a Ti:Sapphire femtosecond regenerative amplifier (Spectra-Physics) operating at 800 nm with 35 fs pulses and a repetition rate of 1 kHz. The excitation pulses at 475 and 550 nm were generated in an optical parametric amplifier (Newport Spectra-Physics). The pump and probe beams were focused on the sample solution, and the transmitted probe light from the samples was collected and focused on the broad-band UV-visible detector to record the time-resolved TA spectra. The difference spectra are corrected for group velocity dispersion. The optical density of DPP-C18 and DPP-Pt(acac) solutions in a 2 mm path length cuvette was adjusted to approximately 0.4 at the lowest absorption band. The solution was constantly stirred using a magnetic stirrer to provide fresh sample solution for each laser shot to avoid photodegradation.

Cyclic voltammetry (CV) study for the samples were performed using BAS CV-50W voltammetric analyzer (Bioanalytical Systems, Inc., www.bioanalytical.com) in dry dichloromethane (CH_2Cl_2) solution in presence of 0.1 M tetra-n-butylammonium hexafluorophosphate (TBAH). The electrodes used were platinum microdisk (2 mm^2) as working electrode, platinum wire as the auxiliary electrode and silver wire as the reference electrode. The sample concentrations were adjusted to 1 mM and a scan rate of 100 mV/s was maintained during the experiment. Solutions were deoxygenated by bubbling with argon prior to the experiment and a positive pressure of argon was

maintained during the experiment. All electrochemical potentials were calibrated with respect to a ferrocene internal standard ($E(Fc/Fc^+)$ = 0.43 V vs SCE in CH_2Cl_2) and the potentials reported here vs SCE.

The calculations were carried out using DFT as implemented in Gaussian 09 Rev. C.01.[198] Geometries were optimized using the B3LYP functional along with the 6-31G(d) basis set for all nonmetals, and the SDD basis set for Pt. To minimize computational cost, solubilizing PBu_3 moieties were replaced with PMe_3, and 2-ethylhexyl groups were replaced with methyls. These models are designated by the addition of a prime (') to their name, thus the model for DPP-Pt-(acac) is termed as DPP-Pt-(acac)'. All singlet optimizations were started from idealized geometries. DPP-Pt-(acac) was optimized under C2 symmetry, while DPP-Pt-(CC) was optimized without symmetry constraints. Triplet optimizations were started from the optimized singlet geometry and used the unrestricted B3LYP functional. All optimized structures were characterized by vibrational frequency calculations and were shown to be minima by the absence of imaginary frequencies. Time-dependent DFT calculations were performed for all optimized structures at the same level of theory with the same basis sets. Structures and orbitals were visualized using Chemcraft Version 1.7[199] which was also used to generate charge difference density plots.

General Methods for Synthesis

All the reactions were performed under argon atmosphere. THF was dried using solvent purification columns (Glass Contour). All the other solvents were used without further purification unless specified. The synthesis of the complexes DPP-Pt(acac) and DPP-Pt(CC) were achieved by following Figure 5-3 and Figure 5-4 respectively. Intermediate compounds 5-1,[200] 5-2,[163] 5-3,[193] 5-5, 5-6[201] and platinum complex 5-9[118]

were synthesized by following literature procedures. 2-octyldodecyl iodide was synthesized also by following literature procedure.[202] The precursor compound for Pt(acac), 2-(5-bromo-2-thienyl)pyridine was purchased from Fisher scientific. Potassium tetrachloroplatinate, bis(triphenylphosphine)palladium(II) dichloride were purchased from Strem Chemicals. $Pd_2(dba)_3$, $Pd(P^tBu_3)_2$ and Potassium phosphate tribasic were purchased from Sigma- Aldrich and used as received. Trimethylsilyl acetylene was purchased from GFS Chemical and was used as received.

Synthesis of Pt(acac)

A solution of 2-(5-bromo-2-thienyl)pyridine (0.614 g, 2.56 mmol), K_2PtCl_4 (0.506 g, 1.24 mmol) in 2-ethoxyethanol (15 mL) and water (5 mL) were deoxygenated by purging with argon for 30 minutes. Then it was heated to 80˚C for 24 hour. It was cooled down to room temperature and the bright yellow colored Pt (II) µ-dichloro-bridged dimer was filtered off, washed with copious amount of water and finally dried under vacuum for 24 hour. The platinum dimer (0.7 g, 0.75 mmol) Na_2CO_3 (0.794 g, 7.5 mmol), 2, 4-pentanedione (0.23 g, 2.3 mmol) was dissolved in 2-ethoxyethanol (30 mL) in a sealed tube and heated to 100˚C for 24 hours. The mixture was cooled down to room temperature, poured into water and extracted with dichloromethane. The combined organic layer was dried with anhydrous Na_2SO_4 and the solvent was evaporated under vacuum to isolate yellow oil. The crude product was purified via flash column chromatography on silica using dichloromethane/hexane (1:1) as eluent to isolate a yellow solid as product in 60% yield. ^{1}H NMR (300 MHz, $CDCl_3$): δ 8.75 (d, 1H, J= 5.8 Hz), 7.65 (t, 1H, J= 8.4 Hz), 7.14 (d, 1H, J= 7.6 Hz), 7.1 (s, 1H), 6.91 (t, 1H, J= 6.1 Hz), 5.47 (s, 1H), 1.99 (s, 1H), 1.96 (s, 1H). ^{13}C NMR (75 MHz, $CDCl_3$): 185.12, 183.86, 147.21, 138.73, 132.87, 118.59, 116.98, 102.51, 28.06, 26.70 (two of the aromatic

quaternary carbon was not observed). MALDI-TOF MS (*m/z*) $[M]^+$ Calcd for $C_{14}H_{12}BrNO_2PtS$, 533.3 ; found, 533.94.

Synthesis of DPP-Pt(acac)

A mixture containing 5-3 (0.135 g, 0.121 mmol), Pt(acac) (0.135 g, 0.253 mmol) and THF(18 mL) were taken in a two necked flask and deoxygenated with argon for 45 minutes. $Pd_2(dba)_3$ (6mg, .007 mmol) and $Pd(P^tBu_3)_2$ (6.2 mg, 0.012 mmol) were added under strong flow of argon. A previously deoxygenated 2 mL solution of K_3PO_4 (0.154 g, 0.725 mmol) was added promptly to the reaction mixture. Immediately the color of the solution changed to bluish green from pink. After the reaction mixture was heated to reflux overnight. The solvent was evaporated to dryness under vacuum and methanol was added to obtain a dark green residue. The crude product was recrystallized from THF/diethylether solvent mixture to obtain a shiny dark green solid (130 mg, 60%). ^{1}H NMR (500 MHz, $CDCl_3$): δ 9.02 (s, 1H), δ 8.79 (d, 1H, J= 5.4 Hz), δ 7.68 (t, 1H, J= 7.6 Hz), δ 7.33 (s, 2H), δ 7.22 (d, 1H, J= 7.7 Hz), δ 6.91 (m, 1H), δ 5.53 (s, 1H), δ 4.07 (d, 2H, J= 7.0 Hz), δ 2.06 (s, 1H), δ 2.03 (s, 1H), δ 2.02 (m, 1H), δ 1.28-1.24 (m, 32H), δ 0.87 (m, 6H). ^{13}C NMR (125 MHz, $CDCl_3$, δ): 185.4, 184.0, 161.5, 147.2, 138.5, 136.8, 128.1, 125.04, 118.4, 117.0, 102.8, 46.4, 38.0, 31.9, 31.3, 30.2, 29.7, 29.6, 29.4, 29.3, 28.1, 26.9, 26.4, 22.8, 14.2 (some of the quaternary carbons is difficult to observe). MALDI-TOF MS (*m/z*) $[M]^+$ Calcd for $C_{82}H_{110}N_4O_6Pt_2S_4$, 1766.21; found, 1766.66.

Synthesis of 5-7

In a 50 mL Schlenk flask (vacuum-argon cycled twice) 5-5 (0.100 g, 0.15 mmol) CuI (2.8 mg, 0.015 mmol) and $PdCl_2(PPh_3)_2$ (5 mg, 0.0073mmol) were dissolved in argon purged THF (6 mL)/diisopropylamine (4mL) solvent mixture. Trimethylsilyl acetylene (0.1 ml, 0.7 mmol) was added to the reaction mixture and heated to 40^0C

overnight under argon atmosphere. Solvents were removed under vacuum and the crude product was further purified by column chromatography on silica with hexane/dichloromethane (1:1) as eluent. The product was isolated as dark purple solid in 76% yield.^{1}H NMR (500 MHz, $CDCl_3$): δ 8.83 (d, 2H, J= 4.1 Hz), δ 7.33 (d, 2H, J= 4.1 Hz), 3.99 (m, 4H), 1.87 (m, 2H), 1.35 (m, 16H), 0.89 (m, 12H), 0.29 (s, 18H). ^{13}C NMR (125 MHz, $CDCl_3$, δ): 161.75, 139.86, 135.52, 133.82, 130.72, 128.62, 109.10, 104.49, 96.95, 46.26, 39.35, 30.41, 28.63, 23.84, 23.40, 14.31, 10.73, 0.00.

Synthesis of 5-8

5-6 (0.1 g, 0.14 mmol) and KF (0.109 g, 1.89 mmol) were taken in a two necked flask and dissolved in a mixture of deoxygenated THF/ water (9 mL/ 2.8 mL). The reaction mixture was stirred overnight under inert atmosphere and stirred vigorously. The product was extracted with dichloromethane; combined organic layer was dried over anhydrous Na_2SO_4 and evaporated to obtain the crude mixture. It was further purified by column chromatography on silica gel using DCM/hexane (7:3) as eluent to obtain the product in 75% yield. ^{1}H NMR (500 MHz, $CDCl_3$): δ 8.85 (d, 2H, J= 4.1 Hz), 7.40 (d, 2H, J= 4.1 Hz), 4.01 (m, 4H), 3.61 (s, 2H), 1.87 (m, 2H), 1.37 (m, 16H), 0.90 (m, 12H). ^{13}C NMR (125 MHz, $CDCl_3$, δ): 161.46, 139.60, 135.18, 134.16, 130.73, 126.99, 108.93, 85.46, 76.26, 46.05, 39.13, 30.12, 28.28, 23.52, 23.04, 14.01, 10.45.

Synthesis of DPP-Pt(CC)

To a 25 mL Schlenk flask 5-8 (0.110 g, 0.15 mmol) was dissolved in THF (7 mL)/ diethylamine (7 mL) and degassed with argon for 45 minutes. 5-7 (0.042 g, 0.073 mmol) and CuI (4 mg, 0.02 mmol) were added to the reaction mixture. The color of the solution was turned from red to dark purple and it was stirred overnight at room temperature under argon atmosphere. Silica gel was added to the resulting reaction mixture and the

solvent was evaporated under vacuum. The crude product was purified by column chromatography on silica gel using ethyl acetate/ hexane (5:95) as eluent. The product was isolated in 63% yield as dark purple solid. ^{1}H NMR (500 MHz, $CDCl_3$): δ 8.98 (d, 2H, J= 4.1 Hz), 7.29 (m, 4H), 7.21 (t, 4H, J= 7.4 Hz), 7.12 (t, 2H, J= 7.0 Hz), 6.95 (d, 2H, J= 4.0 Hz), 4.02 (m, 4H), 2.16 (m, 24H), 1.96 (m, 2H), 1.63 (m, 24H), 1.49 (m, 24H), 1.39 (m, 16H), 0.93 (t, 36H, J= 7.2 Hz), 0.91 (m, 12H). ^{13}C NMR (125 MHz, $CDCl_3$, δ): 161.72, 139.28, 136.58, 135.66, 130.76, 129.00, 128.75, 127.88, 126.18, 125.02, 124.71, 109.76, 107.57, 106.76, 102.06, 46.02, 39.05, 30.12, 28.30, 26.38, 24.41, 23.98, 23.49, 23.13, 14.06, 13.83, 10.50. ^{31}P NMR (121 MHz, $CDCl_3$) δ 3.42 ($J_{Pt\text{-}P}$ = 2334.1 Hz). MALDI-TOF MS (*m/z*) $[M]^+$ Calcd for $C_{98}H_{156}N_2O_2P_4Pt_2S_2$, 1971.9867 ; found, 1971.9866.

CHAPTER 6
CYCLOMETALLATED PLATINUM CONTAINING DIKETOPYRROLOPYRROLE COMPLEXES AND POLYMERS FOR PHOTOVOLTAIC APPLICATIONS

Background

Organic π-conjugated materials have gained a significant amount of attention over the past few years for application in organic photovoltaic devices (OPVs) due to their light weight, cost effectiveness and ease of solution processibility.[4] Among several OPVs, bulk heterojunction solar cells are promising where an interpenetrating network of donor and acceptor materials are present to combat the problems against low diffusion length of the excitons (5-10 nm) and low thickness of the active layer in bilayer devices. The following series of events are necessary for efficient generation of photocurrent: 1) absorption of solar light and efficient generation of exciton (Coulombically coupled electron and hole pair), 2) diffusion of the excitons to the donor-acceptor interface, 3) dissociation of the excitons to electrons and holes and finally, 4) movement of the free charges to the respective electrodes. Heavy atom containing organometallic π-conjugated chromophores have recently drawn attention as a donor materials in bulk heterojunction solar cells because of the facile generation of triplet excited states. There are several reasons at fundamental level that supports the notion why the triplet excited state might be important for photovoltaic devices. It has been shown that triplet exciton can improve the photocurrent by increasing the diffusion length of the exciton (due to longer lifetime of triplet exciton) and also by prohibiting charge recombination of the geminate ion-radical pair.[68,73]

Exciton diffusion length (L_D) depends on lifetime of the exciton (τ) and the diffusivity (D) by following the relation $L_D = (\tau D)^{1/2}$. Diffusivity of an exciton depends in

part on the conjugation length of the chromophore. Although, until now the majority of organometallic polymer for photovoltaics evolves around platinum acetylide systems because of facile generation of triplet exciton; however, it suffers poor diffusivity of the excitons due to inefficient orbital overlap between Pt-5d and C-2p orbital. In an effort to overcome this problem, Frechet and coworkers, incorporated cyclometallated platinum motif to the thiophene and fluorine containing polymer backbone. The thiophene containing cyclometallated polymer gave PCE of 1.3% with PCBM as acceptor.[188] Cheng and coworkers reported a series of polymers containing indacenodithiophene and cyclometallated platinum achieving PCE of 2.9 %.[76] Other than platinum, cyclometallated iridium chromophores are also proved as promising candidates for bulk-heterojunction solar cell devices.[73,82]

We have recently shown enhanced efficiency for generation of triplet excited state in diketopyrrolopyrrole containing cyclometallated donor-acceptor chromophores compared to the analogous platinum acetylide systems.[156] In another line of study we have shown, these materials exhibit fast electron transfer, slow charge recombination to various acceptors which encouraged us to study this metal complex for photovoltaic applications.[203] Unfortunately, the devices made from DPP-Pt(acac) (structure shown below) as donor and $PC_{71}BM$ as acceptor gave poor efficiency (~ 0.1%). In an effort to understand the result, ground state absorption spectra of the thin films were measured for DPP-Pt(acac), $PC_{71}BM$ separately and DPP-Pt(acac)- $PC_{71}BM$ blend. All the spectra are presented in Figure 6-1. The absorption spectrum of DPP-Pt(acac) shows a significant red shift compared to the solution absorption spectra due to aggregation in the solid state. The spectrum is dominated by an intense absorption at 600 - 900 nm

and weak absorption in the region 300 - 500 nm. $PC_{71}BM$ shows a broad absorption spectra between 300 -800 nm. However, when combined for the preparation of the active layer, the absorption of DPP-Pt(acac):$PC_{71}BM$ (1:6) is solely dominated by PCBM absorption in the region of 300 - 800 nm. We speculate that, this is due to the formation of aggregates in the mixture which results in separation of DPP-Pt(acac) during filtration.

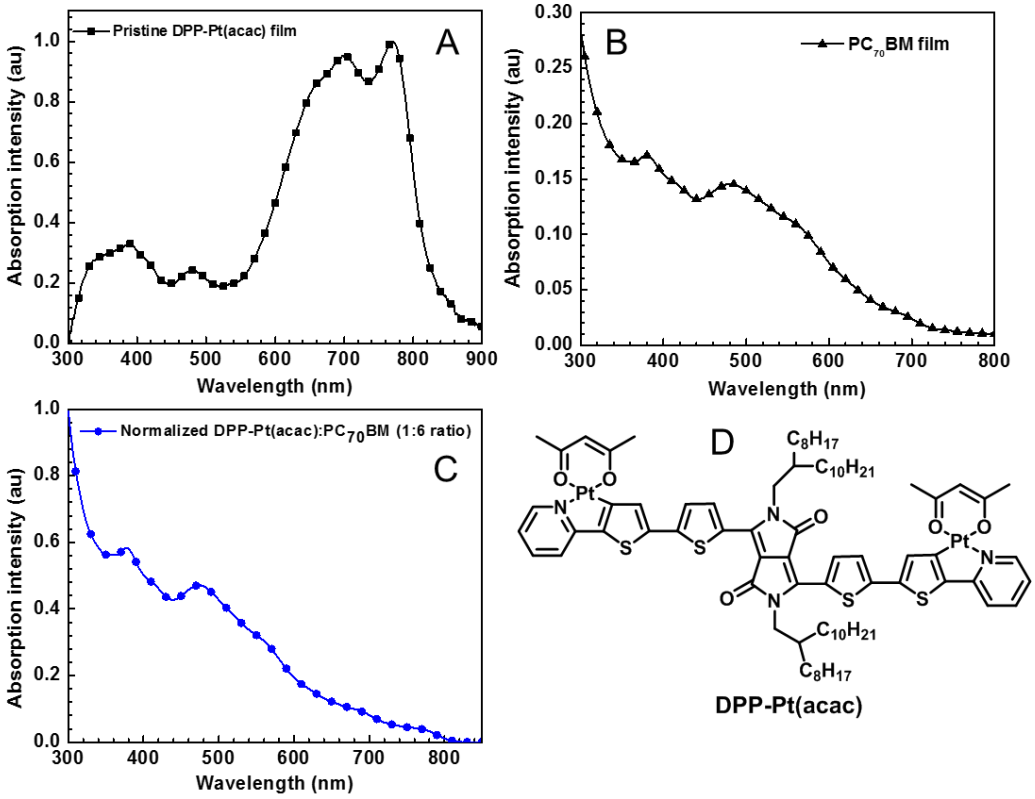

Figure 6-1. Absorption spectra of thin films made from- DPP-Pt(acac) (A), $PC_{70}BM$ (B), DPP-Pt(acac):$PC_{70}BM$ (1:6) (C) and structure of DPP-Pt(acac) (D).

One possible pathway to overcome this problem is to improve the solubility of the platinum containing material. In order to do that, a modified acetylacetonate (acac) ligand “octyl-acac” is synthesized and incorporated into platinum complex. Two DPP complexes were synthesized with ethylhexyl and octyldodecyl side chains at the central nitrogen, named as DPP-C8-Pt(acac) and DPP-C18-Pt(acac) respectively. The ligand

DPP-C8-Th-Py was synthesized to compare the photophysical properties with the metal complexes. The polymers DPP-Th-Pt-P1 and DPP-Ph-Pt-P2 were synthesized with thienyl-pyridine and phenyl-pyridine as cyclometallated ligand respectively.

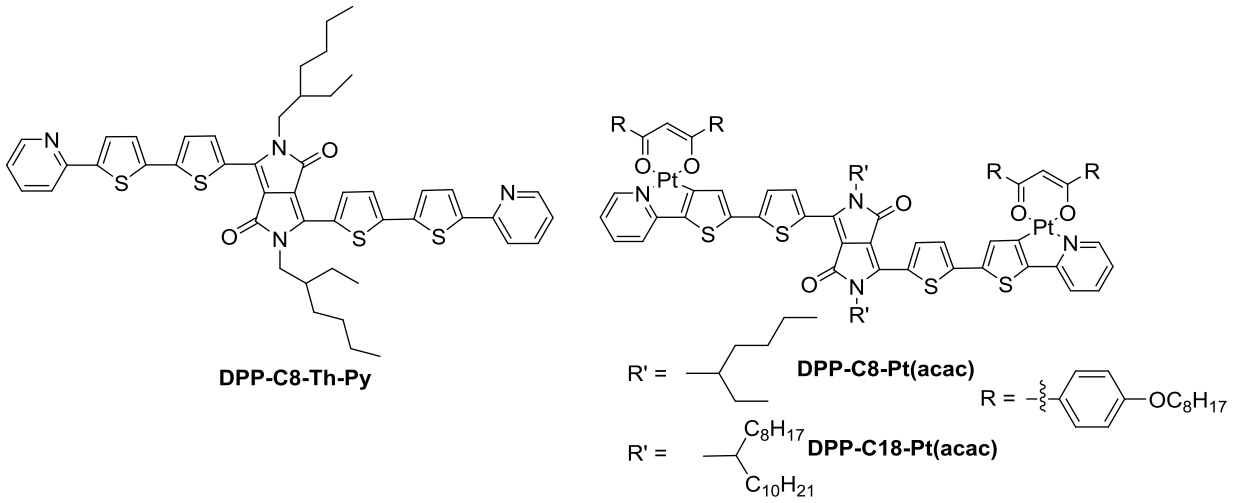

Figure 6-2. Chemical structures of the metal complexes and ligand investigated herein.

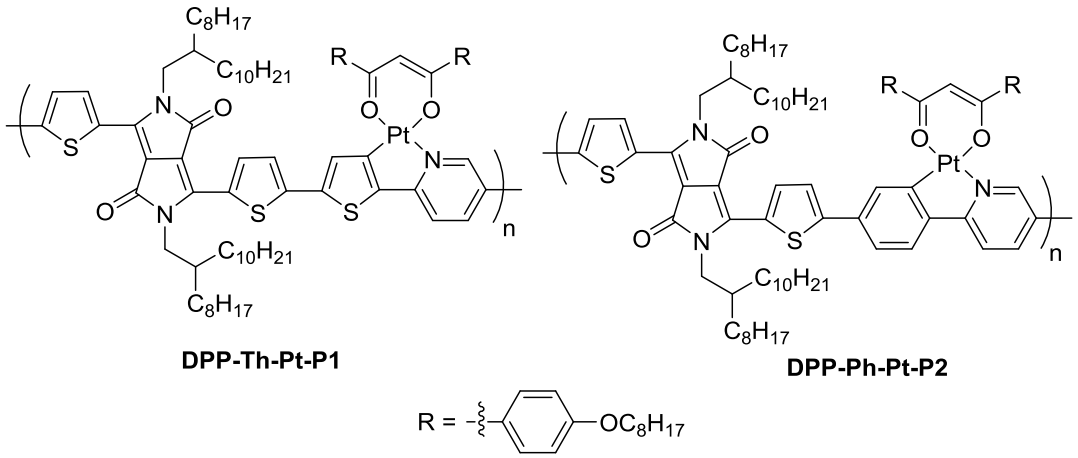

Figure 6-3. Chemical structures of the polymers reported herein.

All the newly synthesized metal complexes and ligands are characterized by ^{1}H NMR, ^{13}C NMR, mass spectra and elemental analysis. The molecular weight of the polymers is estimated by Gel Permeation Chromatography (GPC). The photophysical properties were characterized by ground state absorption, emission and nanosecond transient absorption spectroscopy. The fluorescence quantum yields for the ligand and

metal complexes are much reduced compared to DPP-C18 (DPP without any terminal thienyl-pyridine moiety).[156] The ligand DPP-C8-Th-Py also exhibits triplet excited state in transient absorption spectra possibly due to the presence of four conjugated thiophene rings. Both the polymers are used as donor materials to fabricate bulk-heterojunction solar cells with $PC_{71}BM$ as an acceptor. The thiophene containing polymer DPP-Th-Pt-P1 gave efficiency as high as 1.77% with 1:7 polymer: $PC_{71}BM$ weight ratio compared to DPP-Ph-Pt-P2 which gave 0.45% efficiency. The fill factor for the thiophene containing polymers is ~66%, which is the highest known value to date for an organometallic polymer to the best of our knowledge.

Results and Discussion

Synthesis

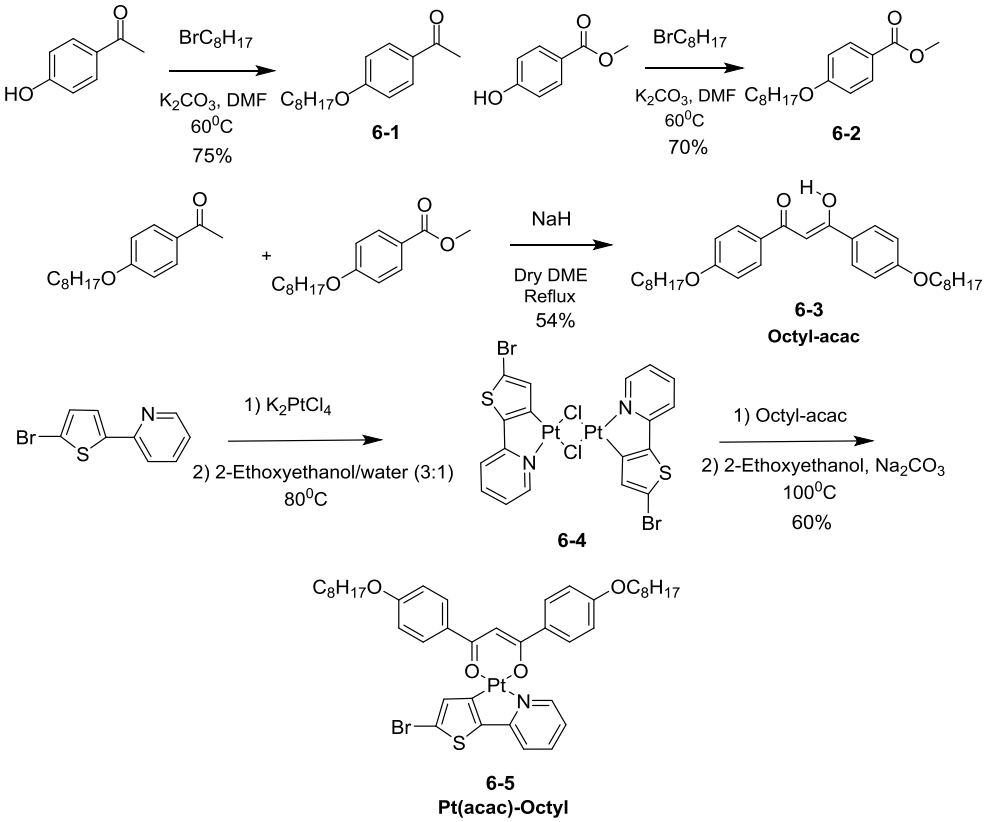

Figure 6-4. Synthetic scheme of octyl-acac and Pt(acac)-Octyl.

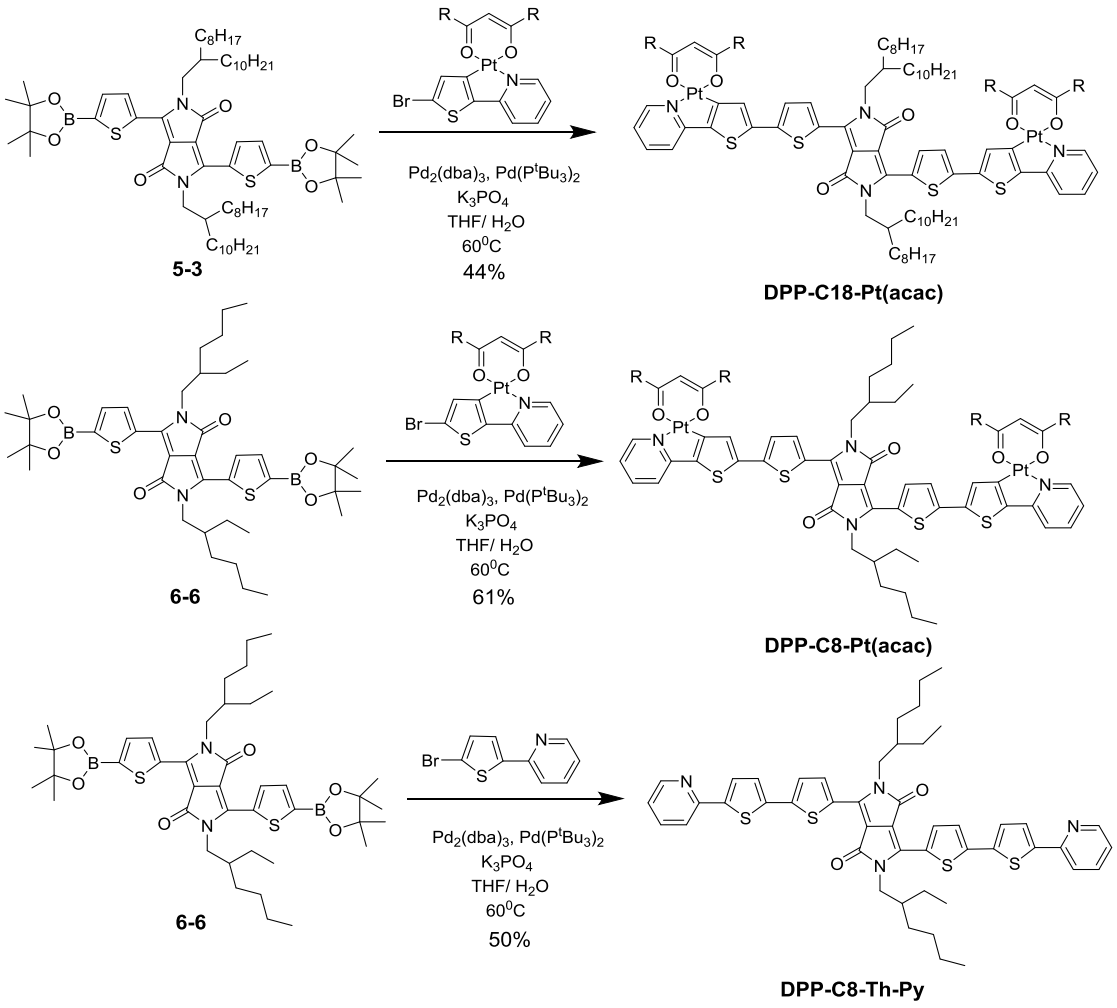

Figure 6-5. Synthetic scheme for the ligand and metal complexes.

The ligand octyl-acac was synthesized by following literature procedure.[188] The commercially available starting materials 4-Hydroxybenzoic acid methyl ester and 4-Hydroxyacetophenone were alkylated in presence of anhydrous K_2CO_3 in anhydrous DMF to obtain 6-2 and 6-1 in good yields. Finally, octyl-acac was obtained by reacting 6-1 and 6-2 in presence of NaH in dry DME under refluxing condition. 2-(5-bromo-2-thienyl)pyridine was reacted with K_2PtCl_4 to obtain bright yellow colored dimer 6-4. The dimer precursor was cleaved by reaction with octyl-acac and Na_2CO_3 in 2-ethoxyethanol at 100˚C to obtain Pt(acac)-Octyl (6-5). Boronate ester derivative 5-3 and 6-6 were

synthesized by following literature procedure. DPP-C18-Pt(acac) and DPP-C8-Pt(acac) were synthesized from boronate ester derivative of respective DPP chromophores 5-3 and 6-6 respectively under Suzuki cross coupling condition.

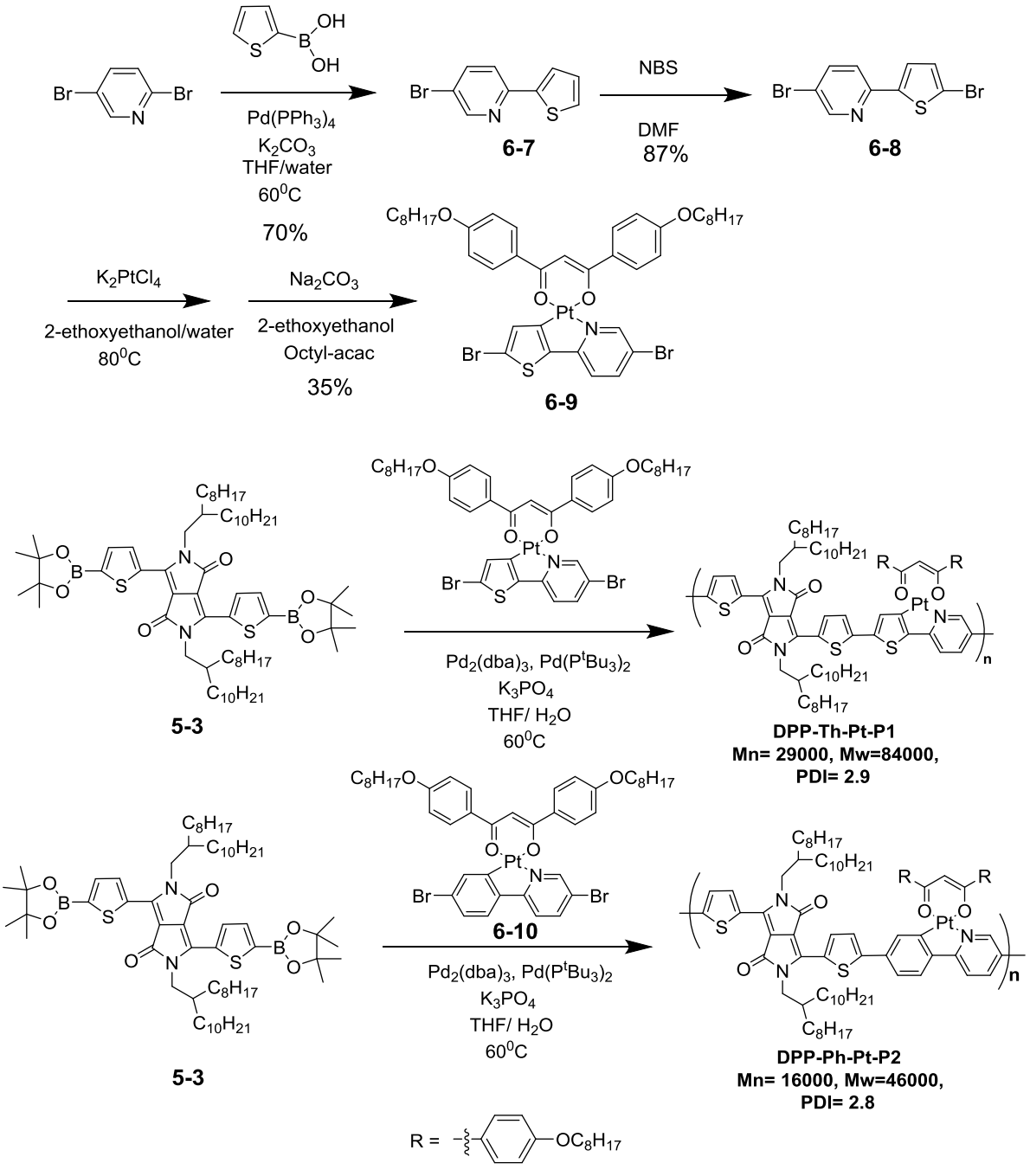

Figure 6-6. Synthetic scheme for the polymer precursor and the polymers.

For the polymerization reactions, the dibromo derivative of the cyclometallated platinum complex 6-9 was synthesized by following a literature procedure to a similar compound. To obtain 6-7, 2,5-Dibromopyridine was reacted with thien-2- yl-2-boronic acid in presence of $Pd(PPh_3)_4$ catalyst and K_2CO_3 base in THF/water solvent mixture. In the next step, 6-7 was brominated with NBS in anhydrous DMF to obtain 6-8 as a white solid. Finally, 6-8 was treated with K_2PtCl_4 to obtain the chloride bridged dimer and subsequently it was cleaved by Na_2CO_3 and Pt(acac)-Octyl in 2-ethoxyethanol at 100˚C to obtain 6-9 as a bright yellow solid. The polymer DPP-Th-Pt-P1 was obtained with molecular weight of 29000 g/mol with a PDI of 2.9, when 5-3 was reacted with 6-9 Phenyl substituted polymer DPP-Ph-Pt-P2 was synthesized by reacting 5-3 with 6-10 under Suzuki cross coupling condition with number average molecular weight 16000 g/mol and PDI 2.8.

Ground State Absorption Spectra

The ground state absorption spectra of the ligand, metal complexes and polymers are recorded in THF solution and presented in Figure 6-7 (A and C). The absorption maxima (λ_{max}) and molar extinction coefficient (ε) values are shown in Table 6-1. In general, the spectra are dominated by an intense absorption at 500 -900 nm and weak absorption in the near UV region (300 - 500 nm). The low energy transition can be attributed to donor-acceptor charge transfer transition while the high energy absorption peak is due to π-π* transition.

Significant red shifts in absorption maxima (~40 nm) and the onset of absorption (~41 nm) were observed for both the metal complexes in comparison to the ligand DPP-C8-Th-Py. This fact suggest extensive increase in conjugation is achieved by

metallation, likely due to increased planarity of the conjugated DPP backbone.[76] In general the spectral shape remained same at longer wavelength region. However, enhanced absorptivity is observed for the metal complexes at 300 -400 nm due to localized absorption of Pt(acac)-octyl. The absorption spectra remain almost the same when the alkyl chain is changed from C8 for DPP-C8-Pt(acac) to C18 for DPP-C18-Pt(acac). Note here, the λ_{max} and ε for the metal complexes are similar to the reported values for DPP-Pt(acac).[156] This fact is in complete agreement with the report from Swager and coworkers where they found increasing the conjugation from "acac" part hardly effects the solution state photophysics as the ligand centered excited state is lowest in energy.[189]

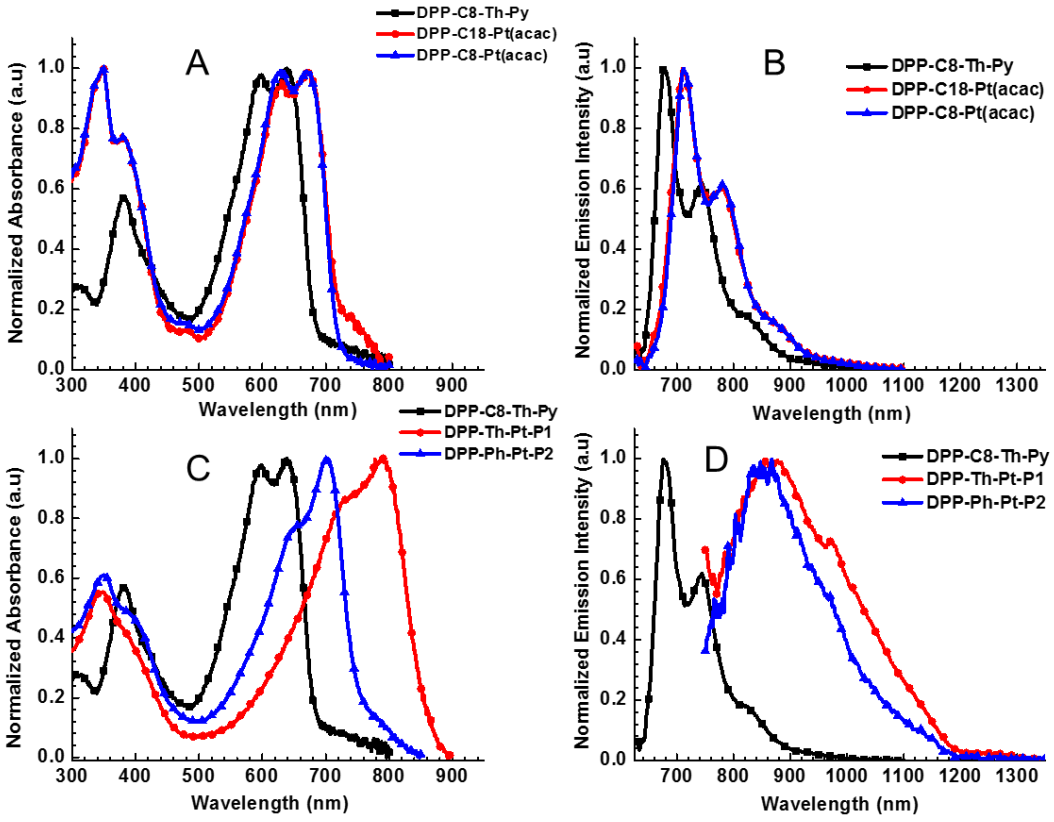

Figure 6-7. Ground state absorption spectra of (A) ligand and metal complexes, (C) ligand and polymers in THF. Steady state photoluminescence spectra of (B) ligand and metal complexes and (D) ligand and polymers in THF.

Both of the polymers exhibit a red shift in absorption compared to the ligand and metal complexes. However, the λ_{max} for phenyl containing polymer DPP-Ph-Pt-P2 is blue shifted compared to thiophene containing polymer DPP-Th-Pt-P1, which has onset of absorption at ~ 900 nm. This fact can be attributed to the lowering of HOMO energy level when a phenyl ring is inserted in between two thiophene rings in DPP system.[204,205] The absorption spectra of the polymers are also broadened compared to the model complexes due to increased conjugation length and possible heterogeneity in conjugation length. The thiophene containing polymer has a higher molar extinction coefficient (25,000 M^{-1} cm^{-1}) compared to the phenyl containing polymer (16,500 $M^{-1}cm^{-1}$). The enhanced molar extinction coefficient of the model complexes compared to the polymer is in part an artifact arising because of the polymer repeat unit (PRU) used for the calculation of molar absorptivity has one cyclometallated platinum motif, whereas model complexes contain two.

Table 6-1. Summary of photophysical properties.[a]

Compound	λ_{max} (nm)	ε x 10^4 ($M^{-1}cm^{-1}$)	λ_{em} (nm)	ϕ_{fl} [b]	τ_{fl} (ns)	τ_{TA} (µs)
DPP-C8-Th-Py	639	2.2	676	0.27	1.2	2.02
DPP-C18-Pt(acac)	672	4.1	710	0.01	<0.2	0.16
DPP-C8-Pt(acac)	670	2.8	711	0.01	<0.2	0.16
DPP-Th-Pt-P1	790	2.5	872	<0.01	<0.2	-
DPP-Ph-Pt-P2	702	1.7	850	<0.01	<0.2	0.43

Note: [a] All the photophysical properties were measured in THF. [b] Quantum yield measured using tetraphenylporphyrin in toluene (ϕ_F=0.09) as actinometer.

Steady-State Photoluminescence Spectroscopy

Room temperature photoluminescence spectra of the ligand, metal complexes and polymers were recorded in THF solution, and are shown in Figure 6-7 (C and D).

Emission maxima (λ_{Fl}), quantum yield of emission (ϕ_{Fl}) and emission lifetime (τ_{Fl}) are listed in Table 6-1.

The ligand DPP-C8-Th-Py and metal complexes DPP-C8-Pt(acac), DPP-C18-Pt(acac) exhibit similar vibronically structured emission spectra. On the basis of minimal Stokes shift from the absorption and short lifetime (<200 ps), the emission is attributed to the fluorescence from $^1\pi,\pi^*$ state. The trends observed in the absorption spectra are mirrored in the emission spectra with the exception of polymers. In particular, for both the polymers, the emission spectra extend far into the IR region until 1300 nm and are significantly broadened compared to the ligand and metal complexes. Surprisingly, there is very minimal difference in λ_{Fl} is observed between two polymers.

It is important to note here, only by incorporation of thienyl pyridine group to DPP-C18 (the central DPP unit with two thiophenes)[156], decreases the fluorescence quantum yield from 86% to 27% and the lifetime of emission from 5.8 ns to 2.7 ns. The quantum yield of emission (ϕ_{Fl}) further decreases from ~27% for ligand DPP-C8-Th-Py to ~1% for the metal complexes. The lifetime of the singlet excited state for the metal complexes was found <200 ps. We postulate, this significant decrease in fluorescence quantum yield is due to efficient intersystem crossing (ISC) from $S_1 \rightarrow T_1$ promoted by strong spin-orbit coupling due to the heavy atom platinum. As fluorescence quantum yield for DPP-Pt(acac) (ϕ_{Fl}= 2.2%)[156] is almost similar to DPP-C8-Pt(acac) and DPP-C18-Pt(acac), we assume the intersystem crossing yield is similar if not higher ($\phi_{ISC} \geq$ 97%).

Transient Absorption Spectroscopy

Overall the moderate to low fluorescence quantum yields and very short emission lifetimes of the chromophores suggest efficient ISC to the triplet excited state for the metal complexes and polymers. In an effort to probe the triplet excited state of these organometallic chromophores, ns-µs transient absorption spectroscopy (TA) was performed with the deoxygenated THF solutions by exciting them at 355 nm. The TA spectra for the ligand DPP-C8-Th-Py along with ground state absorption spectra are plotted and shown in Figure 6-8 and Figure 6-9.

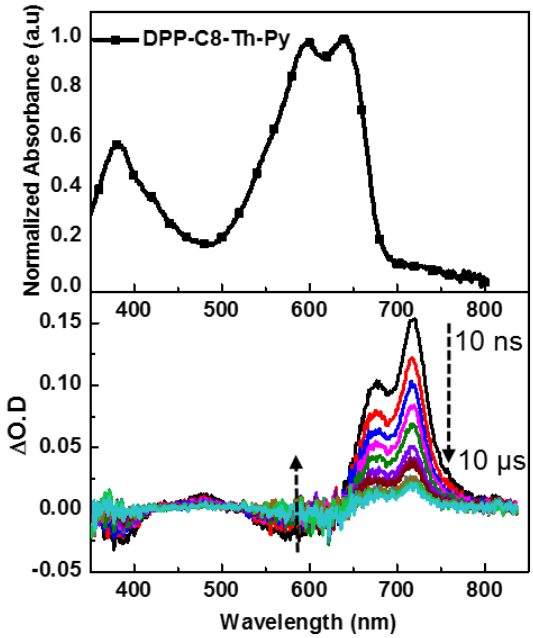

Figure 6-8. Ground state absorption spectra (top panel) and transient absorption spectra (bottom panel) of DPP-C8-Th-Py. Transient absorption spectra were obtained in deoxygenated THF solution. The sample was excited by 355 nm laser pulse, initial delay 10 ns following a 10 ns laser pulse and delay increments of 500 ns was used.

It is interesting to note that although a triplet excited state was not observed from DPP-C18 (only DPP core) by transient absorption: however, here we can see that DPP-C8-Th-Py shows strong transient absorption from a triplet excited state (Figure 6-8). We

believe this is due to the presence of additional thiophene rings from thienyl-pyridine group which enhances ISC to the triplet excited state by heavy atom effect of sulfur.[111]

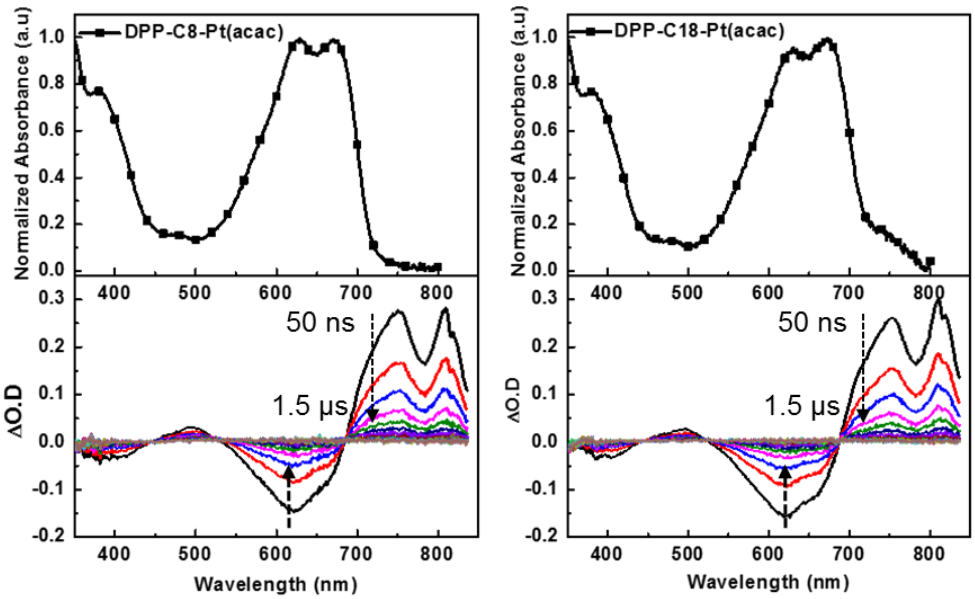

Figure 6-9. Ground state absorption spectra (top panel) and transient absorption spectra (bottom panel) of the metal complexes DPP-C8-Pt(acac) and DPP-C18-Pt(acac). Transient absorption spectra were obtained in deoxygenated THF solution. It was excited by 355 nm laser pulse, Initial delay 50 ns following a 10 ns laser pulse and delay increments of 75 ns was used.

In general both the metal complexes exhibit ground state bleach in between 300 nm to 650 nm and strong transient absorption between 650 to 850 nm. The intensity of the transient absorption signal is almost ~2 times higher for the metal complexes compared to ligand DPP-C8-Th-Py (Figure 6-9). As the experiment was performed with sample solutions of matched absorption at excitation wavelength, with the same laser power and intensity, we assume the stronger transient signal signals a higher triplet yield for the metal complexes. The lifetime of the triplet excited state is calculated from the decay of the transient absorption. The ligand DPP-C8-Th-Py has a longer triplet excited state lifetime (~2.02 μs) compared to the metal complexes (~0.16 μs). Presumably, this shorter lifetime is due to the strong spin-orbit coupling effect of

platinum which enhances the rate of $T_1 \rightarrow S_0$ intersystem crossing. It is important to note here, the spectral shape of the transient absorption along with the triplet excited state lifetimes of the metal complexes are nearly the same as previously reported for DPP-Pt(acac).[156] This is in agreement with the other solution state photophysics, which proves modified "acac" ligand octyl-acac has almost no impact on the electronic properties of the molecule in solution.

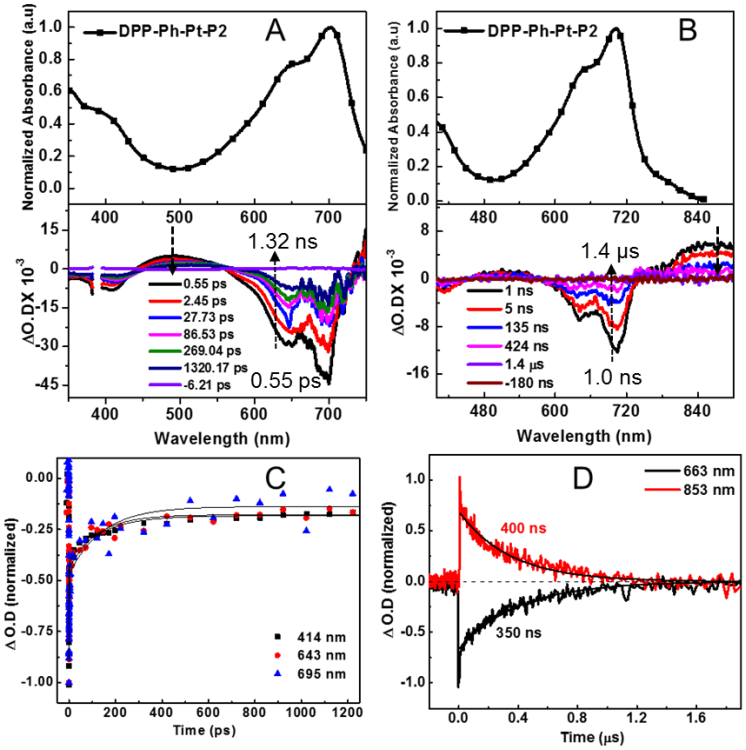

Figure 6-10. (A) Picosecond and (B) nanosecond transient absorption spectra of phenyl containing polymer DPP-Ph-Pt-P2, (C) the kinetic data of the transients at 414, 643 and 695 nm for femtosecond transient absorption spectra (D) the kinetic data of the transients at 853 nm (positive) and 663 nm (negative) for DPP-Ph-Pt-P2, The spectra were recorded at the delay times indicated at the plot legends immediately after excitation at 388 nm in deoxygenated THF.

Ultrafast transient absorption spectroscopy was performed on the Pt polymers in collaboration with Prof. John Papanikolas group and Melissa Gish at the University of North Carolina, Chapel Hill. Time resolved spectra for the polymers were recorded in

THF with an excitation wavelength of 388 nm produced by a 100 fs Ti-sapphire laser. Figure 6-10 (A and B) shows the picosecond and nanosecond transient absorption spectra of DPP-Ph-Pt-2 (bottom panel) along with the ground state absorption spectra (top panel). In general, the spectra consist of ground state bleach in between 350 -450 nm and 600 - 700 nm which correlates well with the ground state absorption spectra. It is important to note here, in femtosecond spectra the feature within 450 -500 nm started growing within 0.6 ps and decayed with a lifetime of ~1.3 ns. Due to the short lifetime, we believe, this is due to singlet excited state absorption from $S_1 \rightarrow S_n$. The nanosecond transient absorption spectra exhibits an additional feature between 750 - 900 nm which started growing within 1 ns and persists for ~1.4 µs. We attribute this feature to the excited state absorption from $T_1 \rightarrow T_n$ due to its relatively longer lifetime compared to the other transient at 500 nm.

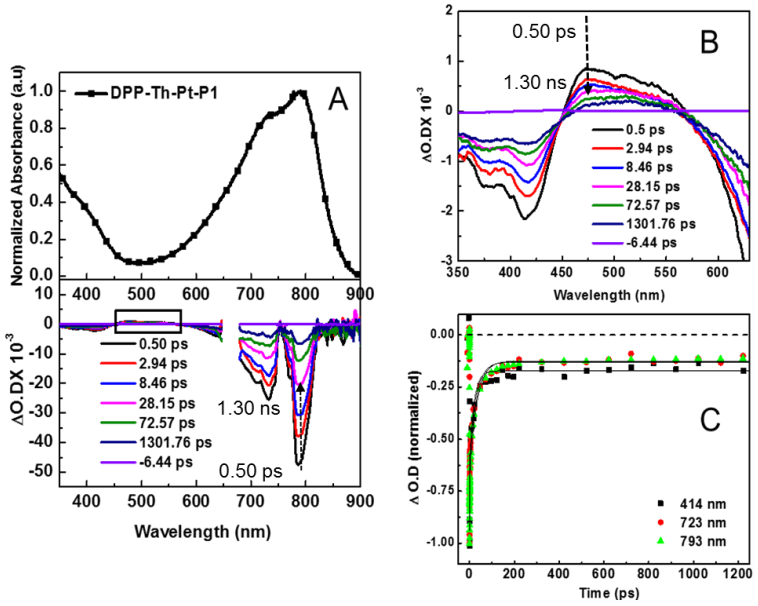

Figure 6-11. (A) Femtosecond transient absorption spectra of DPP-Th-Pt-P1 (bottom panel) and ground state absorption (top panel), (B) Square marked region in A is shown in magnification, (C) kinetic traces of the transients at three different wavelengths. The spectra were recorded immediately after excitation at 388 nm in deoxygenated THF.

Table 6-2. Lifetime of the kinetic traces at three different wavelengths for DPP-Ph-Pt-P2

Wavelength	τ_1, ps	τ_2, ps
414 nm	0.44 (±0.03)	139 (±12)
643 nm	0.54 (±0.07)	117 (±25)
695 nm	0.97 (±0.25	143 (±44)

Table 6-3. Lifetime of the kinetic traces at three different wavelengths for DPP-Th-Pt-P1

Wavelength	τ_1, ps	τ_2, ps
414 nm	0.30 (±0.03)	19.1 (±1.8)
723 nm	0.69 (±0.14)	30.2 (±2.9)
794 nm	1.1 (±0.12)	32.3 (±2.0)

In an effort to understand the dynamics of the singlet excited state of these two polymers, kinetic data are measured and shown in Figure 6-10 (C) and 6-11 (C) and the lifetimes are tabulated at three different wavelengths in Table 6-2 and Table 6-3. In general both the polymers decay via biexponential pathway consisting of a fast component and a long component. It is believed that the fast component is due to singlet excited state decay and the long component decay is influenced by the intersystem crossing to the triplet excited state. The thiophene containing polymer DPP-Th-Pt-P1 shows shorter lifetime of the singlet excited state, indicating faster ISC to the triplet excited state influenced by both additional thiophene rings and coplanarity of the polymer backbone in comparison to DPP-Ph-Pt-P2.

The kinetics for the nanosecond transient absorption decay of DPP-Ph-Pt-P2 is presented in Figure 6-10 (D) at two different wavelengths at 663 nm, 853 nm. The decay of the transient at 663 nm (lifetime ~ 350 ns) correlates well with evolution of the

transient at 853 nm with a lifetime of ~400 ns and can be assigned to the triplet excited state.

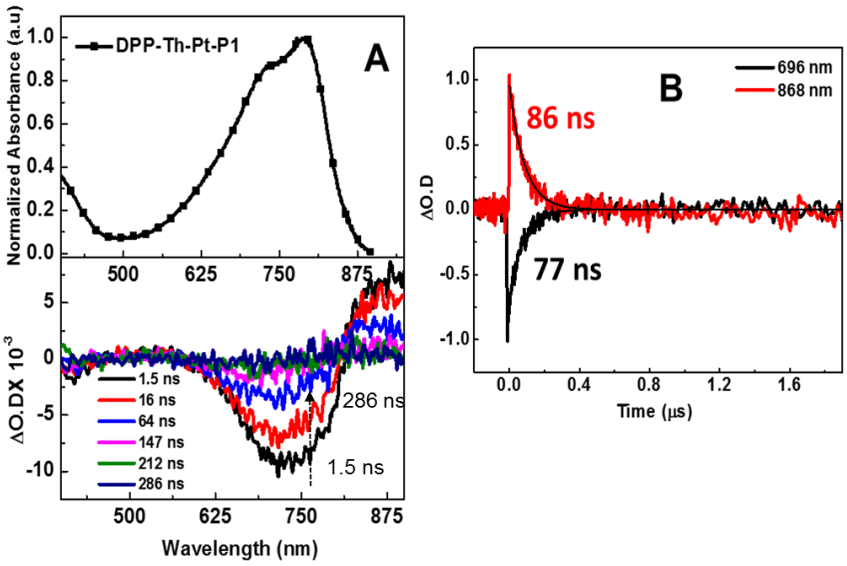

Figure 6-12. The (A) nanosecond transient absorption spectra (bottom panel) and ground state absorption spectra (top panel), (B) kinetic traces at two different wavelengths of DPP-Th-Pt-P1. The spectra were recorded immediately after excitation at 388 nm in deoxygenated THF.

The picosecond transient absorption data for the thiophene containing polymer DPP-Th-Pt-P1 is presented in Figure 6-11. Within 0.5 ps after excitation, a ground state bleach is observed between 650 – 850 nm with an absorption feature between 450 – 600 nm (Figure 6-11 B). The transient at 450 – 600 nm decayed with a lifetime ~ 1.3 ns and can be assigned to the singlet excited state absorption from $S_1 \rightarrow S_n$. The nanosecond transient absorption spectrum of thiophene containing polymer DPP-Th-Pt-P1 is presented in Figure 6-12 (A and B) along with the kinetic traces. At 1.5 ns delay following excitation, the difference spectrum consists of ground state bleach between 600 - 800 nm and transient absorption from 800 nm extending into the near-IR region. The ground state bleach correlates well with the absorption spectrum shown in the top panel. The transient signal at 868 nm was observed within 1.5 ns and decayed to the

ground state within 86 ns. Comparatively faster decay of the triplet excited state for DPP-Th-Pt-P1 than DPP-Ph-Pt-P2 can be attributed to the presence of thiophene rings which is known to promote stronger intersystem crossing due to “heavy atom effect” of sulfur.[111]

Electrochemical properties

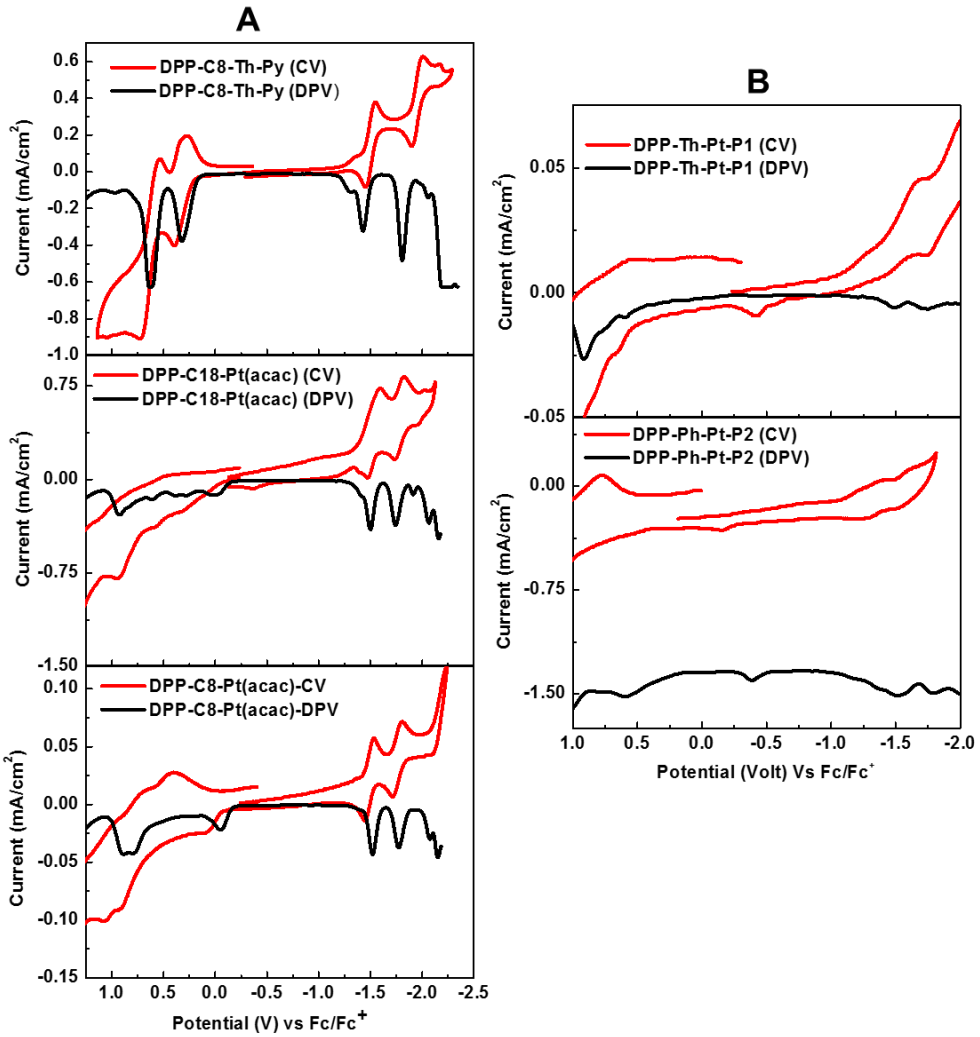

Figure 6-13. The (A) cyclic voltammograms and DPV plot for the ligand and metal complexes, (B) cyclic voltammograms and DPV of the polymers DPP-Th-Pt-P1 and DPP-Ph-Pt-P2 in deoxygenated dichloromethane with 0.1 M TBAPF6 as the supporting electrolyte. It was scanned at 100 mVs^{-1}. All the potentials are referenced to Fc/Fc^{+} couple as an internal standard.

Electrochemical studies of the chromophores were performed in dry dichloromethane solution with 0.1 M NBu_4PF_6 supporting electrolyte. Three electrode system was used for the measurement. Platinum disk and platinum wire was used as working electrode and counter electrode, and Ag/Ag^+ was used as counter electrode. Cyclic voltammograms (CV) along with the differential pulse voltammetry (DPV) for the chromophores are depicted in Figure 6-13. All potentials were reported with respect to Fc/Fc^+ internal standard.

Table 6-4. Electrochemical properties of the ligand, metal complexes and polymers.[a]

Compound	$E_{1/2}$/V		$E_{1/2}$/V	
	Red_1	Red_2	Ox_1	Ox_2
DPP-C8-Th-Py	-1.50	-1.95	0.35	0.63
DPP-C18-Pt(acac)[c]	-1.54	-1.79	0.15[c]	–
DPP-C8-Pt(acac)[c]	-1.49	-1.76	0.23[c]	–
DPP-Th-Pt-P1[b,c]	-1.36	-1.56	0.03[c]	–
DPP-Ph-Pt-P2[b,c]	-1.31	-1.62	0.32[c]	–

Note: [a] Measured in CH_2Cl_2 using 0.1 M NBu_4PF_6 as supporting electrolyte. It was scanned at 100 mV s^{-1}. All the potentials are referenced to Fc/Fc^+ couple as an internal standard. [b] The reduction potentials were estimated from DPV onset, [c] the oxidation potentials for the metal complexes and polymers were ill-defined in electrochemistry. It was measured from LUMO level and optical bandgap.

The cyclic voltammograms of ligand DPP-C8-Th-Py consists of two quasi-reversible oxidations at half wave potential 0.35 V and 0.63 V, along with two reversible reduction waves at -1.50 V and -1.95 V. The HOMO energy level for the ligand was calculated from the onset of oxidation (0.20 V) and found at 5.30 eV, whereas the LUMO level was found at 3.60 eV. The electrochemical bandgap calculated (1.70 eV) is well in accordance with the optical bandgap (1.81 eV). In contrast to a single reduction

wave in DPP-C18 (chapter 5), DPP-C8-Th-Py has two reduction waves. The additional reduction wave can be unambiguously assigned to the thienyl-pyridine moiety.

Interesting differences in the redox properties were observed when thienyl-pyridine part of the ligand is coordinated to Pt(acac)-octyl to in the metal complexes. In Figure 6-13 (A), the middle and bottom panel depicts the electrochemical behavior of the metal complexes. There is very minimal change is observed for the first reduction potential for both the metal complexes (1.49 and 1.54 V) compared to the ligand (~1.50 V). However, the second reduction peak is shifted to slightly less cathodic potential (1.79 V and 1.76 V for DPP-C18-Pt(acac) and DPP-C8-Pt(acac) respectively) compared to the ligand. The similarity in the first reduction potential suggests that the LUMO is mainly localized on the DPP chromophore. However, low bandgap of the metal complexes in comparison to the ligand DPP-C8-Th-Py suggests, cyclometallated platinum auxochrome has significant effect on the HOMO energy level of the metal complexes. The oxidation waves in the metal complexes are irreversible and ill-defined, this is possibly due to the involvement of Pt(II) → Pt(III) oxidation followed by fast chemical reaction.[170] It is interesting to note here, the onset of absorption (721 nm) and 1st reduction potential (1.48 V) for DPP-Pt(acac) (without modified “acac”)[156] are almost similar to the DPP-C18-Pt(acac) (722 nm and 1.55 V). Taken together, we can estimate the oxidation potentials for the metal complexes close to the value of DPP-Pt(acac) (0.28 V).

Figure 6-13 (B) represents the redox property of the polymers DPP-Th-Pt-P1 (top panel) and the model complex DPP-Ph-Pt-P2 (bottom panel). The reduction potential is calculated from the onset of first reduction wave, which is at -1.36 V for DPP-Th-Pt-P1.

However, given the onset of the optical absorption of this polymer (868 nm), we assume the oxidation potential will be close to ~0.03 V. The reduction potential for DPP-Pt-Ph-2 remains almost the same (~-1.31 V) as DPP-Th-Pt-P1 and this is due to localization of the LUMO on the central DPP core which is same for the two polymers. Given the higher bandgap (~1.6 eV) of DPP-Ph-Pt-P2, it is clear that phenyl containing cyclometallated motif has significant effect on polymer HOMO level and it is estimated to be ~0.23 V, much higher than DPP-Th-Pt-P1 oxidation potential (~0.03 V) (detailed calculation of the oxidation potentials showed in the discussion section).

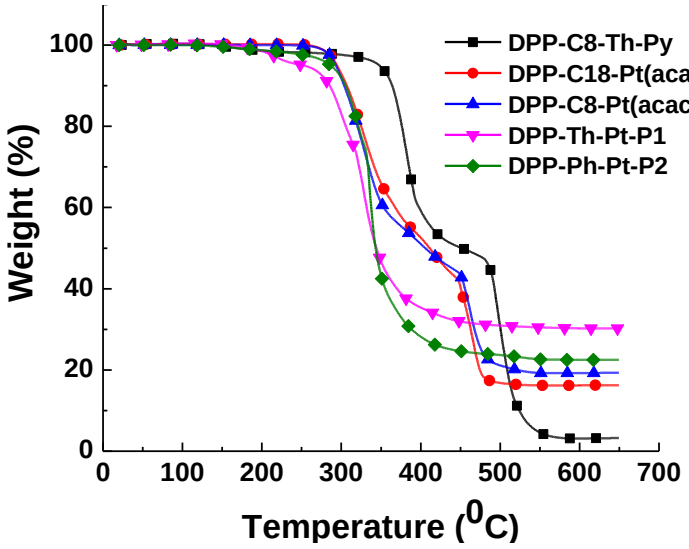

Figure 6-14. Thermal gravimetric analysis of the ligand, metal complexes and polymers under N_2 atmosphere.

Thermal Properties

The thermal stability of the ligand, metal complexes and polymers were measured by thermal gravimetric analysis (TGA) using 3-5 mg of the samples with a heating rate of 20˚C/min and presented in Figure 6-14. The ligand DPP-C8-Th-Py shows the highest thermal stability with a 5% weight loss temperature at 348°C. With the incorporation of cyclometallated motif, thermal stability decreases to 294˚C. This fact

is in agreement with the previous results from Che and coworkers , where they have shown pure organic indacenodithiophene polymers have higher thermal stability compared to the cyclometallated platinum containing polymer.[76] The phenyl containing polymer DPP-Ph-Pt-P2 shows higher thermal stability (T_d = 287˚C) compared to the thiophene containing polymer DPP-Th-Pt-P1 (T_d = 252˚C).

Photovoltaic Properties

Photovoltaic studies described in this section were performed by Jeff Hernandez in Prof. John Reynolds' laboratory at the Georgia Institute of Technology.

Solution processed bulk-heterojunction solar cells were fabricated by using DPP-Th-Pt-P1 and DPP-Ph-Pt-P2 as donor materials with $PC_{71}BM$ as acceptor. The general architecture used to fabricate the device was ITO/PEDOT:PSS (35 nm)/polymer:$PC_{70}BM$/Ca (10 nm)/Al (60 nm). It was found that, increasing the $PC_{71}BM$ loading in the active layer from 1:1 to 1:7 polymer:$PC_{71}BM$ ratio, resulted in an increase in device efficiency. In the literature there are few reports on bulk heterojunction solar cells which operate with very high $PC_{71}BM$ loading ratios.[206,207] For the thiophene containing polymer DPP-Th-Pt-P1 the optimum ratio of polymer:$PC_{71}BM$ was determined to be 1:7, which gave a power conversion efficiency (PCE) of 1.77%. This device structure yields short circuit current (J_{sc}) of 3.90 mA/cm^2, open circuit voltage (V_{oc}) of 0.66 V and fill factor (FF) of 65.8%. For the phenyl containing polymer DPP-Ph-Pt-P2, the best efficiency observed was 0.52% at a polymer:$PC_{71}BM$ ratio of 1:3. However, with the same ratio of DPP-Th-Pt-P1: $PC_{71}BM$ (1:7), the efficiency was 0.46%. The significantly lower power conversion efficiency for DPP-Ph-Pt-P2 compared to DPP-Th-Pt-P1 is partly due to the result of superior spectral overlap of the thiophene containing polymer with the solar spectrum. It is important to note here that even though

incorporation of phenyl group in DPP-Ph-Pt-P2 provides higher V_{oc} due to the low HOMO energy level compared to DPP-Th-Pt-P1, the concomitant increased bandgap in the polymer lowers the efficiency of the device.

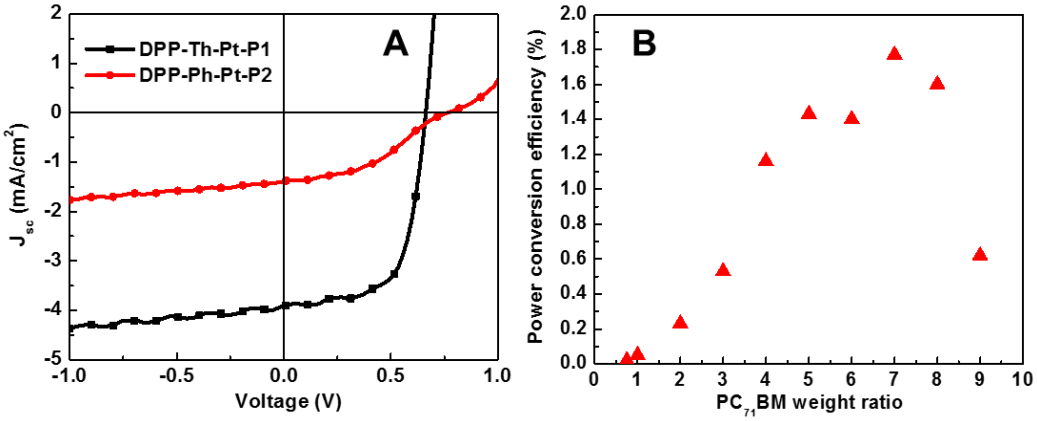

Figure 6-15. (A) Current density/voltage (J-V) curve for the two polymers and (B) power conversion efficiency vs polymer:$PC_{71}BM$ weight ratio plot for device containing DPP-Th-Pt-P1 as the donor polymer.

The high efficiency of the thiophene containing polymer DPP-Th-Pt-P1 can be attributed to the high fill factor (FF) of ~0.66. Fill factor of a device mainly depends on several factors including carrier mobility, charge recombination, and current leakage.[208] It is believed that interchain interaction between the polymer segments can greatly influence the carrier mobility as well as the FF of the device. The majority of organometallic polymers with platinum acetylide architecture show poor FF due to the bulky tributyl phosphine groups on platinum centers which reduces the intermolecular interaction. Previously, Adachi and coworkers reported that diketopyrrolopyrrole chromophores can exhibit self-assembly properties both in solution and solid state.[174] It is believed that the incorporation of planar cyclometallated motifs to the diketopyrrolopyrrole backbone improves the interchain interaction in this polymer and hence the FF.

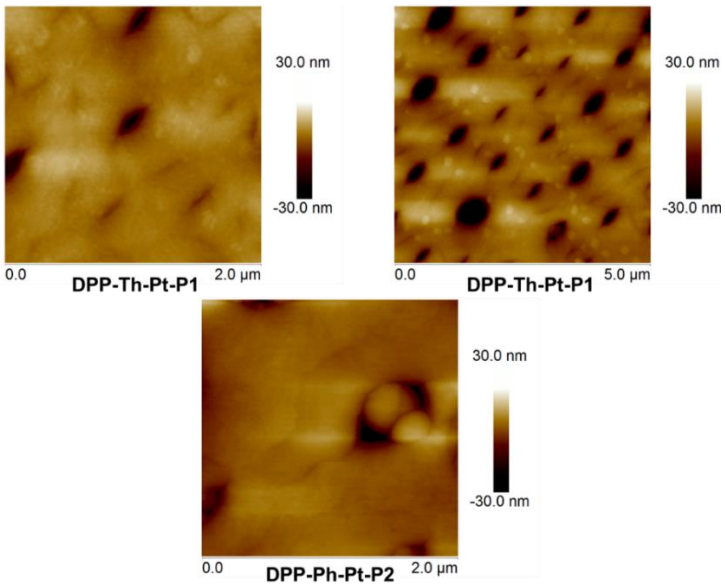

Figure 6-16. AFM height images of the polymers with polymer: $PC_{71}BM$ ratio of 1:7.

Atomic force microscopy (AFM) height images of the devices with donor: acceptor ratio of 1:7 was measured and shown in Figure 6-16. The Thiophene containing polymer DPP-Th-Pt-P1 shows better phase separation compared to DPP-Ph-Pt-P2 within 2 µm scale. Prominent phase separation is observed within 5 µm length scale from thiophene containing polymers as seen in the AFM images. Use of solvent additives to increase the device performance efficiency by improving the phase separation between donor and acceptor is a very popular method. However, in the case of addition of solvent additive 1,4-diiodooctane (DIO) the device efficiency was found to decrease. With the addition of 1%, 2% and 3% DIO, the device efficiency was decreased to 0.70 %, 0.90 % and 0.49 % respectively in chloroform for DPP-Th-Pt-P1. When the active layer solvent is switched from chloroform to the higher boiling point solvent dichlorobenzene, the efficiency drops to 0.77% for DPP-Th-Pt-P1. With the addition of DIO of 1%, 2% and 3%, the device efficiency observed is 0.27%, 0.82% and 0.65% respectively.

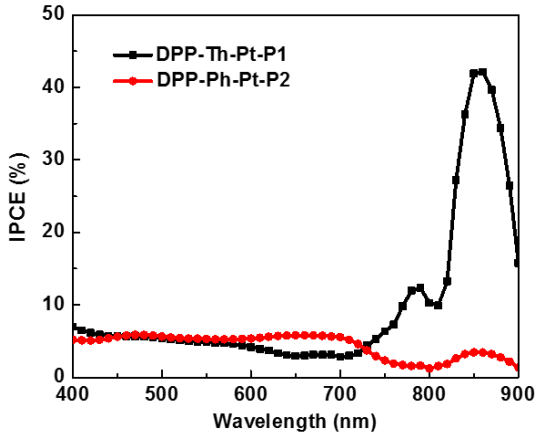

Figure 6-17. IPCE plot of both the polymers with optimized polymer: $PC_{71}BM$ ratio of 1:7.

The external quantum efficiency (EQE) measurement for both the polymers is presented in Figure 6-17 with the donor - acceptor ratio of 1:7. The thiophene containing polymer DPP-Th-Pt-P1 exhibits EQE of 40% with a peak at 850 nm, which is very close to the λ_{max} of the polymer. However, overall the EQE at 400 - 700 nm is very low (<10%). This suggests, that the improvement of photon to current conversion in this region will effectively enhance the PCE of this device. The phenyl containing polymer DPP-Ph-Pt-P2 shows a broad signal with a peak at ~ 700 nm. However, the overall EQE is less than 10% reflecting low PCE of this device.

Table 6-5. Photovoltaic properties of DPP-Th-Pt-P1 with varying PCBM amount

Blend Ratio	J_{sc} (mA cm^{-2})	V_{oc} (V)	FF (%)	PCE (%)
1:1	0.25	0.48	30.8	0.04
1:2	0.76	0.65	42.9	0.22
1:3	1.38	0.64	48.6	0.45
1:4	2.87	0.63	59.0	1.13
1:5	3.20	0.64	63.6	1.37
1:6	3.15	0.65	62.9	1.35
1:7	3.79	0.65	63.9	1.66
1:8	3.53	0.66	60.4	1.50
1:9	2.06	0.70	50.0	0.76

Table 6-6. Photovoltaic properties of DPP-Ph-Pt-P2 with varying PCBM amount.

Blend Ratio	J_{sc} (mA cm^{-2})	V_{oc} (V)	FF (%)	PCE (%)
1:1	1.06	0.75	25.5	0.21
1:2	1.43	0.76	35.8	0.41
1:3	1.61	0.73	41.4	0.52
1:7	1.52	0.75	38.6	0.46

Table 6-7. Photovoltaic properties of DPP-Th-Pt-P1 at 5 different pixels with 1:7 polymer: PCBM ratio

J_{sc} (mA cm^{-2})	V_{oc} (V)	FF (%)	PCE (%)
3.90	0.66	65.8	1.77
3.79	0.66	62.0	1.62
3.85	0.66	63.8	1.70
3.73	0.66	62.5	1.61
3.69	0.64	65.3	1.61
Average - 3.79	0.65	63.9	1.66
Std.Dev - 0.09	0.01	1.65	0.07

Table 6-8. Photovoltaic properties of DPP-Ph-Pt-P2 at 5 different pixels with 1:3 polymer: PCBM ratio

J_{sc} (mA cm^{-2})	V_{oc} (V)	FF (%)	PCE (%)
1.53	0.76	38.9	0.47
1.46	0.74	41.1	0.47
1.52	0.74	40.7	0.48
1.93	0.72	44.9	0.65
1.61	0.72	41.3	0.50
Average – 1.61	0.73	41.4	0.52
Std.Dev - 0.19	0.02	2.15	0.08

Discussion

The objective of this work is to synthesize heavy metal containing cyclometallated donor-acceptor polymers is to probe the effect of triplet excited state in photovoltaic applications. In order to have efficient charge transfer from triplet excited state of the donor to PCBM acceptor, the energetics for photoinduced electron transfer (PET) must be thermodynamically favorable. According to thermodynamics of the PET, the charge separated state must be lower in energy compare to the singlet or triplet

excited state for an efficient charge separation process from that state and given by equation 6-1-

$$\Delta G = E_{cs} - E_{es} \quad (6\text{-}1)$$

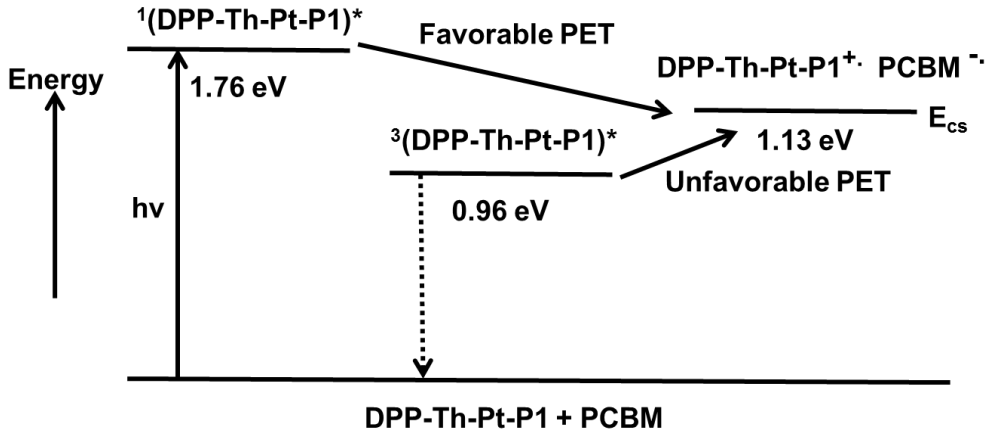

Figure 6-18. Energy level diagram for PET from polymer DPP-Th-Pt-P1 to PCBM.

Here, ΔG is Gibbs free energy change for the PET process, E_{cs} is the energy of the charge separated state and E_{es} is the energy of the excited state. The energy of the charge separated state can be calculated from the difference in energy between the oxidation potential of the polymer and reduction potential of PCBM ($E_{CS} \approx E_{ox}$ (polymer$^{+\cdot/0}$) - E_{red} ($PC_{71}BM^{-\cdot/0}$)). As the oxidation potentials were ill defined for the polymers in electrochemical studies, it can be approximated from the following equations-

$$\text{Bandgap} = \text{HOMO (eV)} - \text{LUMO (eV)} \quad (6\text{-}2)$$

$$E_{HOMO} = -(5.1 + E_{1/2}^{Ox})\ \text{eV} \quad (6\text{-}3) \quad \text{and} \quad E_{LUMO} = -(5.1 + E_{1/2}^{Red})\ \text{eV} \quad (6\text{-}4)$$

From the reduction potential of the polymers and the onset of absorption LUMO energy level and bandgap can be calculated respectively. Using those values in equation 6-2 will give the estimation of HOMO energy level.

From both the electrochemistry and ground state absorption, the oxidation potential calculated for **DPP-Th-Pt-P1** is ~0.03 eV (vs Fc/Fc^+). This value combined with the reduction potential of PCBM (-1.10 V vs Fc/Fc^+)[25], estimated value of E_{cs} is 1.13 eV for DPP-Th-Pt-P1. The second term of the equation 6-1 can be estimated from the onset of emission, which is 1.76 eV for DPP-Th-Pt-P1. As, no phosphorescence was observed from this systems, the triplet energy levels are estimated by considering S_1-T_1 splitting energy of 0.8 eV[185], affording the triplet excited state energy of 0.96 eV. With these values of the energy of the excited states, the ΔG is -0.63 eV for PET from singlet excited state and +0.17 eV for PET from triplet excited state. The energy level diagram for the polymer-PCBM blend is depicted in Figure 6-17. It is very clear from the diagram, the PET process from the singlet excited state of the polymer is energetically favorable (exothermic) being higher in energy than the charge separated state. However, for triplet excited state, it is below the charge separated state and PET from triplet excited state is not possible to take place in an appreciable rate. This fact is in complete agreement with the other reports on donor-acceptor organometallic chromophores where the singlet excited state is responsible for PET instead of triplet excited state.[25,76]

It is interesting to note here, we have recently reported a letter on photophysical studies of structurally similar small molecule DPP-Pt(acac) where the interaction of this complex with several electron acceptors including PCBM was studied.[203] The fluorescence of this complex was found completely quenched with addition of increasing amount of PCBM. The kinetic study of this process showed a rapid rate of electron transfer (1-2 ps) from the singlet excited state to PCBM with a slow charge recombination rate in the order of several nanoseconds.

The maximum output power of a bulk heterojunction solar cell depends on open circuit voltage (V_{OC}), short circuit current (J_{SC}) and fill factor (FF). Open circuit voltage mainly depends on the energy gap between HOMO of the donor and LUMO of the acceptor (Figure 6-19). In order to have donor chromophore with a deeper HOMO level to increase the V_{oc}, phenyl containing polymer DPP-Ph-Pt-P2 is synthesized. The tradeoff for this design is larger HOMO-LUMO bandgap compared to the thiophene containing polymer DPP-Th-Pt-P1. The fill factor (FF) has a large dependence on carrier transport through the active layer. In general, platinum acetylide containing π-conjugated organometallic polymers exhibit low FF due to the presence of bulky solubilizing trialkyl phosphine groups, which reduces interchain interactions. Presumably the introduction of planar cyclometallated motifs to the planar diketopyrrolopyrrole chromophore will improve the charge transport properties and hence the FF.

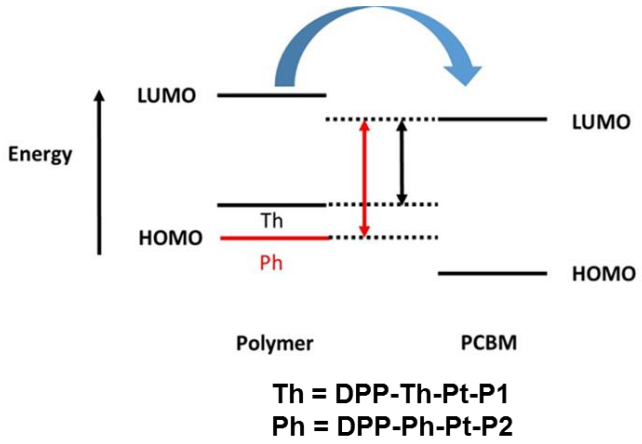

Figure 6-19. Schematic diagram of the design principle for the two polymers

There is a good correlation observed between the design strategy of the polymers and the experimental results. Although, the V_{oc} for DPP-Ph-Pt-P2 is higher compared to DPP-Th-Pt-P1, the more red shifted absorption in the visible region of

DPP-Th-Pt-P1 afforded higher PCE for this polymer. Both the J_{sc} and FF are lower for DPP-Ph-Pt-P2 compared to the thiophene containing polymer. The higher dihedral angle produced by the thiophene-Phenyl linkage in the polymer backbone of DPP-Ph-Pt-P2 may cause less interchain interaction for charge transport and hence low FF.

Summary and Conclusions

In this work we have synthesized two organometallic complexes (DPP-C8-Pt(acac) and DPP-C18-Pt(acac)) with two different alkyl chains on the central nitrogen atom and two organometallic polymers (DPP-Th-Pt-P1 and DPP-Ph-Pt-P2), with varying structure within the cyclometallated motif. The solution state photophysics of the metal complexes remain almost the same as the previous report from our group without the solubilizing acac ligand.[156] However, it is interesting to note here, the incorporation of thienyl-pyridine moiety to the DPP chromophore efficiently populates the triplet excited state and the lifetime of the triplet excited state is reduced from 2.02 μs to 160 ns upon metal coordination. Electrochemical measurements suggest, metal coordination has significant effect on the HOMO energy level compared to the LUMO, which is responsible for the reduced bandgap in these metal complexes compared to DPP-C8-Th-Py. The thiophene containing polymer, DPP-Th-Pt-P1 shows significantly red shifted absorption compared to the phenyl containing polymer DPP-Ph-Pt-P2, possibly due to small dihedral angle between the two thiophene rings which induces planarity in the conjugated backbone. Ultrafast transient absorption studies were performed on both polymers and DPP-Th-Pt-P1 was found to have a shorter triplet excited state lifetime due to spin-orbit coupling effect induced by the additional thiophene rings.

Finally, bulk-heterojunction solar cell devices were fabricated with these two polymers. DPP-Th-Pt-P1 showed efficiency as high as 1.77%. The low efficiency for

DPP-Ph-Pt-P2 (~0.65%) can be attributed to its blue shifted absorption compared to the thiophene containing polymer, as well as its low molar absorptivity. DPP-Th-Pt-P1 exhibits a fill factor up to ~66%, which is the highest known value till date for an organometallic polymer. Interestingly, both these devices shows photocurrent generation with very low polymer loading compared to PCBM. This is the first report on cyclometallated platinum containing diketopyrrolopyrrole polymers as an active materials in photovoltaic devices. However, we anticipate, an improvement in EQE between 400 - 700 nm can produce more efficient devices and further investigation toward this end is currently underway in our lab.

Experimental

Instrumentation and Methods

NMR spectra of the compounds were recorded by using a Mercury-300 FT-NMR spectrometer, which operated at 300 MHz for ^{1}H NMR, and 75.4 MHz for ^{13}C NMR. ^{1}H NMR were also collected from Varian Inova-500 FT-NMR instrument, operating at 500 MHz. The mass spectral analysis of the newly synthesized molecules and complexes were performed in Mass Spectrometry Services, located in house at the University of Florida. The molecular weight of the polymers were analyzed by Gel Permeation Chromatography (GPC) from a system containing Shimadzu SPD-20A photodiode array (PDA) detector and THF as eluent with a flow rate of 1 mL/ min. Before the measurement, the system was calibrated using linear polystyrene in THF.

All the photophysical studies were performed using dry HPLC grade THF as solvent in a 1 x 1 cm^2 quartz cuvette unless otherwise mentioned. The solutions used for the study were diluted from a stock solution according to the experiment. UV-visible absorption spectra were collected from a Shimadzu UV-1800 dual beam

spectrophotometer. The molar absorptivity of the chromophores were recorded by maintaining the solution O.D within 0.1. The calculation of the concentration for polymers were performed by taking the polymer repeat unit (PRU) as the molecular weight. Steady state photoluminescence spectroscopy were obtained from Photon Technology International (PTI) fluorimeter and collected at 90° with respect to the excitation beam. Similar to the absorption measurement, all the measurements were performed with a solution O.D ≤ 0.1 to avoid the self-quenching effect of the chromophores. The fluorescence quantum yields were calculated by taking into account the refractive index correction of THF as well as the standard solvent toluene. Fluorescence lifetime measurements were performed with a PicoQuant FluoTime 100 Compact Fluorescence Lifetime Spectrophotometer by time-correlated single photon counting (TCSPC) and by exciting the solutions by PDL-800B Picosecond Pulsed Diode Laser (375 nm).

The nanosecond-microsecond transient absorption spectroscopy were performed using the third harmonic of a Continuum Surelite series Nd:YAG laser (λ =355 nm, 10 ns FWHM, 7 mJ per pulse). Probe light was produced by a xenon flash lamp and the transient absorption signal was detected with a gated-intensified CCD mounted on a 0.18 m spectrograph (Princeton PiMax/Acton Pro 180). During the measurement the samples were continuously circulated in the pump-probe region and contained in a cuvette of 1 cm pathlength with a total volume of 10 mL. The optical density of the samples were kept ~0.7 at 355 nm and deoxygenated by bubbling argon for at least 45 minutes prior to the measurement.

Femtosecond transient absorption data were taken using a pump-probe configuration with a 1 kHz Ti:sapphire chirped pulse amplifier (Clark-MXR CPA-2001). The 388 nm (600 nJ) pump pulse was generated via frequency doubling a portion of the 775 nm regenerative amplifier beam, while the 665 nm (100 nJ) pump pulse was produced by frequency doubling of the signal from a home-built Optical Parametric Amplifier (OPA). A portion of the 775 nm fundamental was focused in a translating CaF_2 window to generate a white light continuum, which was used as the probe pulse. A mechanical chopper synchronized to the laser chopped the pump at 500 Hz. Pump and probe polarizations were set to magic angle. The two beams were focused to a 150 μm spot size, and spatially overlapped at the sample. A fiber optic coupled multichannel spectrometer with a CMOS sensor collects the probe pulse, where pump-induced changes in the white light continuum were measured on a pulse-to-pulse basis with a sensitivity of 0.1 mOD. Time-resolved transient absorption spectra were collected with an approximate time resolution of 250 fs with a spectral window of 320 nm to 800 nm. The time delay between pump and probe are regulated using a computer controlled delay stage.

Transient absorption measurements from ps-μs were collected with the same pump pulse and CMOS sensor as the femtosecond setup, while the white light probe was obtained from continuum generation in a diode-laser pumped photonic crystal fiber electronically delayed from the pump pulse.

The electrochemical measurements of the samples were performed on a BAS CV-50W voltammetric analyzer (Bioanalytical Systems, Inc., www.bioanalytical.com) using dry dichloromethane solvent and in presence of 0.1 M tetra-n-butylammonium

hexafluorophosphate (TBAH) as electrolyte. The experiments were performed with three electrodes, platinum microdisk (2 mm^2) as the working electrode, a platinum wire as the auxiliary electrode, and a silver wire as the reference electrode. The concentration of the sample solutions were made ~ 1 mM, and the scan rate of 100 mV/s was used during the measurement. The sample solutions were deoxygenated prior to the measurement and also kept under constant pressure of argon during the measurement. All electrochemical potentials were calibrated with respect to a ferrocene internal standard ($E(Fc/Fc^+)$ = 0.43 V vs SCE in CH_2Cl_2). The potentials are reported here vs SCE.

General Methods for Photovoltaic Device Fabrication

Patterned ITO on glass was ultra-sonicated in sodium dodecyl sulfate in water followed by acetone and then isopropanol. ITO was blown dry with Ar gas then UV ozone treated. PEDOT:PSS (Al 4083) was spun coat on clean ITO at 5000 r.p.m. for 60 seconds and then annealed at 120°C for 15 minutes. Solutions of DPP-Th-Pt-P1:$PC_{71}BM$ or DPP-Ph-Pt-P2:$PC_{71}BM$, 1:7 by weight, in chloroform, 9 mg mL^{-1}, were spun coat in an Ar filled glovebox onto PEDOT:PSS substrates at 600 rpm for 50 seconds. After, 10 nm of Ca and 80 nm of Al were evaporated on at 10^{-6} mbar. Devices were tested using a Newport ABB solar simulator with a Keithley SMU for measuring device efficiency under standard AM 1.5 conditions calibrated to 95 mW/cm^2.

General Methods for Synthesis

All the reactions were performed under a dry argon atmosphere unless otherwise mentioned. Tetrahydrofuran was dried using solvent purification columns (Glass Contour) and all the other solvents were used as received. The synthetic scheme of the precursor molecules, metal complexes and the polymers are presented in Figure 6-4, 6-

5 and 6-6. The synthesis of 6-1, 6-2 and 6-3 were performed by literature procedures. The dichloro bridged dimer and 2-octyldodecyl iodide were also synthesized by following literature protocol.[156,202] The boronate ester derivatives 5-3 and 6-6 were also synthesized by following literature procedures.[156,209] For polymerization reaction, the dibromo ligand 6-8 was synthesized by following a literature procedure.[76] The ligand 2-(5-bromo-2-thienyl)pyridine was purchased from Fisher scientific. The metallation agent potassium tetrachloroplatinate and catalysts bis(triphenylphosphine)palladium(II) dichloride were purchased from Strem Chemicals. $Pd_2(dba)_3$, $Pd(P^tBu_3)_2$, potassium phosphate tribasic, thien-2- yl-2-boronic acid, 2,5-dibromopyridine were purchased from Sigma- Aldrich and used without any further purification.

Synthesis of Pt(acac)-Octyl

In a three-neck round bottom flask a solution of 2-(5-bromo-2-thienyl)pyridine (0.614 g, 2.56 mmol) K_2PtCl_4 (0.506 g, 1.24 mmol) in 2-ethoxyethanol (15 mL) and water (5 mL) was deoxygenated by purging argon for 45 minutes. After that, it was heated under an argon atmosphere at 80˚C for 24 hours. It was cooled down to room temperature and the bright yellow precipitate was filtered off. The precipitate was washed with copious amount of water and dried under vacuum to obtain the dichloro bridged dimer 6-13. The dimer (0.35 g, 0.37 mmol), Octyl-acac (0.54 g, 1.12 mmol) and anhydrous Na_2CO_3 (0.395 g, 3.73 mmol) were taken in 20 mL of dry 2-ethoxyethanol solvent. The yellow solution was deoxygenated with argon for 45 minutes and heated to 100˚C for 24 hours. After the complete consumption of the dimer, the reaction mixture was cooled down to room temperature and poured into water. The compound was extracted by using dichloromethane. The dichloromethane layer was collected and dried over anhydrous Na_2SO_4. It was filtered and evaporated to obtain the crude product.

Further purification by silica gel column chromatography using dichloromethane/hexane (1:1) eluent afforded the title compound in 60 % yield (204 mg). ^{1}H NMR (300 MHz, $CDCl_3$): δ 8.93 (d, 1H, J= 5.4 Hz), 7.98 (d, 4H, 8.6 Hz), 7.68 (t, 1H, 6.1 Hz), 7.21 (s, 1H), 7.18 (d, 1H, 7.9 Hz), 6.97-6.94 (m, 5H), 6.67 (s, 1H), 4.04 (t, 4H, 6.5 Hz), 1.87- 1.79 (m, 4H), 1.49-1.31 (m, 20H), 0.90 (t, 6H, 6.4 Hz). ^{13}C NMR (125 MHz, $CDCl_3$) δ: 177.92, 117.03, 163.58, 161.5 (d, J = 9.8 Hz), 147.16, 145.02, 140.00, 138.54, 133.03, 131.99, 130.99, 128.81 (d, J = 5.1 Hz), 118.63, 116.99, 114.31 (d, J = 3.0 Hz), 95.48, 68.23, 31.84, 29.39, 29.27, 29.22, 26.06, 22.68, 14.12. Calculated for $C_{40}H_{48}BrNO_4PtS$ 913.88, found ESI-MS (m/z): 936.20 $[M+Na]^+$.

Synthesis of DPP-C8-Th-Py

In a flame dried flask 6-6 (0.05 g, 0.064 mmol), 2-(5-bromo-2-thienyl)pyridine (0.032 g, 0.132 mmol), $Pd_2(dba)_3$ (3 mg, $3.22x10^{-3}$ mmol), and $Pd(P^tBu_3)_2$ (3.5 mg, $6.44x10^{-3}$ mmol) were combined and vacuum-argon cycled three times to remove residual oxygen from the flask. In a separate flask, K_3PO_4 (0.083 g, 0.39 mmol) was dissolved in deionized water (1 mL) and deoxygenated by bubbling argon for 1 hour. Dry THF (9 mL) was added to the reaction flask and the red colored solution was stirred for 15 minutes. The aqueous solution of K_3PO_4 was added promptly to the reaction mixture under argon and the color of the solution immediately changed to dark blue. The reaction mixture was heated to 60˚C and stirred under an argon atmosphere overnight. It was cooled to room temperature and poured over water. The product was extracted using DCM and the combined organic layer was dried over anhydrous Na_2SO_4. After filtration, the solvents were evaporated under vacuum to obtain the crude product. It was further purified by silica gel column chromatography using DCM-ethyl acetate (90:10) as eluent to obtain the compound as a dark blue crystalline solid in 50%

yield (27 mg). ^{1}H NMR (300 MHz, $CDCl_3$): δ 8.96 (d, 1H, J= 4.2 Hz), 8.59 (m, 1H), 7.69 (m, 2H), 7.52 (d, 1H, J= 3.9 Hz), 7.39 (d, 1H, J = 4.1 Hz), 7.32 (d, 1H, J= 3.9 Hz), 7.18 (m, 1H), 4.06 (d, 2H, J= 8.7 Hz), 1.93 (m, 1H), 1.32 (m, 8H), 0.89 (m, 6H). Calculated for $C_{48}H_{50}N_4O_2S_4$ 843.19, found ESI-MS (m/z): 843.28 $[M+H]^+$.

Synthesis of DPP-C8-Pt(acac)

In a flame dried flask 6-6 (0.1 g, 0.09 mmol), Pt(acac)-Octyl (0.169 g, 0.185 mmol), $Pd_2(dba)_3$ (4 mg, $4.5x10^{-3}$ mmol), and $Pd(P^tBu_3)_2$ (4.6 mg, $8.98x10^{-3}$ mmol) were combined and vacuum-argon cycled three times. Prior to the reaction K_3PO_4 (0.115 g, 0.54 mmol) was dissolved in 2 mL of deionized water and deoxygenated by purging argon for 1 hour. Dry THF (18 mL) and the aqueous solution of K_3PO_4 were added to the reaction mixture and heated to 60˚C overnight under an argon atmosphere. After the reaction, the consumption of the starting material 6-6 was confirmed using thin layer chromatography (TLC). The reaction mixture was cooled to room temperature and the solvents evaporated to dryness under vacuum. The crude product was dissolved in dichloromethane and passed through a silica gel filtration column. The solvents were evaporated under vacuum to reduce the volume and the partially purified product was recrystallized via addition of hexane. The dark blue crystalline precipitate was filtered and subsequently washed with hot hexane and methanol. The precipitate was dried under vacuum to obtain the product as a dark blue solid (120 mg) in 61% yield. ^{1}H NMR (500 MHz, CD_2Cl_2): δ 9.17 (d, 1H, J= 3.8 Hz), 8.71 (d, 1H, J = 5.7 Hz). 7.95 (dd, 4H, J_1= 17.4 Hz, J_2= 8.6 Hz), 7.50 (t, 1H, J = 7.6 Hz), 7.31 (d, 1H, J= 3.8 Hz), 7.22 (s, 1H), 6.94 (dd, 5H, J_1= 22.2 Hz, J_2= 8.5 Hz), 6.80 (t, 1H, J = 6.6 Hz), 6.57 (s, 1H), 4.11 (m, 6H), 1.99-1.84 (m, 5H), 1.38 (m, 26 H), 0.93 (m, 12H). ^{13}C NMR (75 MHz, $CDCl_3$): 175.48, 161.30, 159.87, 159.43, 145.26, 144.84, 141.59, 136.9, 136.2, 135.35, 130.12, 129.12,

127.73, 127.16, 116.78, 115.66, 112.52, 106.42, 93.13, 66.59, 30.30, 30.26, 27.98, 27.86, 27.77, 27.73, 27.69, 24.51, 24.45, 21.58, 21.12, 21.07, 12.41, 12.31, 12.27, 8.68. MALDI-TOF MS (*m/z*) $[M]^+$ Calcd for $C_{110}H_{134}N_4O_{10}Pt_2S_4$, 2189.8289, found 2189.8298. CHN Analysis: Calcd for $C_{110}H_{134}N_4O_{10}Pt_2S_4$: C, 60.31; H, 6.17; N, 2.56. Found: C, 60.017; H, 6.247; N, 2.346.

Synthesis of DPP-C18-Pt(acac)

In a flame dried flask 5-3 (0.1 g, 0.09 mmol), Pt(acac)-Octyl (0.168 g, 0.183 mmol), $Pd_2(dba)_3$ (4.1 mg, $4.5x10^{-3}$ mmol), and $Pd(P^tBu_3)_2$ (4.6 mg, $8.98x10^{-3}$ mmol) were combined and deoxygenated by three vacuum,-argon cycles. In a separate flask K_3PO_4 (0.114 g, 0.54 mmol) was dissolved in 2 mL of deionized water and deoxygenated by bubbling argon for 1 hour. Dry THF (18 mL) was added to the reaction mixture and stirred for 15 minutes. The aqueous solution of K_3PO_4 was added to the bright red solution which resulted in the immediate color change to dark blue and then to dark green. The reaction mixture was heated to 60˚C and stirred under an argon atmosphere overnight. After the consumption of the starting material 5-3, the reaction mixture was cooled down to room temperature and the solvents were evaporated under vacuum. The crude product was dissolved in dichloromethane and passed through a silica gel filtration column to remove the residual catalysts. The filtrate was evaporated under vacuum to remove most of the solvent and recrystallized with hexanes to obtain a dark blue crystalline precipitate. The product was isolated by filtration and washed with hot hexane and hot methanol. It was dried under vacuum to obtain the product in 44% yield (100 mg). ^{1}H NMR (500 MHz, $CDCl_3$): δ 9.13 (d, 1H, J=4.2 Hz), 8.77 (d, 1H, J= 6.0 Hz), 7.96 (dd, 4H, J_1= 22.5 Hz, J_2= 8.9 Hz), 7.49 (t, 1H, J= 7.7 Hz), 7.31 (m, 2H), 7.0 (m, 3H), 6.90 (d, 2H, J= 6.1 Hz), 6.59 (s, 1H), 4.11-3.99 (m, 6H), 2.01 (m, 1H), 1.85 (m,

4H), 1.34-1.17 (m, 63H), 0.93 (m, 6H) and 0.8 (m, 6H). ^{13}C NMR (75 MHz, $CDCl_3$): 177.47, 176.33, 163.17, 161.49, 161.32, 161.26, 147.07, 146.40, 143.16, 139.32, 138.80, 138.68, 137.82, 132.16, 130.87, 128.84, 128.69, 128.29, 124.75, 118.27, 117.30, 114.24, 108.19, 95.06, 68.30, 68.18, 46.54, 38.17, 31.96, 31.91, 29.81, 29.74, 29.46, 29.44, 29.34, 29.30, 22.73, 22.71, 22.70, 14.12. MALDI-TOF MS (*m/z*) $[M]^+$ Calcd for $C_{134}H_{182}N_4O_{10}Pt_2S_4$ 2526.2048, found 2526.2126. CHN Analysis: Anal. Calcd for $C_{134}H_{182}N_4O_{10}Pt_2S_4$: C, 63.68; H, 7.26; N, 2.22. Found: C, 64.027; H, 7.601; N, 2.103.

Synthesis of 6-9

In a three-neck flask, 6-8 (1g, 3.13 mmol) and K_2PtCl_4 (0.62g, 1.5 mmol) were dissolved in 15 mL of 2-ethoxyethanol and 5 mL of deionized water. The yellow reaction mixture was deoxygenated by bubbling argon for 45 minutes. It was then heated to 80˚C and stirred under an argon atmosphere overnight. The reaction mixture was then cooled down to room temperature. The Pt(II) dichloro bridged dimer was then filtered off and subsequently washed with water and methanol. The product was dried under vacuum for 24 hours and used in the next step without any further purification. In the next step, the dimer (1 g, 0.91 mmol), Octyl-acac (1.3 g, 2.73 mmol) and anhydrous Na_2CO_3 (0.627 g, 5.91 mmol) were taken in 50 mL of anhydrous 2-ethoxyethanol. The reaction mixture was deoxygenated by purging with argon for 45 minutes and subsequently heated to 100˚C for 24 hours. It was cooled down to room temperature and poured over water. The product was extracted with dichloromethane. The organic layer was collected, washed with water and brine three times. After drying the organic layer over anhydrous Na_2SO_4, it was evaporated under vacuum to obtain the crude product. It was further purified by silica gel column chromatography using DCM/hexane (1:1) as eluent and washing with hexane. The product was obtained as bright yellowish-orange solid in

35% yield (320 mg). ^{1}H NMR (300 MHz, $CDCl_3$): δ 8.98 (s, 1H), 7.90 (m, 4H), 7.74 (d, 1H, J= 8.7 Hz), 7.06 (s, 1H), 6.91 (m, 5H), 6.54 (s, 1H), 4.06 (m, 4H), 1.88-1.81 (m, 4H), 1.31 (m, 20H), 0.9 (m, 6H). ^{13}C NMR (75 MHz, $CDCl_3$): 177.38, 176.34, 161.91, 161.45, 161.35, 150.57, 150.23, 147.78, 145.01, 140.51, 139.27, 133.03, 131.42, 131.05, 128.81, 128.73, 124.95, 119.21, 118.69, 117.37, 115.65, 114.19, 114.16, 95.26, 68.22, 68.17, 31.86, 29.44, 29.30, 26.10, 22.70, 14.14. Calculated for $C_{40}H_{47}Br_2NO_4PtS$ 992.77, found ESI-MS (m/z): 1016.10 $[M+Na]^+$.

Synthesis of DPP-Th-Pt-P1

In a 10 mL Schlenk tube, 6-9 (0.075g, 0.076 mmol), 5-3 (0.084g, 0.076 mmol), $Pd_2(dba)_3$ (3.5 mg, 3.78x10^{-3} mmol), $Pd(P^tBu_3)_2$ (3.9 mg, 7.55x10^{-3} mmol) were combined and vacuum-argon cycled three times to remove any oxygen from the reaction flask. Anhydrous THF (4 mL) was added to the reaction mixture. In a separate flask, K_3PO_4 (0.096g, 0.45 mmol) was dissolved in 1 mL of deionized water and deoxygenated for 1 hour. The degassed aqueous solution of K_3PO_4 was added to the reaction mixture quickly under an argon atmosphere. It was heated to 60˚C and stirred under argon atmosphere for 48 hours. The reaction mixture was cooled to room temperature and poured over methanol under vigorous stirring. The dark green precipitate was isolated by filtration and transferred to a Soxhlet thimble. It was purified by subsequent Soxhlet extraction using methanol, hexane and chloroform. The chloroform fraction was collected and concentrated under vacuum. The isolated polymer was poured over methanol under vigorous stirring. The dark green fibrous precipitate was isolated by filtration with 90% yield (~ 120 mg). A number average molecular weight (M_n) of 29 kDa, weight average molecular weight (M_w) of 84 kDa and PDI of 2.9 was obtained from GPC for this polymer. The ^{1}H NMR of this polymer was

attempted in chloroform. Although, all peaks were observed in expected regions, integration was unsuccessful due to peak broadening.

Synthesis of DPP-Ph-Pt-P2

In a 10 mL Schlenk tube, 5-3 (0.1 g, 0.09 mmol) and 6-10 (0.088 g, 0.09 mmol) were dissolved in 4 mL of dry THF and deoxygenated by purging argon for 45 minutes. $Pd_2(dba)_3$ (0.004 g, 0.05 eq) and $Pd(P^tBu_3)_2$ (0.0045 g, 0.10 eq) were added to the reaction mixture under a strong flow of argon and the purple solution was further deoxygenated for 10 minutes. After that, K_3PO_4 (0.114 g, 6 eq) in water (1 mL) which was degassed for 1 h, was added quickly by syringe to the reaction mixture and heated to 60°C for 48 hours. After the reaction, the solution was cooled to room temperature and poured over methanol. The dark green color precipitate was isolated and transferred to Soxhlet thimble. It was purified via Soxhlet extraction with methanol, hexane to remove low molecular weight species and finally extracted with chloroform. The chloroform solution was reduced in volume and poured it over methanol to obtain a dark green precipitate. The polymer was isolated by vacuum filtration in 24% yield (50 mg).). A number average molecular weight (M_n) of 16 kDa, and PDI of 2.9 was obtained from GPC of this polymer. The ^1H NMR of this polymer was attempted in chloroform. Although, all the peak regions were observed in the expected place, due to extreme broadness of the peaks, integration was unsuccessful.

.

CHAPTER 7
EFFECT OF CYCLOMETALLATED PLATINUM ON ISOINDIGO: TRIPLET EXCITED STATE OF ISOINDIGO IS REVEALED

Background

The increasing demand of flexible, light weight and cost effective organic photovoltaic devices as an alternative renewable energy resource spurs the interest of the scientific community to come up with novel materials. The efficient generation of photocurrent requires the material to follow all the necessary steps (light absorption, exciton diffusion, charge separation and charge migration) effectively. One effective way of increasing absorption of the solar spectrum is to utilize donor-acceptor π-conjugated chromophores as the donor materials for photovoltaic devices. In this approach, a π-electron rich donor is combined with a π-electron deficient acceptor, and due to the interaction of their frontier orbitals (HOMO and LUMO), the effective bandgap is reduced compared to their individual bandgaps.[210-213] Utilizing this approach, the efficiency of the solar cells have been improved up to 10%.[214] Compared to an abundance of π-electron donors, electron deficient acceptors are rare in literature. Among them, benzothiadiazole (BTD),[215-217] diketopyrrolopyrrole (DPP),[218-220] naphthalene diimide (NDI)[221] have gained popularity. However, to understand the structure property relationship for donor-acceptor (D-A) systems, it is necessary to search for novel acceptor materials.

Isoindigo is a structural isomer of the well-known naturally occurring pigment indigo.[222] It can be also found as a side product in several biological reactions.[212] Although the synthesis of isoindigo was first reported in 1988,[223] it was not before 2010 when Reynolds and coworkers incorporated isoindigo into π-conjugated D-A framework for application in photovoltaic devices. [224] When introduced into polymeric structures,

isoindigo can have two different linkage isomers- 5,5' and 6,6' substituted polymer. However, as 6,6'-substituted isomers can generate conjugated quinoid mesostructure, this isomer gained popularity in organic optoelectronics over the other (Figure 7-1).[222] After the first report on isoindigo based small molecules for solar cells, there has been growing interest of using these materials for both photovoltaics as well as organic field effect transistors (OFETs). For example, Andersson and coworkers reported PCE of 6.3% with isoindigo-terthiophene containing donor-acceptor copolymers,[225] and in 2011 Bao and her group reported siloxane terminated isoindigo containing copolymers with hole mobility as high as 2.48 $cm^2 V^{-1} s^{-1}$.[226] The electron deficient nature of isoindigo can be attributed to the presence of electron withdrawing lactam rings. Isoindigo polymer was also used as acceptor in all polymer solar cell with P3HT as donor providing the overall PCE of 0.5%.[227]

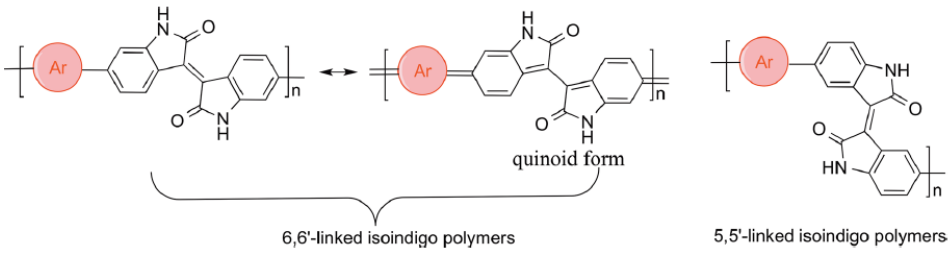

Figure 7-1. The structures of the linkage isomers of isoindigo in polymer backbone.[222] Adapted with permission from Wiley online library.

While most of the studies on isoindigo chromophores are based on singlet excited state properties, the triplet excited state of this versatile acceptor remain unexplored to date. By contrast, the triplet excited state properties of indigo and thioindigo dyes were explored several decades ago.[228-230] One efficient way of populating the triplet excited is to incorporate heavy metals into the conjugated electron system to induce spin-orbit coupling (SOC) and induce intersystem crossing (ISC) to the

triplet excited state. Considering the importance of triplet excited states in optoelectronics,[231] it is necessary to explore the triplet excited state properties of isoindigo.

Since their development in the 1970s,[50] platinum acetylide containing π-conjugated chromophores have gained popularity in the scientific community due to their high ISC efficiency ($\phi_{ISC} \approx 1$) facilitated by strong interactions between the dπ orbital of the metal and the pπ orbital of the chromophore. Recently, Wong and coworkers reported platinum acetylide containing isoindigo polymers and compared their photophysical properties with a diketopyrrolopyrrole analogue.[232] However, triplet excited state photophysics was not explored in their study. It is important to mention that isoindigo-platinum acetylide derivatives were also synthesized in our lab, and triplet excited state was not observed from nanosecond transient absorption spectroscopy. Efficient non-radiative decay likely occurs via rapid twisting around the central olefinic bond. The other non-radiative decay channel could be a low lying triplet excited state which leads to immediate deactivation of the triplet excited state by nonradiative decay according to energy gap law.[185]

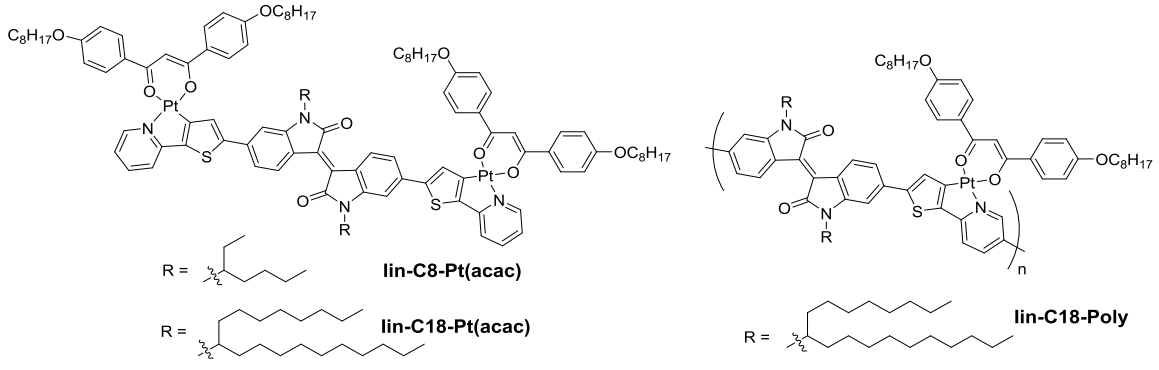

Figure 7-2. Structure of the isoindigo metal complexes and polymer.

Recently we have shown the comparative photophysical and electrochemical studies of platinum acetylide and cyclometallated platinum complex architecture on diketopyrrolopyrrole based donor-acceptor complexes.[156] The planar structure of cyclometallated platinum motif imparts stronger spin-orbit coupling and increased excited state delocalization compared to the platinum acetylide system. Inspired by this result, we have synthesized two cyclometallated platinum containing isoindigo complexes and with varying solubilizing alkyl chains at the central nitrogen atom; named Iin-C8-Pt(acac) and Iin-C18-Pt(acac). The polymer Iin-C18-Poly is synthesized with solubilizing octyldodecyl chains at the central nitrogen atom. Analytical purity of the metal complexes was established by ^{1}H NMR, ^{13}C NMR and mass spectroscopy. The metal complexes and the polymer were characterized by ground state absorption, steady state emission spectroscopy and nanosecond transient absorption spectroscopy. Finally, a preliminary study of photovoltaic measurements with Iin-C18-Poly gave the power conversion efficiency (PCE) of 0.22%. To the best of our knowledge, this is the first detailed report of triplet excited state photophysics of isoindigo containing organometallic chromophores.

Results and Discussion

Synthesis

The synthesis was started with acid catalyzed aldol condensation reaction between commercially available 6-bromoisatin (7-1) and 6-bromooxindole (7-2) in acetic acid under an argon atmosphere. In general, the condensation reaction is high yielding, due to the easy purification of the compound by vacuum filtration and washing with ethyl acetate and ethanol. The obtained product 7-3 was insoluble in any organic solvents due to the presence of strong intermolecular hydrogen bonding and π-π interaction. It

was reacted with corresponding branched alkyl halide in presence of K_2CO_3 as base in DMF under an argon atmosphere to obtain the N-alkylated product 7-4. After that, it was reacted under Miyaura borylation condition to obtain the key intermediate of the reaction 7-5. It was easily purified by successive precipitation in cold methanol to obtain the compound in high purity.

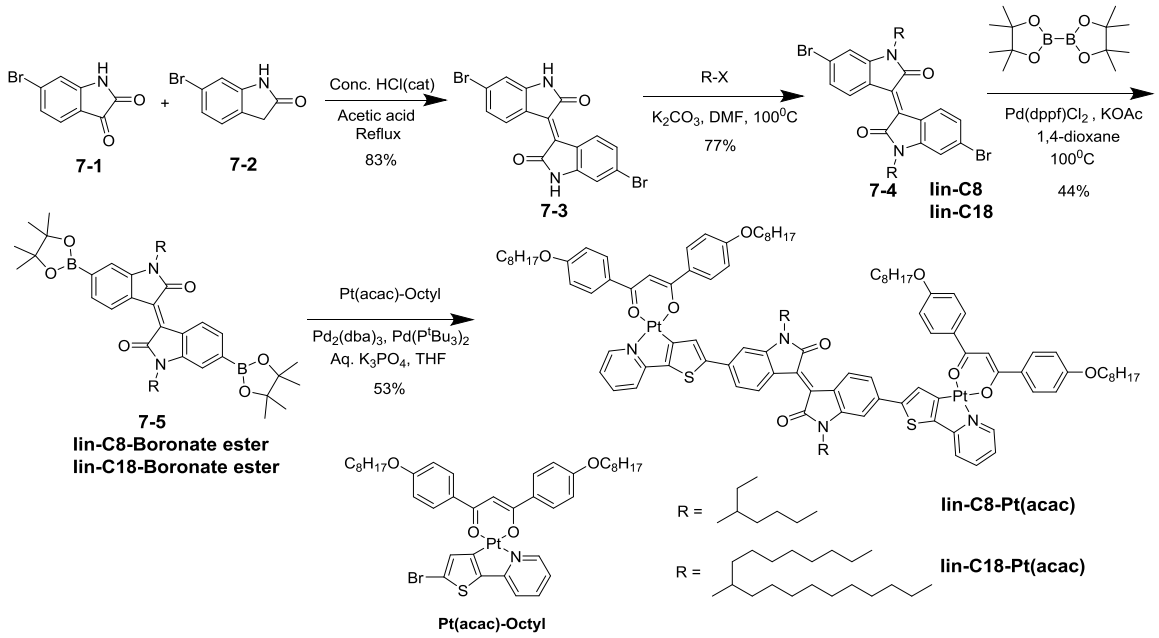

Figure 7-3. Synthetic scheme for the isoindigo metal complexes reported herein.

The cyclometallated precursor Pt(acac)-octyl was synthesized by the same procedure as mentioned before in Chapter 6. Finally, the metal complexes were synthesized under Suzuki-Miyaura cross coupling reaction conditions. The higher solubility of lin-C18-Pt(acac) allows the purification of this complex by traditional silica gel column chromatography and precipitation from hexanes and due to the low solubility of lin-C8-Pt(acac) the compound was purified by successive recrystallization procedure.

The dibromo platinum precursor 6-9 was synthesized by following the same procedure as in chapter 6. Iin-C18-Boronate ester was reacted with 6-9 under Pd catalyzed Suzuki-Miyaura cross coupling condition for 48 hours. The polymer Iin-C18-Poly was purified by Soxhlet extraction subsequently by using methanol, hexane and finally chloroform. It was further purified by precipitation over vigorously stirred methanol.

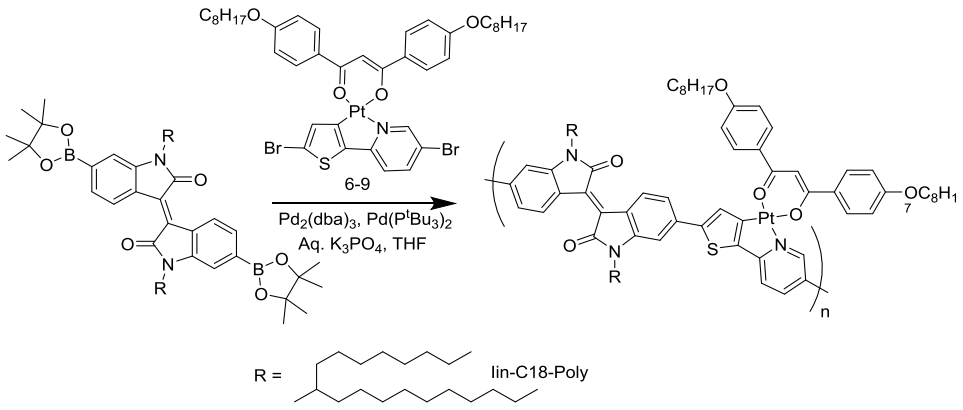

Figure 7-4. The synthetic scheme for the polymer Iin-C18-Poly..

Electrochemistry

In an effort to understand the redox behavior of the isoindigo chromophores, electrochemical studies were performed with the precursor molecule Iin-C18, metal complex Iin-C18-Pt(acac) and the polymer in dry dichloromethane solvent and are presented in Figure 7-5. The electrochemical potentials for the chromophores are listed in Table 7-1.

The electrochemical measurements were performed with three electrode system, where platinum was used as the working and counter electrodes and Ag/Ag^{+} was used as the quasi-reference electrode with 0.1 M NBu_4PF_6 as the electrolyte. All the recorded potentials were vs Fc/Fc^{+} internal standard. The cyclic voltammetric diagram for Iin-C18 is presented in Figure 7-5 (top panel). It consists of two reversible reduction potentials

with half-wave potential value of -1.21 V and -1.69 V. The irreversible oxidative wave shows up above 1.00 V if there is any present. The electrochemical property of Iin-C18 is in accordance with its acceptor nature and similar with the literature report with alkyl chains other than C18.[233] The LUMO energy level was calculated at 3.89 eV from the first reduction potential value of Iin-C18.

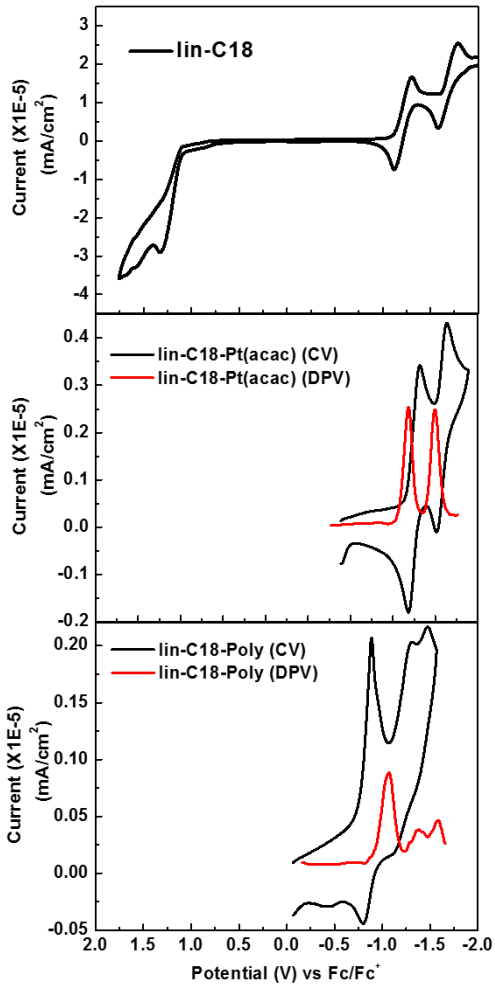

Figure 7-5. Solution electrochemistry and reduction DPVs of isoindigo chromophores in 0.1 M NBu_4PF_6 in DCM with 0.1 M TBAPF6 as the supporting electrolyte. It was scanned at 100 mVs^{-1}. All the potentials are referenced to Fc/Fc^+ couple as an internal standard.

The CV and differential pulse voltammetry (DPV) diagram for the metal complex Iin-C18-Pt(acac) are presented in the middle panel of Figure 7-5. It consists of two

reversible reduction potentials at -1.25 V and -1.60 V. The LUMO energy level was calculated at 3.85 eV. It is interesting to note here the change in reduction potential from Iin-C18 to Iin-C18-Pt(acac) is minimal suggesting negligible impact of the cyclometallated platinum motif on LUMO energy level. This fact indirectly suggests that the reduced bandgap of the metal complex originates from the effect of the cyclometallated platinum on HOMO energy level. However, the oxidation peak for this metal complex architecture was found ill-defined, likely due to the participation of the metal center in the oxidation processes, leading to irreversible changes in the metal complex.[170] Density functional theory (DFT) calculations correlate well with the observed electrochemical data. While the LUMO molecular orbital centered mostly on the isoindigo acceptor, the HOMO is delocalized over the entire molecule with significant contribution from the metal d-orbitals (Figure 7-6 B). For the polymer, the first reduction potential wave shifted to -0.9 V (calculated from onset of DPV) and the LUMO energy level is estimated at 4.2 eV.

Table 7-1. Summary of electrochemical properties.[a]

Compound	$E_{1/2}$/V		$E_{1/2}$/V	
	Red_1	Red_2	Ox_1	Ox_2
Iin-C18	-1.21	-1.69	–	–
Iin-C18-Pt(acac)	-1.25	-1.60	0.51[b]	–
Iin-C18-Poly	-0.90[c]	–	0.72[b]	–

Note: [a] Measured in CH_2Cl_2 using 0.1 M NBu_4PF_6 as supporting electrolyte. It was scanned at 100 mV s^{-1}. All the potentials are referenced to a Fc/Fc^+ couple as an internal standard. [b] oxidation potentials were estimated from the optical bandgap and the reduction potentials derived from electrochemistry. [c] calculated from the onset of DPV.

Ground State Absorption

The ground state absorption spectra of the precursor molecules, metal complexes and polymer were recorded in THF solution and presented in Figure 7-6A. In general, the absorption spectra consists of two bands, which is typical for D-A type chromophores. The precursor molecules Iin-C8 and Iin-C18 show similar absorption spectra which consists of an intense absorption at 300 - 425 nm and a moderately intense band at 425 - 600 nm. The two metal complexes Iin-C8-Pt(acac) and Iin-C18-Pt(acac) also exhibits similar dual absorption bands between 300 - 450 nm and 500-700 nm. For the polymer, the absorption band is further red shifted and the onset of absorption was observed at ~790 nm.

The absorption maxima (λ_{max}) and molar extinction coefficient values (ε) are shown in Table 7-2. From the previous report on D-A based π-conjugate chromophores, the low energy absorption band can be attributed to a charge transfer band and the high energy absorption feature arises from π-π* transition.[234] Isoindigo precursors (Iin-C8 and Iin-C18) also feature a donor-acceptor interaction, and this is believed to originate from a charge transfer interaction between both the central double bond and the nitrogen atom with the carbonyl oxygen atom. In general, the molar absorptivity (ε) for the charge transfer band is lower compared to the ε value of π-π* band. The charge transfer band red shifts from 496 nm for isoindigo precursor molecules to 596 nm for the metal complexes and further down to 690 nm for the polymer. This result can be attributed to increased delocalization imparted by the cyclometallated platinum chromophore. The molar absorptivity (ε) increases from 12,800 $M^{-1}cm^{-1}$ for the precursor molecules to 58,000-60,000 $M^{-1}cm^{-1}$ for the metal complexes. This significant

change in molar absorptivity is due to the increased charge –transfer interaction in the metal complexes. It is important to note here, the low ε value (31,000 $M^{-1}cm^{-1}$) for the polymer is an artifact here, as the polymer repeat unit (PRU) used here for calculation has one cyclometallated unit, whereas the metal complexes contains two.

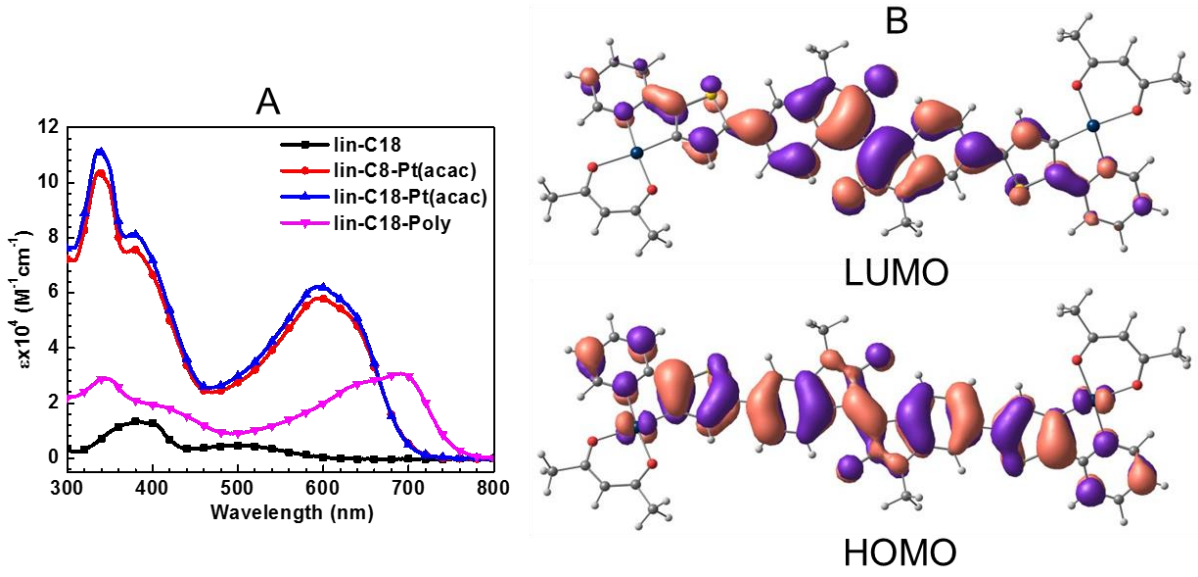

Figure 7-6. The (A) ground state absorption spectra of the precursor molecules, metal complexes and polymer in THF solution, (B) frontier orbitals for Iin-C8-Pt(acac) from DFT calculations.

The ground state absorption spectrum for the model complex is in accordance with the DFT calculation. The HOMO molecular orbital has significant metal orbital contribution whereas the LUMO is mostly localized on the acceptor. Charge difference density (CDD) plots for the longer wavelength absorption bands suggest that the electron density is being lost from cyclometallated platinum part to the central isoindigo acceptor, which is in agreement with the charge transfer transition at longer wavelength (APPENDIX E). From the electrochemical study, it was observed that the LUMO level is nearly unaffected when the conjugation length was increased at the 6,6' position of the isoindigo. This fact clearly suggests that the only way to reduce the HOMO-LUMO

bandgap in cyclometallated platinum chromophores is to affect the HOMO energy level and hence proved from the DFT calculations.

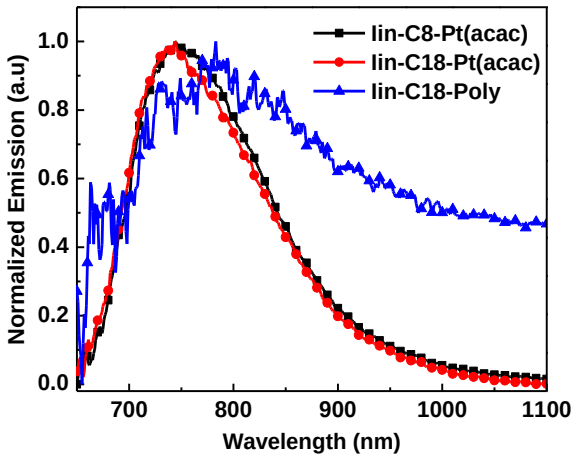

Figure 7-7. The photoluminescence spectra of the metal complexes and the polymer in THF solution.

Steady State Photoluminescence Spectroscopy

The photoluminescence spectra of the metal complexes and the polymer were recorded in THF solution and presented in Figure 7-7. In general, all exhibit broad emission spectra between 600 -1100 nm with a very small Stokes shift relative to the ground state absorption. The time resolved emission spectroscopy indicate that all of the complexes have very short lifetime (<200 ps). Taken together, all these facts indicate that the emission can be assigned to the fluorescence from the lowest singlet excited state. The broad emission spectra also suggests that the singlet excited sate has a significant amount of charge transfer character, which is in agreement with the DFT calculations. There is almost no difference observed between the emission spectra of the two metal complexes with different alkyl chains on the central nitrogen. However, similar to the ground state absorption spectra, the emission from the polymer is red

shifted compared to the metal complexes suggesting delocalization of the singlet excited state. The emission maxima (λ_{em}) and fluorescence quantum yield (ϕ_{Fl}) of the metal complexes and polymer are represented in Table 7-2.

As seen by the data in Table 7-2, the low fluorescence quantum yields (ϕ_{Fl}= 0.04) of the metal complexes and the polymer (ϕ_{Fl}= 0.005) indicates the presence of efficient non-radiative decay from the singlet excited state. We suggest that the alternative pathway is intersystem crossing (ISC) from $S_1 \rightarrow T_1$ due to strong spin-orbit coupling (SOC) from the heavy metal platinum.

Table 7-2. Summary of photophysical properties.[a]

Compound	λ_{max} (nm)	ε x 10^4 ($M^{-1}cm^{-1}$)	λ_{em} (nm)	ϕ_{fl} [b]	τ_{fl} (ns)	τ_{TA} (µs)
Iin-C18	498	1.3	-	-	-	-
Iin-C8-Pt(acac)	595	5.8	748	0.04	<0.2	0.064
Iin-C18-Pt(acac)	595	6.2	742	0.04	<0.2	0.064
Iin-C18-Poly	691	3.1	785	0.005	<0.2	0.082

Note: [a] All the photophysical properties were reported in THF. [b] Quantum yield measured using tetraphenylporphyrin in toluene (ϕ_F=0.09) as actinometer.

Transient Absorption Spectroscopy

One of the major objective to study the cyclometallated platinum containing isoindigo derivatives is to probe the triplet excited state. Although the low fluorescence quantum yields and short singlet excited state lifetimes suggest ISC is taking place to the triplet excited state, no phosphorescence signal was observed from these organometallic complexes. In order to study the triplet excited state, nanosecond-microsecond (ns-µs) transient absorption (TA) spectroscopy was performed with the deoxygenated THF solutions of metal complexes and the polymer. Ultrafast transient absorption spectroscopy was performed on the Pt model complex (Iin-C8-Pt(acac)) and Iin-C8 in collaboration with Prof. John Papanikolas group and Melissa Gish at the

University of North Carolina, Chapel Hill. The ultrafast transient absorption of the isoindigo precursor Iin-C8 along with the ground state absorption is presented in Figure 7-8 (A). It consists of a ground state bleach between (GSB) 300 - 550 nm and broad excited state absorption between 550-800 nm. The ground state bleach correlates well with the ground state absorption spectra. The only spectral evolution observed for Iin-C8 was the slow decay of the peak between 550 -800 nm and no sign of ISC was observed. This spectrum can be assigned to the excited state absorption of S_1 state. The kinetic traces of Iin-C8 are shown in Figure 7-8 (B) at different wavelengths. The decays at 419 nm and 511 nm correlate well with the evolution of the transient at 590 nm. The lifetime of the singlet excited state was found to be ~ 11 ps.

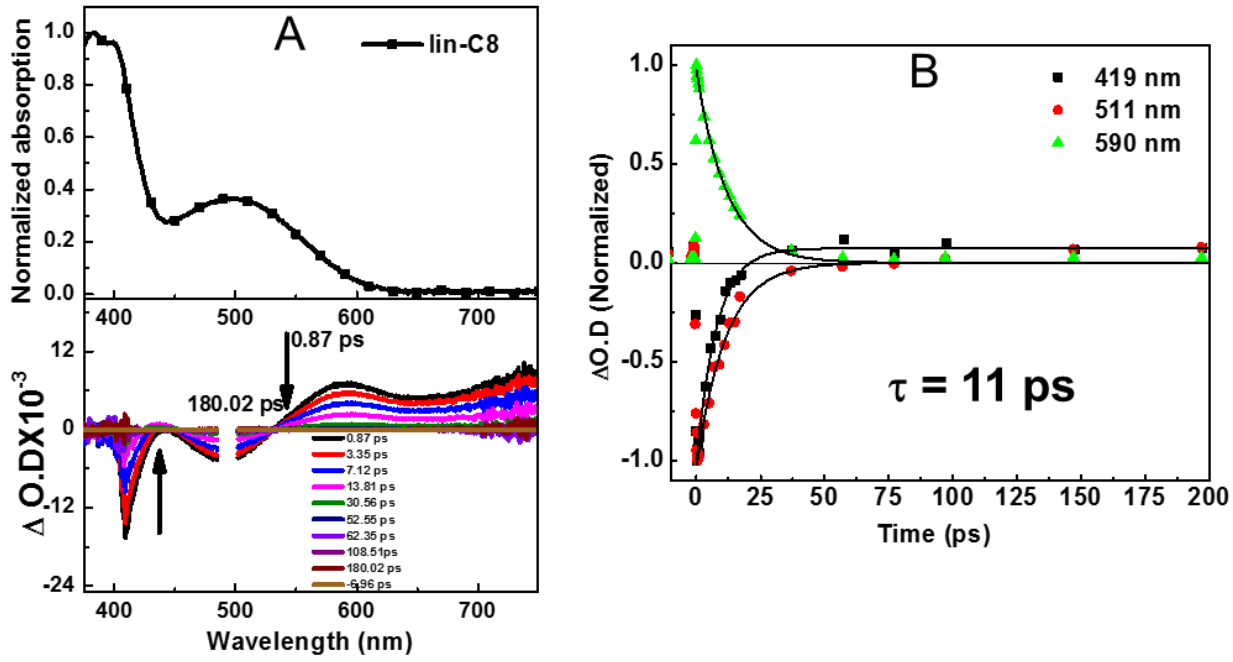

Figure 7-8. (A) Ground state absorption spectra (top panel) and transient absorption spectra (bottom panel) of the isoindigo precursor Iin-C8, (B) kinetic traces at 419 nm, 511 nm and 590 nm for Iin-C8. Transient spectra were obtained in deoxygenated THF solution with 490 nm excitation wavelength (100 nJ/pulse).

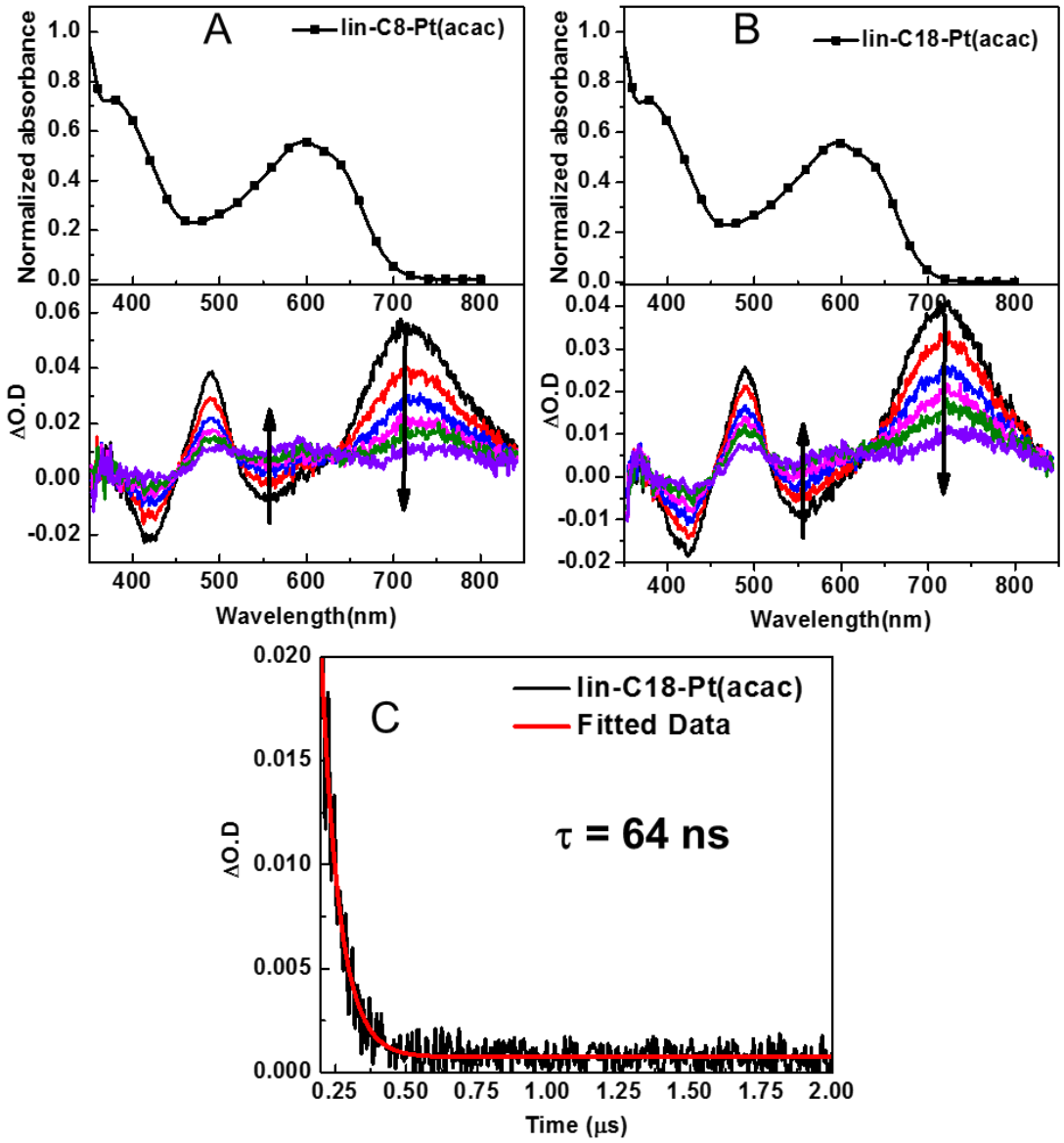

Figure 7-9. (A) and (B) The ground state absorption spectra (top panel) and nanosecond transient absorption spectra (bottom panel) for isoindigo metal complexes, (C) transient decay of Iin-C18-Pt(acac) at 480 nm. Transient spectra were obtained in deoxygenated THF solution with 355 nm excitation wavelength. Initial delay 10 ns following a 15 ns laser excitation pulse.

The ns-μs transient absorption spectra for the metal complexes (Iin-C8-Pt(acac) and Iin-C18-Pt(acac)) were recorded in deoxygenated THF solution by exciting at 355 nm and represented in Figure 7-9. Overall, the spectra consists of a derivative shape

feature with a ground state bleach between 400 - 600 nm and a excited state absorption between 650 -850 nm. The excited state absorption is slightly red shifted compared to the ground state absorption maxima, and the ground state bleach is in accordance with the absorption spectra. Due to the strong interference of the stimulated emission between 700 - 800 nm, the lifetime of the excited state was monitored at 480 nm for Iin-C18-Pt(acac) and found to be ~ 64 ns. The transients were quenched in the presence of oxygen, which is in agreement with their assignment to triplet excited state. As no triplet excited state was observed for Iin-C8, the triplet excited state in the metal complexes is produced by the SOC effect of the cyclometallated platinum “auxochrome.”

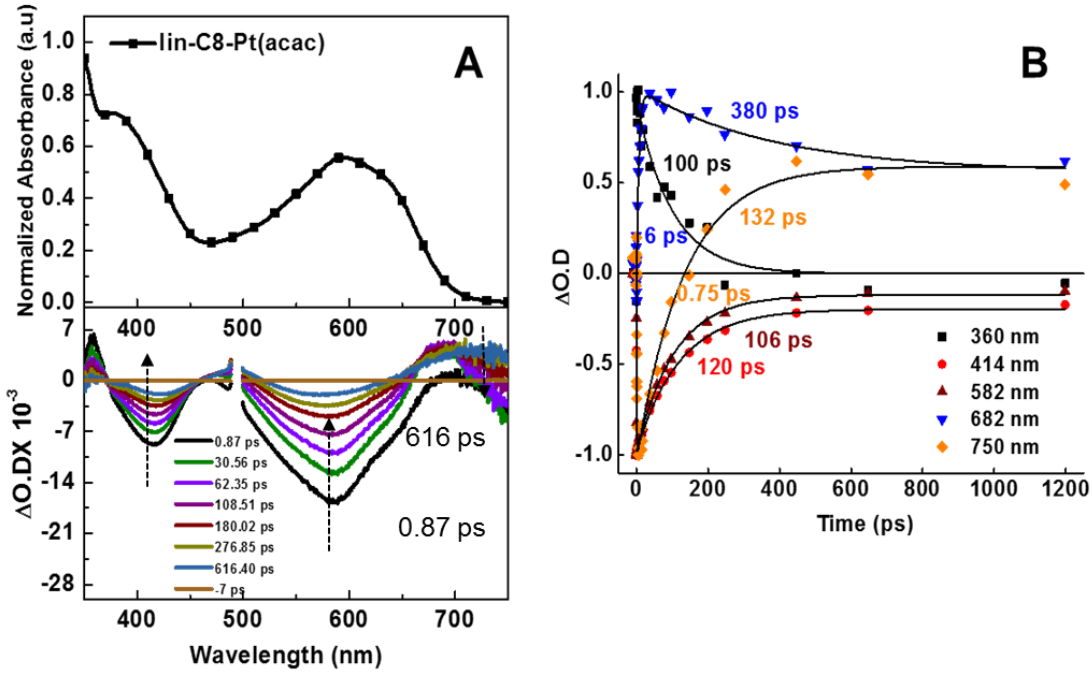

Figure 7-10. (A) The ground state absorption spectra (top panel) and femtosecond transient absorption spectra (bottom) panel for Iin-C8-Pt(acac) in THF. (B) kinetic data of the metal complexes at different wavelengths, lifetimes at the individual wavelengths are shown by respective colors. Transient spectra were obtained in deoxygenated THF solution with 490 nm excitation wavelength (100 nJ/pulse).

Figure 7-10 (A) presents the picosecond transient absorption spectra of the model complex Iin-C8-Pt(acac) measured in THF solution at 388 nm along with the absorption spectra. The ground state bleaches at 350 – 450 nm and 500 -650 nm correlate well with the ground state absorption bands. The kinetic traces at different wavelength are shown in Figure 7-10 (B). Other than the transient at 682 nm, all of transients decay within 100 - 130 ps suggesting this is the lifetime of the singlet state, and the decay rate is controlled by intersystem crossing to the triplet state. The feature at 682 nm is present within 6 ps following excitation and persists for much longer compared to the time scale of the instrument. At longer wavelengths the absorption is due to a superposition of the singlet and the triplet states.

Figure 7-11 represents the ns-µs transient absorption spectra of the polymer Iin-C18-Poly in deoxygenated THF solution. The spectral features observed are similar to those seen for the model complex. However, several features appear upon close inspection of the spectra. As, the TA measurements were performed using sample solutions of matched absorbance of ~0.7 at 355 nm with the same laser power and energy, the low transient absorption intensity of the polymer suggests it has a lower triplet yield than the model complex. The possible explanation could be the presence of triplet-triplet annihilation in the polymer chain.

Notable similarity in structure is found between isoindigo derivatives and stilbene due to the presence of the core double bond.[233] To understand the triplet excited state properties of stilbene derivatives, Schanze and coworkers reported a family of platinum acetylide stilbene derivatives.[235] Although triplet excited state was observed by using nanosecond transient absorption spectroscopy, the lifetime was significantly shorter

(~40 ns) for a triplet excited state. It was proved by ^{1}H NMR study that the twist around the central C=C bond was the major contribution to nonradiative decay of triplet excited state. Similarity in structure and triplet excited state lifetime with stilbene derivatives suggests similar twisting around C=C bond in isoindigo is responsible for the nonradiative decay.

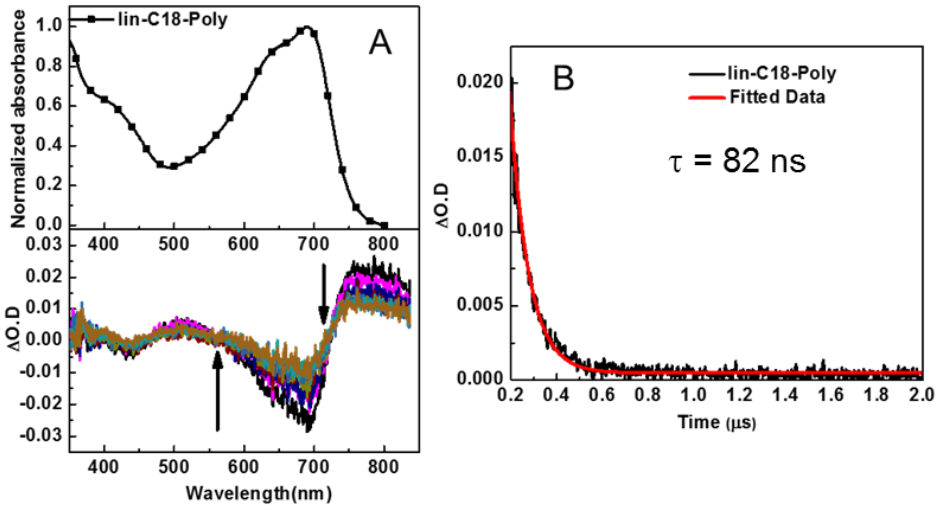

Figure 7-11. The (A) ground state absorption spectra (top panel) and nanosecond transient absorption spectra (bottom panel) for Iin-C18-Poly in THF, (B) triplet excited state lifetime data of the polymer at 480 nm.

In an effort to gain further insight into the triplet-triplet absorption, TD-DFT calculations were performed on the lowest triplet excited state of the metal complex Iin-C18-Pt(acac). The calculation shows, two dominated transitions involved in transient absorption are HSOMO→LUMO+1 and HOMO-1→LSOMO. This fact is in accordance with the red-shifted excited state absorption compared to the ground state absorption which is dominated by a HOMO→LUMO transition. The predicted triplet-triplet absorption maxima (701.8 nm) is very close to the experimental value. Finally, the charge difference density plots in the triplet excited state reveal significant amount of

electron density is lost from the metal center compared to the ground state absorption (see APPENDIX E8).

Photovoltaic Properties

Preliminary studies were performed with Iin-C18-Poly as a donor material for bulk heterojunction solar cell devices in conjunction with $PC_{61}BM$ as an acceptor. The architecture of the photovoltaic devices tested was: ITO/ PEDOT:PSS/ active layer / LiF (0.5 nm)/ Al (100 nm). Chlorobenzene was selected as the solvent to prepare solutions for the active layer.

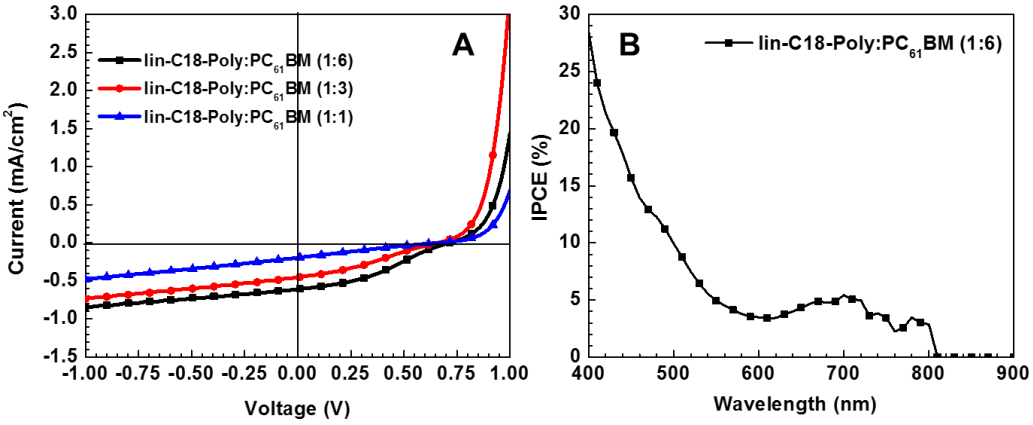

Figure 7-12. (A) J-V plot of the devices made from Iin-C18-Poly as donor and $PC_{61}BM$ as acceptor in varying ratio. (B) IPCE plot of the optimized device with donor –acceptor ratio of 1:6.

Several polymer/ $PC_{61}BM$ ratios were tested to optimize the conditions. With increasing amounts of PCBM from 1:1 to 1:3, and finally to 1:6, the device efficiency increased from 0.04% to 0.22% (Table 7-3). This is in accordance with several reports where organometallic polymers operate in a device with high PCBM fraction.[75,188] The J-V curve for the devices with different ratios of donor and acceptor are shown in 7-12 (A). In optimized ratio, short circuit current (J_{sc}), open circuit voltage (V_{oc}), fill factor (FF) and power conversion efficiency (PCE) observed were 0.9 mA/cm^2, 0.71 V, 35% and 0.22%.

When the amount of PCBM was decreased upto1:1 donor/ acceptor ratio, the PCE decreases to 0.04% with a significant decrease in J_{sc} and FF.

Table 7-3. Photovoltaic properties of Iin-C18-Poly with varying PCBM amount

Blend Ratio	J_{sc} (mA cm^{-2})	V_{oc} (V)	FF (%)	PCE (%)
1:1	0.30	0.65	23	0.04
1:3	0.60	0.66	31	0.13
1:6	0.90	0.71	35	0.22

Note: All numbers are the averages of 8 pixels on each cell.

The IPCE plot for the optimized device is presented in Figure 7-12 (B). Overall, the photon to current conversion efficiency is below 10% which is in accordance with the low efficiency of the device. In general, the IPCE curve consists of a broad absorption from 400 -600 nm and a structured peak at 600 - 800 nm. The longer wavelength and shorter wavelength absorptions can be attributed to the polymer and PCBM respectively. The poor device efficiency of this polymer can be attributed to its low molecular weight and poor phase separation with PCBM in the device together with the frontier energy levels of the polymer.

Discussion

In an effort to understand the multiplicity of the excited state of isoindigo polymer involved in charge transfer to $PC_{61}BM$, the energy diagram of the excited states were constructed and presented in Figure 7-13.

An electron transfer process in bulk heterojunction solar cell is thermodynamically favorable when the energy of the charge separated excited state ($polymer^{+\cdot}PC_{61}BM^{-\cdot}$) is lower compared to energy of the excited state involved.

$$\Delta G = E_{CS} - Ees \qquad (7\text{-}1)$$

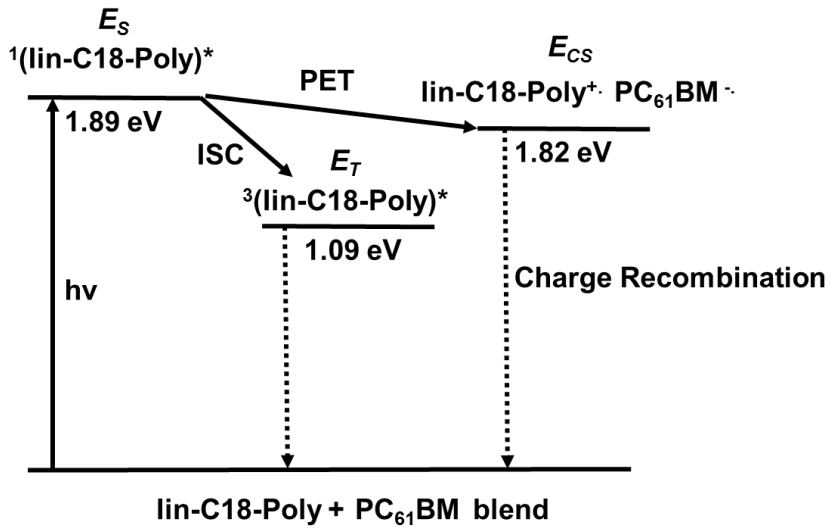

Figure 7-13. Energy level diagram for Iin-C18-Poly.

The energy of the charge separated state can be estimated by taking the difference between oxidation potential of the polymer and reduction potential of the acceptor PCBM

$$E_{cs} = E_{ox(polymer)} - E_{red(PCBM)} \quad (7\text{-}2)$$

From the ground state absorption of the polymer and electrochemical data, the oxidation potential for the polymer was estimated to be ~0.72 V vs Fc/Fc^+. By using the oxidation potential of the polymer together with $E_{red(PCBM)}$ (-1.10 V vs Fc/Fc^+),[25] the estimated E_{cs} value for the polymer is ~1.82 eV. The singlet excited state energy was estimated from the onset of fluorescence and found to be ~1.89 eV which is the second term of equation 7-1. As phosphorescence was not observed from Iin-C18-Poly, the triplet excited state energy was estimated from S_1-T_1 energy gap of 0.8 eV and calculated as 1.09 eV.[185]

It is clearly observed that the PET from singlet excited state is exothermic whereas it is endothermic from the triplet excited state being lower in energy as compared to the charge separated state. However, for singlet excited state, the energy

difference between charge separated state and singlet excited state is only ~0.07 eV, which gives weakly exothermic electron transfer.

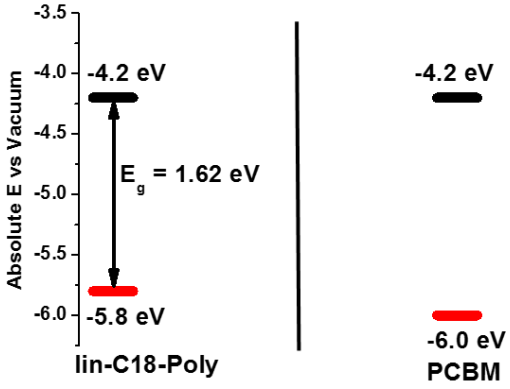

Figure 7-14. HOMO-LUMO energy levels for Iin-C18-Poly and PCBM.

From the onset of reduction potential value (-0.9 V), the LUMO level of the polymer Iin-C18-Poly was estimated at ~ - 4.2 eV which is same LUMO energy level as PCBM. We believe such a low LUMO energy level is responsible for low PCE of this polymer. Reynolds and coworkers reported a family of n-type poly-isoindigo, where they estimated the LUMO energy levels at -3.80 and -3.90 eV for two polymers.[227] When used as an acceptor in bulk-heterojunction solar cell with P3HT as donor, PCE of 0.5% was achieved. Being closer in LUMO energy level with PCBM, this material has the potential to act as an acceptor in all polymer solar cells.

Summary and Conclusions

This work demonstrated the detailed synthetic and photophysical study of two cyclometallated platinum containing isoindigo metal complexes Iin-C8-Pt(acac), Iin-C18-Pt(acac) and one polymer Iin-C18-Poly. The results clearly demonstrate the effect of cyclometallated auxochrome on isoindigo chromophores through photophysical and electrochemical studies. The electrochemical data suggests, cyclometallated motif has

significant impact on the HOMO energy level which is manifested by bathochromic shift in absorption spectra compared to the nonmetallated isoindigo precursors. This fact is also in accordance with the DFT calculations for the metal complexes where significant contribution of the platinum orbital to the HOMO is observed. Nanosecond transient absorption spectroscopy of the metal complexes and the polymer showed the presence of triplet excited state in these chromophores with a lifetime of 64 ns and 82 ns respectively. Such a short lifetime can be attributed to the low energy of the triplet excited state along with the twist around central olefinic bond which contributes to the nonradiative decay of the excited state.

Finally, we have studied the polymer Iin-C18-Poly as a donor material in bulk heterojunction solar cells. Preliminary studies have shown 0.22% efficiency with $PC_{61}BM$ in a 1:6 donor-acceptor ratio. Interestingly, the LUMO energy level of the polymer is estimated at ~4.2 eV, which is exactly the same value as for PCBM. Future work in our lab will focus on using this material as an acceptor in all polymer solar cell device. Taken together, this is the first detailed study of the triplet excited state photophysics of organometallic isoindigo chromophores and it is shown that this could be a promising candidate for bulk heterojunction solar cell device.

Experimental

Instrumentation and Methods

^{1}H NMR spectra and ^{13}C NMR spectra were recorded by using Inova-500 FT-NMR instrument operating at 500 MHz for ^{1}H NMR and 125 MHz for ^{13}C NMR. Mass spectra analysis of the newly synthesized compounds were performed in Mass spectrometry services, which is present in house at the University of Florida. The molecular weight of the polymer was analyzed by Gel Permeation Chromatography

(GPC) from a system containing Shimadzu SPD-20A photodiode array (PDA) detector and THF as eluent with a flow rate of 1 mL/ min. Before the measurement, the system was calibrated using linear polystyrene in THF.

The photophysical measurements were performed with dry, HPLC grade THF, unless otherwise mentioned in 1 x 1 cm^2 cuvettes. All the experiments were performed with a diluted solution, prepared from a stock solution, unless otherwise mentioned. Ground state absorption spectra were obtained by Shimadzu UV-1800 dual beam spectrophotometer. Steady state emission spectra were collected from a Photon Technology International (PTI) spectrophotometer and the data was collected at 90˚ relative to the excitation beam. The optical density (O.D) of the sample solutions were kept $\leq$ 0.1 for optical measurements unless otherwise mentioned. For quantum yield calculations, corrections for refractive index of the sample solvent and the standard solvent were incorporated. Fluorescence lifetime data was obtained from PicoQuant FluoTime 100 Compact Fluorescence Lifetime Spectrophotometer by time-correlated single photon counting (TCSPC). Sample solutions were excited a 375 nm by PDL-800B Picosecond Pulsed Diode Laser.

Nanosecond transient absorption spectroscopy data was obtained from an in-house instrument using the third harmonic of a continuum Surelite series Nd:YAG laser. The probe light was generated from a xenon flash lamp and the signal was detected by using gated intensified CCD mounted on a 0.18 M spectrograph (Princeton PiMax/Acton Pro 180). The optical density of the samples was kept at ~ 0.7 at 355 nm and deoxygenated by purging argon for at least 45 minutes. The sample solutions contained

in 1 cm path length flow cell (10 mL) and continuously circulated at pump-probe region to protect the sample from degradation.

The cyclic voltammetry studies were performed on a BAS CV-50W voltammetric analyzer (Bioanalytical Systems, Inc., www.bioanalytical.com) in dry dichloromethane (CH_2Cl_2) solution in the presence of 0.1 M tetra-n-butylammonium hexafluorophosphate (TBAH) as electrolyte. The measurements were performed with three electrodes: a platinum microdisk with area of 2 mm^2 as working electrode, a platinum wire as the auxiliary electrode and a silver wire as the reference electrode. Sample concentrations were maintained to 1 mM and the scan rate of 100 mV/s was used for the study. The sample solutions were deoxygenated prior to the measurement and constant flow of argon was maintained during the data collection. All the potentials collected were corrected against ferrocene as internal standard ((E(Fc/Fc+) = 0.43 V vs SCE in CH_2Cl_2).

General Methods for Synthesis

All the reactions were performed under an argon atmosphere and tetrahydrofuran (THF) used for the reactions was dried using solvent purification columns (Glass Contour). All the other solvents for the reaction were used without any purification unless otherwise mentioned. The metal complexes were synthesized by following the reaction scheme in Figure 7-3. Isoindigo precursor 7-3 and the soluble derivative with 2-ethylhexyl chain Iin-C8 was synthesized by following literature procedure.[224] Iin-C18, isoindigo precursor with solubilizing octyldodecyl chain was synthesized according to the reported procedure.[236] $Pd_2(dba)_3$, $Pd(P^tBu_3)_2$, Potassium phosphate tribasic were purchased from Sigma Aldrich and used as received. 7-1 and

7-2 were obtained from TCI America. The synthesis of cyclometallated platinum precursors were synthesized by following the procedure from Chapter-6.

Methods for Device Fabrication

Photovoltaic devices were fabricated by using pre patterned Indium tin oxide coated glass slides obtained from Kintec Company. The ITO coated glass substrates are subsequently treated with aqueous sodium dodecyl sulfate (Fisher Scientific), deionized water (Milli-Q), isopropyl alcohol and acetone in an ultrasonic bath for 15 minutes. The substrates were then treated with oxygen plasma for 15 minutes in a Plasma Cleaner (Harrick PDC-32G). An aqueous solution of PEDOT:PSS (Baytron P VP Al 4083) was spin coated at a rate of 5000 rpm for 1 minute and subsequently annealed on a hot plate at 130˚C for 20 minutes. A solution of the active layer with the desired ratio of polymer:$PC_{61}BM$ was prepared in chlorobenzene and stirred at 60˚C overnight under argon filled M-Braun glove box. The active layer solution was then spin coated onto the PEDOT-PSS coated substrates at 1000 rpm in the glove box and the resulting films were dried under high vacuum overnight at room temperature. LiF (0.5 nm) and Al (100 nm) were deposited by thermal evaporation under high vacuum overnight on the active layer in sequence. The cathode pattern on the substrates was created by using copper mask, resulting pixel size of the cathodes of 0.07 cm^2.

The current-voltage (J-V) plot was measured with a Keithley 2400 source measurement unit (SMU) under illumination of A.M. 1.5 with an incident power density of 100 mW/cm^2 supplied by a xenon arc lamp power supply (Oriel Instruments). The external quantum efficiency (EQE) of the devices were evaluated by measuring the IPCE (%). IPCE measurements were performed with monochromatic light generated by a monochromator (Oriel Instruments) with a xenon arc lamp as the light source. A

power meter (S350, UDT Instruments), equipped with a calibrated silicon detector (221, UDT Instruments) was used to measure the intensity of the source at each wavelength (10 nm increment). A Keithley 2400 source meter was used with no voltage bias to record the current at each illumination wavelength. All the measurements were performed under air and without encapsulation.

General procedure for synthesis of boronate esters of Isoindigo (8-5)

Iin-C18 (0.2 g, 0.2 mmol), pinacol ester of diboron (0.21 g, 0.82 mmol), [$PdCl_2$(dppf)] (9 mg, 0.012 mmol) and potassium acetate (0.12 g, 1.2 mmol) were combined in a flame dried three necked flask and vacuum-argon cycled to remove the residual oxygen. Dry 1, 4-dioxane (3 mL) was added to the reaction mixture and heated to 80˚C. The reaction mixture was stirred at that temperature for 30 hour under argon atmosphere. It was cooled to room temperature and filtered by passing through a short pad of silica gel, eluting with dichloromethane/hexane (1:1). The solvents were evaporated under vacuum to concentrate and poured over vigorously stirring cold methanol (50 mL). The precipitate was isolated by filtration and washed with methanol. The product was dried to give a dark red shiny powder (97 mg, 44%).

Iin-C18-boronate ester: ^{1}H NMR (300 MHz, $CDCl_3$): δ 9.14 (d, 1H, J= 7.9 Hz), 7.47 (d, 1H, J= 7.9 Hz), 7.15 (s, 1H), 3.68 (d, 2H, 7.2 Hz), 1.96 (m, 1H), 1.36 (m, 44H), 0.87 (m, 6H).

Iin-C8-boronate ester: ^{1}H NMR (300 MHz, $CDCl_3$): δ 9.12 (d, 1H, J= 7.9 Hz), 7.47 (d, 1H, J = 7.9 Hz), 7.16 (s, 1H), 3.70 (m, 2H), 1.90 (m, 1H), 1.36 (m, 40H), 0.93 (m, 12H).

General procedure for synthesis of metal complexes [Example-Iin-C18-Pt(acac)]

In a flame dried flask, Iin-C18-boronate ester (0.075 g, 0.07 mmol), Pt(acac)-Octyl (0.13 g, 0.14 mmol), $Pd_2(dba)_3$ (3.2 mg, 3.5 x 10^{-3} mmol), $Pd(P^tBu_3)_2$ (3.6 mg, 6.97 x 10^{-3} mmol) were combined and vacuum-argon cycled for three times to remove the oxygen from the reaction medium. In the meantime, K_3PO_4 (0.088 g, 0.42 mmol) was dissolved in 2 mL of Millipore water and deoxygenated by purging argon for 1 hour. Dry THF (18 mL) was added to the reaction mixture and the dark brown reaction mixture was stirred for 15 minutes. Aqueous K_3PO_4 solution was added to the reaction mixture and the color of the reaction mixture immediately turned into dark blue color. It was heated to 60˚C and stirred under argon atmosphere overnight. After the consumption of the boronate ester, the reaction mixture was cooled down to room temperature. The solvents were stripped off under vacuum and the crude product was extracted with dichloromethane. It was dried with anhydrous Na_2SO_4 , filtered and the solvent was evaporated to obtain the crude product. It was further purified by silica gel column chromatography with DCM/hexane (60/40) as eluent mixture to obtain a dark solid. It was dissolved into minimum amount of DCM and methanol was added to obtain a precipitate. It was isolated by vacuum filtration, washed with methanol, and dried to obtain the product as a dark blue solid (90 mg, 53% yield).

Iin-C18-Pt(acac): ^{1}H NMR (500 MHz, CD_2Cl_2): δ 9.17 (d, 1H, J = 8.3 Hz), 8.88 (d, 1H, J = 5.6 Hz), 8.06 (dd, 5H, J_1 = 22.3 Hz, J_2 = 8.7 Hz), 7.63 (t, 1H, 6.3 Hz), 7.49 (s, 1H), 7.33 (d, 1H, 8.6 Hz), 7.19 (d, 1H, J = 7.7 Hz), 7.05 (m, 5H), 6.94 (t, 1H, J = 6.2 Hz), 6.71 (s, 1H), 4.1 (m, 4H), 3.76 (d, 2H, J = 6.3 Hz), 1.99 (m, 1H), 1.89 (m, 4H), 1.34 (m, 52H), 0.96 (m, 6H), 0.86 (t, 6H, J = 6.9 Hz). ^{13}C NMR (75 MHz, $CDCl_3$): δ 177.58, 176.54, 168.73, 163.63, 161.49, 161.37, 147.11, 146.89, 146.24, 145.33, 139.71,

137.92, 137.50, 132.26, 131.23, 130.95, 130.20, 128.83, 128.74, 127.35, 121.22, 119.00, 118.36, 117.27, 114.32, 104.93, 95.11, 68.29, 68.21, 44.64, 36.68, 31.98, 31.96, 31.90, 31.87, 29.53, 29.45, 29.43, 29.34, 29.30, 26.10, 22.73, 22.70, 14.12.

Iin-C8-Pt(acac): ^{1}H NMR (500 MHz, $CDCl_3$): δ 9.13 (d, 1H, J = 8.3 Hz), 8.87 (d, 1H, J = 5.5 Hz), 8.02 (dd, 4H, J_1 = 25.4 Hz, J_2 = 8.7 Hz), 7.59 (t, 1H, 5.7 Hz), 7.49 (s, 1H), 7.32 (d, 1H, J = 8.3 Hz), 7.16 (d, 1H, 7.9 Hz), 6.99 (m, 5H), 6.88 (t, 1H, J = 6.5 Hz), 6.66 (s, 1H), 4.11 (t, 2H, 6.5 Hz), 4.05 (t, 2H, 6.6 Hz), 3.76 (d, 2H, J = 6.1 Hz), 1.92 (m, 5H), 1.50-1.36 (m, 28H), 1.02 (t, 3H, 7.6 Hz), 0.93 (m, 9H). ^{13}C NMR (75 MHz, $CDCl_3$): δ 168.73, 163.59, 161.45, 138.01, 137.59, 132.21, 131.03, 128.83, 128.75, 128.74, 128.70, 121.20, 114.24, 68.27, 68.03, 37.78, 31.88, 30.91, 29.73, 29.48, 29.44, 29.29, 28.92, 29.13, 26.09, 24.34, 23.16, 22.71, 22.69, 14.21, 14.13, 10.92 (some of the peaks in the aromatic region were not observed due to low solubility of this complex). MALDI-TOF MS (*m/z*) $[M]^+$ Calcd for $C_{112}H_{126}N_4O_{10}Pt_2S_2$ 2152.9084, found 2152.9084.

Synthesis of Iin-C18-Poly

In a 10 mL Schlenk tube, Iin-C18-boronate ester (0.05 g, 0.05 mmol), 6-9 (0.046 g, 0.05 mmol), $Pd_2(dba)_3$ (2.13 mg, 2.33 x 10^{-3} mmol), $Pd(P^tBu_3)_2$ (2.4 mg, 4.65 x 10^{-3} mmol) were combined and vacuum-argon cycled for three times to remove the oxygen from the reaction medium. Dry THF (4 mL) was added via syringe through the septum. Previously deoxygenated aqueous K_3PO_4 solution (0.06 g, 0.3 mmol in 1 mL of Millipore water) was added to the reaction mixture under argon atmosphere. It was heated to 60˚C and stirred under argon for 48 hours. After the reaction, it was cooled down to room temperature and poured it over vigorously stirred methanol. The precipitate was isolated and transferred to a Soxhlet thimble. The crude polymer was purified via Soxhlet extraction with methanol, hexane to remove low molecular weight species and

residual catalyst. Finally, the polymer was extracted with chloroform, reduced in volume and poured it over vigorously stirred methanol. The precipitate was collected via vacuum filtration to obtain the polymer as dark green fibrous solid (25 mg). The exact molecular weight of the polymer was not obtained due to the low solubility of the polymer in THF.

CHAPTER 8
PLATINUM ACETYLIDE DERIVATIVES OF DIKETOPYRROLOPYRROLE

Background

Since the development of π- conjugated chromophores as potential materials for organic photovoltaics, there has been growing interest for chemists in this field to design new materials with improved properties. One of the major advantages of organic photovoltaics over their inorganic counterparts is the solution processibility which reduces production cost of these devices. Bulk-heterojunction (BHJs) solar cells are favored over bilayer devices due to the presence of an interpenetrating network of donor and acceptor molecules which favors the exciton dissociation process. Although π-conjugated polymers are widely known as active donor materials in BHJs, batch to batch variation, structural defects, and purification have detrimental effects on device efficiency. Small electroactive molecules have recently caught attention as an alternative over polymers due to their ease of purification and batch to batch consistency. However, unlike polymers, small molecules can suffer weak intermolecular interactions in which can reduce charge transport properties and hence overall efficiency.

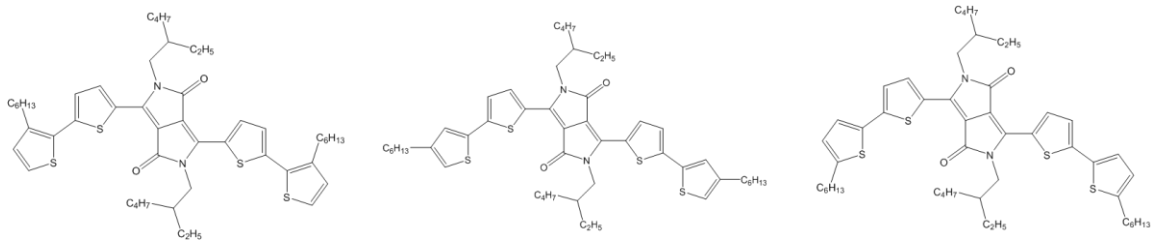

Figure 8-1. The small molecules synthesized by Janssen and coworkers.[237]

One way to improve the morphology and interconnectivity is to introduce non-covalent interactions among the donor molecules. Janssen and coworkers designed

and synthesized diketopyrrolopyrrole based small molecules (Figure 8-1) by varying substitution position of the hexyl chain on terminal thiophene rings.[237] It was observed that although the solution state photophysics were the same for all molecules, significant differences were observed in the solid state. DPP2T-4 aggregates in *H*-type aggregation, while DPP2T-3 showed *J*-type aggregation. Overall, DPP2T-4 exhibited the highest solar cell efficiency due to its favorable morphology for phase separation and charge transport. Lee and coworkers have synthesized TH-P and TH-Q molecules by varying the acceptor as well as the chain length at the core acceptor moiety.[238] TH-P was found to form a 3D network even without the presence of PCBM and showed power conversion efficiency of 0.38% in bulk heterojunction solar cell. However, TH-Q was found to form small needle-like fibrous structures in the absence of PCBM and a continuous network in the presence of PCBM only.

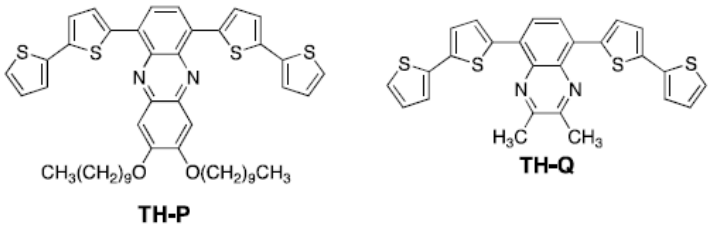

Figure 8-2. Phenazine and quinoxaline based donor-acceptor-donor small molecules reported by Lee et al.[238]

Adachi and coworkers have reported two diketopyrrolopyrrole based small molecules DPP-TP6 and DPP-TP12 with different alkyl chain lengths at the terminal phenyl group.[239] Between these two molecules, DPP-TP6 exhibited liquid crystalline properties which can produce nanostructured domains in the presence of PCBM, facilitating efficient charge separation at the donor-acceptor interface. Films cast from a

chloroform solution of DPP-TP6 were found to form *H*-aggregates in contrast to *J*-aggregates formed by DPP-TP12 films following annealing condition.

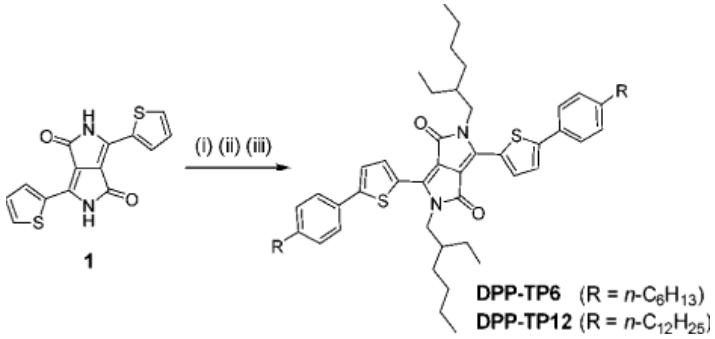

Figure 8-3. Adachi and coworkers synthesized DPP-based small molecules with varying chain lengths for photovoltaic studies.[239]

Considering the importance of triplet excited states in optoelectronics, in this work we have synthesized a series of diketopyrrolopyrrole platinum acetylide complexes by varying the number of solubilizing alkyl chains- DPP-Pt-Ph (no alkyl chain at terminal Ph), DPP-Pt-Dodecyl (single dodecyl chain at terminal Ph) and DPP-Pt-Gallic (three dodecyl chains at terminal Ph) to understand their effect on optical properties in solution as well as solid state.

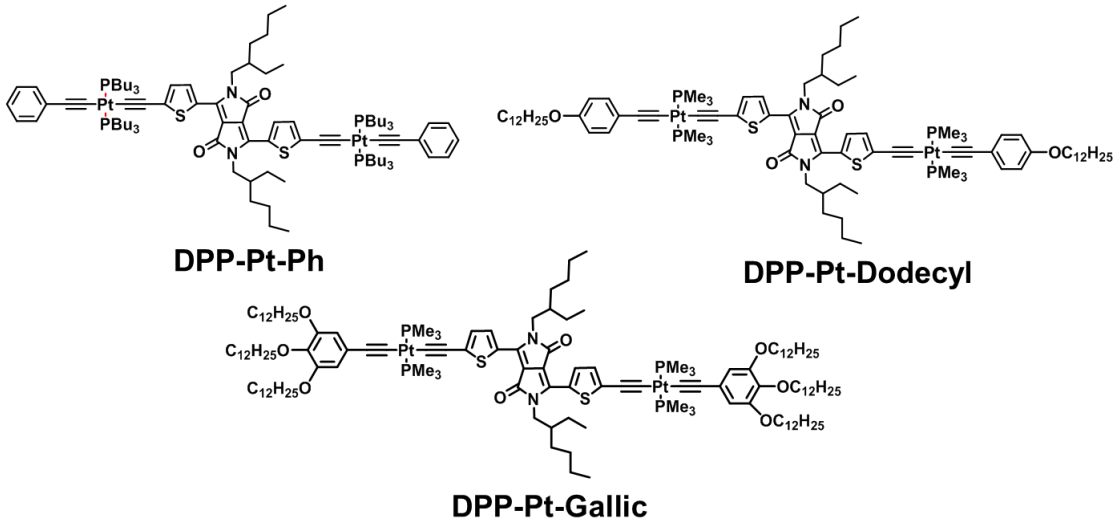

Figure 8-4. Structures of diketopyrrolopyrrole platinum acetylide complexes synthesized in this work.

The diketopyrrolopyrrole chromophore is selected because of its high absorption coefficient in the visible spectrum[163] and the dodecyloxy group is favored over other alkyl chains due to its ability to form self-assembled structures.[240] The analytical purity of the complexes were confirmed from ^{1}H NMR, ^{13}C NMR, ^{31}P NMR spectroscopy and mass spectrometry. The optical properties were characterized by solution state absorption, photoluminescence, emission lifetime and nanosecond transient absorption spectroscopy. Although the solution state absorption remains almost unaffected by alkyl chain substitution, significant differences are observed in the solid state. Preliminary studies on photovoltaic properties of these materials with $PC_{60}BM$ as an acceptor have shown that DPP-Pt-Ph has power conversion efficiency (PCE) ~0.3% which is the highest of the three. Overall, the results clearly demonstrates that the morphology of platinum acetylide materials can be controlled by number of solubilizing groups at the terminal phenyl groups and has direct correlation with photovoltaic properties.

Results and Discussion

Synthesis

All of the metal complexes were synthesized by following Hagihara coupling reactions between the terminally deprotected acetylide containing diketopyrrolopyrrole chromophore 5-8 and the platinum acetylide precursors in the presence of CuI catalyst. Synthesis of DPP-Pt-Ph and 5-8 were already described in Chapter 5. The platinum acetylide precursor molecule 8-1 and 8-2 were synthesized by reacting cis-$Pt(PMe_3)_2Cl_2$ and their respective phenyl acetylene precursor under Hagihara coupling conditions. DPP-Pt-Ph was obtained in high yield (~75%) and the other two metal complexes DPP-Pt-Dodecyl and DPP-Pt-Gallic were synthesized in low to moderate yields. All the metal

complexes were isolated as dark viscous oil immediately after column chromatography; however recrystallization with hexane turned them into dark purple crystalline solids.

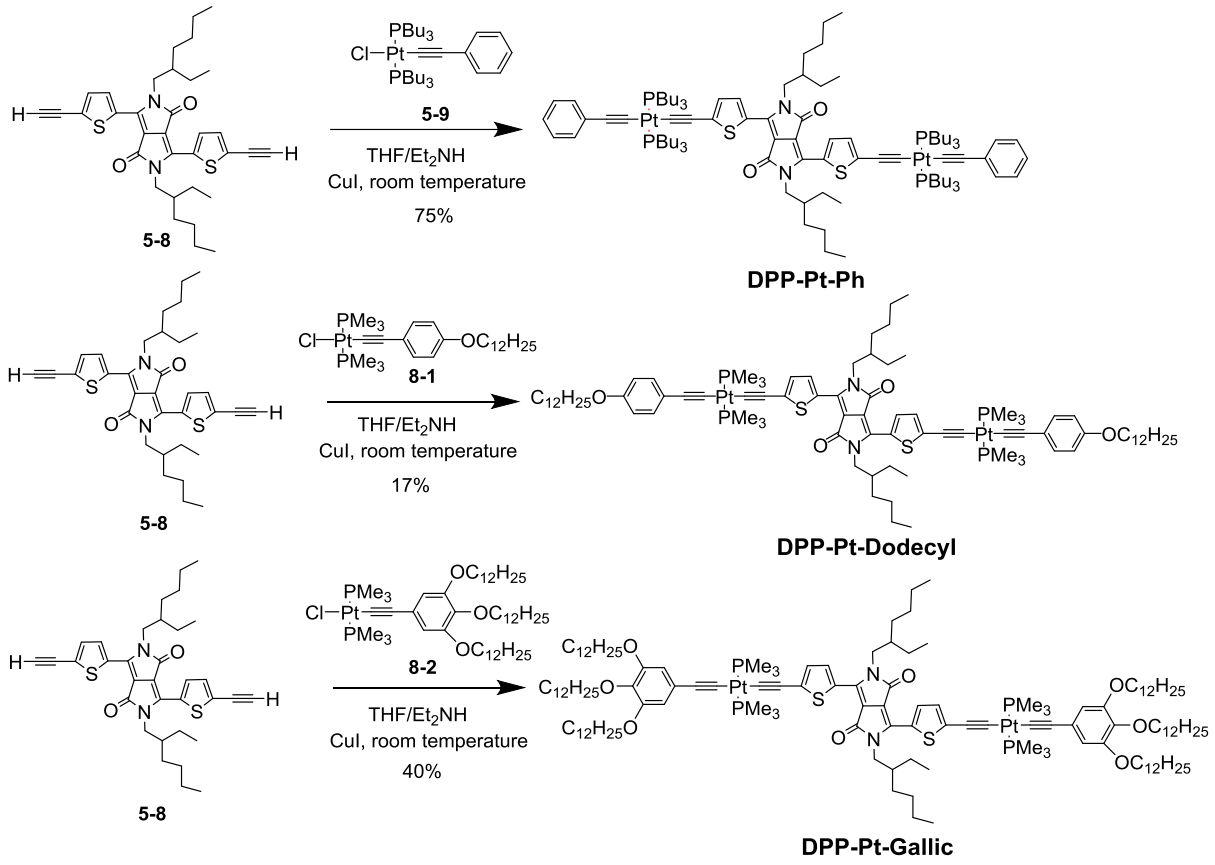

Figure 8-5. Synthetic scheme for diketopyrrolopyrrole platinum acetylide complexes.

Ground State Absorption Spectra

Ground state absorption spectra of the metal complexes were recorded in chloroform solution and presented in Figure 8-6 (A). In an effort to understand the differences in solid state absorption, the spectra of thin films cast from these metal complexes are shown in Figure 8-6 (B). The absorption maxima (λ_{max}) and molar extinction coefficient (ε) are shown in Table 8-1.

In general, the absorption spectra consist of weak absorption bands in the 300 - 500 nm region and strong vibronic absorption band from 500 - 700 nm region. The low

energy transition can be attributed to the donor-acceptor charge transfer transition and the high energy transition is due to π-π* transitions. In solution, there is very minimal change observed in absorption spectra between different metal complexes. The λ_{max} of DPP-Pt-Ph exhibits a 5 nm red shift in absorption compared to both DPP-Pt-Gallic and DPP-Pt-Dodecyl. However, the onset of absorption differs slightly in these metal complexes, which is 666 nm, 671 nm and 676 nm for DPP-Pt-Dodecyl, DPP-Pt-Gallic and DPP-Pt-Ph respectively.

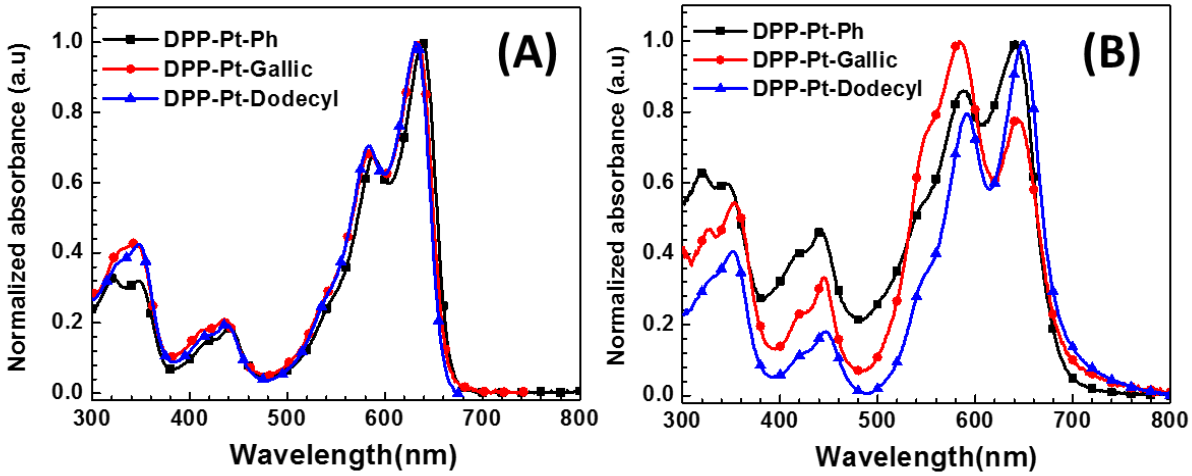

Figure 8-6. Ground state absorption spectra of the metal complexes-(A) in chloroform solution and (B) thin films deposited from chloroform solution.

In comparison to solution, interesting differences were observed in the absorption spectra of metal complexes cast as thin films. First, the ratio of absorptivity between two vibronic bands at charge transfer band (500 – 700 nm) decreases in comparison to solution state. As expected, DPP-Pt-Ph and DPP-Pt-Dodecyl exhibit red shifts in absorption compared to the solution state, possibly due to *J*-type or slipped stacking aggregation.[239,241] The shift in absorption maxima is higher for DPP-Pt-Dodecyl, possibly due to interactions among the long dodecyl chains in the solid state.

Surprisingly, for the film DPP-Pt-Gallic, a blue shift is observed in λ_{max} compared to the solution state. This fact can be attributed to *H*-type or cofacial stacking aggregate formation in the solid state due to hydrophobic interactions between the three dodecyl chains.[239,241] Unlike the solution state, DPP-Pt-Ph films show the most blue shifted onset of absorption (700 nm), compared to DPP-Pt-Dodecyl (748 nm) and DPP-Pt-Gallic (726 nm) due to aggregation induced by the long hydrophobic alkyl chains. The molar extinction coefficient ε for the metal complexes in chloroform follows as DPP-Pt-Ph > DPP-Pt-Dodecyl > DPP-Pt-Gallic.

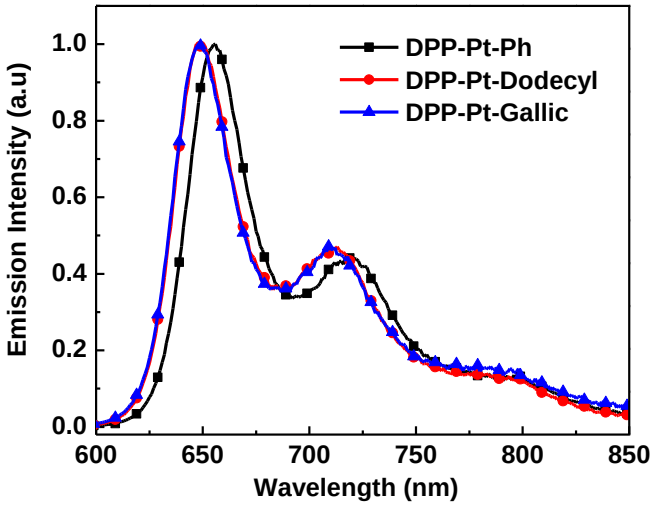

Figure 8-7. Photoluminescence spectra of metal complexes in THF solution.

Photoluminescence Spectroscopy

Photoluminescence spectroscopic measurements were performed in chloroform and presented in Figure 8-7. In general vibronically structured emission was observed for all the metal complexes between 600 nm and 850 nm which is slightly red shifted from their absorption maxima. The trend in emission spectra is mostly similar to the ground state absorption, DPP-Pt-Ph shows the more red shifted emission compared to the other two metal complexes. It is interesting to note here, DPP-Pt-Ph and the other

metal complexes showed solvatochromic shifts in their emission spectra, suggesting charge transfer character in the vibronically relaxed excited state. Emission lifetimes were recorded in chloroform and found in between 2.4 ns and 2.5 ns for all the metal complexes. Such a short lifetime of the excited state and minimal Stokes shift from absorption maxima indicates the emission is from, $S_1 \rightarrow S_0$ fluorescence decay.

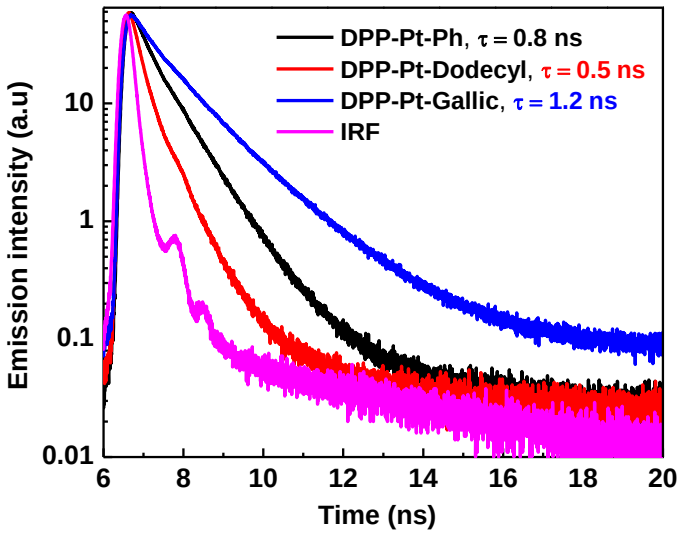

Figure 8-8. Fluorescence lifetime plot of thin films of the metal complexes.

Thin film emission lifetimes were measured from films cast from sample solutions of weight concentration 10 mg/ ml in chloroform, the same as UV-Vis absorption spectra. Unlike the solution lifetime data, significant differences were observed in the lifetime data of the films. Fluorescence lifetime for DPP-Pt-Gallic was found to be much longer (τ_{Av} = 1.2 ns) compared to DPP-Pt-Dodecyl (τ_{Av} = 0.5 ns) and DPP-Pt-Ph (τ_{Av} = 0.8 ns). The longer lifetime for DPP-Pt-Gallic is in accordance with the low energy exciton- coupled *H*-configuration assignment of the excited state which is lower in energy and has lower transition probability. The shorter lifetimes of the other metal complexes can be explained by dipole-allowed low-energy transitions, which are a characteristic of *J*-type of aggregation.[133,237] In general, the exciton diffusion is much

faster in *J*-type aggregation due to enhanced Forster transfer.[242] The fluorescence quantum yield of the metal complexes was measured in THF and follows the order of DPP-Pt-Ph (53%) > DPP-Pt-Dodecyl (49%) > DPP-Pt-Gallic (43%). Low fluorescence quantum yield and lifetime compared to the ligand DPP-H (ϕ_{Fl} = 66% and τ_{Fl} = 4.3 ns)[156] suggests a non-radiative decay pathway is in effect and we have assigned this as intersystem crossing (ISC) to the triplet excited state.

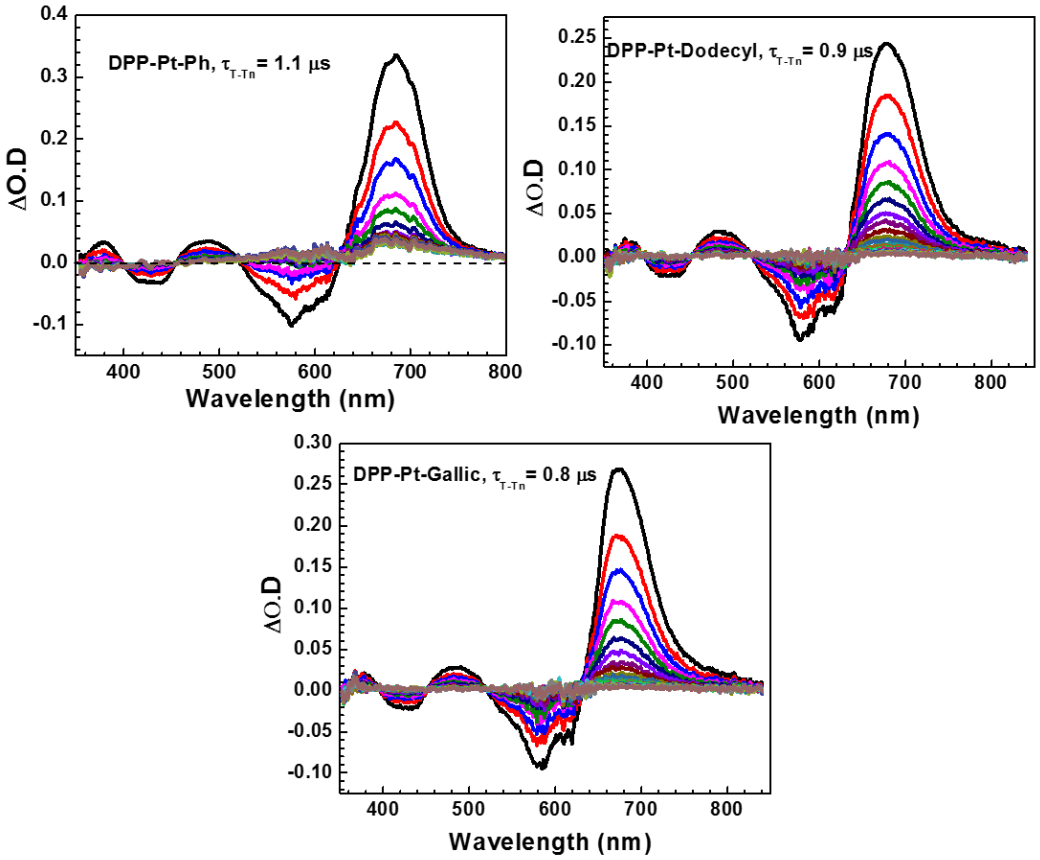

Figure 8-9. Nanosecond transient absorption spectra of the metal complexes in THF solution. Transient spectra were obtained in deoxygenated THF solution with 355 nm excitation wavelength. Initial delay 50 ns following a 15 ns laser excitation pulse with 500 ns camera delay increment were used.

Nanosecond Transient Absorption

As no phosphorescence was observed from these molecular systems, in order to probe the triplet excited state, nanosecond transient absorption spectroscopy was

performed with THF solutions of this metal complexes. In general, the transient absorption spectra consists of a ground state bleach between 350 – 650 nm and excited state absorption in between 650 – 850 nm. The ground state bleach correlated well with the ground state absorption spectra of the metal complexes in THF solution. The quenching of the transients in presence of oxygen and lifetime in the order of microseconds (μs), suggests the excited state absorption is due to $T_1 \rightarrow T_n$. Similar to the ground state absorption spectra, there is no difference observed in the shape of the transient absorption spectra among different complexes. However, the lifetime of the triplet excited state decreases slightly from 1.1 μs to 0.8 μs with increased number of alkyl chains. This is possibly due to aggregation induced quenching of the triplet exciton in DPP-Pt-Dodecyl and DPP-Pt-Gallic.

Table 8-1. Summary of photophysical properties of the metal complexes.[a]

Compound	λ_{max} (nm)	λ_{max} Thin film (nm)	ε x 10^4 ($M^{-1}cm^{-1}$)	λ_{em} (nm)	ϕ_{fl}[b,c]	τ_{fl} (ns)	τ_{fl} (ns) (Thin film)	τ_{TA}[b]/ (μs)
DPP-Pt-Ph	638	641	9.3	656	0.53	2.4	0.8	1.1
DPP-Pt-Dodecyl	631	649	8.3	649	0.49	2.5	0.5	0.9
DPP-Pt-Gallic	633	585	7.7	648	0.43	2.4	1.2	0.8

Note: [a] All the photophysical properties were measured in chloroform unless otherwise mentioned. [b] Measured in THF. [c] The fluorescence quantum yield was measured with respect to tetraphenylporphyrin in toluene (ϕ_F=0.09) as actinometer.

Thermal Properties and Morphology of Films

Thermal property of these materials were studied by thermal gravimetric analysis (TGA) and differential scanning calorimetry (DSC) and are presented in Figure 8-10. The 5% weight loss temperature is ~50˚C higher for DPP-Pt-Dodecyl and DPP-Pt-Gallic compared to DPP-Pt-Ph, suggesting the dodecyloxy alkyl chains increase the thermal stability of the complexes, which is in accordance with the literature where dodecyl chain containing DPP shows higher thermal stability compared to hexyl chain.[239] DSC

analysis reveals a melting point (T_m) of ~110˚C for DPP-Pt-Ph which is shifted to ~198˚C for DPP-Pt-Dodecyl. Surprisingly, for DPP-Pt-Gallic, the melting point shifted to much lower temperature at ~54˚C. While cooling, crystallization point (T_c) was not observed for DPP-Pt-Ph. DPP-Pt-Gallic and DPP-Pt-Dodecyl exhibit crystallization at ~141˚C and 30˚C respectively. The higher T_m and T_c for DPP-Pt-Dodecyl suggest greater crystallization tendency of this complex compared to the other metal complexes. It is anticipated that, bulky tributylphosphine (PBu_3) ligands in DPP-Pt-Ph compared to less bulky trimethylphosphine (PMe_3) ligands in other two metal complexes, prevent crystallization in the former.

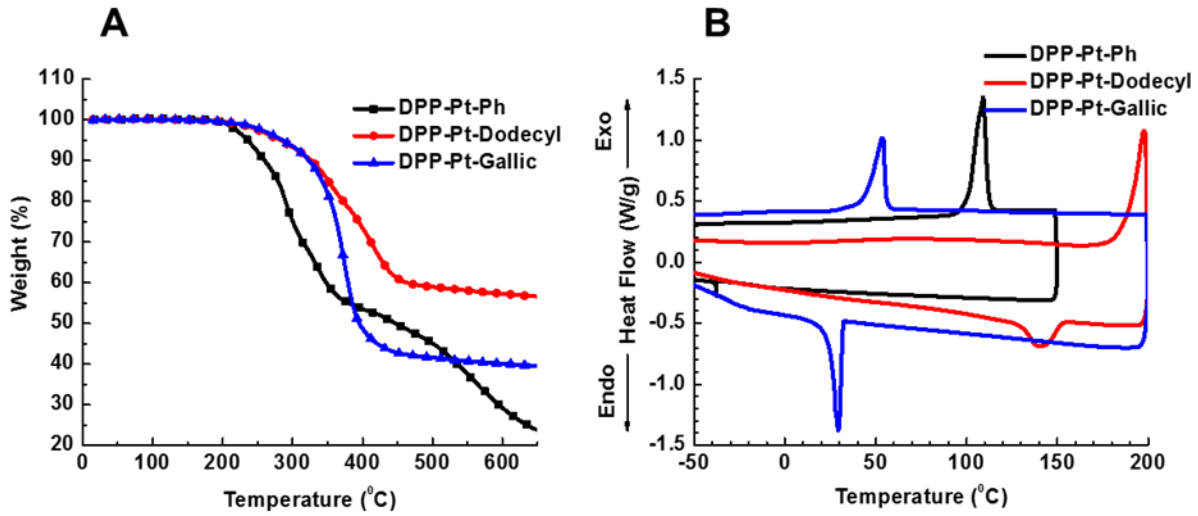

Figure 8-10. (A) TGA analysis and (B) DSC analysis of the metal complexes. For both the experiments scan rate of 20˚C/minute was used with 2-5 mg of the sample. DSC was performed in a sealed aluminum pan with respect to an aluminum reference pan. Only the second and third cycle are shown.

Morphological differences of the thin films were examined by scanning electronic microscopy on films deposited from chloroform solution. In general no differences were observed between DPP-Pt-Ph and DPP-Pt-Dodecyl. However, a globule like aggregated structure was observed for DPP-Pt-Gallic complex. This observation is in

accordance with the different aggregation behavior shown by DPP-Pt-Gallic in photophysical characterizations compared to DPP-Pt-Ph and DPP-Pt-Dodecyl which have similar morphology.

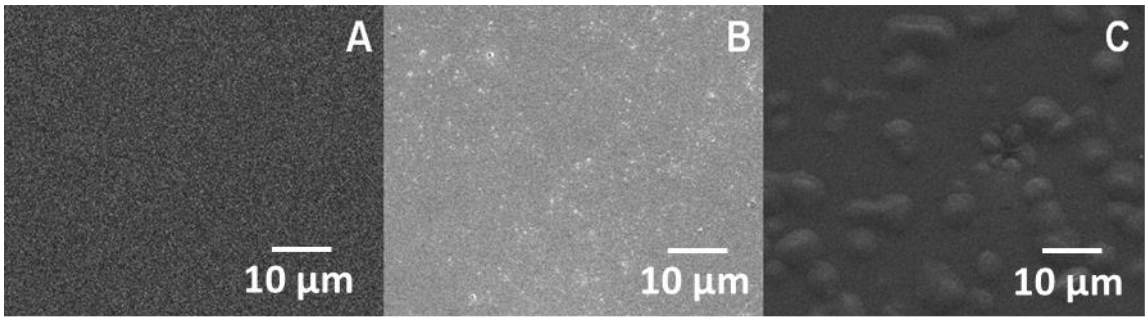

Figure 8-11. Scanning Electronic Microscopic images of the metal complexes deposited on glass slide from concentrated solution of chloroform-(A) DPP-Pt-Ph, (B) DPP-Pt-Dodecyl, (C) DPP-Pt-Gallic. The images are shown with scale bar of 10 µm.

Electrochemical Properties

In an effort to understand the fact if there is any change in the redox behavior of the DPP metal complexes with varying number of terminal alkyl chains, electrochemical measurements were performed with two metal complexes, DPP-Pt-Ph and DPP-Pt-Gallic in dry dichloromethane solvent and are presented in Figure 8-12.

In general, the cyclic voltammograms consists of a reversible reduction wave and two reversible oxidation waves. It is important to mention that the spectral shape remained the same as compared to central DPP unit without the platinum acetylide auxochromes.[156] The reduction potential of DPP-Pt-Ph remains same as with the core DPP unit (~-1.68 V), although the oxidation potential changes to 0.16 V and 0.45 V with respect to 0.53 V and 1.04 V respectively.[156] For DPP-Pt-Gallic, the peak potentials remain almost the same (E_{red} ~ -1.61 V, E_{ox1} ~ 0.2 V and E_{ox2} ~ 0.5 V) with DPP-Pt-Ph, however, the shape of the peaks in cyclic voltammograms are broadened. The similarity

in the peak potentials of these two metal complexes is manifested in similar solution state photophysical properties.

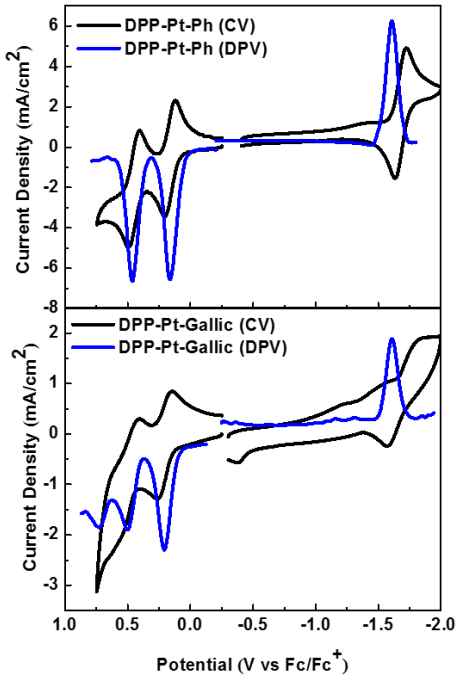

Figure 8-12. Cyclic voltammetry (CV) and differential pulse voltammetry (DPV) for DPP-Pt-Ph and DPP-Pt-Gallic in dry dichloromethane solvent in presence of $TBAPF_6$ (scan rate 100 mV/sec). All the potentials are referenced to Fc/Fc^+ couple as an internal standard.

Table 8-2. Summary of electrochemical properties.[a]

Compound	$E_{1/2}$/V		$E_{1/2}$/V	
	Red_1	Red_2	Ox_1	Ox_2
DPP-Pt-Ph	-1.68	—	0.16	0.45
DPP-Pt-Gallic	-1.61	—	0.20	0.50

Note: [a] Measured in CH_2Cl_2 using 0.1 M NBu_4PF_6 as supporting electrolyte. It was scanned at 100 mV s^{-1}. All the potentials are referenced to a Fc/Fc^+ couple as an internal standard.

Photovoltaic Properties

Bulk heterojunction solar cells (BHJs) were made using these metal complexes as donor and $PC_{61}BM$ as acceptor in the active layer. The architecture of the photovoltaic devices tested was ITO/ poly (3,4-

ethylene−dioxythiophene):poly(styrenesulfonic acid) (PEDOT:PSS)/ active layer/ LiF/ Al. The active layer for the BHJs were fabricated from chlorobenzene solution by spin coating at 1000 rpm. Several ratios of donor: acceptor blend were tested for device optimization. For DPP-Pt-Ph, the optimized ratio of donor: acceptor was 1:4. 5 mg/ml of the donor material and 20 mg/ml of PCBM were dissolved in chlorobenzene and heated to 60˚C overnight to make the active layer solution. For a 1:2 ratio of DPP-Pt-Ph: $PC_{61}BM$, two weight percentages of donor materials (5 mg/ml and 10 mg/ml) were tried but gave low efficiency compared to 1:4 ratio devices. The efficiency observed for DPP-Pt-Ph and DPP-Pt-Dodecyl was 0.3% and 0.12% respectively. However, near zero efficiency was observed for DPP-Pt-Gallic complex. The J-V plot for the two working devices is shown in Figure 8-11.

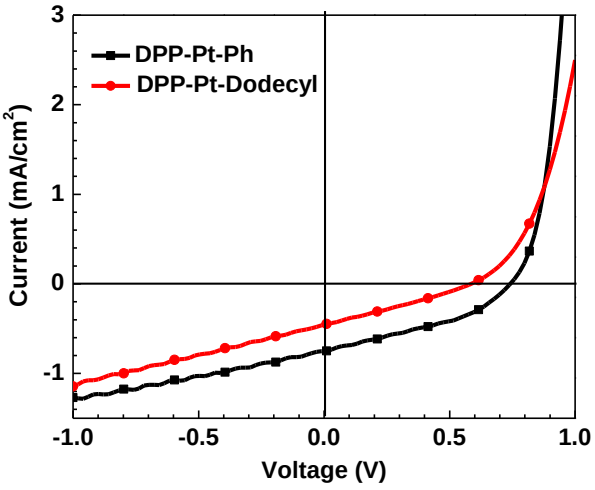

Figure 8-13. Characteristic J-V curves of bulk heterojunction solar cells using DPP-Pt-Ph and DPP-Pt-Dodecyl as the donor material.

For DPP-Pt-Ph, under optimized device conditions short circuit current (J_{sc}), open circuit voltage (V_{oc}), fill factor (FF) and power conversion efficiency (PCE) observed were 1mA/cm^2, 0.73 V, 41% and 0.3% respectively. When the device was annealed for 10 minutes, a slight decrease in efficiency was observed from 0.3% to 0.2%. DPP-Pt-

Dodecyl containing devices exhibited lower PCE compared to DPP-Pt-Ph with similar 1:4 donor/acceptor ratios. Similar to DPP-Pt-Ph, devices with increased donor amount (10 mg/ml) or reduced PCBM amount (1:2 ratio) showed lower efficiency compared to 1:4 ratio devices. All the device parameters for DPP-Pt-Dodecyl are lower compared to DPP-Pt-Ph. Among all the complexes, DPP-Pt-Gallic showed almost no efficiency when used as the donor material in the device (0.02%). The major decrease was observed for J_{sc} and FF, 0.1 mA/cm^2 and 23% respectively. It is assumed that as DPP-Pt-Ph forms J aggregates in the solid state and Forster energy transfer is efficient in these aggregates, charge separation is more efficient in this metal complex compared to DPP-Pt-Gallic which form H-aggregates in the solid state.

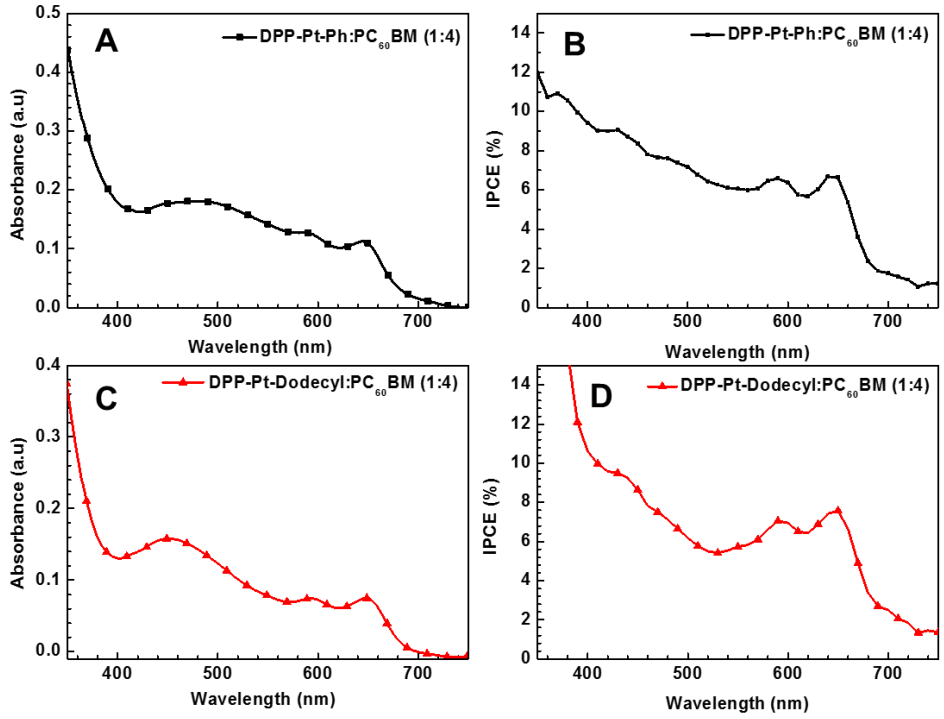

Figure 8-14. (A) and (B) shows absorption spectra and IPCE of DPP-Pt-Ph containing devices, (C) and (D) shows the absorption spectra and IPCE of DPP-Pt-Dodecyl containing devices.

Ground state absorption spectra and IPCE plots of devices made from DPP-Pt-Ph and DPP-Pt-Dodecyl are presented in Figure 8-14. In general, the IPCE from both complexes is below 10% which is in agreement with the low power conversion efficiency observed from the metal complexes. In the longer wavelength region, IPCE consists of two vibronic peaks whereas the short wavelength region is dominated by broad absorption. The vibronic bands between 500 - 700 nm can be attributed to the DPP chromophores as evidenced from their ground state absorption spectra. The shorter wavelength region from 300 - 500 nm is mostly due to $PC_{61}BM$ absorption. Further characterization of the devices are currently underway where AFM is applied to gain an understanding of the morphological differences which cause these difference in device efficiency.

Table 8-3. Summary of photovoltaic properties of the metal complexes.[a]

Complex	J_{sc} (mA cm^{-2})	V_{oc} (V)	FF (%)	PCE (%)
DPP-Pt-Ph	1.00	0.73	41.00	0.30
DPP-Pt-Dodecyl	0.70	0.62	26.00	0.11
DPP-Pt-Gallic	0.10	0.69	23.00	0.02

Note: [a] All the devices are optimized with donor:$PC_{61}BM$ ratio of 1:4. All numbers are the average of 8 pixels on each cells. The details of the device fabrication are given in experimental section.

Discussion

In an effort to understand the energetics involved into the mechanism of charge separation in DPP metal complex/$PC_{61}BM$ blend, Figure 8-15 is constructed. The efficient photoinduced electron transfer (PET) process depends on the energy gap between the singlet (S_1) or triplet excited state (T_1) and the charge separated state (CS). The energy of the charge separated state is evaluated by taking the difference between the oxidation potential of the donor (E_{OX1}) and reduction potential of the

acceptor $PC_{61}BM$ (E_{RD1} ~ -1.10 V vs Fc/Fc^+). Using the oxidation potential of DPP-Pt-Ph (0.16 V vs Fc/Fc^+)[156] , the energy of the charge separated state was estimated to be 1.26 V.

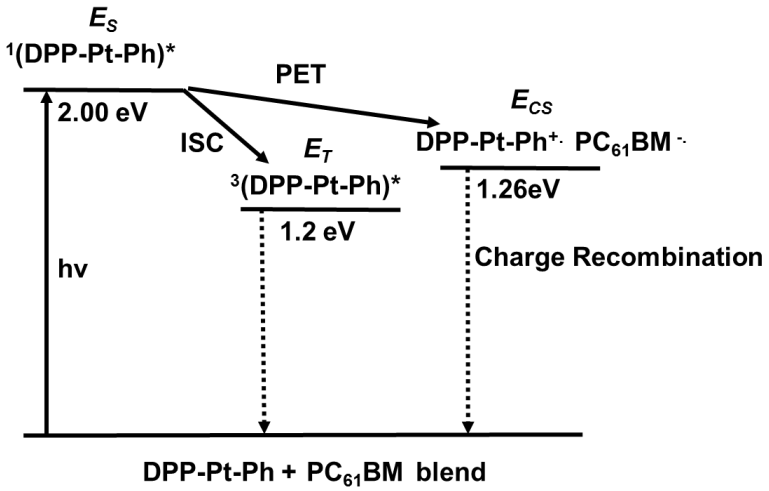

Figure 8-15. Energy level diagram for DPP-Pt-Ph.

Singlet excited state energy for DPP-Pt-Ph was estimated from the onset of emission and determined to be ~ 2.00 eV. As phosphorescence was not detected from this donor-acceptor chromophores, the triplet excited state energy was estimated by using the approximation S_1-T_1 energy gap of 0.8 eV and determined at 1.2 eV. It can be clearly observed from the energy diagram, the singlet excited state is higher in energy compare to the charge separated state, which makes the PET process thermodynamically favorable. In contrast, PET from triplet excited state is thermodynamically unfavorable being a weakly endothermic process. As, the solution state photophysics of the metal complexes are similar and redox potential values of DPP-Pt-Ph are similar to DPP-Pt-Gallic, we can assume for the other metal complexes, PET is also taking place from the singlet excited state.

It is interesting to note here, the energy difference between the LUMO level of DPP-Pt-Ph (~3.42 eV) and PCBM (~4.2 eV) is ~0.78 eV, which is greater than minimum requirement of 0.3 eV and favorable for PET process to occur.

Summary and Conclusion

In summary, a series of platinum acetylide complexes with varying numbers of terminal alkyl chains are designed and synthesized. Although the solution state UV-Visible absorption and emission spectra remains mostly similar for all the metal complexes, significant differences were observed in the solid state. While DPP-Pt-Ph and DPP-Pt-Dodecyl aggregate in the solid state via *J*-type aggregation showing a characteristic red shift in the absorption spectra compared to solution state, DPP-Pt-Gallic shows blue shifted absorption due to *H*-aggregation. Photoluminescence lifetime measurement in thin films showed shorter lifetimes for DPP-Pt-Ph (~0.8 ns) and DPP-Pt-Dodecyl (~0.5 ns) compared to DPP-Pt-Gallic (~1.2 ns). This fact is in accordance with the dipole allowed emission from *J*-type aggregates. A large triplet excited state population was observed from nanosecond transient absorption spectroscopy with slight differences in lifetimes on the order of ~100 ns among the metal complexes. DPP-Pt-Dodecyl and DPP-Pt-Gallic exhibits higher thermal stability compared to DPP-Pt-Ph suggesting additional thermal stability provided by the long dodecyl chains. DPP-Pt-Dodecyl shows the higher tendency of crystallization among all the metal complexes with highest T_m and T_c.

Preliminary photovoltaic studies with these metal complexes as donor and $PC_{61}BM$ as acceptor exhibit low to moderate efficiency. Among them, DPP-Pt-Ph exhibits the highest efficiency of 0.3%. Overall, these results demonstrate that the morphology of the platinum acetylide materials can be fine-tuned by appending longer

alkyl chains. Further research on understanding these materials device properties and improving the efficiency is underway in our lab.

Experimental

General Methods for Synthesis

All reactions were performed under a dry argon atmosphere unless otherwise mentioned. Tetrahydrofuran (THF) used for the reactions was dried using solvent purification columns (Glass Contour). All other solvents for the reactions were used without any purification unless otherwise mentioned. The synthesis of the metal complex DPP-Pt-Ph and ligand DPP-H was described in Chapter 5 and also reported by our group recently.[156] The platinum acetylide precursor 8-2 was synthesized by following literature procedure.[240] I would like to thank our former group member Eminie Demir for providing me the platinum acetylide precursor 8-1.

Methods for Device Fabrication

Photovoltaic devices were fabricated using pre patterned Indium tin oxide coated glass slides obtained from Kintec Company. The ITO-coated glass substrates were subsequently treated with aqueous sodium dodecyl sulfate (Fisher Scientific), deionized water (Milli-Q), isopropyl alcohol and acetone in an ultrasonic bath for 15 minutes. The substrates were then treated with oxygen plasma for 15 minutes in a plasma cleaner (Harrick PDC-32G). An aqueous solution of PEDOT:PSS (Baytron P VP Al 4083) was spin coated at a rate of 5000 rpm for 1 minute and subsequently annealed on a hot plate at 130˚C for 20 minutes. A solution of the active layer with the desired ratio of metal complex:$PC_{61}BM$ was prepared in chlorobenzene and stirred at 60˚C overnight in an argon filled M-Braun glove box. The active layer solution was then spin coated onto the PEDOT-PSS coated substrates at 1000 rpm in the glove box and the resulting films

were dried under high vacuum overnight at room temperature. LiF (0.5 nm) and Al (100 nm) were sequentially deposited by thermal evaporation under high vacuum overnight on the active layer. The cathode pattern on the substrates was created by using copper mask, resulting in a cathode pixel size of 0.07 cm^2.

The current-voltage (J-V) plot was measured with a Keithley 2400 source measurement unit (SMU) under A.M. 1.5 illumination with an incident power density of 100 mW/cm^2 supplied by a xenon arc lamp power supply (Oriel Instruments). The external quantum efficiency (EQE) of the devices were evaluated by measuring the IPCE (%). IPCE measurements were performed with monochromatic light generated by a monochromator (Oriel Instruments) with a xenon arc lamp as the light source. A power meter (S350, UDT Instruments), equipped with a calibrated silicon detector (221, UDT Instruments) was used to measure the intensity of the source at each wavelength (10 nm increment). A Keithley 2400 source meter was used with no voltage bias to record the current at each illumination wavelength. All the measurements were performed in air and without encapsulation.

Synthesis of DPP-Pt-Dodecyl

In a Schlenk flask DPP-H (0.05g, 0.09 mmol) and 8-1 (0.122 g, 0.2 mmol) were dissolved in diethylamine/ tetrahydrofuran (7 mL/ 7 mL) and deoxygenated by purging with argon for 45 minutes. Copper iodide (CuI, 4.3 mg, 0.02 mmol) was added to the reaction mixture under a strong flow of argon. Immediately the color of the reaction mixture changed from wine red to dark blue. It was stirred under an argon atmosphere overnight at room temperature. Silica gel was added to the reaction mixture and the solvents were evaporated under vacuum. The product was purified by silica gel column chromatography with ethyl acetate/hexane (3:7) as eluent. The solvents were

evaporated under vacuum to obtain a dark blue viscous oil. It was then dissolved in a minimum amount of dichloromethane and methanol was added to obtain a precipitate. The product was isolated by filtration under vacuum as a dark purple solid in 17% yield (~27 mg). ^{1}H NMR (300 MHz, CD_2Cl_2): δ 8.9 (d, 1H, *J* = 3.9 Hz), 7.21 (d, 2H, *J* = 8.5 Hz), 7.00 (d, 1H, *J* = 4.0 Hz), 6.77 (d, 2H, *J* = 8.5 Hz), 3.97 (m, 4H), 1.90 (s, 1H), 1.76 (t, 18H, *J* = 3.8 Hz), 1.37 (m, 26H), 0.90 (m, 9H). ^{31}P NMR (121 MHz, CD_2Cl_2) δ -20.55 ($J_{Pt\text{-}P}$ = 2288.11 Hz). ^{13}C NMR (75 MHz, $CDCl_3$): δ 161.70, 157.28, 139.21, 136.21, 134.84, 132.18, 129.43, 123.42, 120.15, 114.12, 109.12, 107.74, 103.41, 101.07, 68.02, 45.92, 39.17, 31.86, 30.27, 30.25, 29.66, 29.63, 29.60, 29.57, 29.40, 29.34, 29.29, 28.38, 26.05, 23.55, 23.13, 22.69, 15.58, 15.42, 15.27, 14.08, 10.56.

Synthesis of DPP-Pt-Gallic

In a Schlenk flask, DPP-H (0.05g, 0.09 mmol) and 8-2 (0.185g, 0.18 mmol) were dissolved in a solvent mixture of THF/diethylamine (7 mL/ 7 mL) and deoxygenated by purging argon for 45 minutes. Under a strong flow of argon, CuI (5 mg, 0.03 mmol) was added to the reaction mixture. Immediately the color of the reaction mixture changed to dark purple from dark red. It was stirred at room temperature an under argon atmosphere for 15 hours. Silica gel was added to the purple solution and the solvents were evaporated under vacuum. It was purified by silica gel column chromatography using hexane/ethyl acetate as eluent. The dark purple band was collected and solvents were evaporated to isolate a viscous oil. Addition of methanol and solvent evaporation gave the product as a dark blue amorphous solid in 40% yield (90 mg). ^{1}H NMR (300 MHz, $CDCl_3$): δ 8.91 (d, 2H, *J* = 4.1 Hz), 6.99 (d, 2H, *J* = 4.1 Hz), 6.53 (s, 4H), 3.95 (m, 16H), 1.92 (m, 1.69), 1.76 (m, 36H), 1.45-1.26 (m, 124H), 0.88 (m, 30H). ^{31}P NMR (121 MHz, $CDCl_3$) δ -20.35 ($J_{Pt\text{-}P}$ = 2289.32 Hz). ^{13}C NMR (75 MHz, $CDCl_3$): δ 161.66,

152.67, 139.21, 137.44, 136.19, 134.72, 129.43, 126.75, 122.65, 122.58, 109.90, 107.77, 100.97, 73.48, 69.12, 45.92, 39.18, 31.95, 31.94, 29.76, 29.75, 29.72, 29.67, 29.66, 29.63, 29.45, 29.38, 23.55, 23.13, 22.70, 15.63, 15.47, 15.31, 14.12, 10.69.

APPENDIX A
SUPPORTING INFORMATION FOR CHAPTER 2

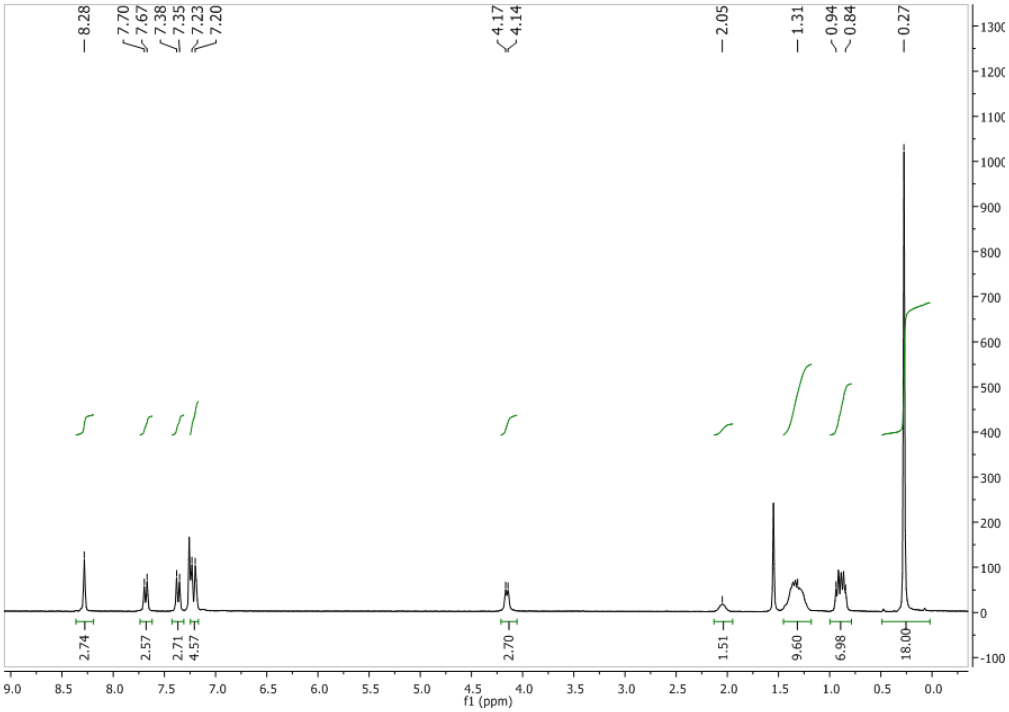

Figure A-1. ^{1}H NMR (300 MHz, $CDCl_3$) of CBZ-TMS.

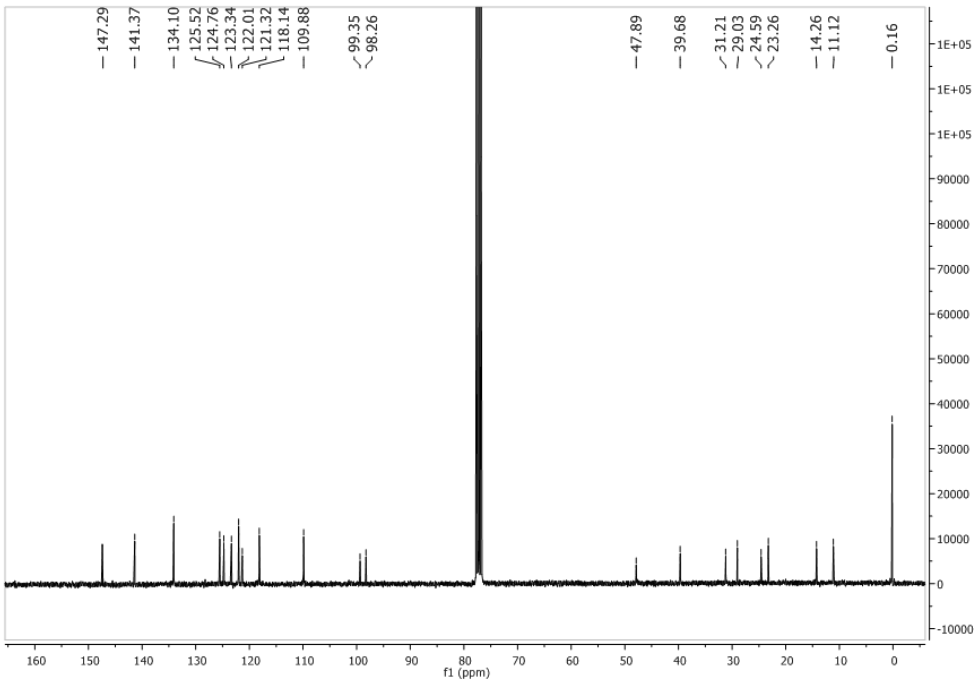

Figure A-2. ^{13}C NMR (75 MHz, $CDCl_3$) of CBZ-TMS.

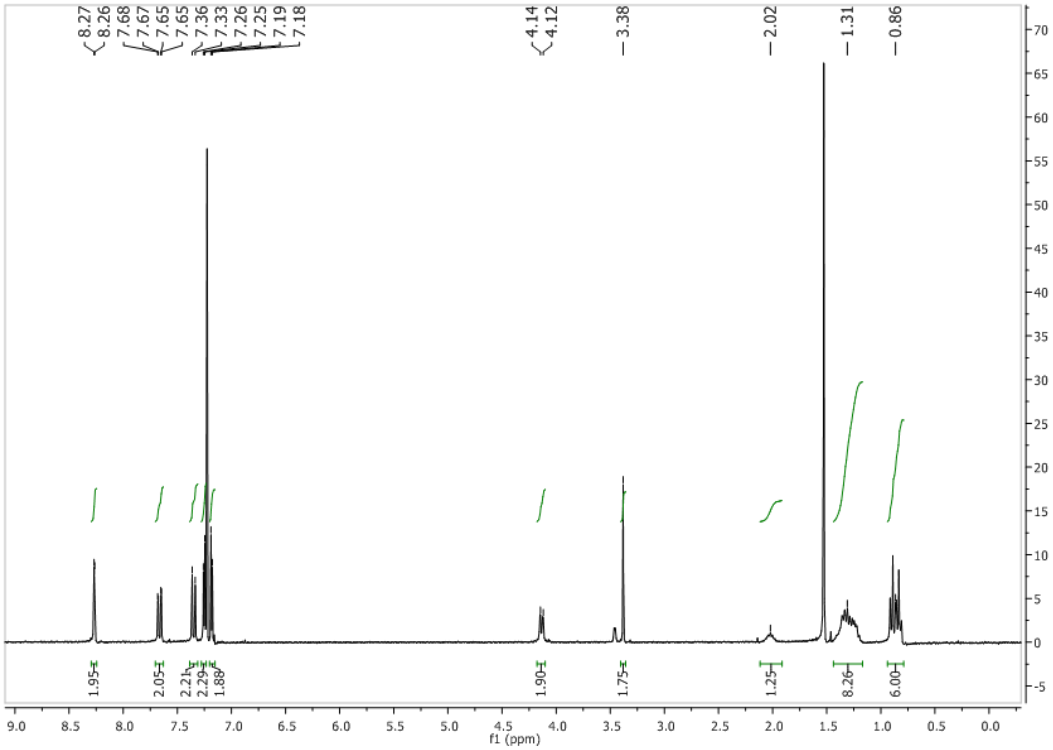

Figure A-3. ^{1}H NMR (300 MHz, $CDCl_3$) of L1.

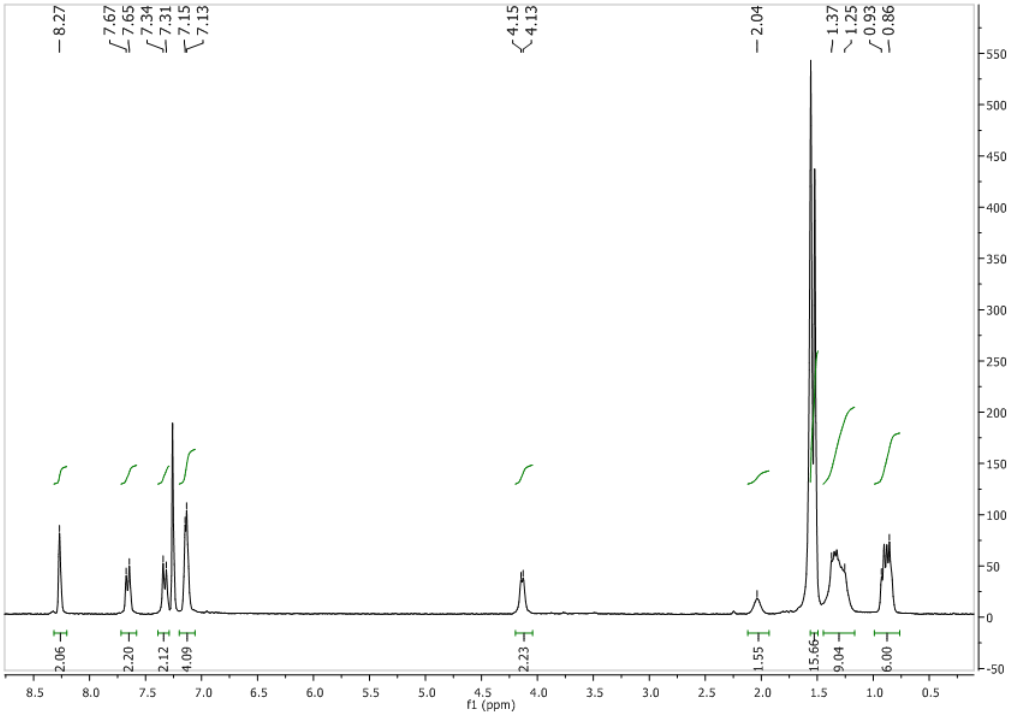

Figure A-4. ^{1}H NMR (300 MHz, $CDCl_3$) of CBZ-Au-1.

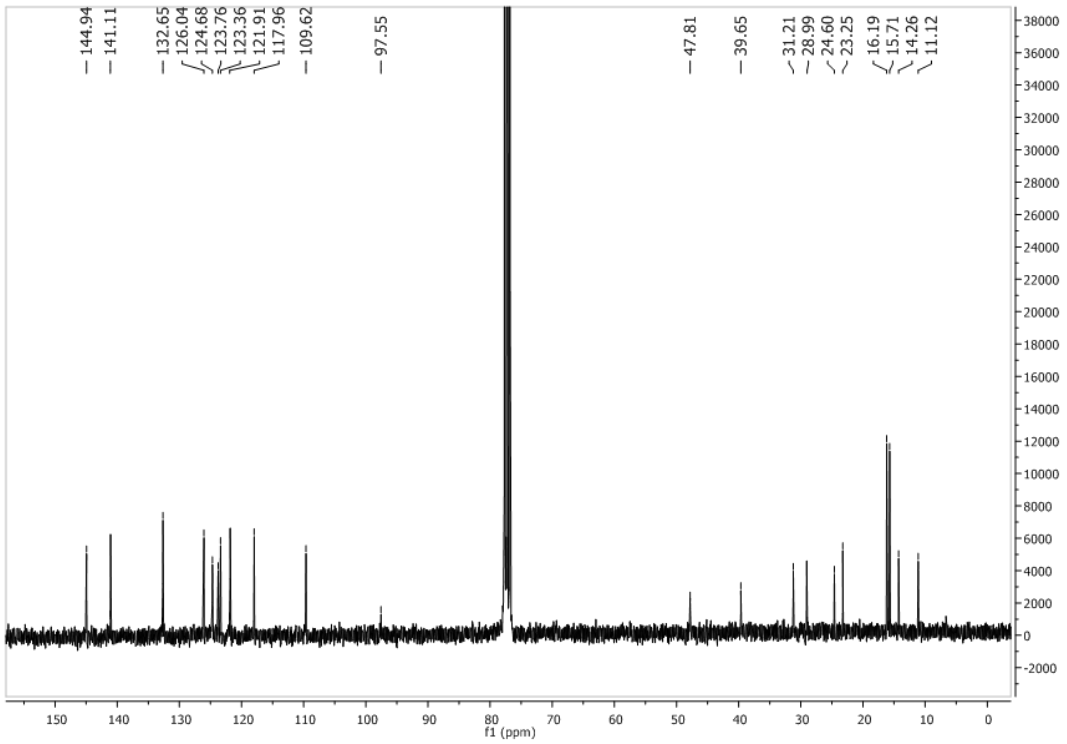

Figure A-5. ^{13}C NMR (75 MHz, $CDCl_3$) of CBZ-Au-1.

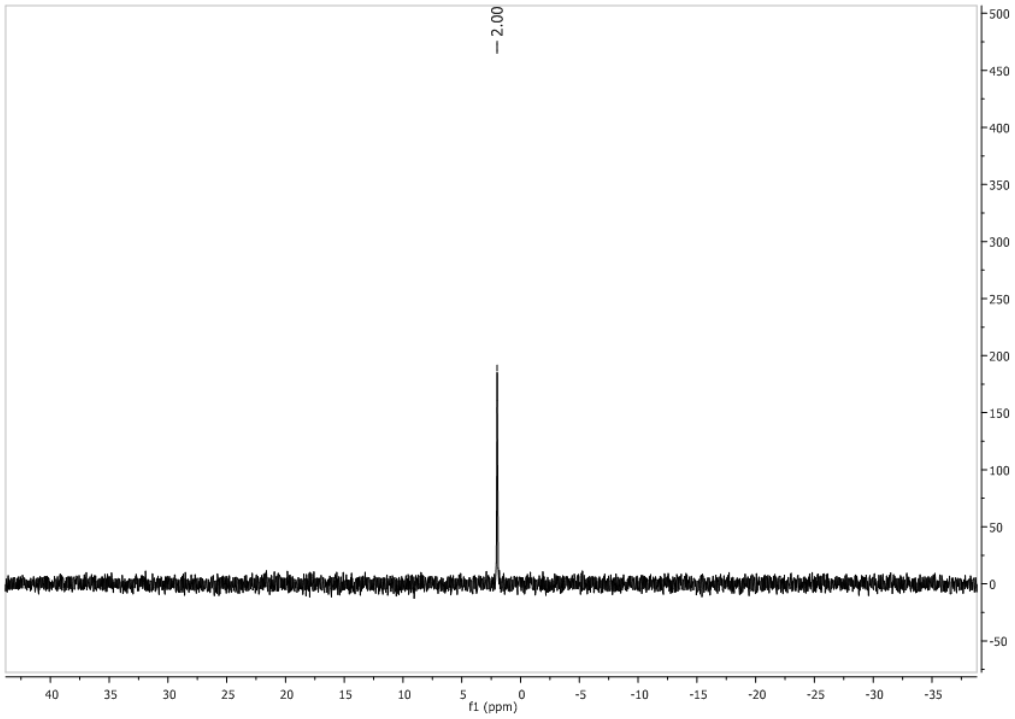

Figure A-6. ^{31}P NMR (121 MHz, $CDCl_3$) of compound CBZ-Au-1.

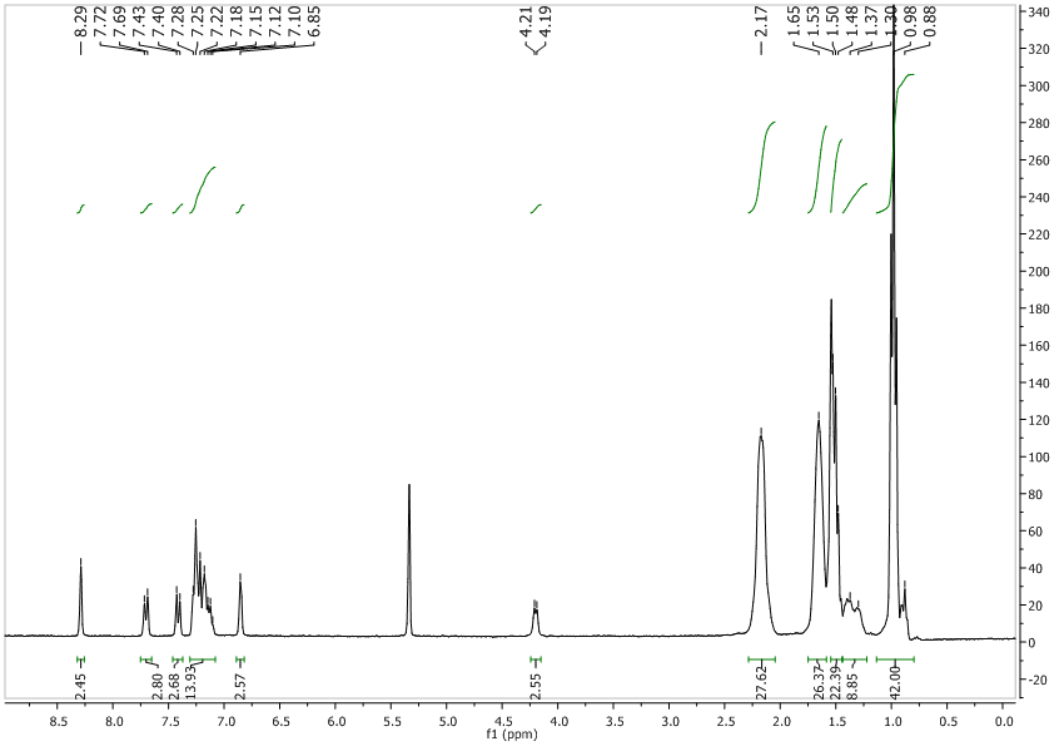

Figure A-7. ^{1}H NMR (300 MHz, CD_2Cl_2) of compound CBZ-Pt-1.

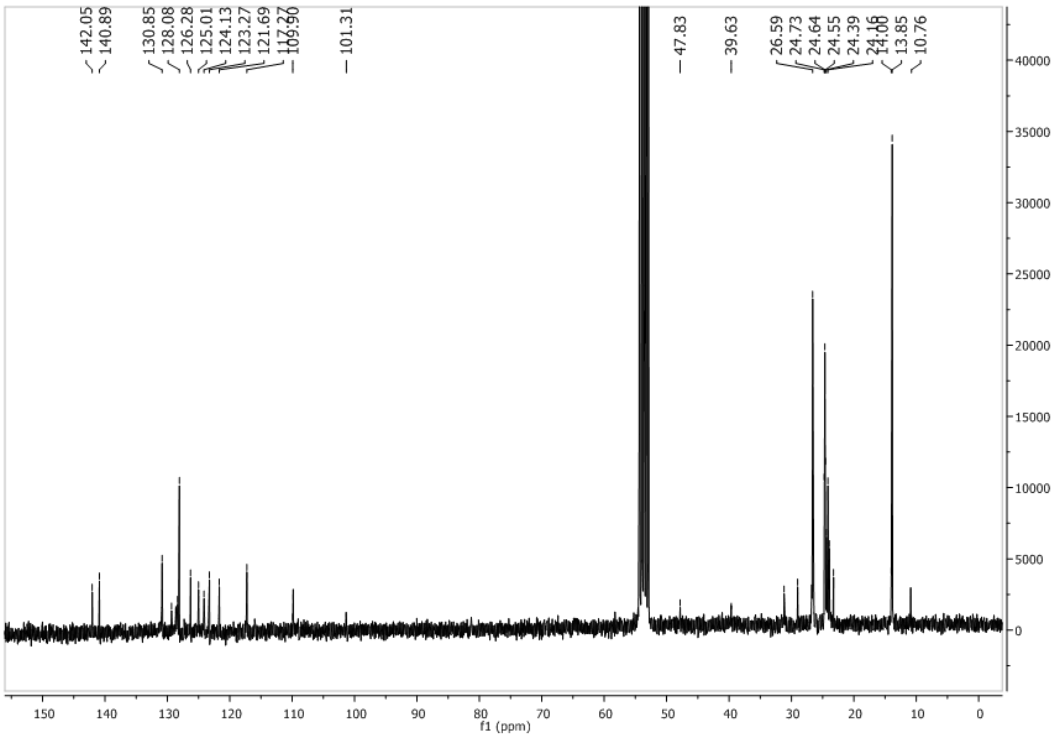

Figure A-8. ^{13}C NMR (75 MHz, CD_2Cl_2) of compound CBZ-Pt-1.

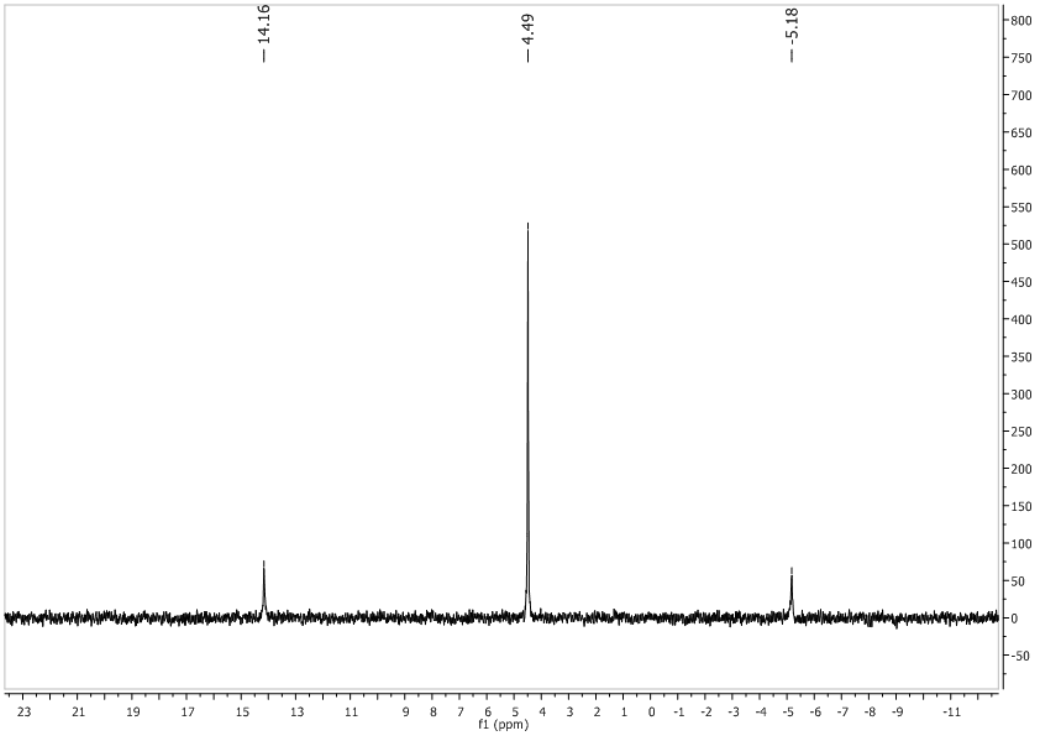

Figure A-9. ^{31}P NMR (121 MHz, CD_2Cl_2) of compound CBZ-Pt-1.

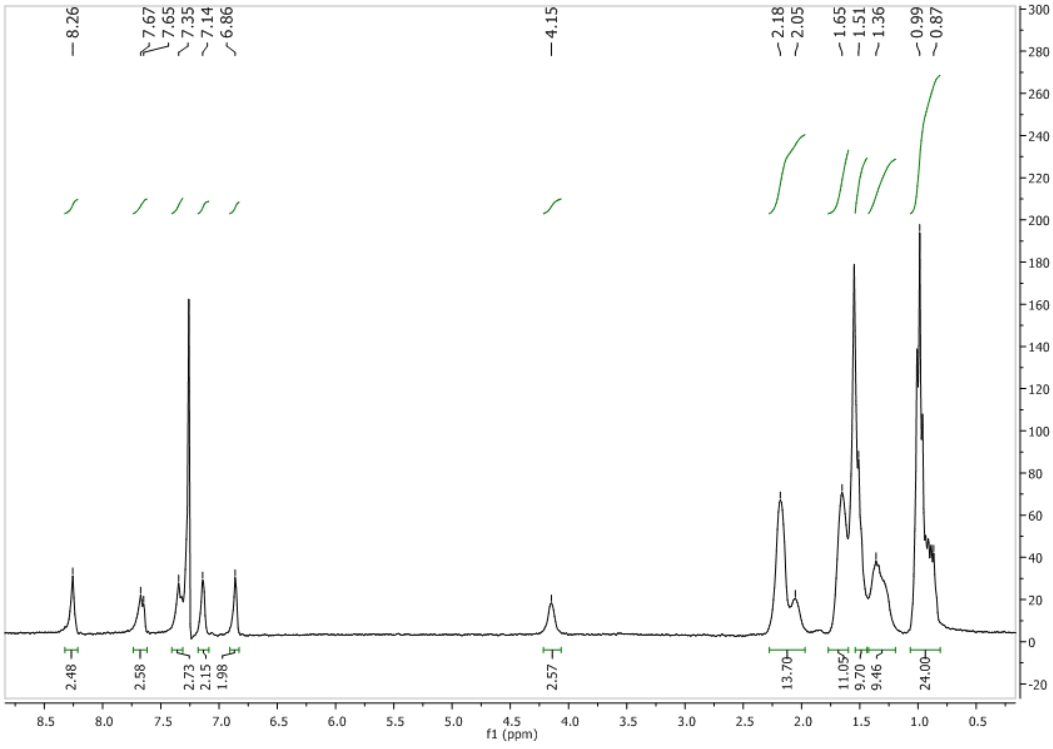

Figure A-10. ^{1}H NMR (300 MHz, $CDCl_3$) of compound CBZ-Poly-Pt.

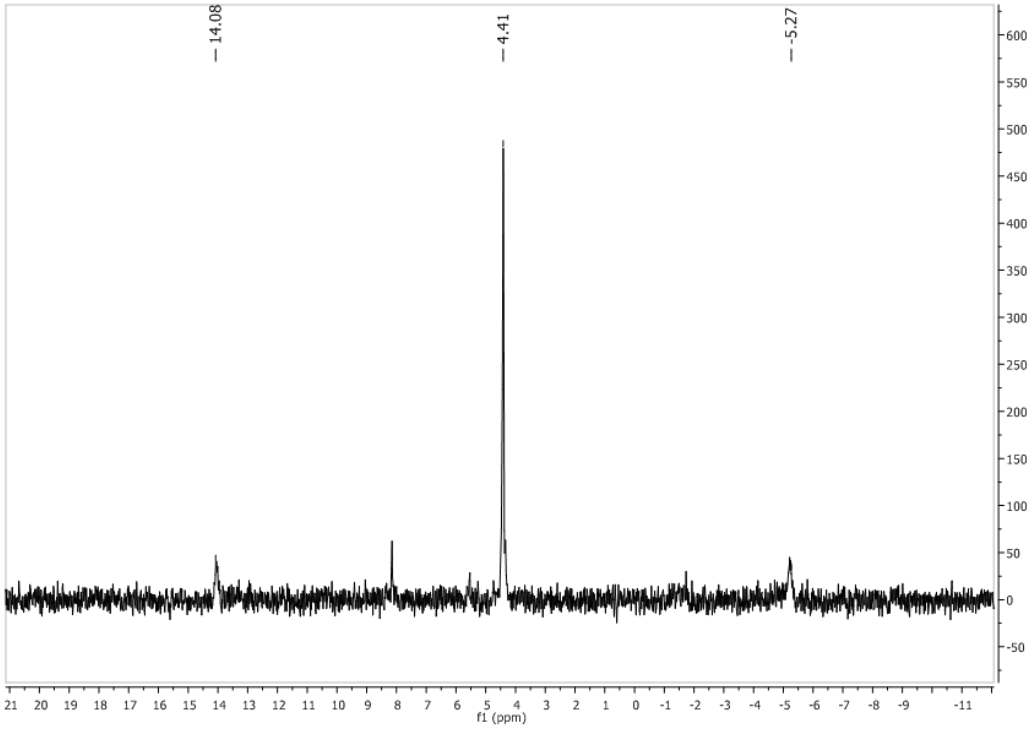

Figure A-11. ^{31}P NMR (121 MHz, $CDCl_3$) of compound CBZ-Poly-Pt.

APPENDIX B
SUPPORTING INFORMATION FOR CHAPTER 3

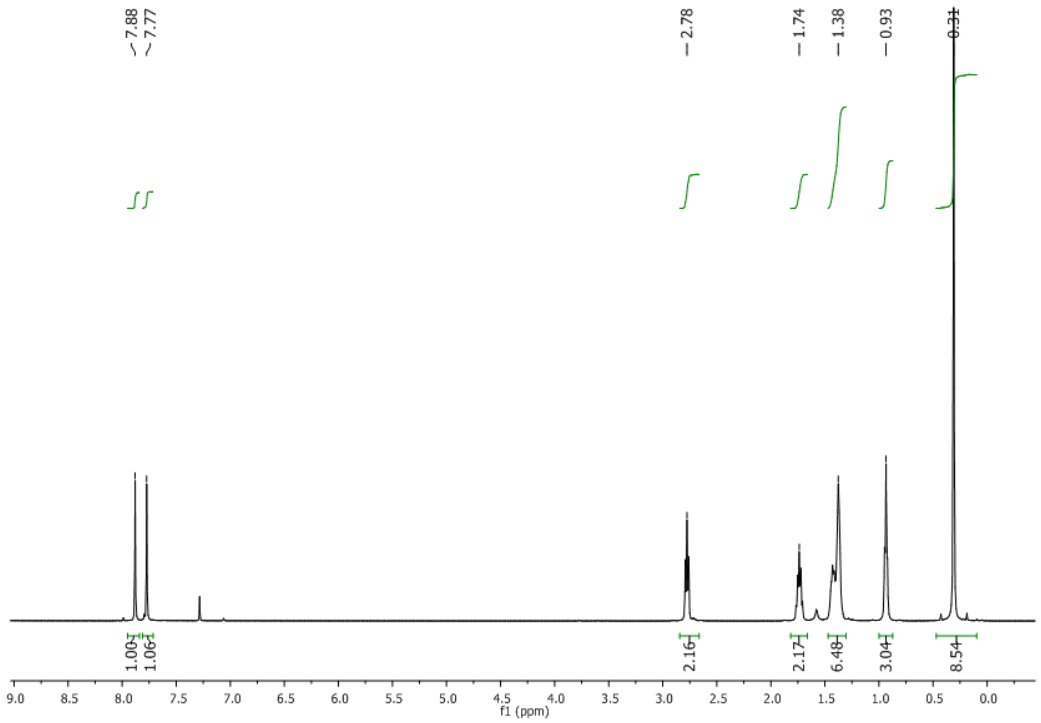

Figure B-1. ^{1}H NMR spectra of TBT-TMS in $CDCl_3$.

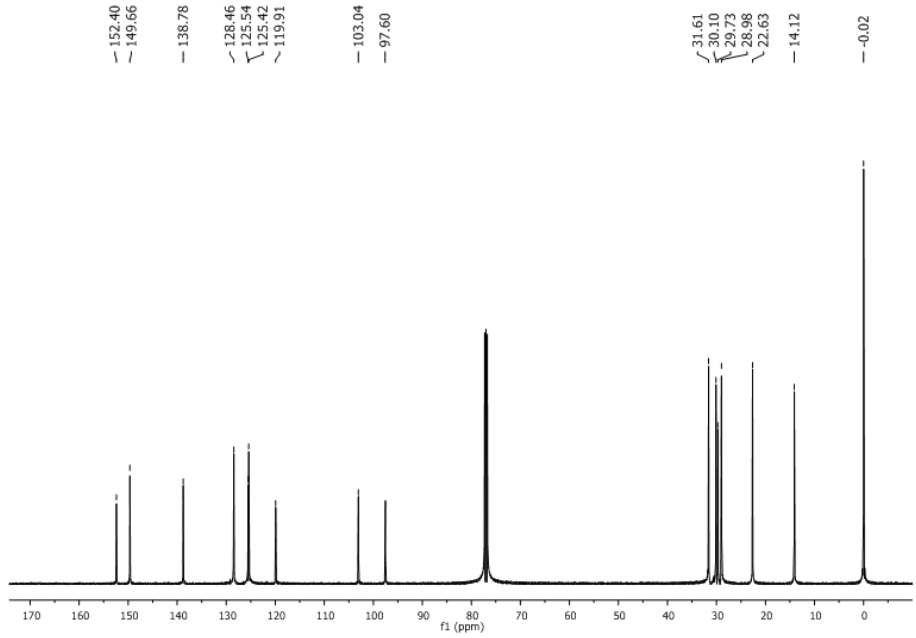

Figure B-2. ^{13}C NMR spectra of TBT-TMS in $CDCl_3$.

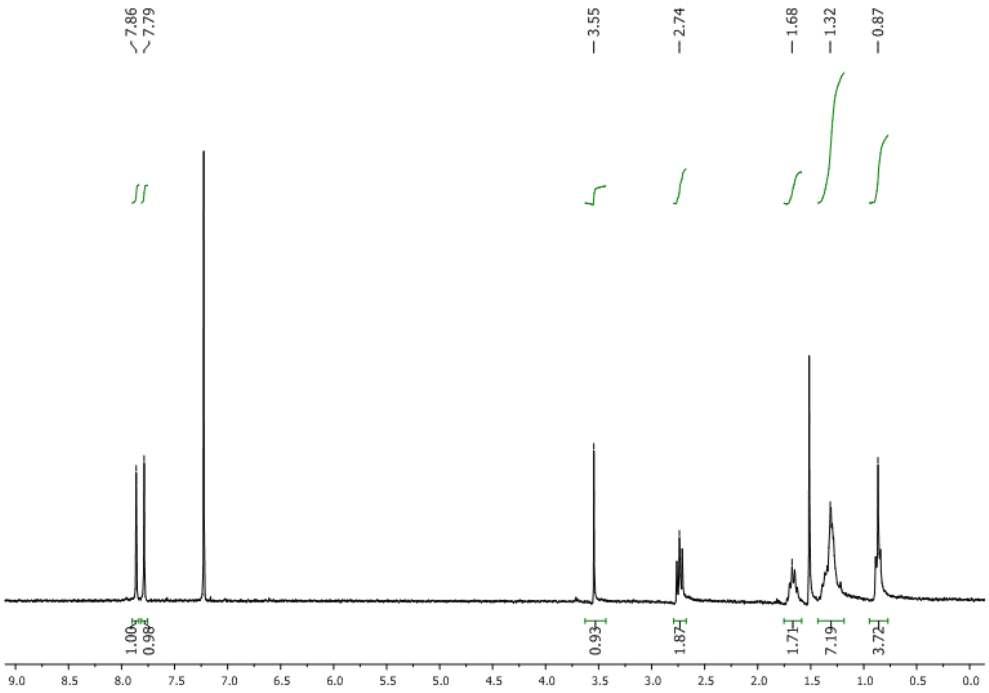

Figure B-3. ^{1}H NMR spectra of TBT-H in $CDCl_3$.

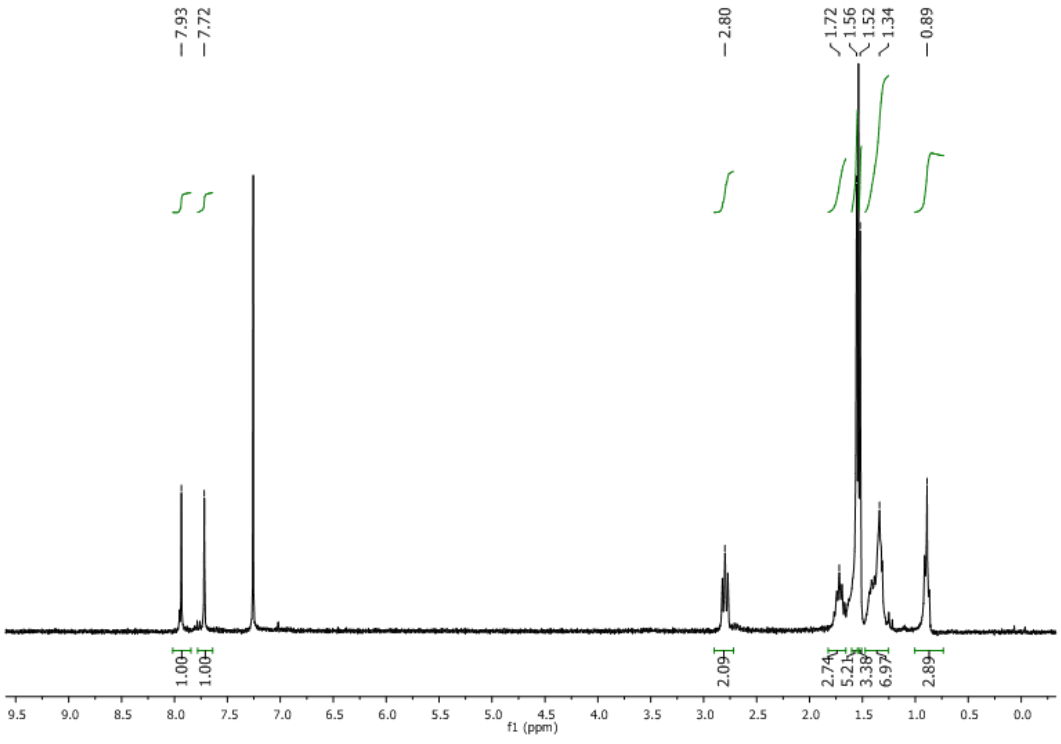

Figure B-4. ^{1}H NMR spectra of TBT-Au-PMe_3 in $CDCl_3$.

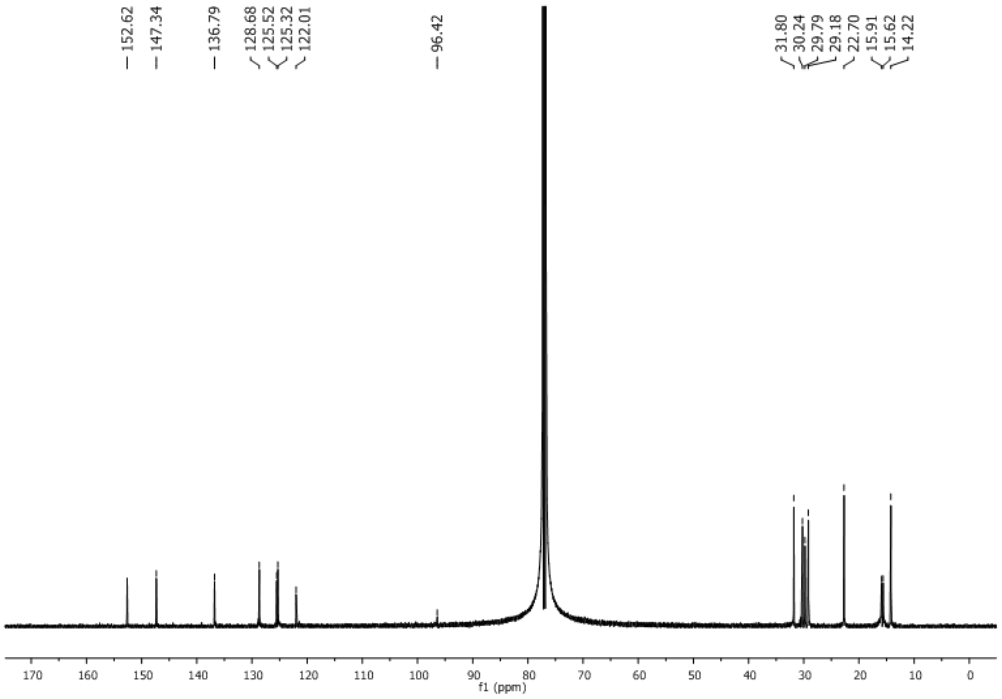

Figure B-5. ^{13}C NMR spectra of TBT-Au-PMe_3 in $CDCl_3$.

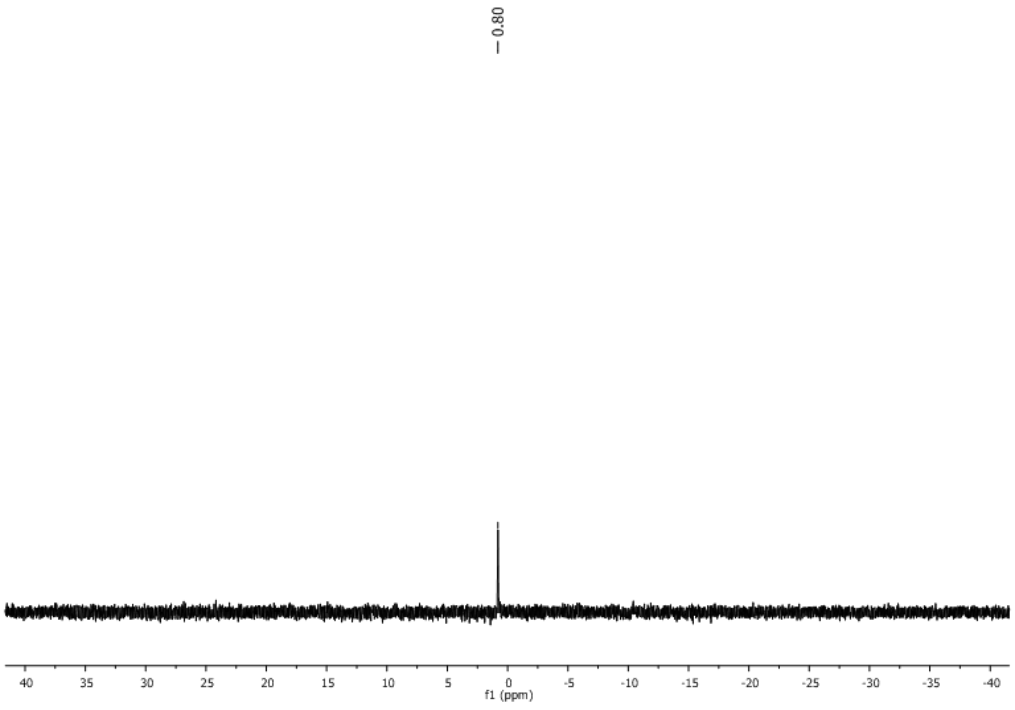

Figure B-6. ^{31}P NMR spectra of TBT-Au-PMe_3 in $CDCl_3$.

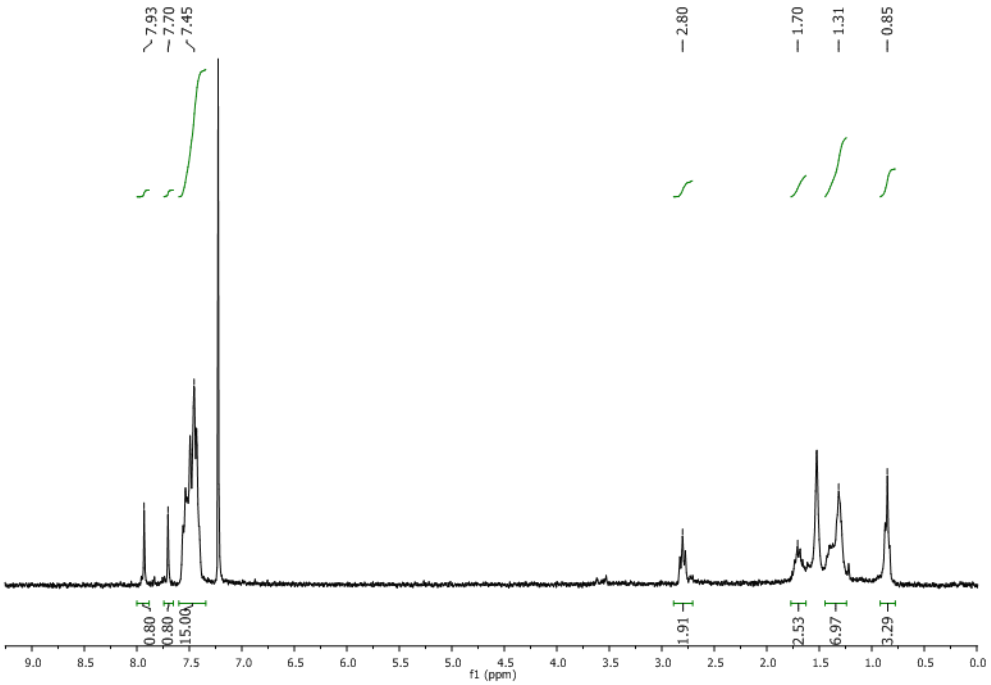

Figure B-7. ^{1}H NMR spectra of TBT-Au-PPh_3 in $CDCl_3$.

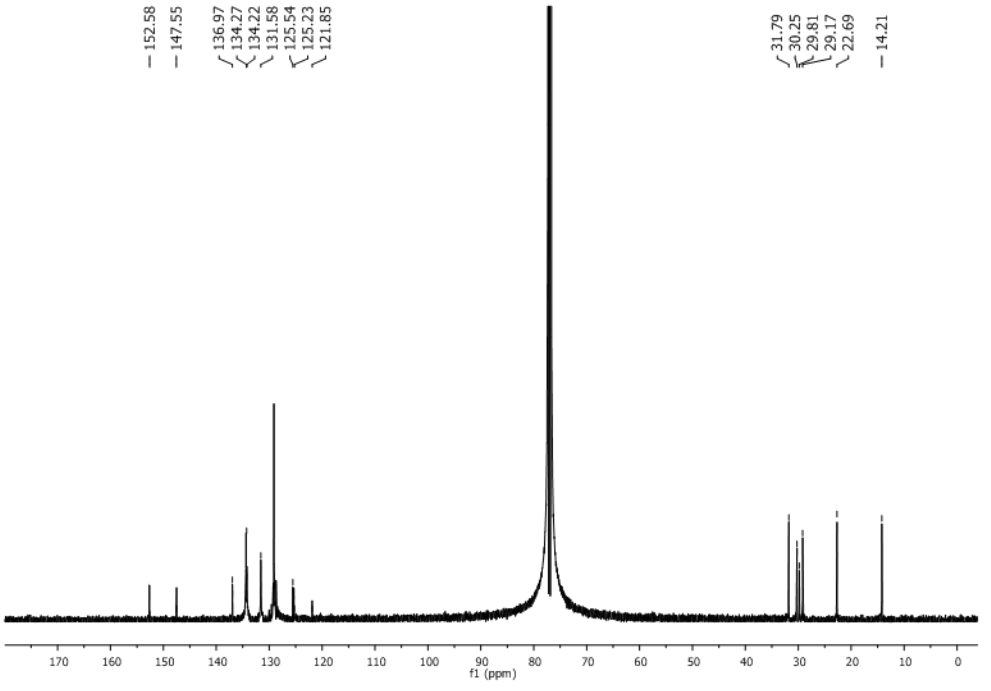

Figure B-8. ^{13}C NMR spectra of TBT-Au-PPh_3 in $CDCl_3$.

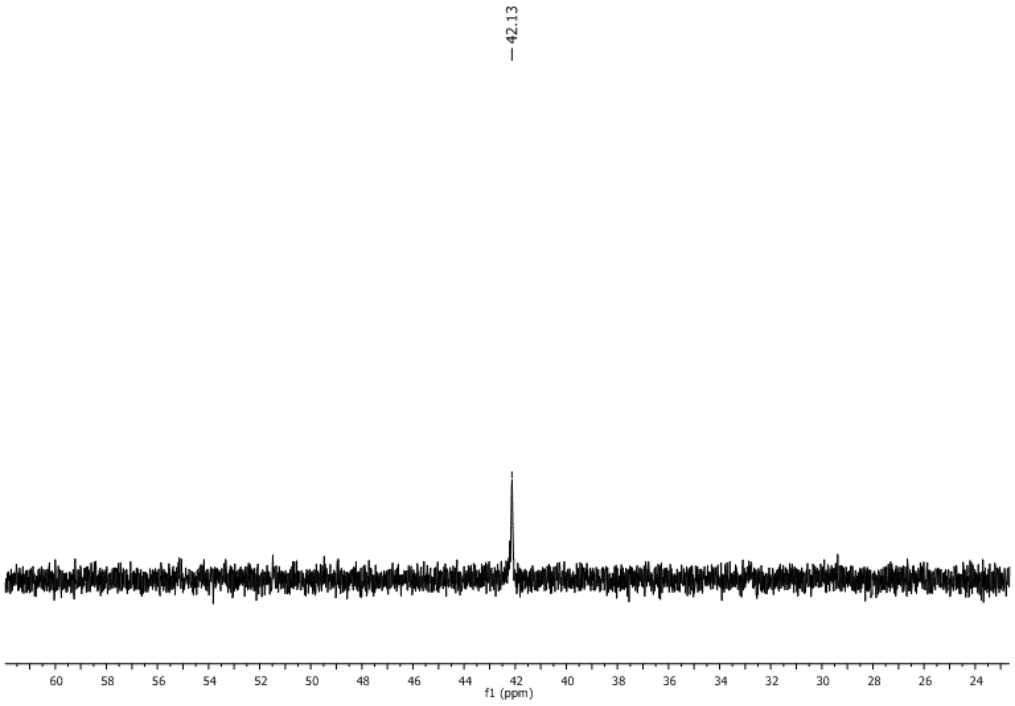

Figure B-9. ^{31}P NMR spectra of TBT-Au-PPh_3 in $CDCl_3$.

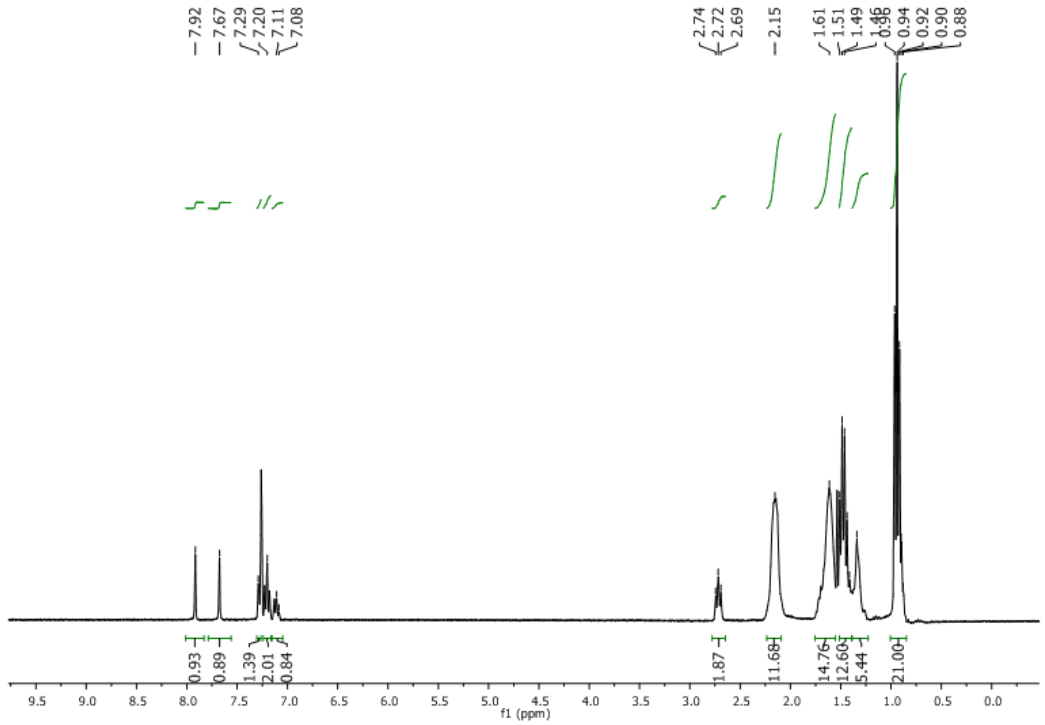

Figure B-10. ^{1}H NMR spectra of TBT-Pt-PBu_3 in $CDCl_3$.

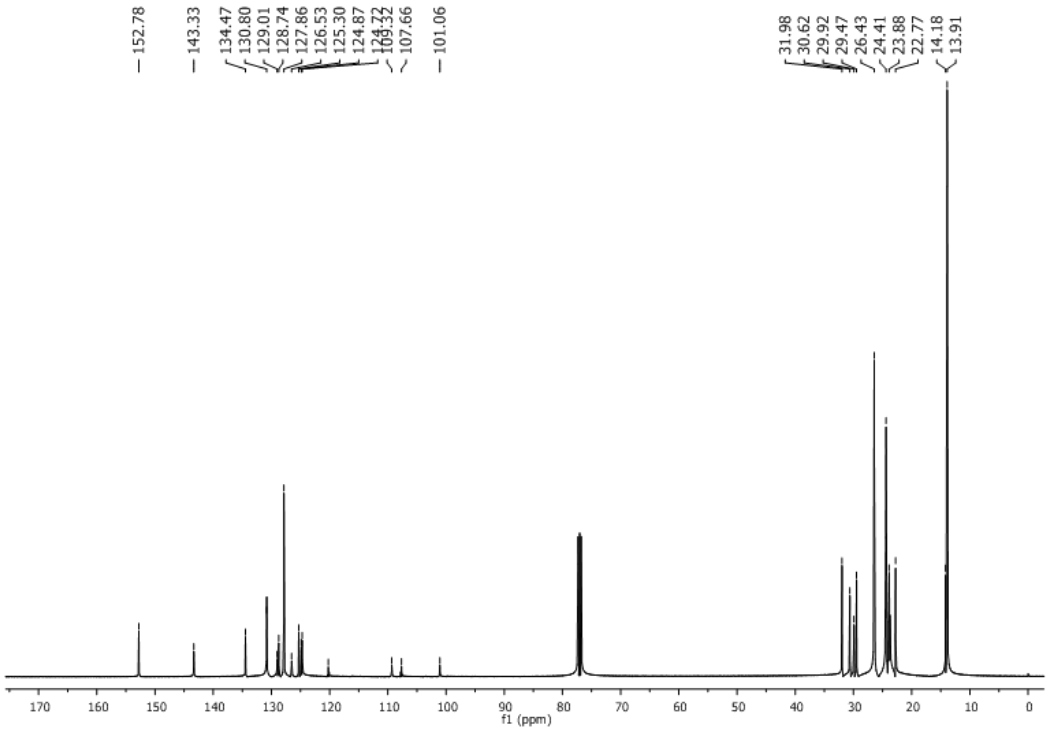

Figure B-11. ^{13}C NMR spectra of TBT-Pt-PBu_3 in $CDCl_3$.

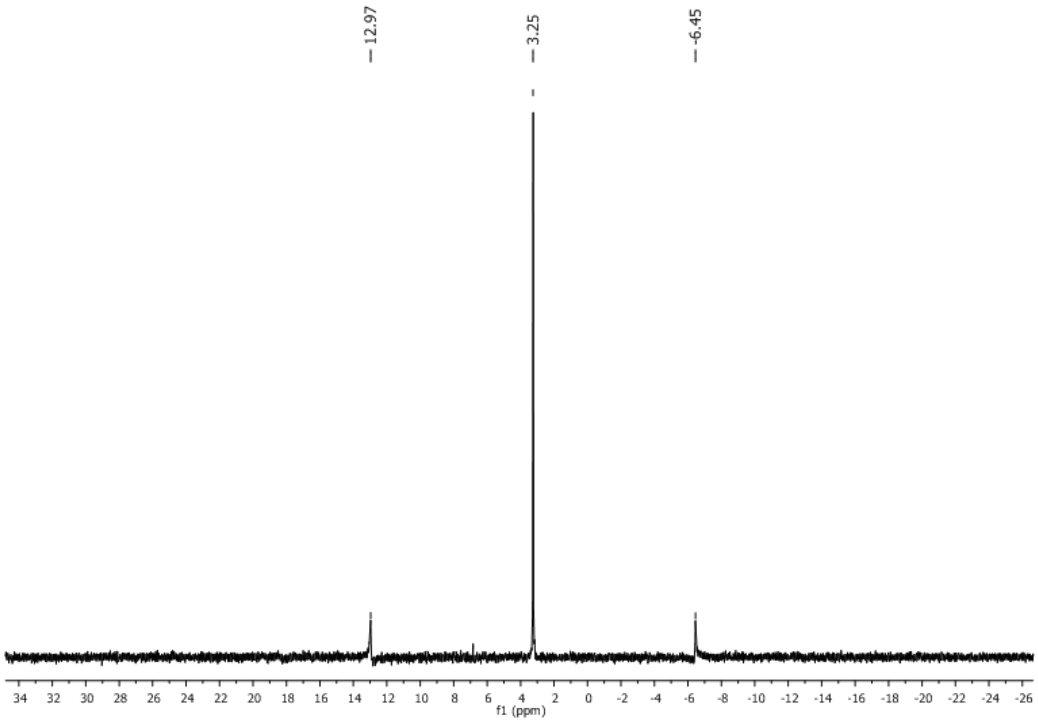

Figure B-12. ^{31}P NMR spectra of TBT-Pt-PBu_3 in $CDCl_3$.

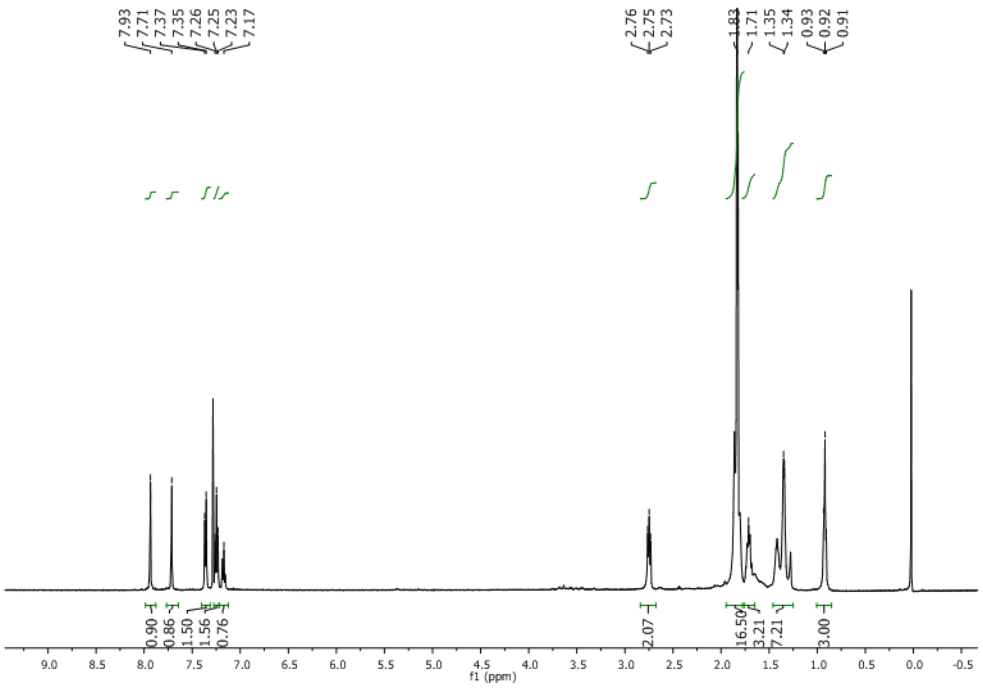

Figure B-13. ^{1}H NMR spectra of TBT-Pt-PMe_3 in $CDCl_3$.

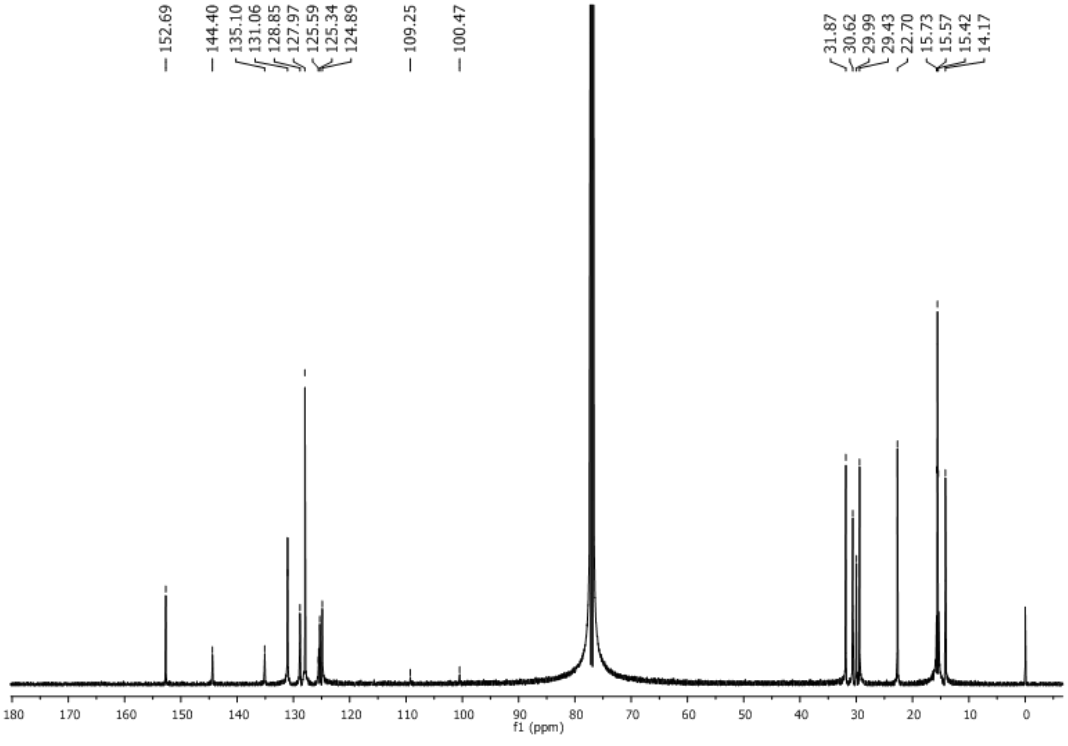

Figure B-14. ^{13}C NMR spectra of TBT-Pt-PMe_3 in $CDCl_3$.

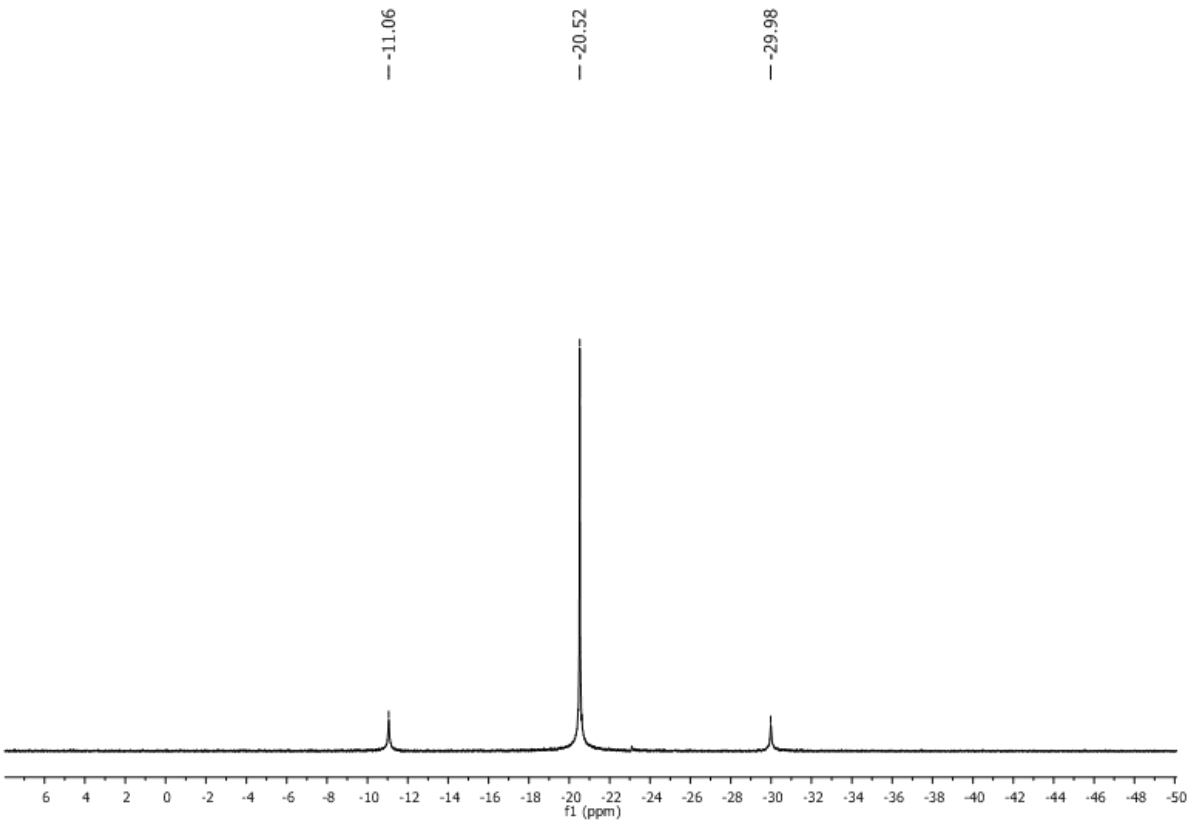

Figure B-15. ^{31}P NMR spectra of TBT-Pt-PMe_3 in $CDCl_3$.

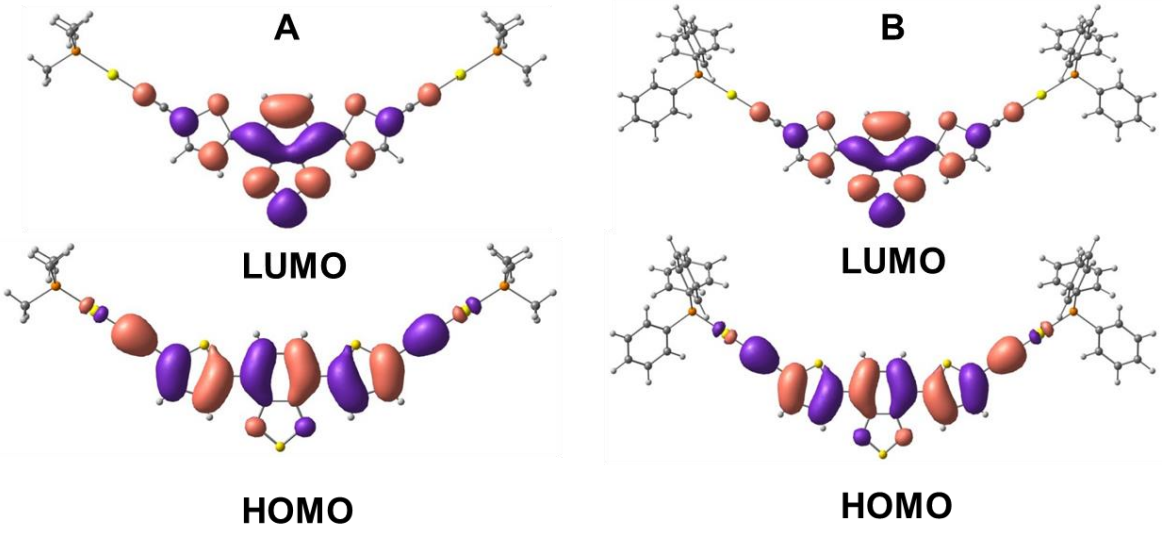

Figure B-16. Frontier molecular orbitals of (A) TBT-Au-PMe_3 and (B) TBT-Au-PPh_3.

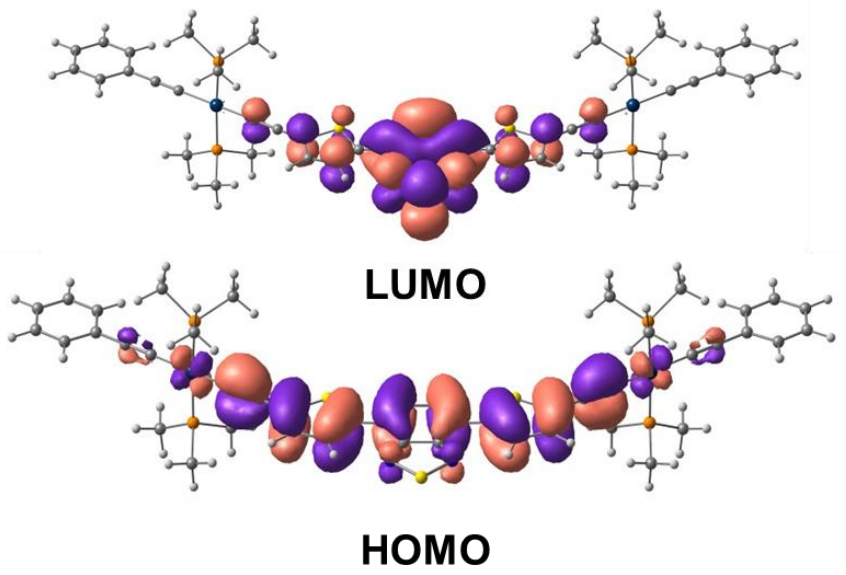

Figure B-17. Frontier molecular orbitals of TBT-Pt-PMe_3.

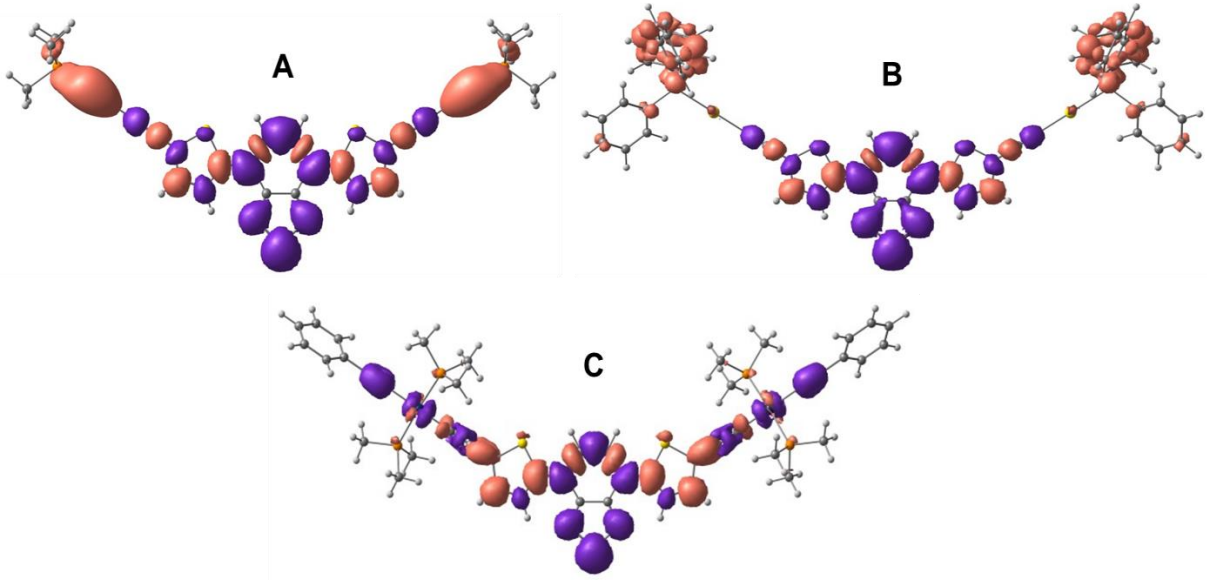

Figure B-18. Charge Difference Density (CDD) for the triplet electronic transition predicted (A) at 621.8 nm for TBT-Au-PMe_3, (B) at 593.0 nm for TBT-Au-PPh_3, (C) at 635.1 nm for TBT-Pt-PMe_3. Blue coloring indicates electron density being lost, while red coloring indicates electron density being gained. CDD plot was imaged with an isovalue of 0.0004.

APPENDIX C
SUPPORTING INFORMATION FOR CHAPTER 5

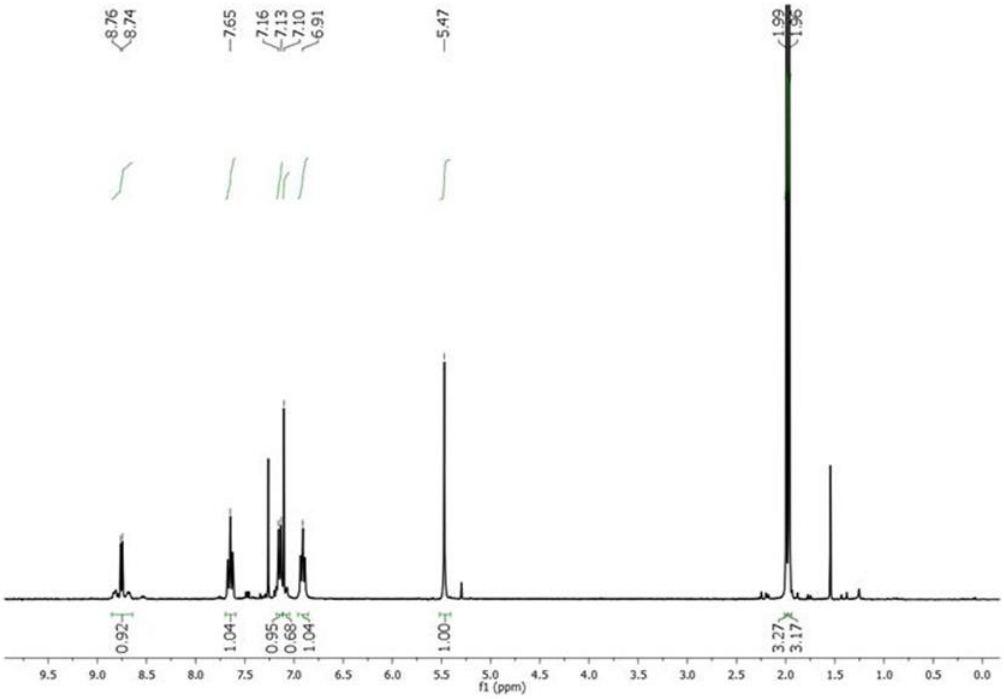

Figure C-1. ^{1}H NMR (300 MHz, $CDCl_3$) spectra of Pt(acac).

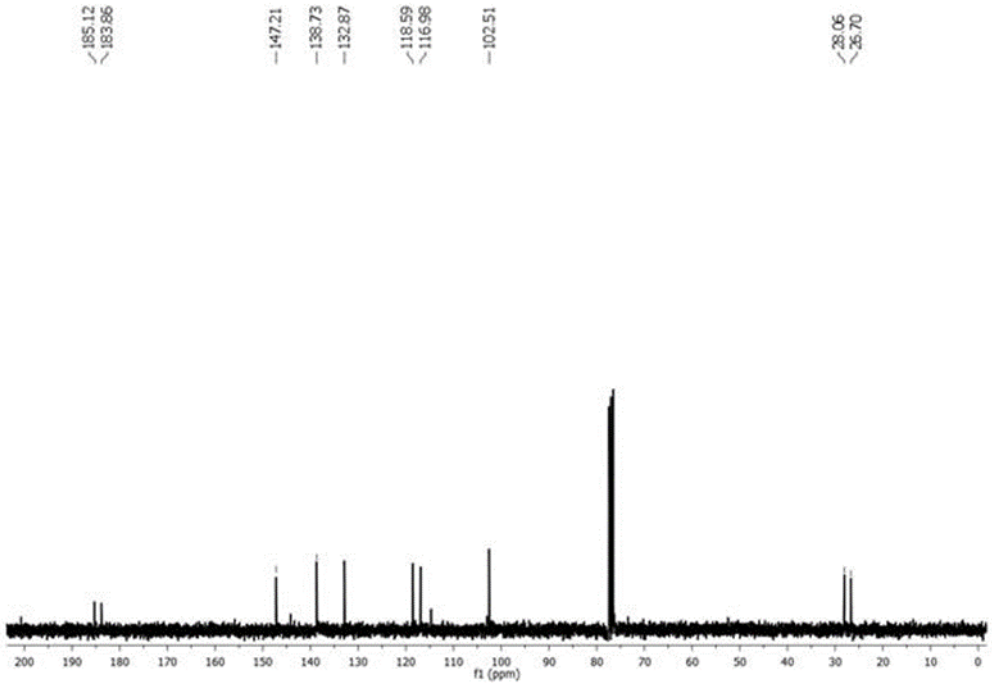

Figure C-2. ^{13}C NMR (75 MHz, $CDCl_3$) spectra of Pt(acac).

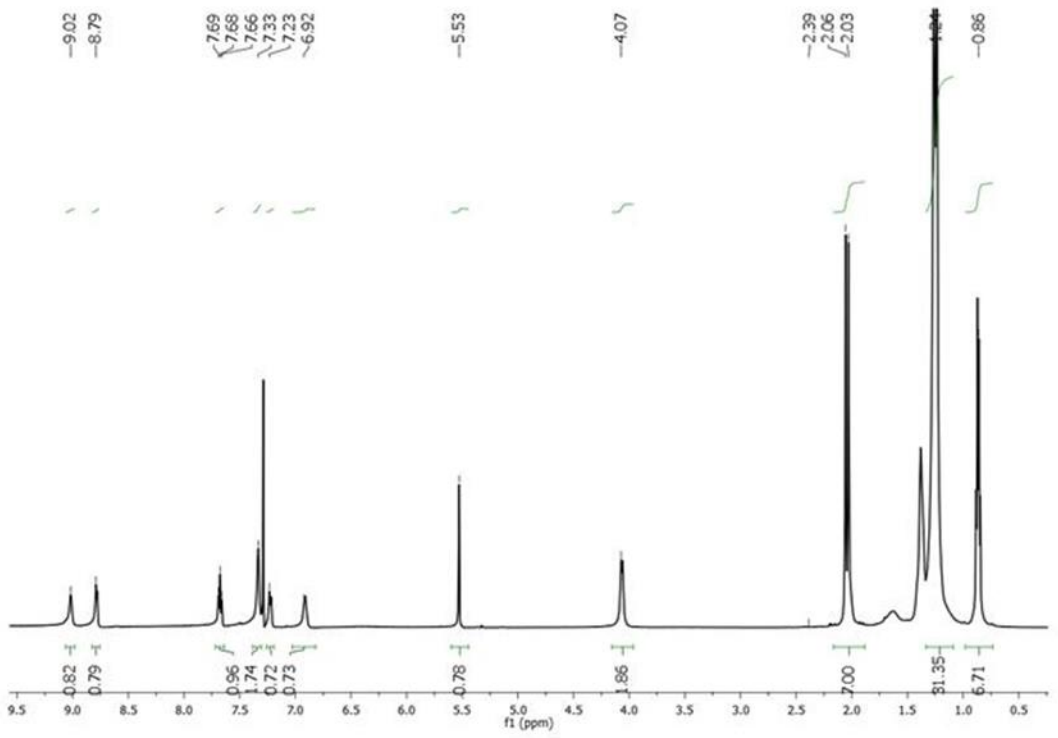

Figure C-3. ^{1}H NMR (500 MHz, $CDCl_3$) spectra of DPP-Pt(acac).

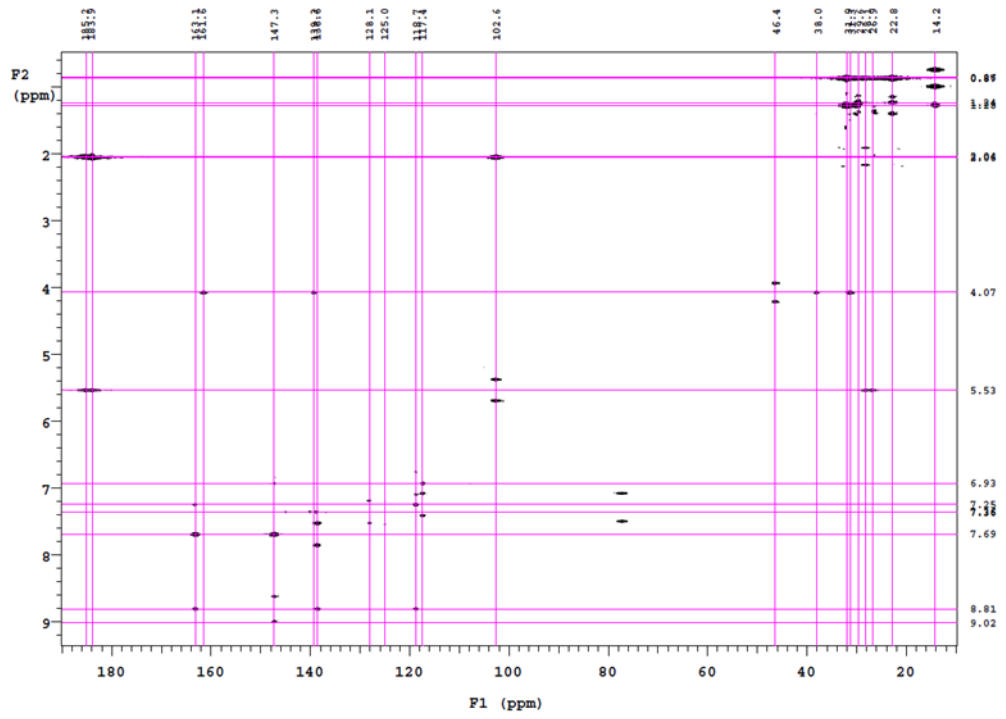

Figure C-4. ^{1}H-^{13}C gHMBC spectrum of DPP-Pt(acac) in $CDCl_3$.

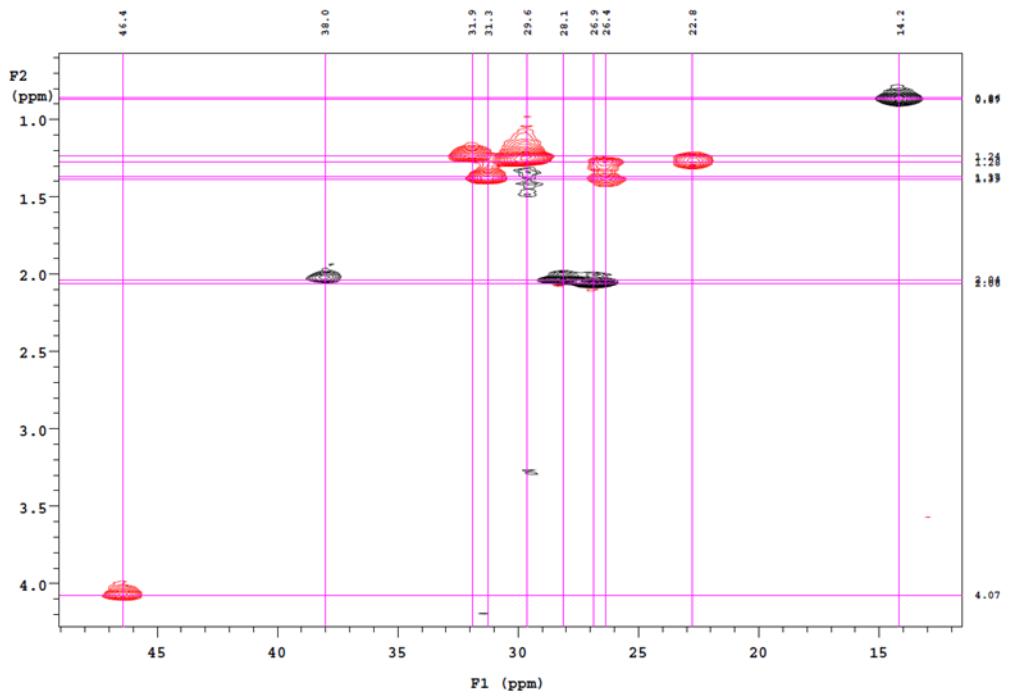

Figure C-5. ^{1}H-^{13}C gHMBC spectrum of DPP-Pt(acac) in $CDCl_3$ (aliphatic region).

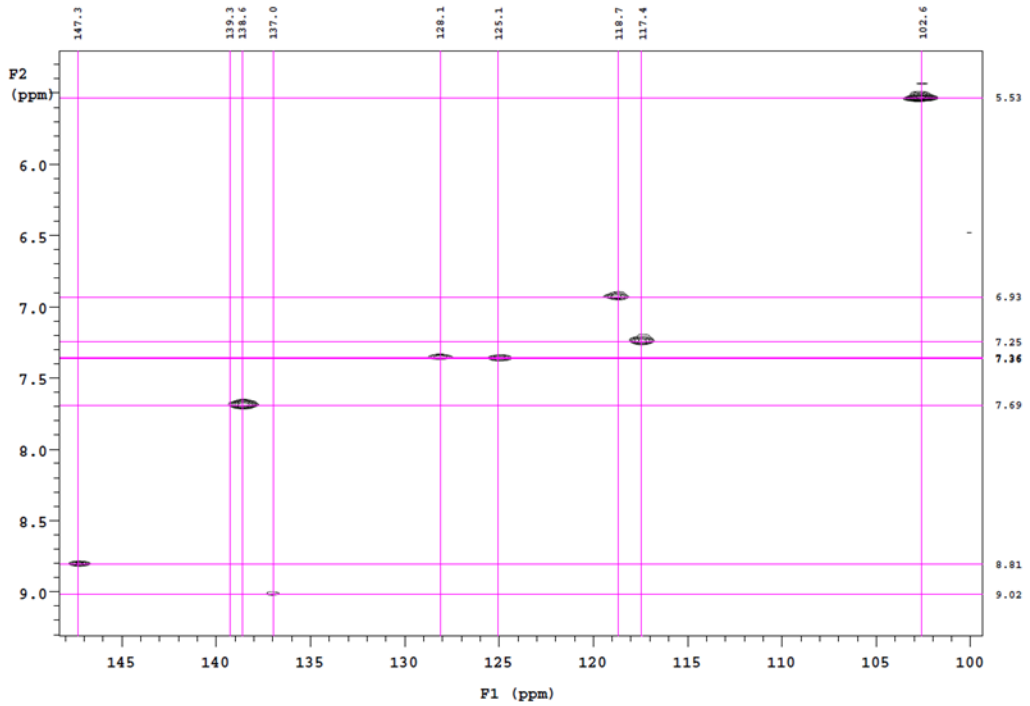

Figure C-6. ^{1}H-^{13}C gHMBC spectrum of DPP-Pt(acac) in $CDCl_3$ (aromatic region).

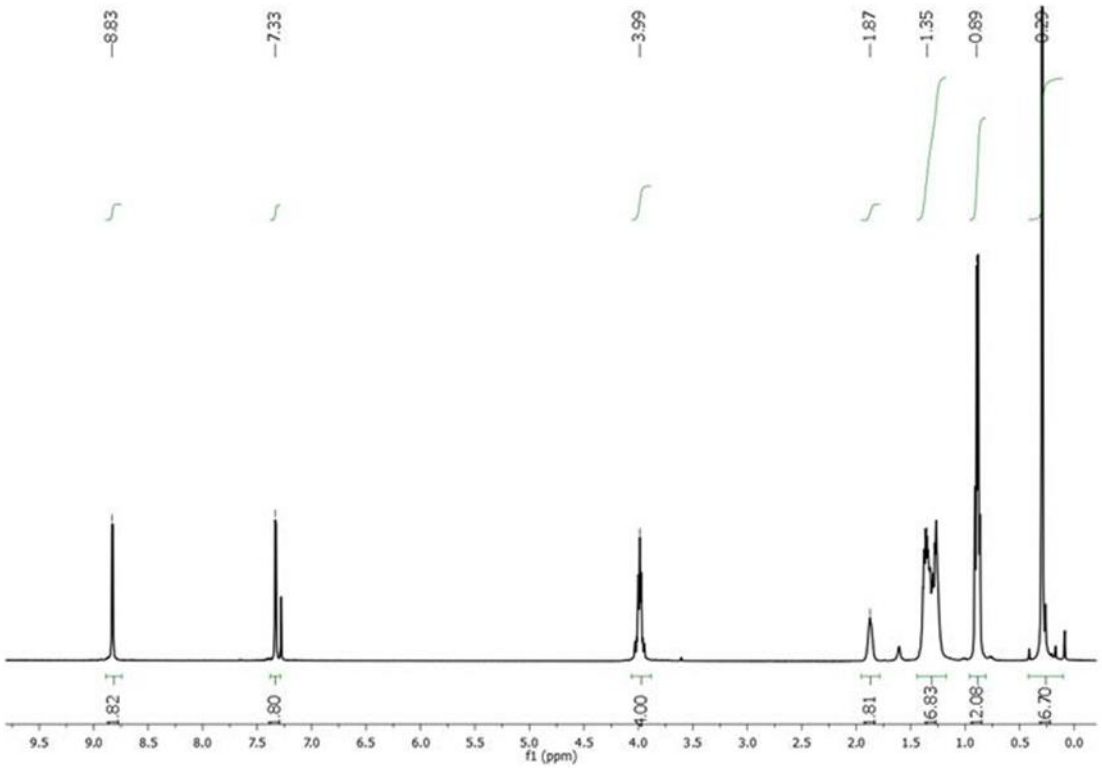

Figure C-7. ^{1}H NMR (500 MHz, $CDCl_3$) spectra of 5-7.

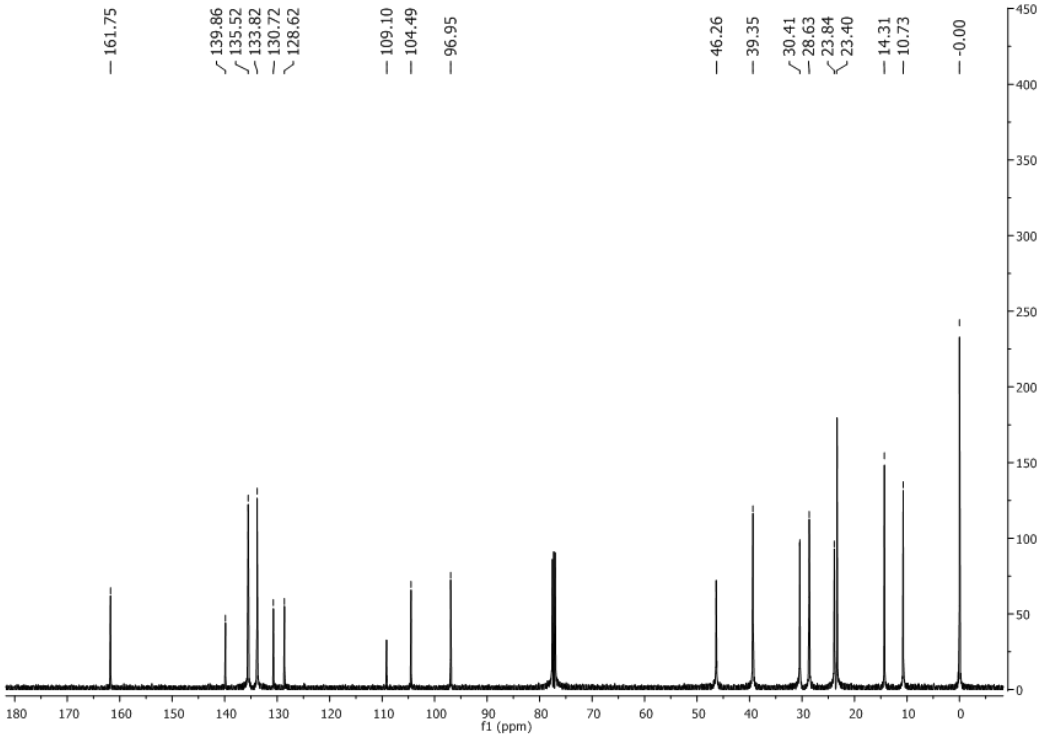

Figure C-8. ^{13}C NMR (125 MHz, $CDCl_3$) spectra of 5-7.

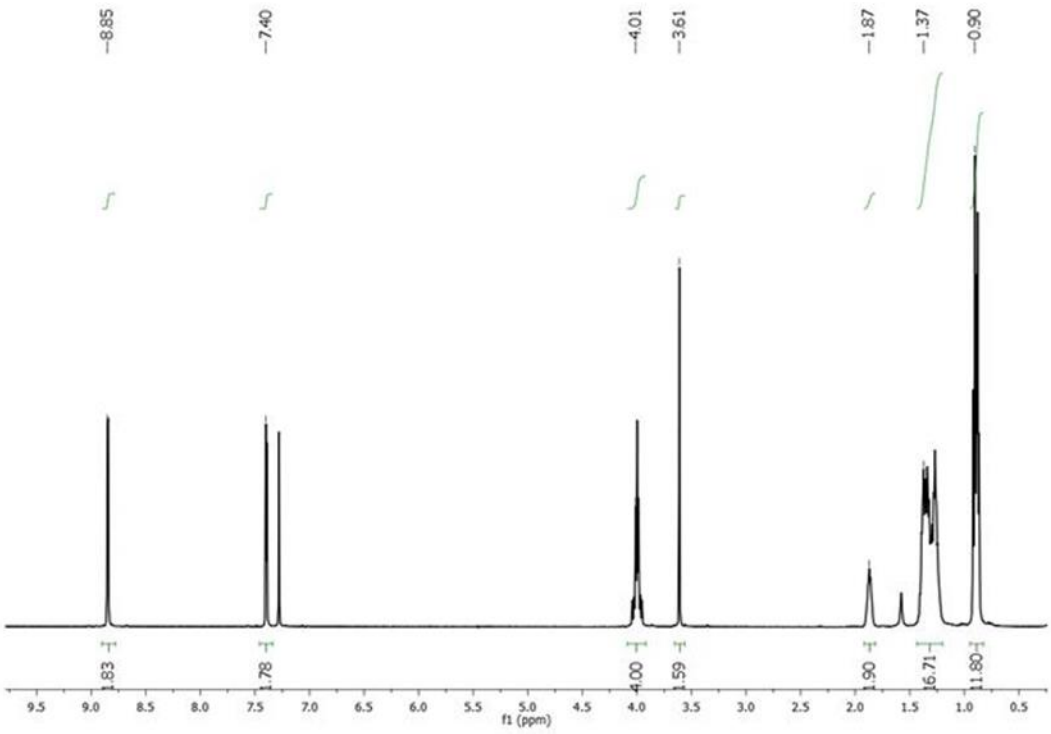

Figure C-9. ^{1}H NMR (500 MHz, $CDCl_3$) spectra of DPP-H.

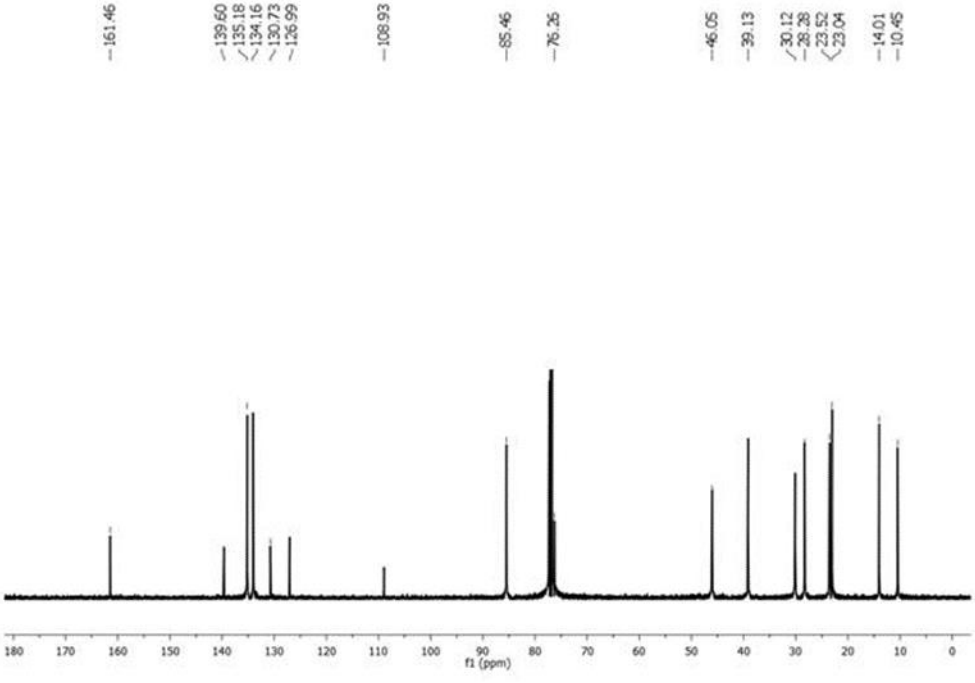

Figure C-10. ^{13}C NMR (125 MHz, $CDCl_3$) spectra of DPP-H.

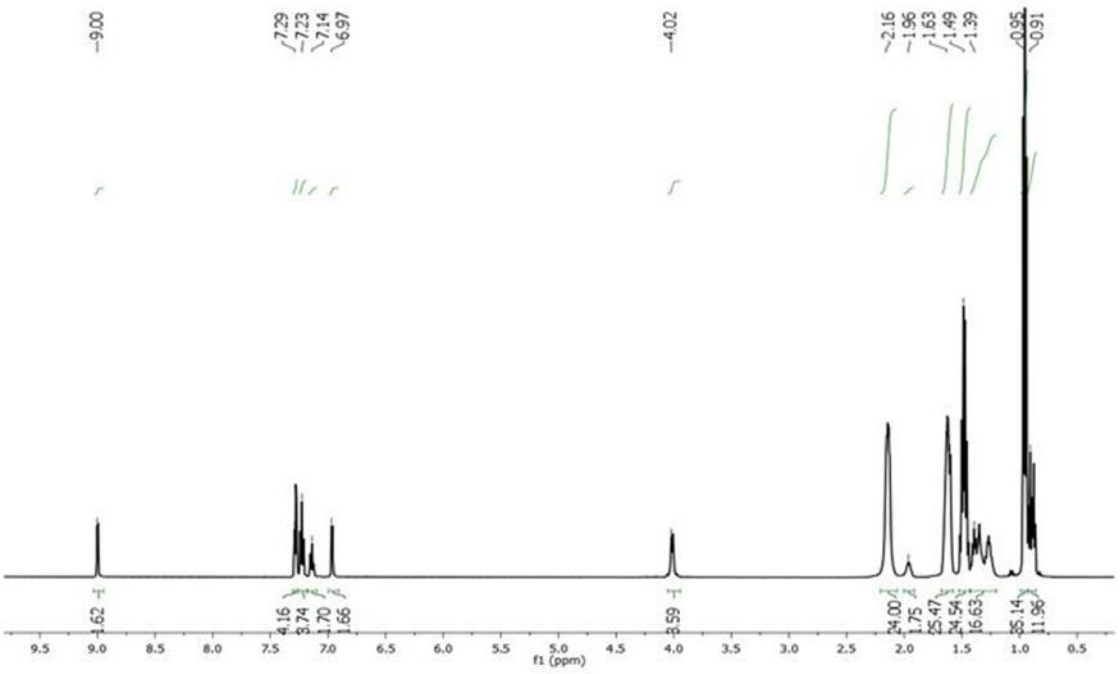

Figure C-11. ^{1}H NMR (500 MHz, $CDCl_3$) spectra of DPP-Pt(CC).

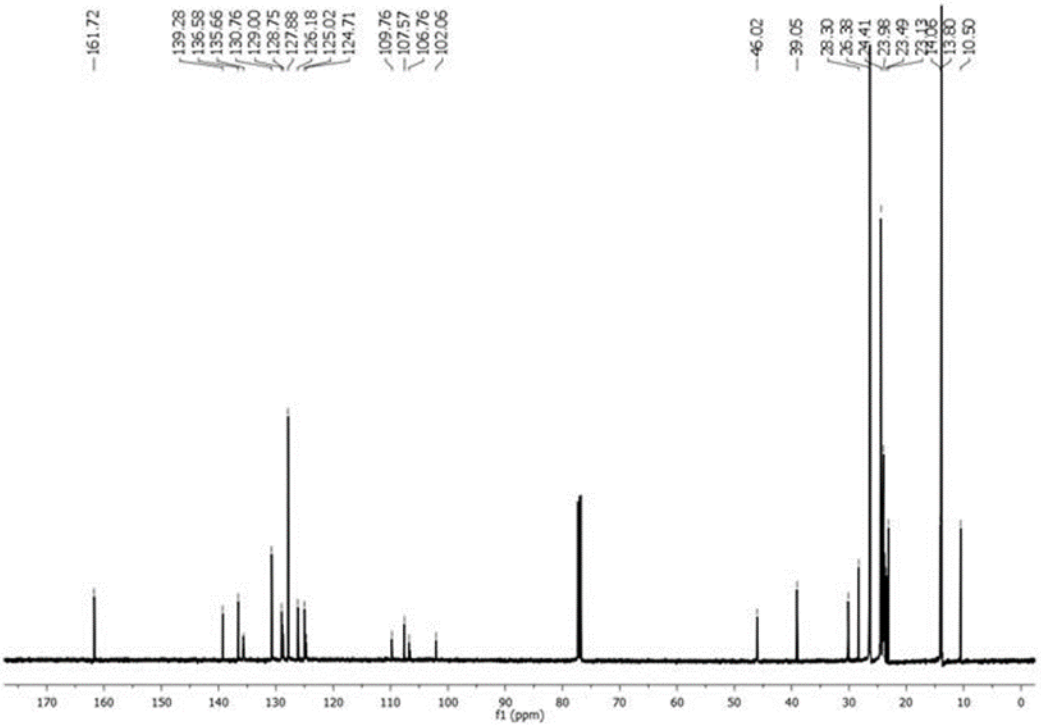

Figure C-12. ^{13}C NMR (125 MHz, $CDCl_3$) spectra of DPP-Pt(CC).

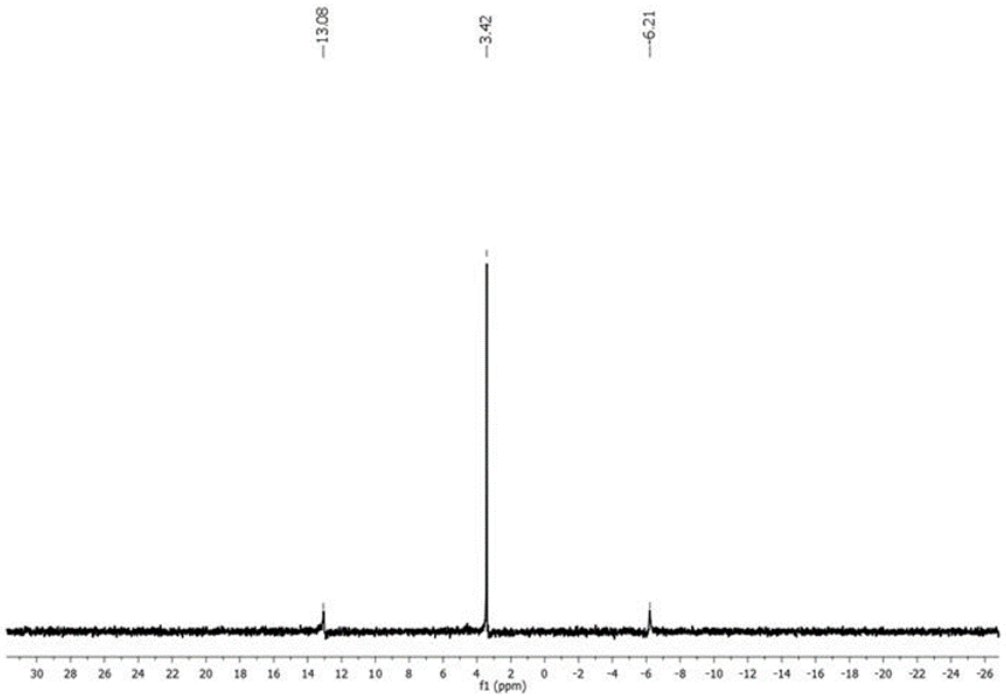

Figure C-13. ^{31}P NMR (121 MHz, $CDCl_3$) of compound DPP-Pt(CC).

Table C1. Computed HOMO and LUMO energies for comparison with electrochemical results

Compound	HOMO (eV)	LUMO (eV)	Bandgap
DPP-C18’	-4.97	-2.51	2.46
DPP-Pt(acac)’	-4.59	-2.70	1.89
DPP-Pt(CC)’	-4.37	-2.21	2.16

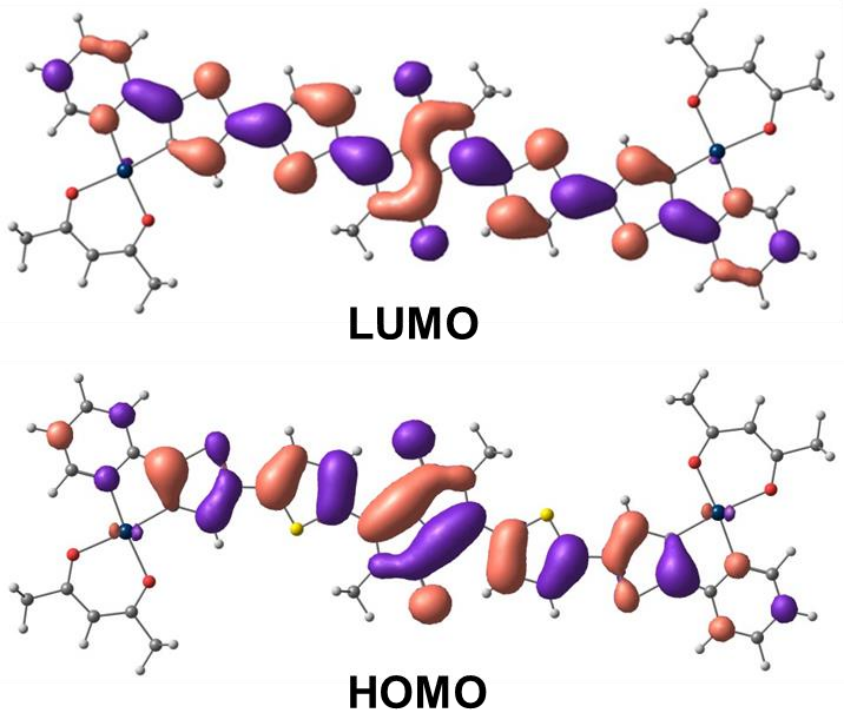

Figure C-14. Molecular Orbitals for the LUMO and HOMO of DPP-Pt(acac)**'**. Orbitals are imaged with an isovalue of 0.02.

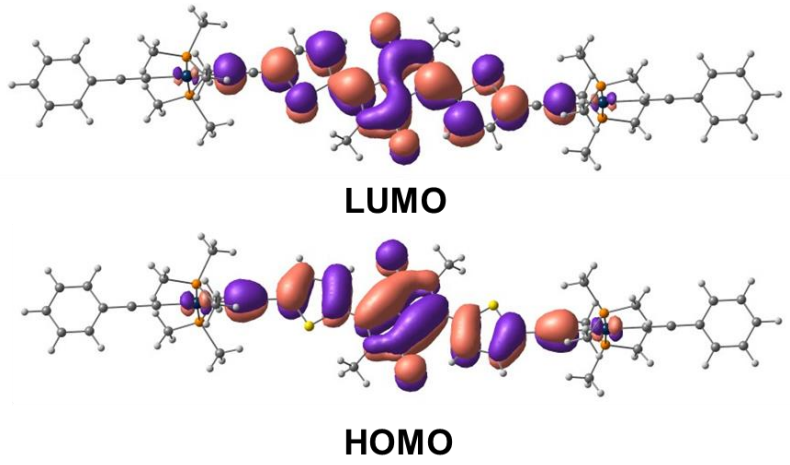

Figure C-15. Molecular Orbitals for the LUMO and HOMO of DPP-Pt(CC)'. Orbitals are imaged with an isovalue of 0.02.

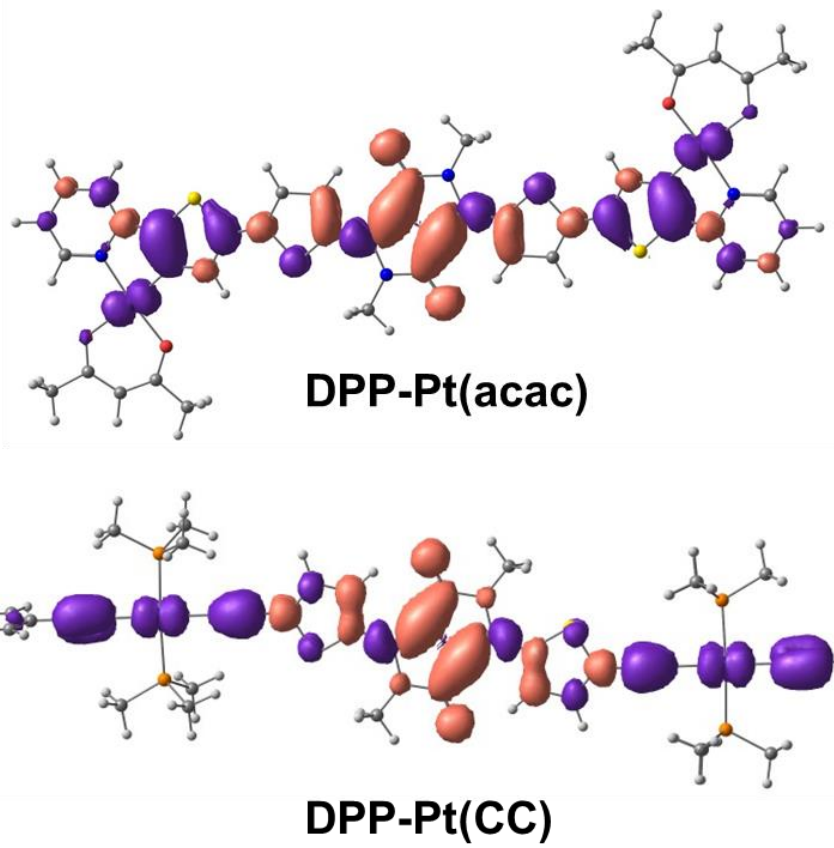

Figure C-16. Charge Difference Density (CDD) for the triplet electronic transition predicted at 804.6 nm for DPP-Pt(acac)' and at 676.6 nm for DPP-Pt(CC)**'**. Blue coloring indicates electron density being lost, while red coloring indicates electron density being gained. CDD plot was imaged with an isovalue of 0.0004.

APPENDIX D
SUPPORTING INFORMATION FOR CHAPTER 6

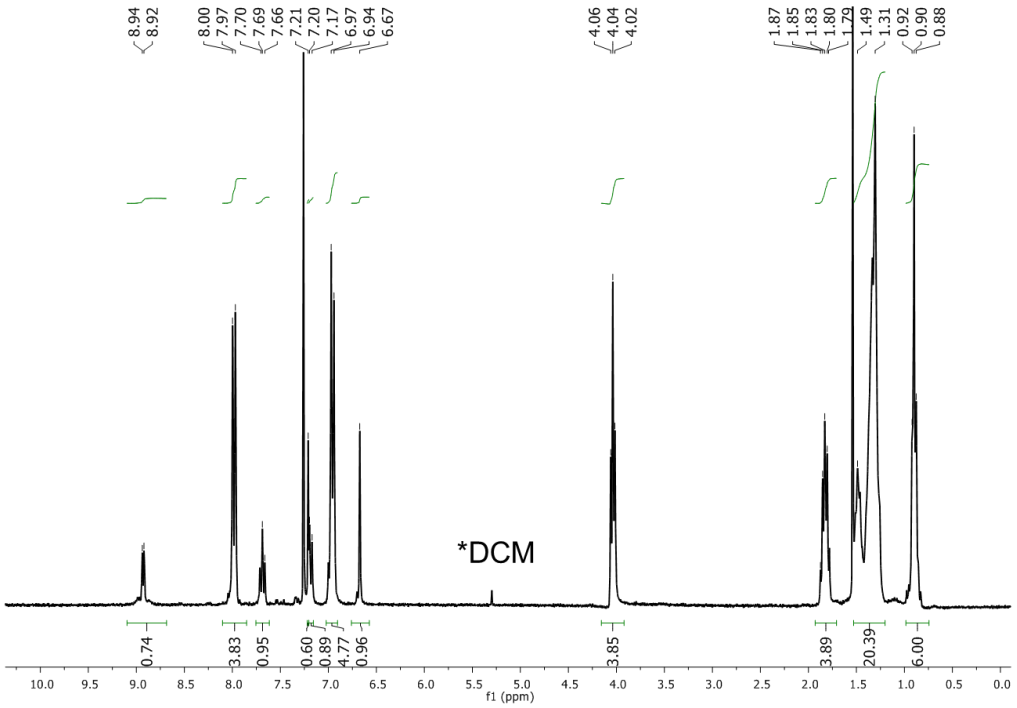

Figure D-1. ^{1}H NMR spectra of Pt(acac)-Octyl in $CDCl_3$.

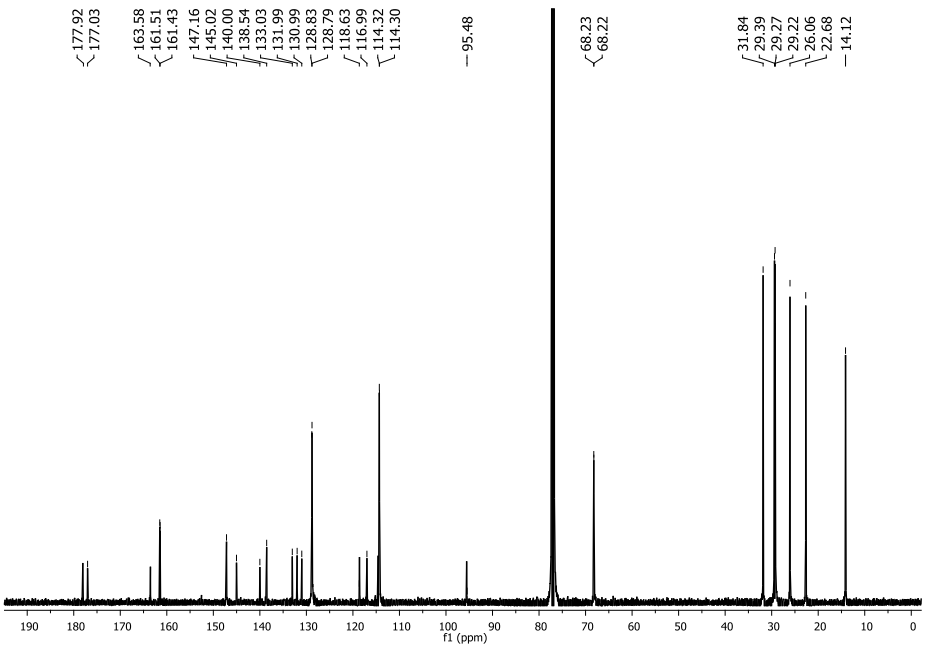

Figure D-2. ^{13}C NMR spectra of Pt(acac)-Octyl in $CDCl_3$.

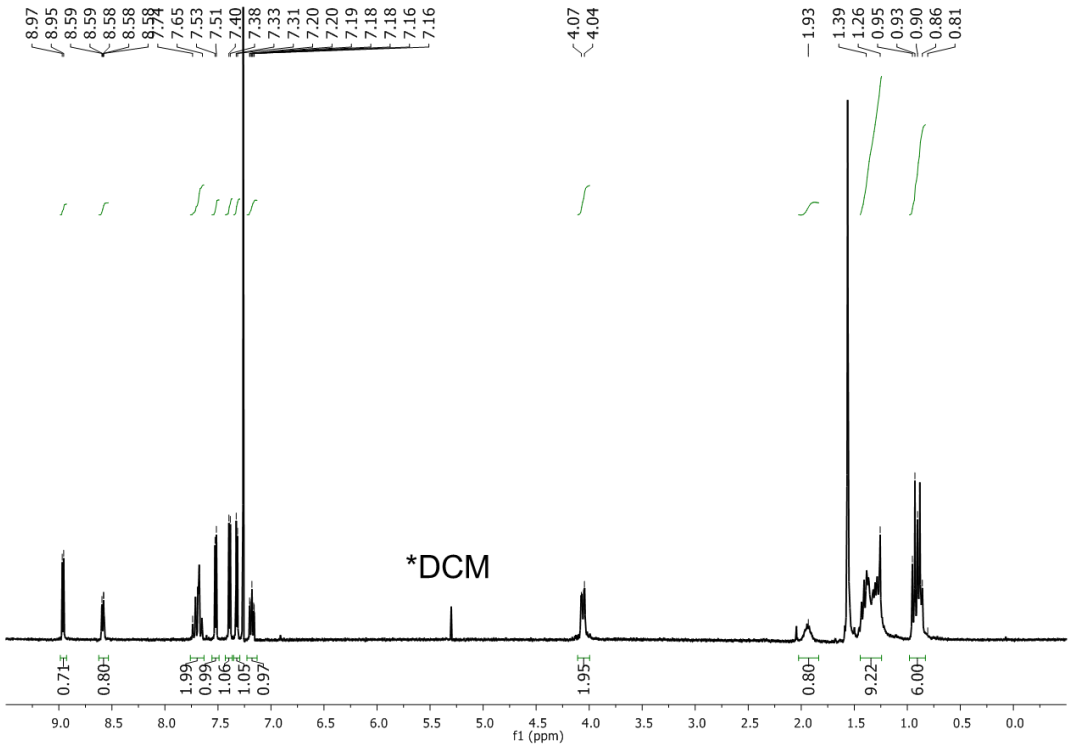

Figure D-3. ^{1}H NMR spectra of DPP-C8-Th-Py in $CDCl_3$.

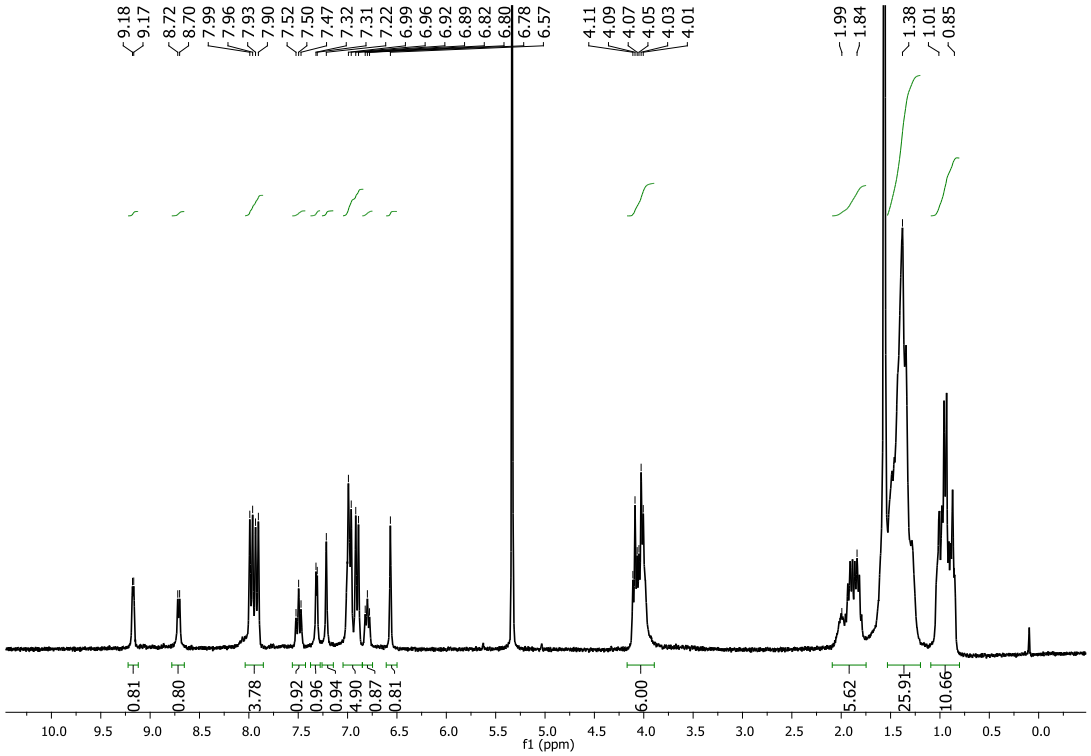

Figure D-4. ^{1}H NMR spectra of DPP-C8-Pt(acac) in CD_2Cl_2.

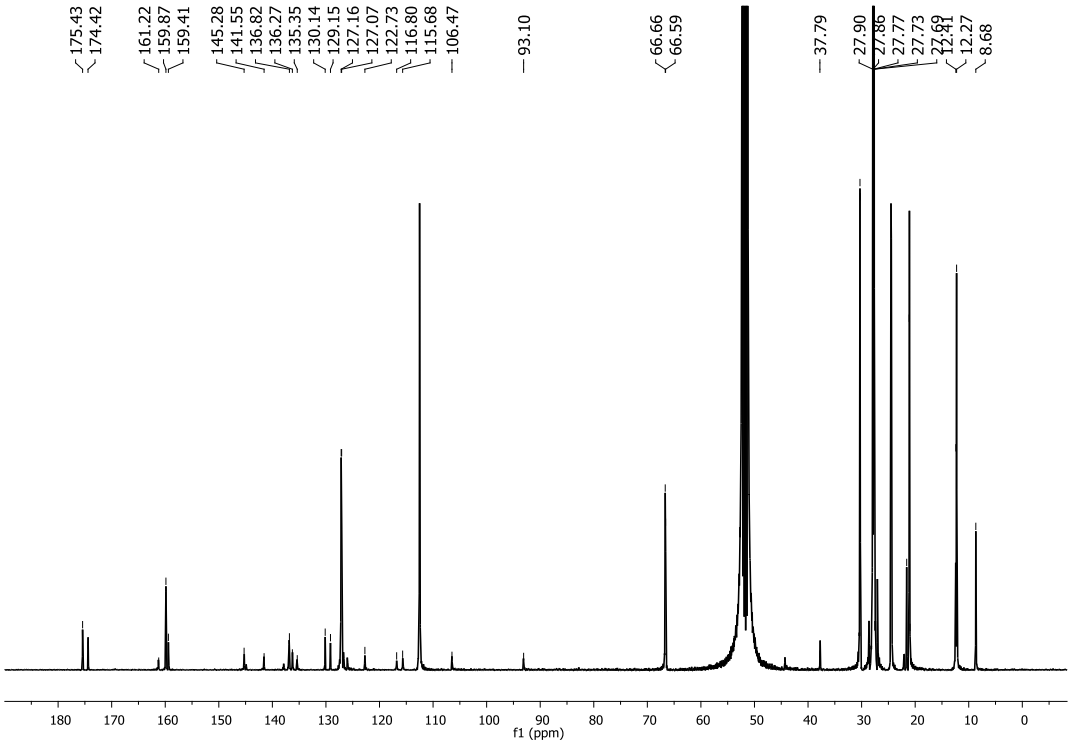

Figure D-5. ^{13}C NMR spectra of DPP-C8-Pt(acac) in CD_2Cl_2.

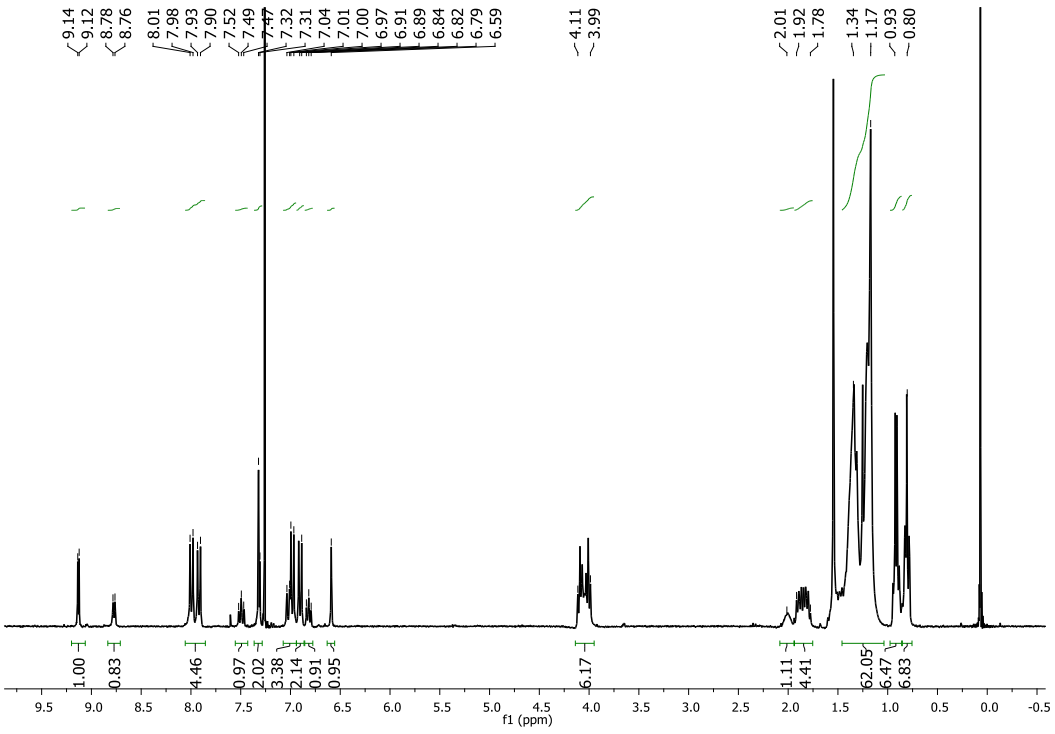

Figure D-6. ^{1}H NMR spectra of DPP-C18-Pt(acac) in $CDCl_3$.

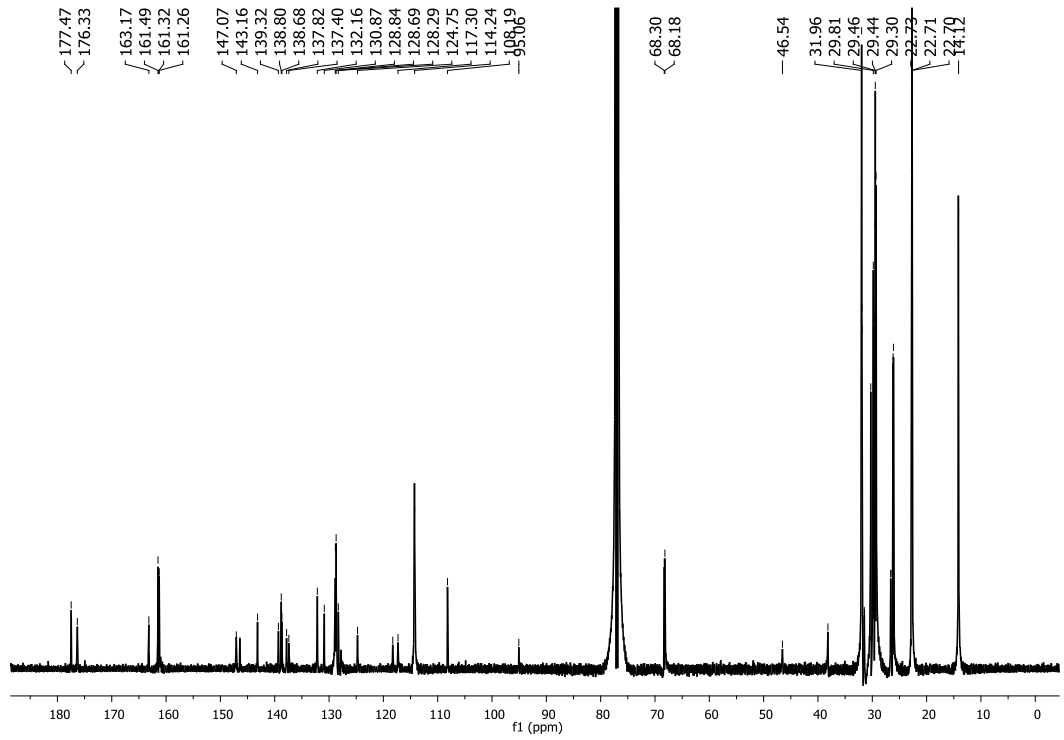

Figure D-7. ^{13}C NMR spectra of DPP-C18-Pt(acac) in $CDCl_3$.

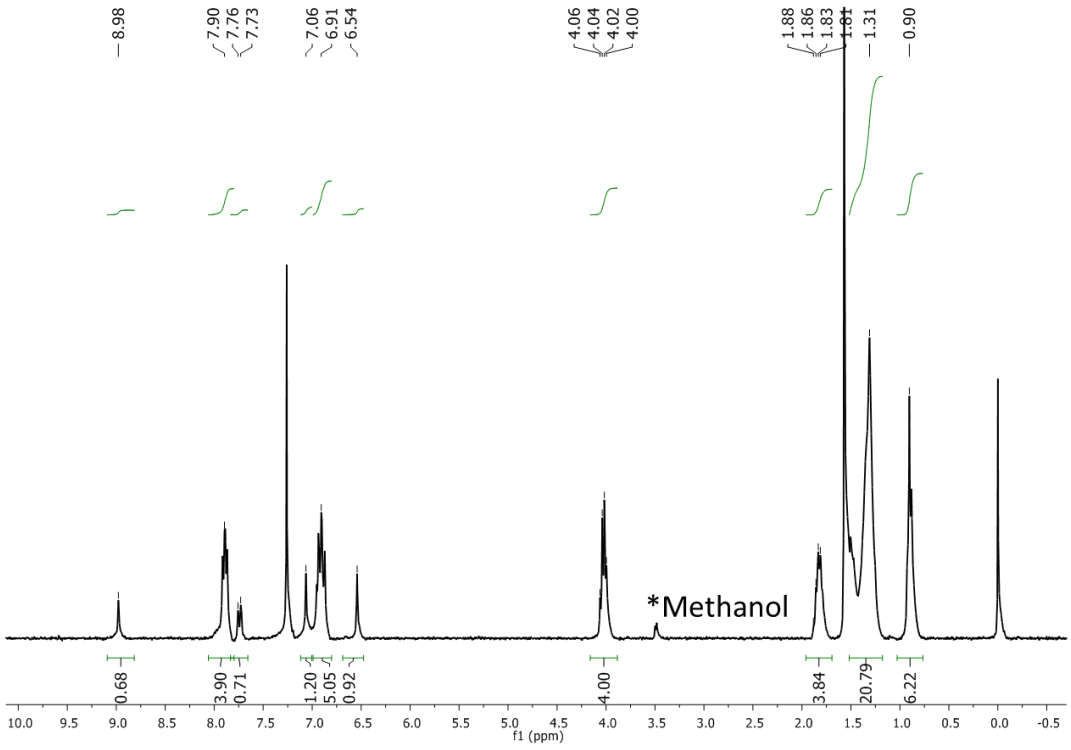

Figure D-8. ^{1}H NMR spectra of 6-9 in $CDCl_3$.

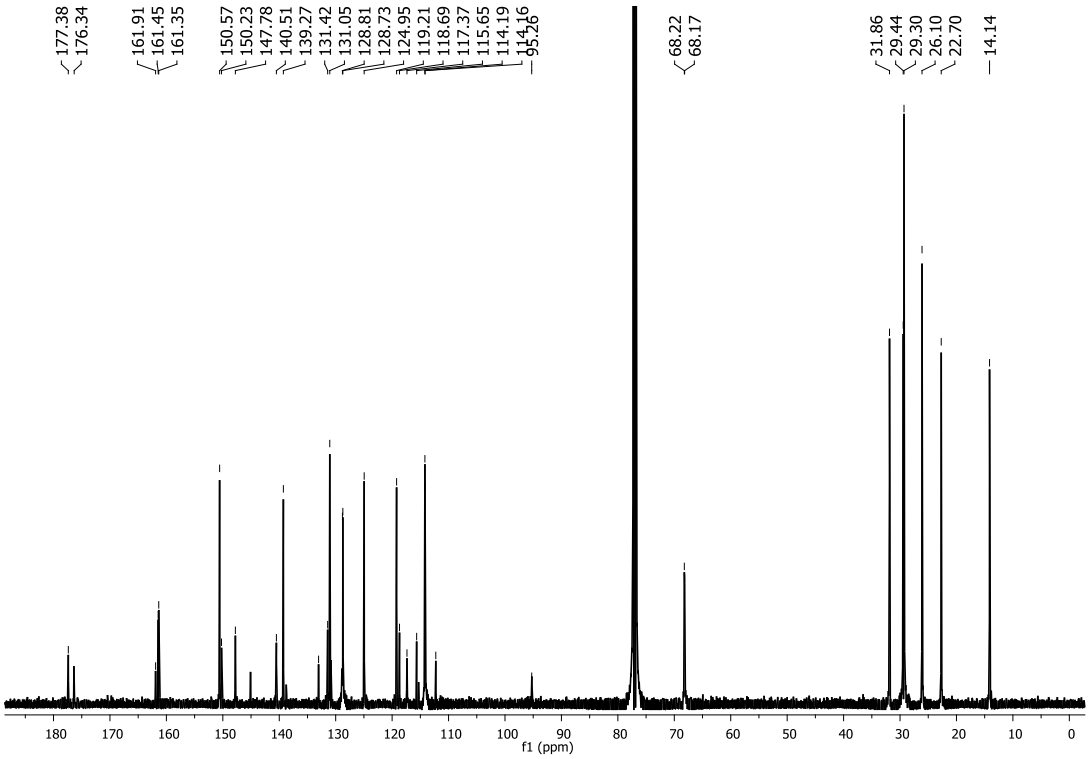

Figure D-9. ^{13}C NMR spectra of 6-9 in $CDCl_3$.

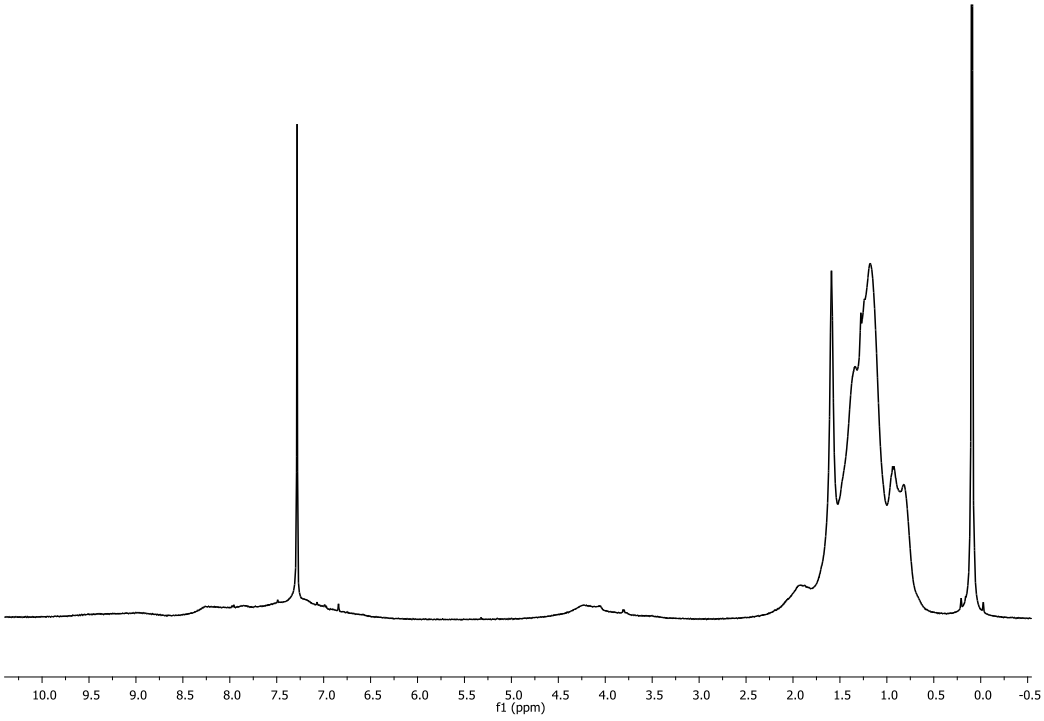

Figure D-10. ^{1}H NMR spectra of DPP-Ph-Pt-P2 in $CDCl_3$.

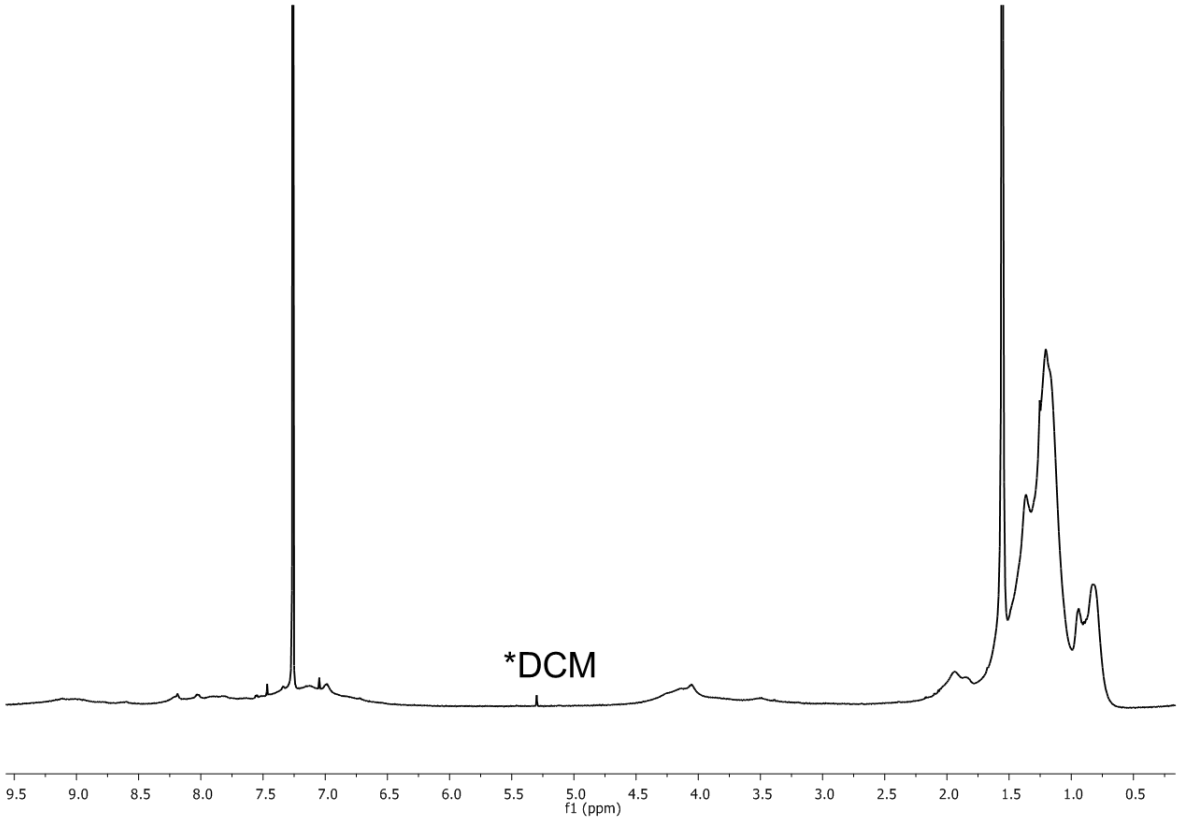

Figure D-11. ^{1}H NMR spectra of DPP-Th-Pt-P1 in $CDCl_3$.

APPENDIX E
SUPPORTING INFORMATION FOR CHAPTER 7

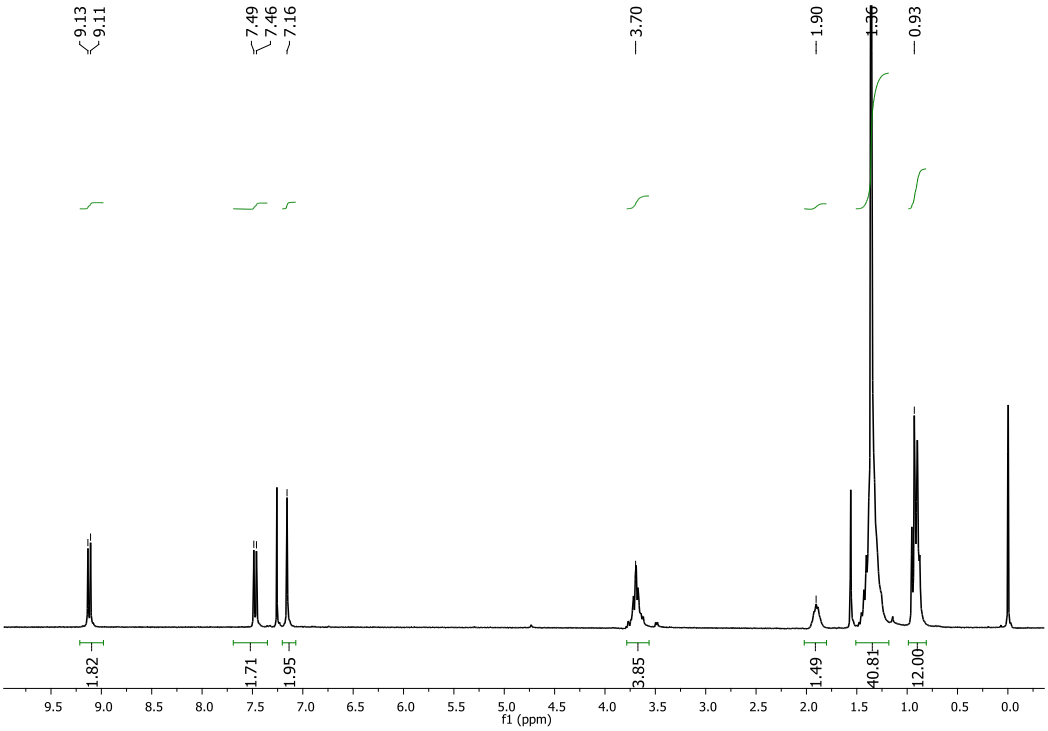

Figure E-1. ^{1}H NMR spectra of Iin-C8-Boronate ester.

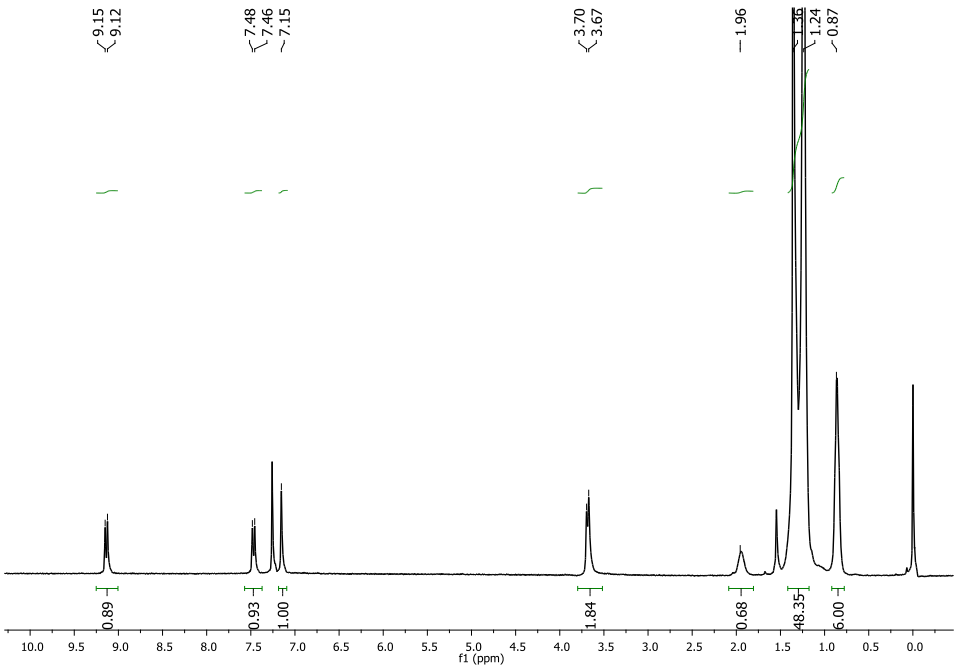

Figure E-2. ^{1}H NMR spectra of Iin-C18-Boronate ester.

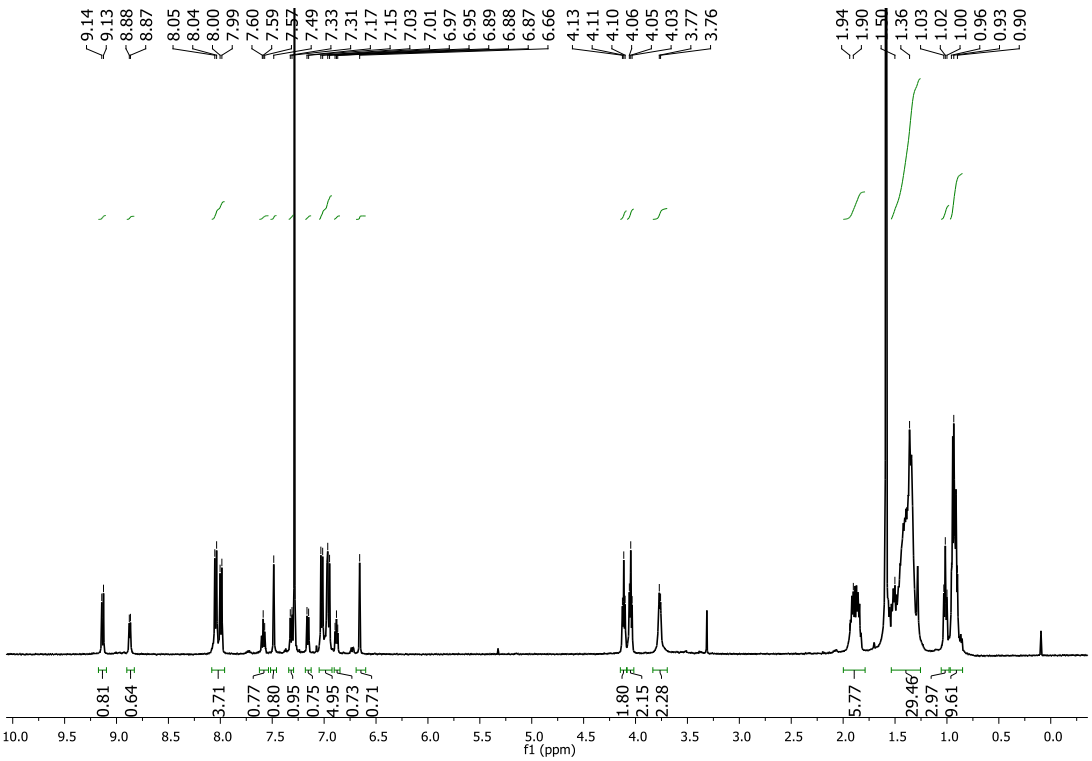

Figure E-3. ^{1}H NMR spectra of Iin-C8-Pt(acac).

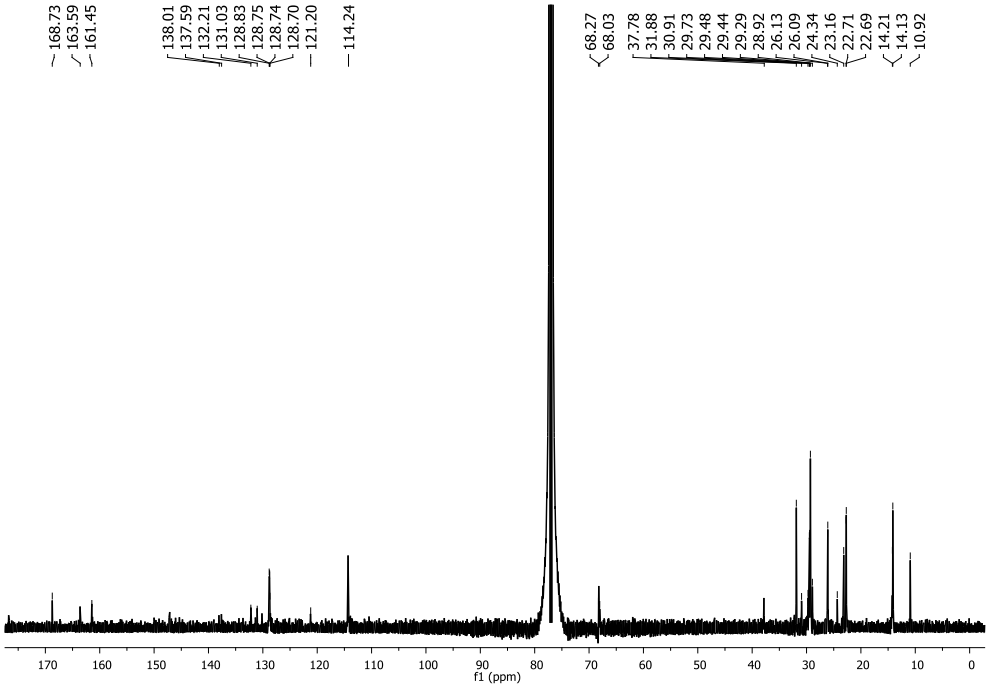

Figure E-4. ^{13}C NMR spectra of Iin-C18-Pt(acac) in $CDCl_3$.

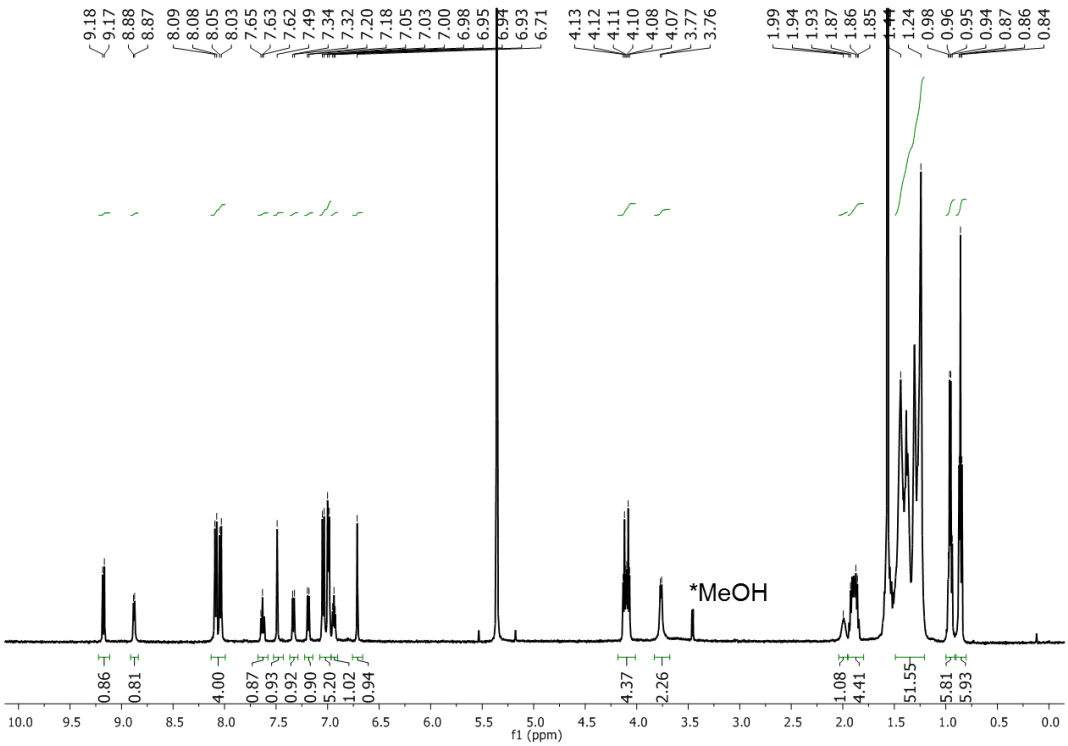

Figure E-5. ^{1}H NMR spectra of Iin-C18-Pt(acac) in $CDCl_3$.

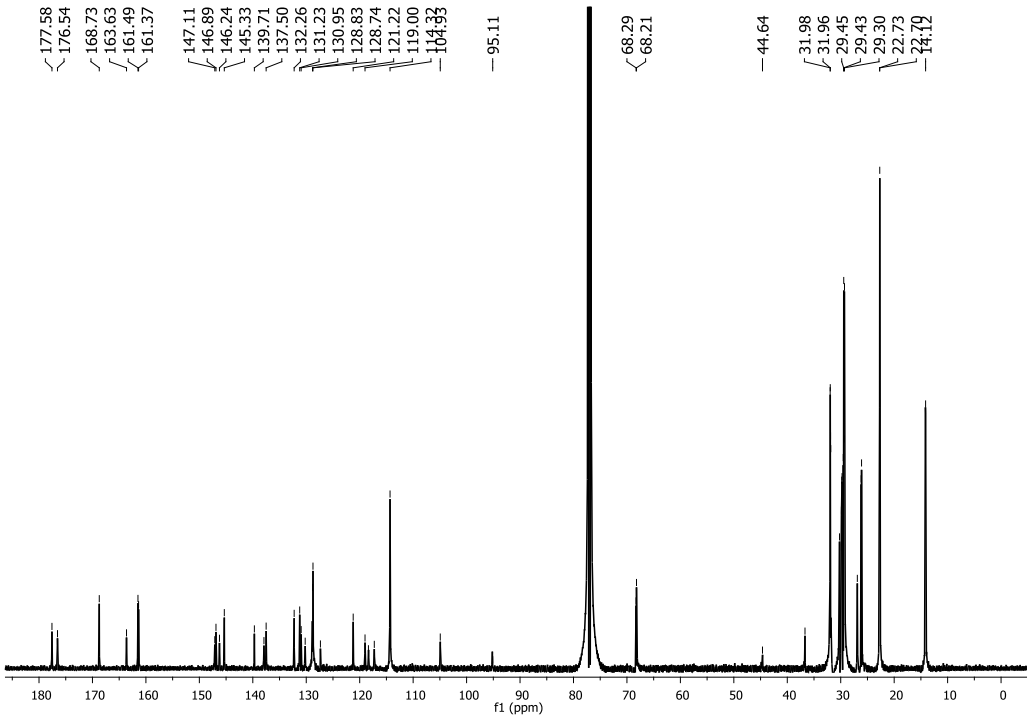

Figure E-6. ^{13}C NMR spectra of Iin-C18-Pt(acac) in $CDCl_3$.

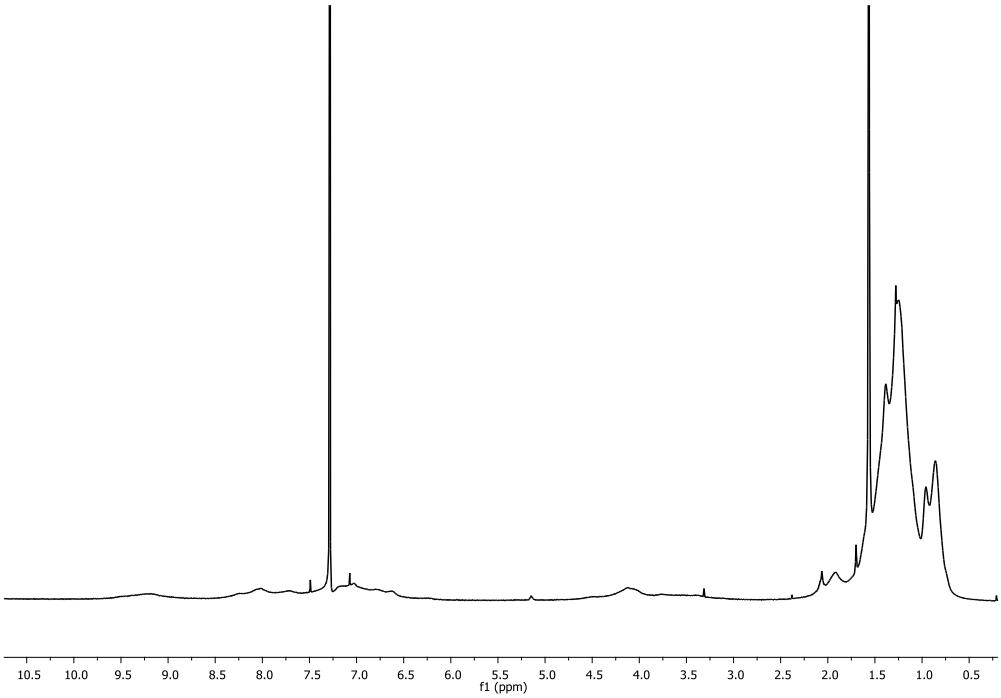

Figure E-7. ^{1}H NMR spectra of Iin-C18-Poly.

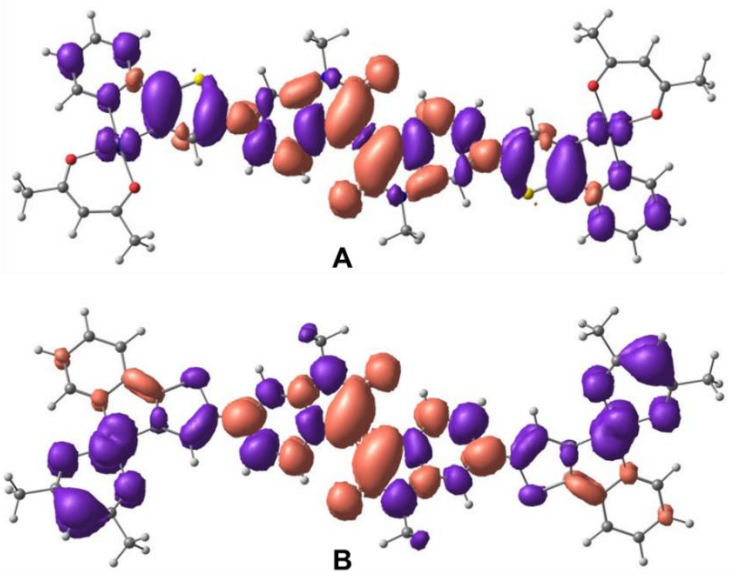

Figure E-8. Charge Difference Density (CDD) for the singlet electronic transition predicted at (A) 627.8 nm and (B) 446.0 nm for Iso-Pt-(acac).

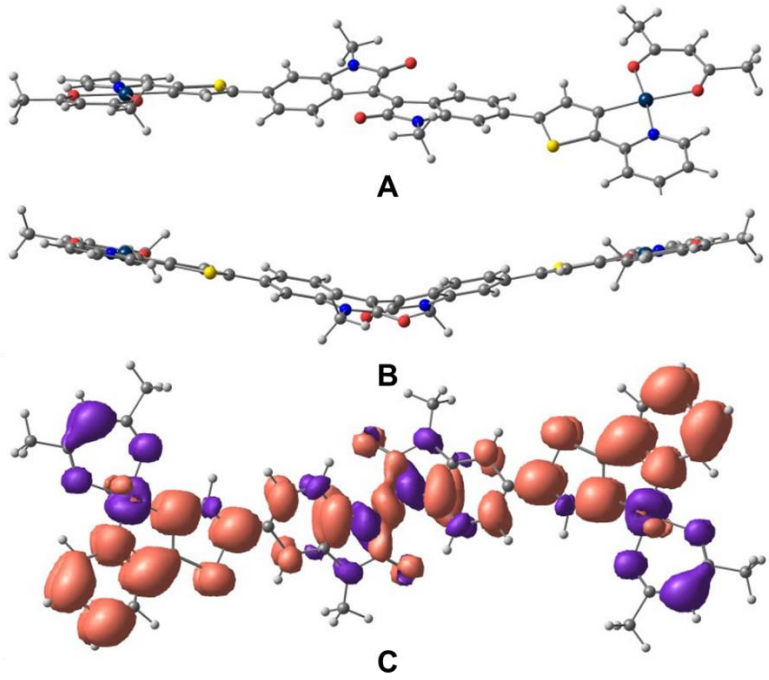

Figure E9. (A) Singlet excited state optimized geometry, (B) triplet excited state optimized geometry and (C) Charge Difference Density (CDD) for the triplet electronic transition predicted at 701.8 nm for **Iso-Pt-(acac)'**. Blue coloring indicates electron density being lost, while red coloring indicates electron density being gained. CDD plot was imaged with an isovalue of 0.0004.

APPENDIX F
SUPPORTING INFORMATION FOR CHAPTER 8

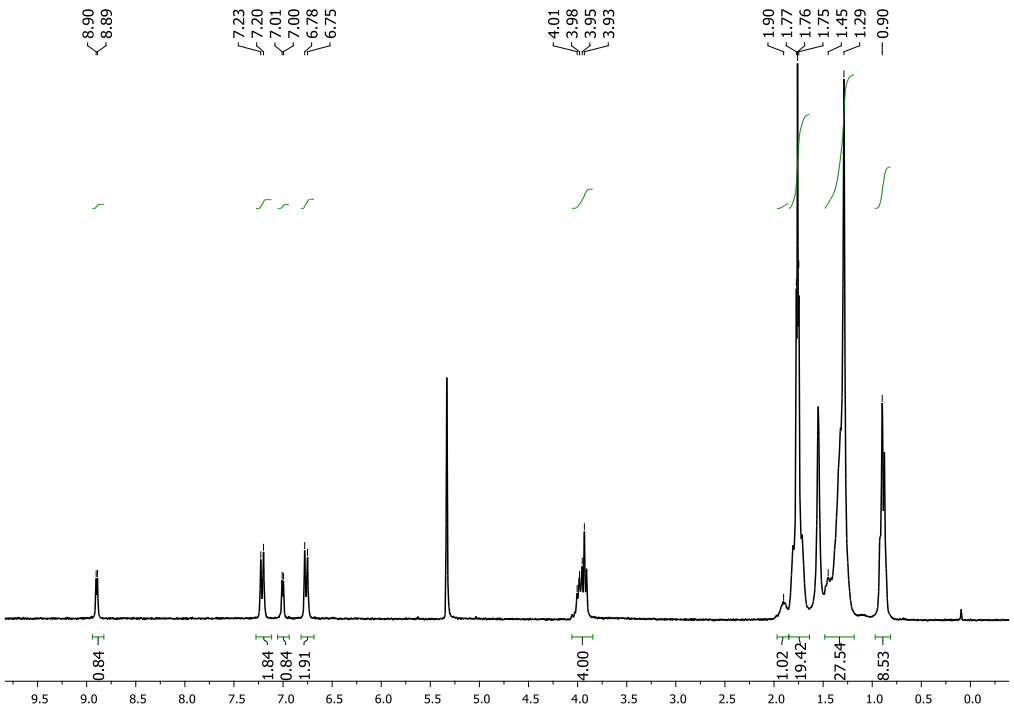

Figure F-1. ^{1}H NMR spectra of DPP-Pt-Dodecyl in CD_2Cl_2.

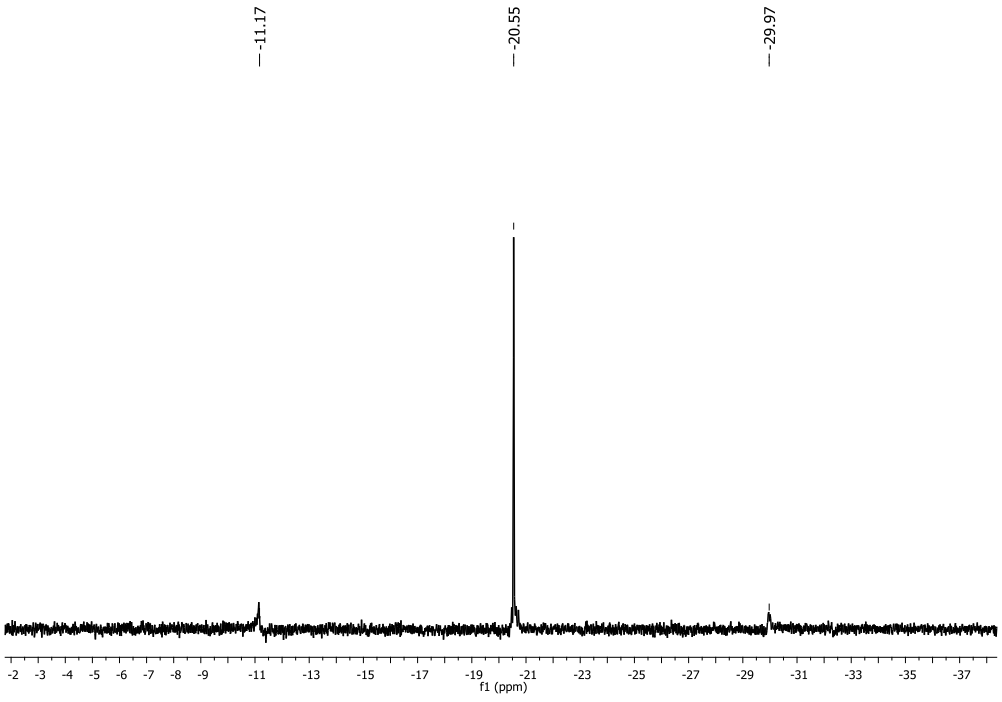

Figure F-2. ^{31}P NMR spectra of DPP-Pt-Dodecyl in CD_2Cl_2.

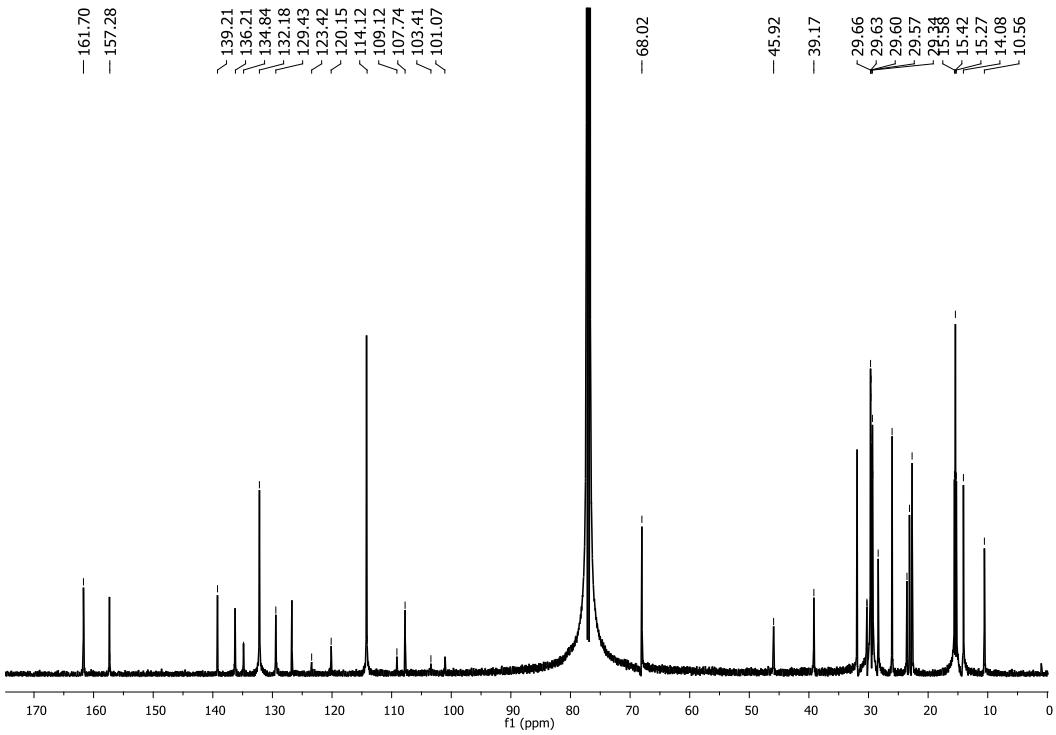

Figure F-3. ^{13}C NMR spectra of DPP-Pt-Dodecyl in $CDCl_3$.

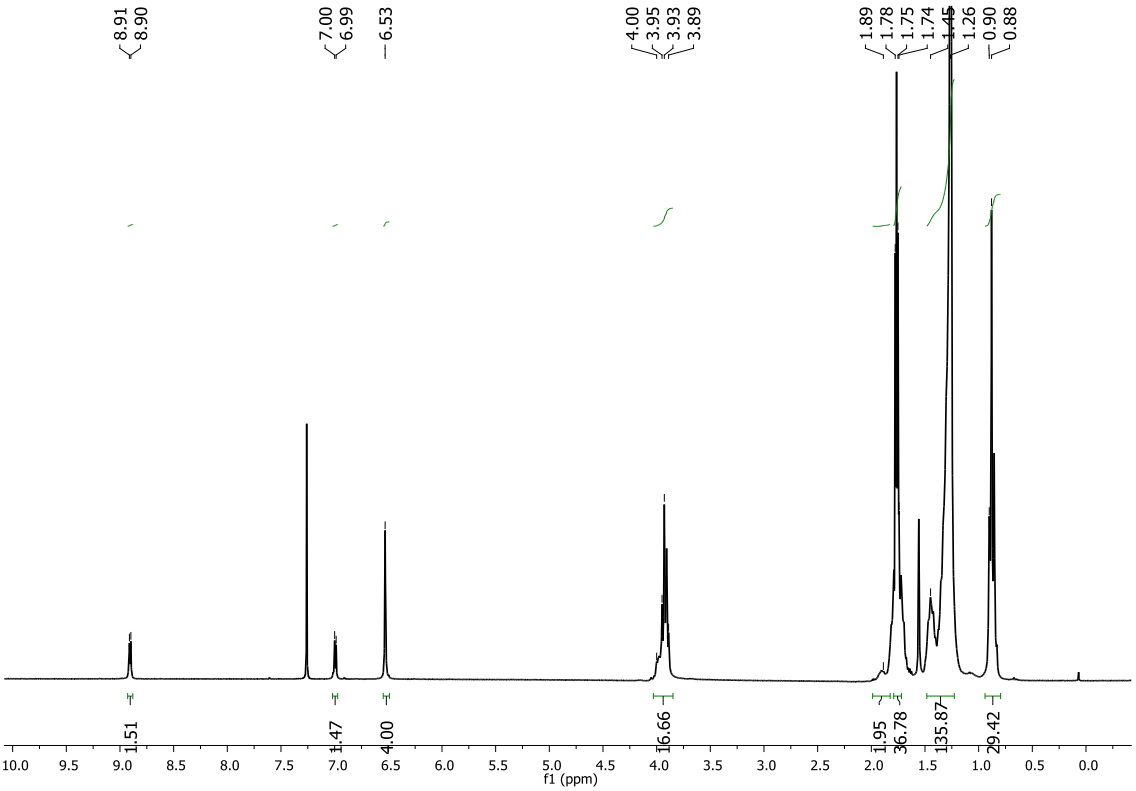

Figure F-4. ^{1}H NMR spectra of DPP-Pt-Gallic in $CDCl_3$.

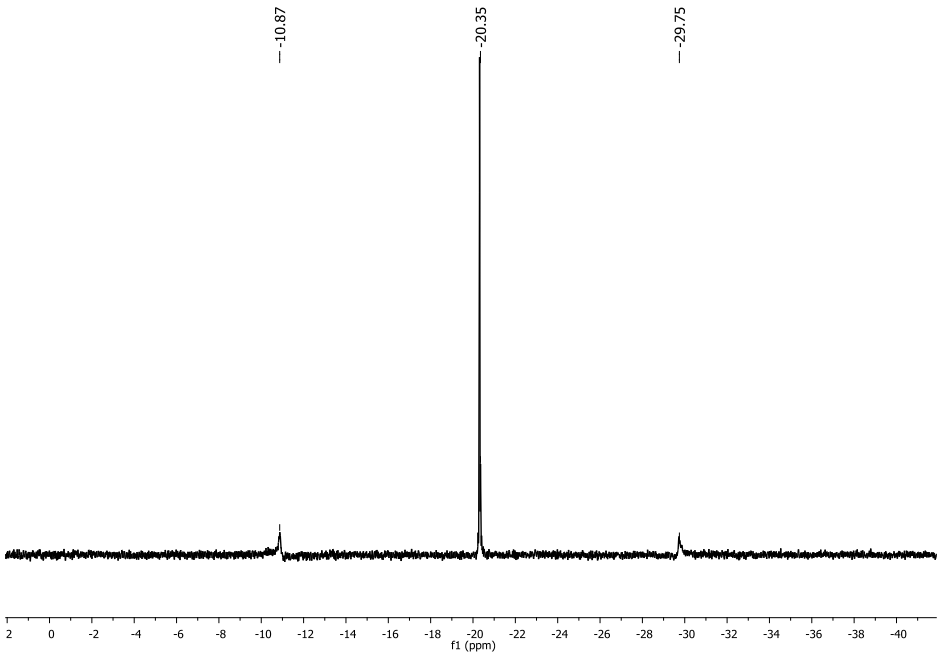

Figure F-5. ^{31}P NMR spectra of DPP-Pt-Gallic in $CDCl_3$.

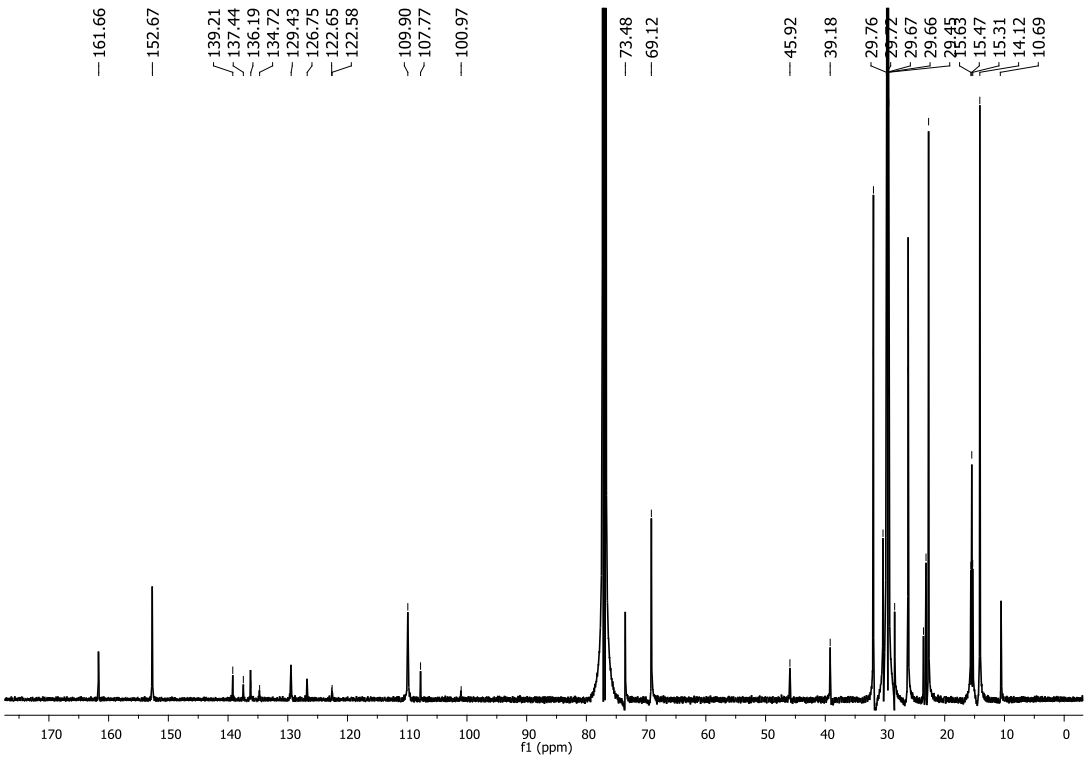

Figure F-6. ^{13}C NMR spectra of DPP-Pt-Gallic in $CDCl_3$.

REFERENCES

(1) Shirakawa, H.; Louis, E. J.; MacDiarmid, A. G.; Chiang, C. K.; Heeger, A. J. *J. Chem. Soc., Chem. Commun.* **1977**, 578.

(2) Stalder, R., Universty of Florida, 2012.

(3) Su, W. P.; Schrieffer, J. R.; Heeger, A. J. *Physical Review B* **1980**, *22*, 2099.

(4) Thompson, B. C.; Fréchet, J. M. J. *Angew. Chem. Int. Ed.* **2008**, *47*, 58.

(5) Dennler, G.; Scharber, M. C.; Brabec, C. J. *Adv. Mater.* **2009**, *21*, 1323.

(6) Kim, Y.; Cook, S.; Tuladhar, S. M.; Choulis, S. A.; Nelson, J.; Durrant, J. R.; Bradley, D. D. C.; Giles, M.; McCulloch, I.; Ha, C.-S.; Ree, M. *Nat. Mater.* **2006**, *5*, 197.

(7) Li, Y. *Acc. Chem. Res.* **2012**, *45*, 723.

(8) Gross, M. D. C. N. H.-G. U. D. C. K. *Nature* **2000**, *405*, 661.

(9) Gong, X.; Robinson, M. R.; Ostrowski, J. C.; Moses, D.; Bazan, G. C.; Heeger, A. J. *Adv. Mater.* **2002**, *14*, 581.

(10) Janata, J.; Josowicz, M. *Nat. Mater.* **2003**, *2*, 19.

(11) Fan, L.-J.; Jones, W. E. *J. Am. Chem. Soc.* **2006**, *128*, 6784.

(12) Jiang, H.; Taranekar, P.; Reynolds, J. R.; Schanze, K. S. *Angew. Chem. Int. Ed.* **2009**, *48*, 4300.

(13) Duarte, A.; Pu, K.-Y.; Liu, B.; Bazan, G. C. *Chem. Mater.* **2011**, *23*, 501.

(14) Ji, E.; Corbitt, T. S.; Parthasarathy, A.; Schanze, K. S.; Whitten, D. G. *ACS Appl. Mater. Interfaces* **2011**, *3*, 2820.

(15) Pinto, M. R.; Schanze, K. S. *Proc. Natl. Acad. Sci. U. S. A.* **2004**, *101*, 7505.

(16) Keller, J. M.; Schanze, K. S. *Organometallics* **2009**, *28*, 4210.

(17) Ramakrishna, G.; Goodson, T.; Rogers-Haley, J. E.; Cooper, T. M.; McLean, D. G.; Urbas, A. *J. Phys. Chem. C* **2009**, *113*, 1060.

(18) Rogers, J. E.; Slagle, J. E.; Krein, D. M.; Burke, A. R.; Hall, B. C.; Fratini, A.; McLean, D. G.; Fleitz, P. A.; Cooper, T. M.; Drobizhev, M.; Makarov, N. S.; Rebane, A.; Kim, K.-Y.; Farley, R.; Schanze, K. S. *Inorg. Chem.* **2007**, *46*, 6483.

(19) Dubinina, G. G.; Price, R. S.; Abboud, K. A.; Wicks, G.; Wnuk, P.; Stepanenko, Y.; Drobizhev, M.; Rebane, A.; Schanze, K. S. *J. Am. Chem. Soc.* **2012**, *134*, 19346.

(20) Zhou, G.-J.; Wong, W.-Y. *Chem. Soc. Rev.* **2011**, *40*, 2541.

(21) Colombo, A.; Nisic, F.; Dragonetti, C.; Marinotto, D.; Oliveri, I. P.; Righetto, S.; Lobello, M. G.; De Angelis, F. *Chem. Commun.* **2014**, *50*, 7986.

(22) Farinola, G. M.; Ragni, R. *Chem. Soc. Rev.* **2011**, *40*, 3467.

(23) Ren, X.; Alleyne, B. D.; Djurovich, P. I.; Adachi, C.; Tsyba, I.; Bau, R.; Thompson, M. E. *Inorg. Chem.* **2004**, *43*, 1697.

(24) Graham, K. R.; Yang, Y.; Sommer, J. R.; Shelton, A. H.; Schanze, K. S.; Xue, J.; Reynolds, J. R. *Chem. Mater.* **2011**, *23*, 5305.

(25) Mei, J.; Ogawa, K.; Kim, Y.-G.; Heston, N. C.; Arenas, D. J.; Nasrollahi, Z.; McCarley, T. D.; Tanner, D. B.; Reynolds, J. R.; Schanze, K. S. *ACS Appl. Mater. Interfaces* **2009**, *1*, 150.

(26) Wu, P.-T.; Bull, T.; Kim, F. S.; Luscombe, C. K.; Jenekhe, S. A. *Macromolecules* **2009**, *42*, 671.

(27) Liu, L.; Ho, C.-L.; Wong, W.-Y.; Cheung, K.-Y.; Fung, M.-K.; Lam, W.-T.; Djurišić, A. B.; Chan, W.-K. *Adv. Funct. Mater.* **2008**, *18*, 2824.

(28) Göppert-Mayer, M. *Annalen der Physik* **1931**, *401*, 273.

(29) Kaiser, W.; Garrett, C. G. B. *Phys. Rev. Lett.* **1961**, *7*, 229.

(30) He, G. S.; Tan, L.-S.; Zheng, Q.; Prasad, P. N. *Chem. Rev.* **2008**, *108*, 1245.

(31) Picot, A.; D'Aléo, A.; Baldeck, P. L.; Grichine, A.; Duperray, A.; Andraud, C.; Maury, O. *J. Am. Chem. Soc.* **2008**, *130*, 1532.

(32) Krishna, T. R.; Parent, M.; Werts, M. H. V.; Moreaux, L.; Gmouh, S.; Charpak, S.; Caminade, A.-M.; Majoral, J.-P.; Blanchard-Desce, M. *Angew. Chem. Int. Ed.* **2006**, *45*, 4645.

(33) Wang, X.; Nguyen, D. M.; Yanez, C. O.; Rodriguez, L.; Ahn, H.-Y.; Bondar, M. V.; Belfield, K. D. *J. Am. Chem. Soc.* **2010**, *132*, 12237.

(34) Koo, C.-K.; Wong, K.-L.; Man, C. W.-Y.; Lam, Y.-W.; So, L. K.-Y.; Tam, H.-L.; Tsao, S.-W.; Cheah, K.-W.; Lau, K.-C.; Yang, Y.-Y.; Chen, J.-C.; Lam, M. H.-W. *Inorg. Chem.* **2009**, *48*, 872.

(35) Arnbjerg, J.; Jiménez-Banzo, A.; Paterson, M. J.; Nonell, S.; Borrell, J. I.; Christiansen, O.; Ogilby, P. R. *J. Am. Chem. Soc.* **2007**, *129*, 5188.

(36) Velusamy, M.; Shen, J.-Y.; Lin, J. T.; Lin, Y.-C.; Hsieh, C.-C.; Lai, C.-H.; Lai, C.-W.; Ho, M.-L.; Chen, Y.-C.; Chou, P.-T.; Hsiao, J.-K. *Adv. Funct. Mater.* **2009**, *19*, 2388.

(37) Schmitt, J.; Heitz, V.; Sour, A.; Bolze, F.; Ftouni, H.; Nicoud, J.-F.; Flamigni, L.; Ventura, B. *Angew. Chem. Int. Ed.* **2015**, *54*, 169.

(38) Hammerer, F.; Garcia, G.; Chen, S.; Poyer, F.; Achelle, S.; Fiorini-Debuisschert, C.; Teulade-Fichou, M.-P.; Maillard, P. *J.Org.Chem.* **2014**, *79*, 1406.

(39) W. Spangler, C. *J. Mater. Chem.* **1999**, *9*, 2013.

(40) Lin, T.-C.; Chen, Y.-F.; Hu, C.-L.; Hsu, C.-S. *J. Mater. Chem.* **2009**, *19*, 7075.

(41) Cumpston, B. H.; Ananthavel, S. P.; Barlow, S.; Dyer, D. L.; Ehrlich, J. E.; Erskine, L. L.; Heikal, A. A.; Kuebler, S. M.; Lee, I. Y. S.; McCord-Maughon, D.; Qin, J.; Rockel, H.; Rumi, M.; Wu, X.-L.; Marder, S. R.; Perry, J. W. *Nature* **1999**, *398*, 51.

(42) Strickler, J. H.; Webb, W. W. *Opt. Lett.* **1991**, *16*, 1780.

(43) Sun, H.-B.; Matsuo, S.; Misawa, H. *Appl. Phys. Lett.* **1999**, *74*, 786.

(44) Pucher, N.; Rosspeintner, A.; Satzinger, V.; Schmidt, V.; Gescheidt, G.; Stampfl, J.; Liska, R. *Macromolecules* **2009**, *42*, 6519.

(45) Lu, Y.; Hasegawa, F.; Goto, T.; Ohkuma, S.; Fukuhara, S.; Kawazu, Y.; Totani, K.; Yamashita, T.; Watanabe, T. *J. Mater. Chem.* **2004**, *14*, 75.

(46) Álvarez, M.; Best, A.; Unger, A.; Alonso, J. M.; del Campo, A.; Schmelzeisen, M.; Koynov, K.; Kreiter, M. *Adv. Funct. Mater.* **2010**, *20*, 4265.

(47) Sutherland, R. L.; Brant, M. C.; Heinrichs, J.; Rogers, J. E.; Slagle, J. E.; McLean, D. G.; Fleitz, P. A. *J. Opt. Soc. Am. B* **2005**, *22*, 1939.

(48) Silly, M. G.; Porrès, L.; Mongin, O.; Chollet, P.-A.; Blanchard-Desce, M. *Chem. Phys. Lett.* **2003**, *379*, 74.

(49) Liao, C.; Shelton, A. H.; Kim, K.-Y.; Schanze, K. S. *ACS Appl. Mater. Interfaces* **2011**, *3*, 3225.

(50) Sonogashira, K.; Fujikura, Y.; Yatake, T.; Toyoshima, N.; Takahashi, S.; Hagihara, N. *J. Organomet. Chem.* **1978**, *145*, 101.

(51) D'Amato, R.; Furlani, A.; Colapietro, M.; Portalone, G.; Casalboni, M.; Falconieri, M.; Russo, M. V. *J. Organomet. Chem.* **2001**, *627*, 13.

(52) Liu, Y.; Jiang, S.; Glusac, K.; Powell, D. H.; Anderson, D. F.; Schanze, K. S. *J. Am. Chem. Soc.* **2002**, *124*, 12412.

(53) Williams, J. A. G. In *Photochemistry and Photophysics of Coordination Compounds II*; Balzani, V., Campagna, S., Eds.; Springer Berlin Heidelberg: 2007; Vol. 281, p 205.

(54) Frapper, G.; Kertesz, M. *Inorg. Chem.* **1993**, *32*, 732.

(55) Sacksteder, L.; Baralt, E.; DeGraff, B. A.; Lukehart, C. M.; Demas, J. N. *Inorg. Chem.* **1991**, *30*, 2468.

(56) Wilson, J. S.; Köhler, A.; Friend, R. H.; Al-Suti, M. K.; Al-Mandhary, M. R. A.; Khan, M. S.; Raithby, P. R. *J. Chem. Phys.* **2000**, *113*, 7627.

(57) Schull, T. L.; Kushmerick, J. G.; Patterson, C. H.; George, C.; Moore, M. H.; Pollack, S. K.; Shashidhar, R. *J. Am. Chem. Soc.* **2003**, *125*, 3202.

(58) Jones, S. C.; Coropceanu, V.; Barlow, S.; Kinnibrugh, T.; Timofeeva, T.; Brédas, J.-L.; Marder, S. R. *J. Am. Chem. Soc.* **2004**, *126*, 11782.

(59) Glimsdal, E.; Carlsson, M.; Eliasson, B.; Minaev, B.; Lindgren, M. *J. Phys. Chem. A* **2007**, *111*, 244.

(60) Kim, K.-Y.; Shelton, A. H.; Drobizhev, M.; Makarov, N.; Rebane, A.; Schanze, K. S. *J. Phys. Chem. A* **2010**, *114*, 7003.

(61) Price, R. S.; Dubinina, G.; Wicks, G.; Drobizhev, M.; Rebane, A.; Schanze, K. S. *ACS Appl. Mater. Interfaces* **2015**.

(62) Tang, C. W. *Appl. Phys. Lett.* **1986**, *48*, 183.

(63) Jenekhe, S. A.; Yi, S. *Appl. Phys. Lett.* **2000**, *77*, 2635.

(64) Stevens, D. M.; Qin, Y.; Hillmyer, M. A.; Frisbie, C. D. *J. Phys. Chem. C* **2009**, *113*, 11408.

(65) Wong, W. Y.; Ho, C. L. *Acc. Chem. Res.* **2010**, *43*, 1246.

(66) Scholes, G. D.; Rumbles, G. *Nat. Mater.* **2006**, *5*, 683.

(67) Gélinas, S.; Paré-Labrosse, O.; Brosseau, C.-N.; Albert-Seifried, S.; McNeill, C. R.; Kirov, K. R.; Howard, I. A.; Leonelli, R.; Friend, R. H.; Silva, C. *J. Phys. Chem. C* **2011**, *115*, 7114.

(68) Guo, F.; Kim, Y.-G.; Reynolds, J. R.; Schanze, K. S. *Chem. Commun.* **2006**, 1887.

(69) Köhler, A.; Wilson, J. S.; Friend, R. H.; Al-Suti, M. K.; Khan, M. S.; Gerhard, A.; Bässler, H. *J. Chem. Phys.* **2002**, *116*, 9457.

(70) Köhler, A.; Wittmann, H. F.; Friend, R. H.; Khan, M. S.; Lewis, J. *Synth. Met.* **1996**, *77*, 147.

(71) Shao, Y.; Yang, Y. *Adv. Mater.* **2005**, *17*, 2841.

(72) Yang, C.-M.; Wu, C.-H.; Liao, H.-H.; Lai, K.-Y.; Cheng, H.-P.; Horng, S.-F.; Meng, H.-F.; Shy, J.-T. *Appl. Phys. Lett.* **2007**, *90*, 133509.

(73) Schulz, G. L.; Holdcroft, S. *Chem. Mater.* **2008**, *20*, 5351.

(74) Zhao, X.; Piliego, C.; Kim, B.; Poulsen, D. A.; Ma, B.; Unruh, D. A.; Fréchet, J. M. J. *Chem. Mater.* **2010**, *22*, 2325.

(75) Baek, N. S.; Hau, S. K.; Yip, H.-L.; Acton, O.; Chen, K.-S.; Jen, A. K. Y. *Chem. Mater.* **2008**, *20*, 5734.

(76) Liao, C.-Y.; Chen, C.-P.; Chang, C.-C.; Hwang, G.-W.; Chou, H.-H.; Cheng, C.-H. *Sol. Energy Mater. Sol. Cells* **2013**, *109*, 111.

(77) Yun, M. H.; Lee, E.; Lee, W.; Choi, H.; Lee, B. R.; Song, M. H.; Hong, J.-I.; Kwon, T.-H.; Kim, J. Y. *J. Mater. Chem. C* **2014**, *2*, 10195.

(78) Colombo, A.; Dragonetti, C.; Roberto, D.; Ugo, R.; Falciola, L.; Luzzati, S.; Kotowski, D. *Organometallics* **2011**, *30*, 1279.

(79) Zhen, H.; Hou, Q.; Li, K.; Ma, Z.; Fabiano, S.; Gao, F.; Zhang, F. *J. Mater. Chem. A* **2014**, *2*, 12390.

(80) Bertrand, G. H. V.; Tortech, L.; Gandon, V.; Aubert, C.; Fichou, D. *Chem. Commun.* **2014**, *50*, 8663.

(81) Lai, S.-L.; Wang, L.; Yang, C.; Chan, M.-Y.; Guan, X.; Kwok, C.-C.; Che, C.-M. *Adv. Funct. Mater.* **2014**, *24*, 4655.

(82) Qian, M.; Zhang, R.; Hao, J.; Zhang, W.; Zhang, Q.; Wang, J.; Tao, Y.; Chen, S.; Fang, J.; Huang, W. *Adv. Mater.* **2015**, n/a.

(83) Westlund, R.; Malmström, E.; Lopes, C.; Öhgren, J.; Rodgers, T.; Saito, Y.; Kawata, S.; Glimsdal, E.; Lindgren, M. *Adv. Funct. Mater.* **2008**, *18*, 1939.

(84) Tang, C.; Zheng, Q.; Zhu, H.; Wang, L.; Chen, S.-C.; Ma, E.; Chen, X. *J. Mater. Chem. C* **2013**, *1*, 1771.

(85) Belfield, K. D.; Bondar, M. V.; Hernandez, F. E.; Przhonska, O. V. *J. Phys. Chem. C* **2008**, *112*, 5618.

(86) Kim, S.; Ohulchanskyy, T. Y.; Pudavar, H. E.; Pandey, R. K.; Prasad, P. N. *J. Am. Chem. Soc.* **2007**, *129*, 2669.

(87) Denk, W.; Strickler, J.; Webb, W. *Science* **1990**, *248*, 73.

(88) PARTHENOPOULOS, D. A.; RENTZEPIS, P. M. *Science* **1989**, *245*, 843.

(89) Long, N. J. *Angew. Chem. Int. Ed.* **1995**, *34*, 21.

(90) Haley, J. E.; Krein, D. M.; Monahan, J. L.; Burke, A. R.; McLean, D. G.; Slagle, J. E.; Fratini, A.; Cooper, T. M. *J. Phys. Chem. A* **2011**, *115*, 265.

(91) Nguyen, K. A.; Day, P. N.; Pachter, R. *J. Phys. Chem. A* **2009**, *113*, 13943.

(92) McEwan, K.; Lewis, K.; Yang, G. Y.; Chng, L. L.; Lee, Y. W.; Lau, W. P.; Lai, K. S. *Adv. Funct. Mater.* **2003**, *13*, 863.

(93) Wen, T. C.; Tsai, C. Y. *Chem. Phys. Lett.* **1999**, *311*, 173.

(94) Humphrey, J. L.; Kuciauskas, D. *J. Am. Chem. Soc.* **2006**, *128*, 3902.

(95) Screen, T. E. O.; Thorne, J. R. G.; Denning, R. G.; Bucknall, D. G.; Anderson, H. L. *J. Mater. Chem.* **2003**, *13*, 2796.

(96) Perry, J. W.; Alvarez, D.; Choong, I.; Mansour, K.; Marder, S. R.; Perry, K. J. *Opt. Lett.* **1994**, *19*, 625.

(97) Swain, D.; Singh, R.; Singh, V. K.; Krishna, N. V.; Giribabu, L.; Rao, S. V. *J. Mater. Chem. C* **2014**, *2*, 1711.

(98) Wang, B. S.; Wang, J.; Chen, J.-Y. *J. Mater. Chem. C.* **2014**, *2*, 1594.

(99) Liu, R.; Chen, H.; Chang, J.; Li, Y.; Zhu, H.; Sun, W. *Dalton Trans.* **2013**, *42*, 160.

(100) Aly, S. M.; Ho, C.-L.; Wong, W.-Y.; Fortin, D.; Harvey, P. D. *Macromolecules* **2009**, *42*, 6902.

(101) Ho, C.-L.; Chui, C.-H.; Wong, W.-Y.; Aly, S. M.; Fortin, D.; Harvey, P. D.; Yao, B.; Xie, Z.; Wang, L. *Macromol. Chem. Phys.* **2009**, *210*, 1786.

(102) Zhou, G.-J.; Wong, W.-Y.; Cui, D.; Ye, C. *Chem. Mater.* **2005**, *17*, 5209.

(103) Tao, C.-H.; Yang, H.; Zhu, N.; Yam, V. W.-W.; Xu, S.-J. *Organometallics* **2008**, *27*, 5453.

(104) Tacca, A.; Po, R.; Caldararo, M.; Chiaberge, S.; Gila, L.; Longo, L.; Mussini, P. R.; Pellegrino, A.; Perin, N.; Salvalaggio, M.; Savoini, A.; Spera, S. *Electrochim. Acta* **2011**, *56*, 6638.

(105) Lu, W.; Kwok, W.-M.; Ma, C.; Chan, C. T.-L.; Zhu, M.-X.; Che, C.-M. *J. Am. Chem. Soc.* **2011**, *133*, 14120.

(106) Ma, C.; Chan, C. T.-L.; Kwok, W.-M.; Che, C.-M. *Chem. Sci.* **2012**, *3*, 1883.

(107) Tong, G. S. M.; Chow, P. K.; Che, C.-M. *Angew. Chem. Int. Ed.* **2010**, *49*, 9206.

(108) Chao, H.-Y.; Lu, W.; Li, Y.; Chan, M. C. W.; Che, C.-M.; Cheung, K.-K.; Zhu, N. *J. Am. Chem. Soc.* **2002**, *124*, 14696.

(109) Wong, W.-Y.; Liu, L.; Poon, S.-Y.; Choi, K.-H.; Cheah, K.-W.; Shi, J.-X. *Macromolecules* **2004**, *37*, 4496.

(110) Kato, S.-i.; Shimizu, S.; Taguchi, H.; Kobayashi, A.; Tobita, S.; Nakamura, Y. *J.Org.Chem.* **2012**, *77*, 3222.

(111) Parthasarathy, A.; Goswami, S.; Corbitt, T. S.; Ji, E.; Dascier, D.; Whitten, D. G.; Schanze, K. S. *ACS Appl. Mater. Interfaces* **2013**, *5*, 4516.

(112) Terenziani, F.; Painelli, A.; Katan, C.; Charlot, M.; Blanchard-Desce, M. *J. Am. Chem. Soc.* **2006**, *128*, 15742.

(113) Makarov, N. S.; Drobizhev, M.; Rebane, A. *Opt. Express* **2008**, *16*, 4029.

(114) Rebane, A.; Drobizhev, M.; Makarov, N. S.; Wicks, G.; Wnuk, P.; Stepanenko, Y.; Haley, J. E.; Krein, D. M.; Fore, J. L.; Burke, A. R.; Slagle, J. E.; McLean, D. G.; Cooper, T. M. *J. Phys. Chem. A* **2014**, *118*, 3749.

(115) Sheik-Bahae, M.; Said, A. A.; Wei, T. H.; Hagan, D. J.; Van Stryland, E. W. *Quantum Electronics, IEEE Journal of* **1990**, *26*, 760.

(116) Oulianov, D. A.; Tomov, I. V.; Dvornikov, A. S.; Rentzepis, P. M. *Opt. Commun.* **2001**, *191*, 235.

(117) Promarak, V.; Ruchirawat, S. *Tetrahedron* **2007**, *63*, 1602.

(118) Cardolaccia, T.; Funston, A. M.; Kose, M. E.; Keller, J. M.; Miller, J. R.; Schanze, K. S. *J. Phys. Chem. B* **2007**, *111*, 10871.

(119) Baldo, M. A.; O'Brien, D. F.; You, Y.; Shoustikov, A.; Sibley, S.; Thompson, M. E.; Forrest, S. R. *Nature* **1998**, *395*, 151.

(120) Giridhar, T.; Saravanan, C.; Cho, W.; Park, Y. G.; Lee, J. Y.; Jin, S.-H. *Chem. Commun.* **2014**, *50*, 4000.

(121) Rausch, A. F.; Murphy, L.; Williams, J. A. G.; Yersin, H. *Inorg. Chem.* **2011**, *51*, 312.

(122) Yi, J.; Zhang, B.; Shao, P.; Li, Y.; Sun, W. *J. Phys. Chem. A* **2010**, *114*, 7055.

(123) Hrobárik, P.; Hrobáriková, V.; Semak, V.; Kasák, P.; Rakovský, E.; Polyzos, I.; Fakis, M.; Persephonis, P. *Org. Lett.* **2014**, *16*, 6358.

(124) Purc, A.; Sobczyk, K.; Sakagami, Y.; Ando, A.; Kamada, K.; Gryko, D. T. *J. Mater. Chem. C* **2015**, *3*, 742.

(125) Gao, Y.; Qu, Y.; Jiang, T.; Zhang, H.; He, N.; Li, B.; Wu, J.; Hua, J. *J. Mater. Chem. C* **2014**, *2*, 6353.

(126) Ellinger, S.; Graham, K. R.; Shi, P.; Farley, R. T.; Steckler, T. T.; Brookins, R. N.; Taranekar, P.; Mei, J.; Padilha, L. A.; Ensley, T. R.; Hu, H.; Webster, S.; Hagan, D. J.; Van Stryland, E. W.; Schanze, K. S.; Reynolds, J. R. *Chem. Mater.* **2011**, *23*, 3805.

(127) Grelaud, G.; Cifuentes, M. P.; Paul, F.; Humphrey, M. G. *J. Organomet. Chem.* **2014**, *751*, 181.

(128) Goswami, S.; Wicks, G.; Rebane, A.; Schanze, K. S. *Dalton Trans.* **2014**, *43*, 17721.

(129) Pomestchenko, I. E.; Polyansky, D. E.; Castellano, F. N. *Inorg. Chem.* **2005**, *44*, 3412.

(130) Shang, H.; Fan, H.; Liu, Y.; Hu, W.; Li, Y.; Zhan, X. *Adv. Mater.* **2011**, *23*, 1554.

(131) Li, P.; Ahrens, B.; Bond, A. D.; Davies, J. E.; Koentjoro, O. F.; Raithby, P. R.; Teat, S. J. *Dalton Trans.* **2008**, 1635.

(132) Pina, J.; de Melo, J. S.; Breusov, D.; Scherf, U. *PCCP* **2013**, *15*, 15204.

(133) Karunakaran, V.; Prabhu, D. D.; Das, S.; Varughese, S. *PCCP* **2015**.

(134) Xu, C.; Webb, W. W. *J. Opt. Soc. Am. B* **1996**, *13*, 481.

(135) Barzoukas, M.; Blanchard-Desce, M. *J. Chem. Phys.* **2000**, *113*, 3951.

(136) Rebane, A.; Drobizhev, M.; Makarov, N. S.; Beuerman, E.; Haley, J. E.; Krein, D. M.; Burke, A. R.; Flikkema, J. L.; Cooper, T. M. *J. Phys. Chem. A* **2011**, *115*, 4255.

(137) Whittall, I. R.; Humphrey, M. G.; Samoc, M.; Luther-Davies, B. *Angew. Chem. Int. Ed.* **1997**, *36*, 370.

(138) Hu, Q. Y.; Lu, W. X.; Tang, H. D.; Sung, H. H. Y.; Wen, T. B.; Williams, I. D.; Wong, G. K. L.; Lin, Z.; Jia, G. *Organometallics* **2005**, *24*, 3966.

(139) Raubenheimer, H. G.; Schmidbaur, H. *Organometallics* **2011**, *31*, 2507.

(140) Li, J.-C.; Lee, H.-Y.; Lee, S.-H.; Zong, K.; Jin, S.-H.; Lee, Y.-S. *Synth. Met.* **2009**, *159*, 201.

(141) Haskins-Glusac, K.; Pinto, M. R.; Tan, C.; Schanze, K. S. *J. Am. Chem. Soc.* **2004**, *126*, 14964.

(142) Lin, T.-C.; Liu, C.-Y.; Li, M.-H.; Liu, Y.-Y.; Tseng, S.-Y.; Wang, Y.-T.; Tseng, Y.-H.; Chu, H.-H.; Luo, C.-W. *J. Mater. Chem. C* **2014**, *2*, 821.

(143) Dvornikov, A. S.; Walker, E. P.; Rentzepis, P. M. *J. Phys. Chem. A* **2009**, *113*, 13633.

(144) Pudavar, H. E.; Joshi, M. P.; Prasad, P. N.; Reinhardt, B. A. *Appl. Phys. Lett.* **1999**, *74*, 1338.

(145) Day, D.; Gu, M.; Smallridge, A. *Opt. Lett.* **1999**, *24*, 948.

(146) Wu, C.; Szymanski, C.; Cain, Z.; McNeill, J. *J. Am. Chem. Soc.* **2007**, *129*, 12904.

(147) Chateau, D.; Chaput, F.; Lopes, C.; Lindgren, M.; Brännlund, C.; Öhgren, J.; Djourelov, N.; Nedelec, P.; Desroches, C.; Eliasson, B.; Kindahl, T.; Lerouge, F.; Andraud, C.; Parola, S. *ACS Appl. Mater. Interfaces* **2012**, *4*, 2369.

(148) Zieba, R.; Desroches, C.; Chaput, F.; Carlsson, M.; Eliasson, B.; Lopes, C.; Lindgren, M.; Parola, S. *Adv. Funct. Mater.* **2009**, *19*, 235.

(149) Shelton, A. H.; Price, R. S.; Brokmann, L.; Dettlaff, B.; Schanze, K. S. *ACS Appl. Mater. Interfaces* **2013**, *5*, 7867.

(150) Fox, R. B.; Cozzens, R. F. *Macromolecules* **1969**, *2*, 181.

(151) Breul, A. M.; Schäfer, J.; Pavlov, G. M.; Teichler, A.; Höppener, S.; Weber, C.; Nowotny, J.; Blankenburg, L.; Popp, J.; Hager, M. D.; Dietzek, B.; Schubert, U. S. *J. Polym. Sci., Part A: Polym. Chem.* **2012**, *50*, 3192.

(152) Chen, Z.; Grumstrup, E. M.; Gilligan, A. T.; Papanikolas, J. M.; Schanze, K. S. *J. Phys. Chem. B* **2014**, *118*, 372.

(153) Chen, Z.; Hsu, H.-Y.; Arca, M.; Schanze, K. S. *J. Phys. Chem. B* **2014**.

(154) Chen, Z.; Grumstrup, E. M.; Gilligan, A. T.; Papanikolas, J. M.; Schanze, K. S. *J. Phys. Chem. B* **2014**, *118*, 372.

(155) Liao, C.; Yarnell, J. E.; Glusac, K. D.; Schanze, K. S. *J. Phys. Chem. B* **2010**, *114*, 14763.

(156) Goswami, S.; Winkel, R. W.; Alarousu, E.; Ghiviriga, I.; Mohammed, O. F.; Schanze, K. S. *J. Phys. Chem. A* **2014**, *118*, 11735.

(157) Qu, S.; Tian, H. *Chem. Commun.* **2012**, *48*, 3039.

(158) Robb, M. J.; Ku, S.-Y.; Brunetti, F. G.; Hawker, C. J. *J. Polym. Sci., Part A: Polym. Chem.* **2013**, *51*, 1263.

(159) Wu, Y.; Zhu, W. *Chem. Soc. Rev.* **2013**, *42*, 2039.

(160) Kanimozhi, C.; Yaacobi-Gross, N.; Chou, K. W.; Amassian, A.; Anthopoulos, T. D.; Patil, S. *J. Am. Chem. Soc.* **2012**, *134*, 16532.

(161) Cheng, C.; Yu, C.; Guo, Y.; Chen, H.; Fang, Y.; Yu, G.; Liu, Y. *Chem. Commun.* **2013**, *49*, 1998.

(162) Farnum, D. G.; Mehta, G.; Moore, G. G. I.; Siegal, F. P. *Tetrahedron Lett.* **1974**, *15*, 2549.

(163) Naik, M. A.; Patil, S. *J. Polym. Sci., Part A: Polym. Chem.* **2013**, *51*, 4241.

(164) Chandran, D.; Lee, K.-S. *Macromol. Res.* **2013**, *21*, 272.

(165) Tamayo, A. B.; Tantiwiwat, M.; Walker, B.; Nguyen, T.-Q. *J. Phys. Chem. C* **2008**, *112*, 15543.

(166) Dhar, J.; Venkatramaiah, N.; A, A.; Patil, S. *J. Mater. Chem. C* **2014**, *2*, 3457.

(167) Sonar, P.; Singh, S. P.; Williams, E. L.; Li, Y.; Soh, M. S.; Dodabalapur, A. *J. Mater. Chem.* **2012**, *22*, 4425.

(168) Hendsbee, A. D.; Sun, J.-P.; Rutledge, L. R.; Hill, I. G.; Welch, G. C. *J. Mater. Chem. A* **2014**, *2*, 4198.

(169) McCusker, C. E.; Hablot, D.; Ziessel, R.; Castellano, F. N. *Inorg. Chem.* **2012**, *51*, 7957.

(170) Brooks, J.; Babayan, Y.; Lamansky, S.; Djurovich, P. I.; Tsyba, I.; Bau, R.; Thompson, M. E. *Inorg. Chem.* **2002**, *41*, 3055.

(171) Glusac, K.; Köse, M. E.; Jiang, H.; Schanze, K. S. *J. Phys. Chem. B* **2007**, *111*, 929.

(172) Hirani, B.; Li, J.; Djurovich, P. I.; Yousufuddin, M.; Oxgaard, J.; Persson, P.; Wilson, S. R.; Bau, R.; Goddard, W. A.; Thompson, M. E. *Inorg. Chem.* **2007**, *46*, 3865.

(173) Liao, C.; Shelton, A. H.; Kim, K.-Y.; Schanze, K. S. *ACS Appl. Mater. Interfaces* **2011**, *3*, 3225.

(174) Adachi, C.; Baldo, M. A.; Thompson, M. E.; Forrest, S. R. *Journal of Applied Physics* **2001**, *90*, 5048.

(175) Gareth Williams, J. A.; Develay, S.; Rochester, D. L.; Murphy, L. *Coord. Chem. Rev.* **2008**, *252*, 2596.

(176) Langhals, H.; Limmert, M.; Lorenz, I.-P.; Mayer, P.; Piotrowski, H.; Polborn, K. *Eur. J. Inorg. Chem.* **2000**, *2000*, 2345.

(177) Beljonne, D.; Wittmann, H. F.; Köhler, A.; Graham, S.; Younus, M.; Lewis, J.; Raithby, P. R.; Khan, M. S.; Friend, R. H.; Bredas, J. L. *J. Chem. Phys.* **1996**, *105*, 3868.

(178) Rogers, J. E.; Cooper, T. M.; Fleitz, P. A.; Glass, D. J.; McLean, D. G. *J. Phys. Chem. A* **2002**, *106*, 10108.

(179) Liu, Y.; Jiang, S.; Glusac, K.; Powell, D. H.; Anderson, D. F.; Schanze, K. S. *J. Am. Chem. Soc.* **2002**, *124*, 12412.

(180) Liu, Y.; Li, Y.; Schanze, K. S. *J. Photochem. Photobiol. C: Photochem. Rev.* **2002**, *3*, 1.

(181) Silverman, E. E.; Cardolaccia, T.; Zhao, X. M.; Kim, K. Y.; Haskins-Glusac, K.; Schanze, K. S. *Coord. Chem. Rev.* **2005**, *249*, 1491.

(182) Kim, K. Y.; Liu, S. X.; Kose, M. E.; Schanze, K. S. *Inorg. Chem.* **2006**, *45*, 2509.

(183) Rogers, J. E.; Slagle, J. E.; Krein, D. M.; Burke, A. R.; Hall, B. C.; Fratini, A.; McLean, D. G.; Fleitz, P. A.; Cooper, T. M.; Drobizhev, M.; Makarov, N. S.; Rebane, A.; Kim, K. Y.; Farley, R.; Schanze, K. S. *Inorg. Chem.* **2007**, *46*, 6483.

(184) Ramakrishna, G.; Goodson, T.; Rogers-Haley, J. E.; Cooper, T. M.; McLean, D. G.; Urbas, A. *J. Phys. Chem. C* **2008**, *113*, 1060.

(185) Wilson, J. S.; Chawdhury, N.; Al-Mandhary, M. R. A.; Younus, M.; Khan, M. S.; Raithby, P. R.; Köhler, A.; Friend, R. H. *J. Am. Chem. Soc.* **2001**, *123*, 9412.

(186) Wong, W. Y. *Dalton Trans.* **2007**, 4495.

(187) Wong, W. Y.; Wang, X. Z.; He, Z.; Djurisic, A. B.; Yip, C. T.; Cheung, K. Y.; Wang, H.; Mak, C. S. K.; Chan, W. K. *Nature Mater.* **2007**, *6*, 521.

(188) Clem, T. A.; Kavulak, D. F. J.; Westling, E. J.; Fréchet, J. M. J. *Chem. Mater.* **2009**, *22*, 1977.

(189) Thomas Iii, S. W.; Yagi, S.; Swager, T. M. *J. Mater. Chem.* **2005**, *15*, 2829.

(190) Aly, S. M.; Goswami, S.; Alsulami, Q. A.; Schanze, K. S.; Mohammed, O. F. *J. Phys. Chem. Lett.* **2014**, *5*, 3386.

(191) Gevaerts, V. S.; Herzig, E. M.; Kirkus, M.; Hendriks, K. H.; Wienk, M. M.; Perlich, J.; Müller-Buschbaum, P.; Janssen, R. A. J. *Chem. Mater.* **2013**, *26*, 916.

(192) Dou, L.; You, J.; Yang, J.; Chen, C.-C.; He, Y.; Murase, S.; Moriarty, T.; Emery, K.; Li, G.; Yang, Y. *Nat Photon* **2012**, *6*, 180.

(193) Mohebbi, A. R.; Yuen, J.; Fan, J.; Munoz, C.; Wang, M. f.; Shirazi, R. S.; Seifter, J.; Wudl, F. *Adv. Mater.* **2011**, *23*, 4644.

(194) Cooper, T. M.; Blaudeau, J. P.; Hall, B. C.; Rogers, J. E.; McLean, D. G.; Liu, Y. L.; Toscano, J. P. *Chem. Phys. Lett.* **2004**, *400*, 239.

(195) Sheng, C. X.; Singh, S.; Gambetta, A.; Drori, T.; Tong, M.; Tretiak, S.; Vardeny, Z. V. *Sci. Rep.* **2013**, *3*.

(196) Batista, E. R.; Martin, R. L. *J. Phys. Chem. A* **2005**, *109*, 9856.

(197) Patil, A. O.; Heeger, A. J.; Wudl, F. *Chem. Rev.* **1988**, *88*, 183.

(198) Frisch, M. J.; Trucks, G. W.; Schlegel, H. B.; Scuseria, G. E.; Robb, M. A.; Cheeseman, J. R.; Scalmani, G.; Barone, V.; Mennucci, B.; Petersson, G. A.; Nakatsuji, H.; Caricato, M.; Li, X.; Hratchian, H. P.; Izmaylov, A. F.; Bloino, J.; Zheng, G.; Sonnenberg, J. L.; Hada, M.; Ehara, M.; Toyota, K.; Fukuda, R.; Hasegawa, J.; Ishida, M.; Nakajima, T.; Honda, Y.; Kitao, O.; Nakai, H.; Vreven, T.; Montgomery Jr., J. A.; Peralta, J. E.; Ogliaro, F.; Bearpark, M. J.; Heyd, J.; Brothers, E. N.; Kudin, K. N.; Staroverov, V. N.; Kobayashi, R.; Normand, J.; Raghavachari, K.; Rendell, A. P.; Burant, J. C.; Iyengar, S. S.; Tomasi, J.; Cossi, M.; Rega, N.; Millam, N. J.; Klene, M.; Knox, J. E.; Cross, J. B.; Bakken, V.; Adamo, C.; Jaramillo, J.; Gomperts, R.; Stratmann, R. E.; Yazyev, O.; Austin, A. J.; Cammi, R.; Pomelli, C.; Ochterski, J. W.; Martin, R. L.; Morokuma, K.; Zakrzewski, V. G.; Voth, G. A.; Salvador, P.; Dannenberg, J. J.; Dapprich, S.; Daniels, A. D.; Farkas, Ö.; Foresman, J. B.; Ortiz, J. V.; Cioslowski, J.; Fox, D. J.; Gaussian, Inc.: Wallingford, CT, USA, 2009.

(199) Zhurko, G. A. 2012; Vol. 2012.

(200) Zhang, G.; Fu, Y.; Xie, Z.; Zhang, Q. *Solar Energy Materials and Solar Cells* **2011**, *95*, 1168.

(201) Huo, L.; Hou, J.; Chen, H.-Y.; Zhang, S.; Jiang, Y.; Chen, T. L.; Yang, Y. *Macromolecules* **2009**, *42*, 6564.

(202) Letizia, J. A.; Salata, M. R.; Tribout, C. M.; Facchetti, A.; Ratner, M. A.; Marks, T. J. *J. Am. Chem. Soc.* **2008**, *130*, 9679.

(203) Aly, S. M.; Goswami, S.; Alsulami, Q. A.; Schanze, K. S.; Mohammed, O. F. *J. Phys. Chem. Lett* **2014**, *5*, 3386.

(204) Bijleveld, J. C.; Gevaerts, V. S.; Di Nuzzo, D.; Turbiez, M.; Mathijssen, S. G. J.; de Leeuw, D. M.; Wienk, M. M.; Janssen, R. A. J. *Adv. Mater.* **2010**, *22*, E242.

(205) Li, W.; Furlan, A.; Roelofs, W. S. C.; Hendriks, K. H.; van Pruissen, G. W. P.; Wienk, M. M.; Janssen, R. A. J. *Chem. Commun.* **2014**, *50*, 679.

(206) Chen, G.; Sasabe, H.; Wang, Z.; Wang, X.-F.; Hong, Z.; Yang, Y.; Kido, J. *Adv. Mater.* **2012**, *24*, 2768.

(207) Chen, G.; Sasabe, H.; Wang, Z.; Wang, X.; Hong, Z.; Kido, J.; Yang, Y. *PCCP* **2012**, *14*, 14661.

(208) Lee, O. P.; Yiu, A. T.; Beaujuge, P. M.; Woo, C. H.; Holcombe, T. W.; Millstone, J. E.; Douglas, J. D.; Chen, M. S.; Fréchet, J. M. J. *Adv. Mater.* **2011**, *23*, 5359.

(209) Bürckstümmer, H.; Weissenstein, A.; Bialas, D.; Würthner, F. *J.Org.Chem.* **2011**, *76*, 2426.

(210) Li, G.; Zhu, R.; Yang, Y. *Nat Photon* **2012**, *6*, 153.

(211) Dou, L.; Gao, J.; Richard, E.; You, J.; Chen, C.-C.; Cha, K. C.; He, Y.; Li, G.; Yang, Y. *J. Am. Chem. Soc.* **2012**, *134*, 10071.

(212) Yuen, J. D.; Wudl, F. *Energy & Environmental Science* **2013**, *6*, 392.

(213) Patel, D. G.; Feng, F.; Ohnishi, Y.-y.; Abboud, K. A.; Hirata, S.; Schanze, K. S.; Reynolds, J. R. *J. Am. Chem. Soc.* **2012**, *134*, 2599.

(214) You, J.; Dou, L.; Yoshimura, K.; Kato, T.; Ohya, K.; Moriarty, T.; Emery, K.; Chen, C.-C.; Gao, J.; Li, G.; Yang, Y. *Nat Commun* **2013**, *4*, 1446.

(215) Park, S. H.; Roy, A.; Beaupre, S.; Cho, S.; Coates, N.; Moon, J. S.; Moses, D.; Leclerc, M.; Lee, K.; Heeger, A. J. *Nat Photon* **2009**, *3*, 297.

(216) Hou, J.; Chen, H.-Y.; Zhang, S.; Li, G.; Yang, Y. *J. Am. Chem. Soc.* **2008**, *130*, 16144.

(217) Blouin, N.; Michaud, A.; Leclerc, M. *Adv. Mater.* **2007**, *19*, 2295.

(218) Bronstein, H.; Chen, Z.; Ashraf, R. S.; Zhang, W.; Du, J.; Durrant, J. R.; Shakya Tuladhar, P.; Song, K.; Watkins, S. E.; Geerts, Y.; Wienk, M. M.; Janssen, R. A. J.; Anthopoulos, T.; Sirringhaus, H.; Heeney, M.; McCulloch, I. *J. Am. Chem. Soc.* **2011**, *133*, 3272.

(219) Bijleveld, J. C.; Zoombelt, A. P.; Mathijssen, S. G. J.; Wienk, M. M.; Turbiez, M.; de Leeuw, D. M.; Janssen, R. A. J. *J. Am. Chem. Soc.* **2009**, *131*, 16616.

(220) Zhou, E.; Yamakawa, S.; Tajima, K.; Yang, C.; Hashimoto, K. *Chem. Mater.* **2009**, *21*, 4055.

(221) Schubert, M.; Dolfen, D.; Frisch, J.; Roland, S.; Steyrleuthner, R.; Stiller, B.; Chen, Z.; Scherf, U.; Koch, N.; Facchetti, A.; Neher, D. *Adv. Energy Mater.* **2012**, *2*, 369.

(222) Wang, E.; Mammo, W.; Andersson, M. R. *Adv. Mater.* **2014**, *26*, 1801.

(223) Papageorgiou, C.; Borer, X. *Helv. Chim. Acta* **1988**, *71*, 1079.

(224) Mei, J.; Graham, K. R.; Stalder, R.; Reynolds, J. R. *Org. Lett.* **2010**, *12*, 660.

(225) Wang, E.; Ma, Z.; Zhang, Z.; Vandewal, K.; Henriksson, P.; Inganäs, O.; Zhang, F.; Andersson, M. R. *J. Am. Chem. Soc.* **2011**, *133*, 14244.

(226) Mei, J.; Kim, D. H.; Ayzner, A. L.; Toney, M. F.; Bao, Z. *J. Am. Chem. Soc.* **2011**, *133*, 20130.

(227) Stalder, R.; Mei, J.; Subbiah, J.; Grand, C.; Estrada, L. A.; So, F.; Reynolds, J. R. *Macromolecules* **2011**, *44*, 6303.

(228) Grellmann, K. H.; Hentzschel, P. *Chem. Phys. Lett.* **1978**, *53*, 545.

(229) Karstens, T.; Kobs, K.; Memming, R. *Berichte der Bunsengesellschaft für physikalische Chemie* **1979**, *83*, 504.

(230) Schanze, K. S.; Giannotti, C.; Whitten, D. G. *J. Am. Chem. Soc.* **1983**, *105*, 6326.

(231) Xu, H.; Chen, R.; Sun, Q.; Lai, W.; Su, Q.; Huang, W.; Liu, X. *Chem. Soc. Rev.* **2014**, *43*, 3259.

(232) Liu, Q.; Ho, C.-L.; Lo, Y.; Li, H.; Wong, W.-Y. *J. Inorg. Organomet. Polym. Mater.* **2015**, *25*, 159.

(233) Estrada, L. A.; Stalder, R.; Abboud, K. A.; Risko, C.; Brédas, J.-L.; Reynolds, J. R. *Macromolecules* **2013**, *46*, 8832.

(234) Stalder, R.; Mei, J.; Reynolds, J. R. *Macromolecules* **2010**, *43*, 8348.

(235) Haskins-Glusac, K.; Ghiviriga, I.; Abboud, K. A.; Schanze, K. S. *J. Phys. Chem. B* **2004**, *108*, 4969.

(236) Zhang, G.; Fu, Y.; Xie, Z.; Zhang, Q. *Macromolecules* **2011**, *44*, 1414.

(237) Gevaerts, V. S.; Herzig, E. M.; Kirkus, M.; Hendriks, K. H.; Wienk, M. M.; Perlich, J.; Müller-Buschbaum, P.; Janssen, R. A. J. *Chem. Mater.* **2014**, *26*, 916.

(238) Lee, D.-C.; Brownell, L. V.; Yan, L.; You, W. *ACS Appl. Mater. Interfaces* **2014**, *6*, 15767.

(239) Shin, W.; Yasuda, T.; Watanabe, G.; Yang, Y. S.; Adachi, C. *Chem. Mater.* **2013**, *25*, 2549.

(240) Cardolaccia, T.; Li, Y.; Schanze, K. S. *J. Am. Chem. Soc.* **2008**, *130*, 2535.

(241) Kirkus, M.; Wang, L.; Mothy, S.; Beljonne, D.; Cornil, J.; Janssen, R. A. J.; Meskers, S. C. J. *J. Phys. Chem. A* **2012**, *116*, 7927.

(242) Siebbeles, L. D. A.; Huijser, A.; Savenije, T. J. *J. Mater. Chem.* **2009**, *19*, 6067.

BIOGRAPHICAL SKETCH

Subhadip Goswami was born in a small village called Baradhemo, India in 1986, as a first child to Debdas Goswami and Tripti Goswami. After he received his high school education from E.Rly.Boys.H.S.School, Asansol, he moved to one of the renowned missionary colleges in India - Ramakrishna Mission Vidyamandira in Belur Math to study Chemistry. After finishing his bachelor's in 2008 he joined the chemistry department of country's prestigious institute Indian Institute of Technology, Kanpur (IITK) to pursue his masters. After 5 years of studying chemistry, he decided to pursue career in chemistry and moved to University of Florida, USA (UF) to attend the graduate school in 2010. In UF, he joined the research group of Professor Kirk Schanze and entered into the field of light-materials interaction. During his stay in the Schanze group, he exposed himself to many aspects of research. He gained experience in synthesis of pi-conjugated organic small molecules and polymers for biocidal activity, synthesis of organometallic complexes and polymers for nonlinear optical phenomenon, bulk-heterojunction solar cells. Apart from that he worked with his colleagues briefly in various aspects of device fabrication. During his graduate studies, he got married to Sucharita Chakraborty in 2014. Subhadip obtained his PhD from University of Florida in summer, 2015. He will work with Professor Joe Hupp as a postdoctoral fellow, in the department of chemistry, Northwestern University.